UNIVERSITY OF
KWAZULU-NATAL

INYUVESI
YAKWAZULU-NATALI

# AN INVESTIGATION INTO THE USE OF FLUORINATED HYDRATING AGENTS IN THE DESALINATION OF INDUSTRIAL WASTEWATER


**by**
**Cassandra Petticrew (BSc. Eng)**


This dissertation (ENNO8RPH1) is submitted for the degree of Master of Science in Engineering (MScEng) in the School of Chemical Engineering at the University of Kwa-Zulu Natal.

December 2011


**Supervisor:** Prof. Deresh Ramjugernath
**Co-Supervisors:** Dr. Paramespri Naidoo
Dr. Amir H. Mohammadi
Prof. Chris Buckley



The financial assistance of the National Research Foundation (NRF) towards this research is hereby acknowledged. Opinions expressed and conclusions arrived at, are those of the author and are not necessarily to be attributed to the NRF.

# DECLARATION

I, Cassandra Petticrew, declare that:

(i) The research reported in this dissertation/thesis, except where otherwise indicated, is my original work.
(ii) This dissertation/thesis has not been submitted for any degree or examination at any other university.
(iii) This dissertation/thesis does not contain other persons‟ data, pictures, graphs or other information, unless specifically acknowledged as being sourced from other persons.
(iv) This dissertation/thesis does not contain other persons‟ writing, unless specifically acknowledged as being sourced from other researchers. Where other written sources have been quoted, then:
a) their words have been re-written but the general information attributed to them has been referenced;
b) where their exact words have been used, their writing has been placed inside quotation marks, and referenced.
(v) Where I have reproduced a publication of which I am an author, co-author or editor, I have indicated in detail which part of the publication was actually written by myself alone and have fully referenced such publications.
(vi) This dissertation/thesis does not contain text, graphics or tables copied and pasted from the Internet, unless specifically acknowledged, and the source being detailed in the dissertation/thesis and in the References sections.

Cassandra Petticrew December 2011

As the candidate‟s Supervisor/Co-Supervisor I agree to the submission of this dissertation:

Supervisor:

Prof. Deresh Ramjugernath

Co-Supervisors:

Dr. Paramespri Naidoo Dr. Amir H. Mohammadi Prof. Chris Buckley

# ACKNOWLEDGEMENTS

The author would like to acknowledge the contribution and assistance of the following individuals: The supervisors in this project: Prof. Deresh Ramjugernath, Dr. Paramespri Naidoo, Dr. Amir H. Mohammadi and Prof. Chris Buckley; the workshop staff especially Mr Ken Jack and the postgraduate students and colleagues in the Thermodynamics Research Unit: Ayanda Khanyile, Lindinkosi Mkhize, Nicholas Rice and Armel Kaniki Tumba. Additionally the author would like to thank Angela Petticrew, Alexander Petticrew and Alastair Petticrew for their support.

# ABSTRACT

Salts in solution should be removed by desalination techniques to prevent equipment fouling and corrosion. Common desalination technologies are energy intensive such as Multi Stage Flash (MSF) distillation which requires 14.5 J/$m^3$ (Ribeiro. J, 1996) of energy. Desalination technologies produce purified water and a concentrated salt solution, where the salt concentration is dependent on the desalination technology used. This work investigates gas hydrate technology as a possible desalination technology.

Hydrates are composed of guest molecules and host molecules. Guest molecules may be in the form of a liquid or gas. During hydrate formation, host molecules, water, form a cage enclosing the guest molecule. Common hydrate formers or guest molecules such as; methane, ethane, propane and carbon dioxide are currently being investigated in literature, for use in gas hydrate desalination technology. Common hydrate formers form hydrates at low temperatures; below 288 K and high pressures; above 2 MPa. To increase the temperature and reduce the pressure at which gas hydrates form, commercially available hydrofluorocarbon hydrate formers such as R14, R32, R116, R134a, R152a, R218, R404a, R407c, R410a and R507 are preliminarily investigated in this work.

The criteria for choosing the most suitable fluorine-based formers require the former to be: environmentally acceptable where it is approved by the Montreal Protocol; non-toxic where it has a low acute toxicity; non-flammable; chemically stable; a structure II hydrate to simplify the washing process; available in commercial quantities; low cost in comparison to other hydrate formers; compatible with standard materials and contain a high critical point for a large heat of vaporisation (McCormack and Andersen, 1995). Taking all these criteria into account, R134a was chosen for further investigation as a possible hydrate former.

In this work, hydrate-liquid-vapour phase equilibrium measurements are conducted using the isochoric method with a static high pressure stainless steel equilibrium cell. The Combined Standard Uncertainty for the 0-1 MPa pressure transducer, 0-10 MPa pressure transducer and the Pt100 temperature probes are ±0.64 MPa, ±5.00 MPa and ±0.09 K respectively. Vapour pressure measurements for Hydrofluoropropyleneoxide, $CO_2$, R22 and R134a were measured to verify the pressure and temperature calibrations. Hydrate test systems for R22 (1) + water (2) and R134a (1) + water (2) were measured to verify calibrations, equipment and procedures. New systems measured included R134a (1) + water (2) + {5wt%, 10wt% or 15wt%} NaCl (3).

For the system R134 (1) + water (2) at 281 K the dissociation pressure is 0.269 MPa. However, addition of NaCl to the system resulted in a shift of the HVL equilibrium phase boundary to lower temperatures or higher pressures. The average shift in temperature between the system R134a (1) + water (2) containing no salt and the systems containing {5, 10 and 15} wt% NaCl are -1.9K, -4.8K and -8.1K respectively.

In this work, the measured systems were modelled using two methods of approach. The first method is where hydrofluorocarbon hydrate former solubility is included, (Parrish et al., 1972) and the second is where hydrofluorocarbon hydrate former solubility is ignored, (Eslamimanesh et al., 2011). From these models, it is found that hydrofluorocarbon solubility could not be neglected.

In this work, the hydrate phase was modelled using modifications of the van der Waals and Platteeuw model, (Parrish et al., 1972). The liquid and vapour phases are modelled using the Peng-Robinson equation of state with classical mixing rules (Peng, 1976). The electrolyte component is modelled using the Aasberg-Peterson model (Aasberg-Petersen et al., 1991) modified by Tohidi (Tohidi et al., 1995). The percent absolute average deviation (%AAD) for the systems, which includes solubility, is 0.41 for R22 (1) + water (2) and 0.33 for R134a (1) + water (2). For the system R134a (1) + water (2) + {5 wt%, 10 wt% or 15 wt%} NaCl (3) the % AAD is 5.14.

Using the hydrate former, R134a, is insufficient to ensure gas hydrate technology is competitive with other desalination technologies. Hydrate dissociation temperature should be increased and pressure decreased further to ambient conditions. As evident in literature, promoters, such as cyclopentane, are recommended to be added to the system to shift the HLV equilibrium phase boundary as close to ambient conditions as possible.

# TABLE OF CONTENTS

# LIST OF FIGURES

# LIST OF TABLES

# NOMENCLATURE

| | | |
|---|---|---|
| a | Distance of closest approach | m or cm* |
| $a_i$ | Empirical parameters | K/MPa |
| $å_i$ | Hard core diameter | m |
| $\overset{0}{A}$ | Angstrőm unit | |
| $a_r$ | Radial coordinate | |
| $a_w$ | Activity of water | |
| $A_\varphi$ | Debye-Hűckel coefficient | |
| $A_{ml}$ | Fitted constant for component l in cavity m | K |
| $A_p$ | Surface area of the particle | |
| b | Empirical parameter | K/MPa |
| $B_\gamma$ | Debye-Hűckel B parameter | |
| $\dot{B}$ | B-dot parameter | |
| $B_{ml}$ | Fitted constant for component l in cavity m | K |
| c | Empirical parameter | K/MPa |
| $c^0_{AB}$ | Stoichiometric molarity of electrolyte AB | $gmol/dm^3$* |
| C | Adjustable parameter | |
| $C_{ml}$ | Langmuir constant for component l in cavity m | |
| Cp | Heat capacity | J/(mol.K) |
| d | Density | $kg/m^3$ |
| d | Empirical parameter | K/MPa |
| D | Macroscopic static dielectric constant of the solution | |
| $D_s$ | Dielectric constant of pure liquid constant | |
| $f_l$ | Fugacity of guest l | Pa or MPa** |
| $\overset{\Lambda}{f}{}^{L}_{w}$ | Fugacity of water in the water rich aqueous phase | Pa or MPa** |
| $\overset{\Lambda}{f}{}^{+}_{w}$ | Fugacity of pure water in the reference state (at the T and P of mixture) | Pa or MPa** |
| $h_{ws}$ | Interaction coefficient between dissolved salt and non electrolyte | |
| H | Enthalpy | J/kg or J/mol |
| I | Ionic strength | $gmol/dm^3$* |

| | | |
|---|---|---|
| k | Boltzmann constant | $1.3805410\times10^{-23}$ J/K.mol |
| $K_d$ | Mass transfer coefficient for hydrate desorption | m/s |
| $K^o$ | Reciprocal Debye length | $m^{-1}$ or $cm^{-1}$* |
| $K^*$ | Mass transfer coefficient of diffusion and adsorption | m/s |
| m | Molality | mol/kg or gmol/kg* |
| M | Molecular weight | kg/kgmol or g/gmol |
| n | Adjustable parameter | |
| N | Number of moles / Number of phases | |
| $N_I$ | Integer constant | |
| $N_o$ | Avogadro‟s number | $6.02252\times10^{23}$ $gmol^{-1}$ |
| P | Pressure | Pa |
| $P_w^{MT}$ | Pressure of water in empty hydrate | atm |
| r | Core radius | m |
| $r_i^{\circ}$ | Ionic saturated cavity radius | cm* |
| R | Gas constant | $MPa.m^3/kgmol.K$** or J/K.gmol |
| $R_{cav}$ | Cavity radius | m |
| T | Absolute temperature | K |
| v | Number of ions | |
| V | Molar volume | $m^3/mol$ |
| w(r) | Spherically symmetric cell potential | J |
| x | Mole fraction / liquid phase | |
| z | Electronic charge | |
| $z_z$ | Coordination number | |

**Greek letters**

| | | |
|---|---|---|
| α | Numerical parameter / core radius | Å |
| $\alpha_d$ | Dissociation coefficient of the electrolyte | |
| β | Interaction energy parameter | |
| Γ | Non random factor | |
| $\gamma_\pm$ | Mean ionic activity coefficient | |
| $\gamma_i$ | Species Activity coefficient | |
| ε | Solvent relative permittivity / depth of binary potential well | erg |
| $\varepsilon_m$ | Free salt mixture dielectric constant | |
| $\varepsilon_N$ | Dielectric constant of water | |

| | | |
|---|---|---|
| $\Theta$ | Fraction of cage occupation | |
| $\lambda$ | NRTL-NRF parameter | |
| $\mu$ | Chemical potential | J/mol |
| $\nu$ | $\nu_- + \nu_+$ | |
| $\nu_{-,+}$ | Stoichiometric numbers of ions in the dissociation equation | |
| $\nu^c$ | Molar volume of the saturated cavity around the ions | $cm^3/gmol$* |
| $\nu^o$ | Molar volume | |
| $\bar{\nu}$ | Partial molar volume | $cm^3/gmol$* |
| $\nu_m$ | Number of cages per water molecule in a unit hydrate cell | |
| $\xi$ | True mole fraction | |
| $\tau$ | NRTL binary interaction energy parameters | J/mol |
| $\sigma$ | Molecular distance parameter | Å |
| $\Phi$ | Fugacity coefficient | |
| $\varphi$ | Correction for the deviation of the saturated vapour of the pure, hypothetical, lattice from ideal behaviour | |
| $\omega$ | Apparent volume fraction of component in the liquid phase | |

**Superscripts**

| | |
|---|---|
| a | Anion |
| c | Cation |
| SR | Short range electrolyte interactions |
| LR | Long range electrolyte interactions |
| $\beta$ | Empty hydrate |
| $\alpha$ | Pure water |
| - | Average |
| H | Hydrate |
| L | Liquid |
| V | Vapour |
| MT | Hypothetical empty hydrate |
| o | Reference point |

**Subscripts**

| | |
|---|---|
| $\pm$ | Mean ionic |
| AB | Electrolyte |

| | |
|---|---|
| i | Component |
| o | Reference state |
| sat | Saturated |
| s | Solvent |
| t | Salt |
| v | Volume |
| w | Water |
| x | Mole fraction |
| E | Electrolyte |
| b | Solution (bulk) phase |
| eq | Equilibrium |

**Abbreviations**

| | |
|---|---|
| ED | Electrodialysis |
| EOS | Equation of state |
| H | Hydrate |
| I | Ice |
| LDHI | Low dosage hydrate inhibitors |
| LR | Long Range |
| $L_a$ | Liquid additive |
| $L_g$ | Liquid guest molecules |
| $L_{HC}$ | Liquid hydrocarbon |
| $L_w$ | Liquid water |
| MED | Multiple effect distillation |
| MSF | Multi stage flash |
| PR | Peng Robinson |
| PRSV | Peng-Robinson-Stryjek-Vera |
| PT | Patel and Teja |
| RO | Reverse osmosis |
| sI | Structure I hydrate |
| sII | Structure II hydrate |
| sH | Structure H hydrate |
| SR | Short Range |
| SRK | Soave-Redlich-Kwong |

| | |
|---|---|
| TB | Trebble-Bishnoi |
| TDS | Total dissolved solids |
| V | Vapour |
| VC | Vapour compression |
| VP | Valderrama |

* Units are not defined according to the International System of Units, these units correspond to NRTL, Debye-McAulary (Cruz and Renon, 1978)

** These units correspond to (Englezos and Ngan, 1993)

# CHAPTER ONE

## INTRODUCTION

Water shortages are common in many countries due to increased industrial, domestic and agricultural use. Currently 70% of water used worldwide is for irrigation, 22% is used for industry and 8% is used for domestic consumption. Water shortages are prevented by reusing industrial water. The presence of chemical pollutants such as metals, organic compounds, inorganic compounds, solvents, polymers, oil, salts, and dissolved or solid compounds in industrial wastewater make re-use difficult and lead to numerous problems such as fouling and corrosion of equipment. The presence of chlorides such as NaCl, $CaCl_2$ and $MgCl_2$ results in unit operation corrosion while the presence of sulphates such as $CaSO_4$, $Na_2SO_4$ and $MgSO_4$ results in scaling, fouling and plugging of equipment.

Desalination technologies reduce the total dissolved solids (TDS) of seawater, brackish water or treated wastewater to less than 0.5 g TDS/L. Commercial desalination technologies include thermal processes and membrane processes. Thermal processes include multi stage flash distillation (MSF), vapour compression (VC), and multiple effect distillation (MED). Membrane processes include electrodialysis (ED) and reverse osmosis (RO), (Javanmardi and Moshfeghian, 2003). Membrane distillation (MD) and hydrate technology are emerging technologies which are under investigation in literature for high feed salt concentrations. The desalination technology used is dependent on plant cost, feed and product water quality, energy sources, pre-treatment requirements, chemical costs, labour requirements and training and plant capacity.

Table 1.1: Desalination process economic requirement for a plant with a capacity of 1000 000 kg/day.

| **Process** | **Total capital investment / R million** | **Total product cost / R million/1000kg** |
|---|---|---|
| MSF | 21.36 | 23.68 |
| MD | 18.08 | 22.00 |
| RO | 18.40 | 35.76 |
| Hydrate technology* | 43.68 | 22.08 |

Ref: (Javanmardi and Moshfeghian, 2003)

MSF: Multi stage flash distillation, MD: Membrane distillation, RO: Reverse osmosis
*Using propane as a former

The most competitive technologies include RO and MED since VC is limited to small scale application. ED is limited to feed concentrations of up to 12 g TDS/L. MD has limited application due to low productivity, fouling, a low durability membrane and high thermal conductivity (Mariah et al., 2006). RO and MED are used for large scale applications however, biofouling, scaling due to the low salt solubility limit such as $Ca_2SO_4$, corrosion and additional cleaning prove them to be unfavourable (Van Der Bruggen et al., 2002). Additionally, RO is highly sensitive to changes in feed quality and its application is limited to feed concentrations less than 32 g TDS/L. Refer to Appendix A for further details on each technology.

An alternative technology currently under investigation in this work is hydrate desalination technology. It proves advantageous due to its low energy requirement: the latent heat of fusion of ice is one seventh of the latent heat of vaporisation of water. Scaling, fouling and corrosion are reduced due to low operating temperatures. Low cost materials may be used due to the low operating temperature compared to MED. A high heat transfer coefficient and surface area may be achieved as there is direct contact between the brine and the refrigerant. Additional chemicals and pre-treatment are not required as opposed to RO (McCormack and Andersen 1995).

For hydrate desalination technology to be applied industrially, several concerns should be addressed. These include the use of high quality energy for crystallization, washing the hydrate with fresh water to remove excess salt from the purified water product, high energy requirements when using compressors, complex operation due to handling ice slurries, retention of undesirable odours in the product stream and trapping the salt in the ice which requires crushing and re-crystallization (McCormack and Andersen 1995).

It is necessary to measure hydrate phase boundaries to determine the conditions (temperature and pressure) at which hydrates dissociate. From phase equilibrium data, operating conditions for the desalination of industrial wastewater using hydrate technology can be identified. Research on hydrates conducted in literature include the use of common gases such as methane, ethane, propane and carbon dioxide (refer to Tables A1 to A4 in Appendix C). Gas hydrates using common formers have been measured in the presence of salts (refer to Tables A10 to A13 in Appendix C). Common gases aid in low temperature and high pressure hydrate formation, increasing operating conditions

for gas hydrate desalination technology. Commercial hydrofluorocarbon gases were investigated in this work, to replace common gases, to reduce the operating costs to more competitive values. Research has been conducted in literature for several fluorinated gases (refer to Tables A5 to A9 in Appendix C). Additionally, measurements have been conducted in literature for R22 (1) + water (2) + {5, 10 and 15} wt% NaCl (refer to Table A14 in Appendix C for further details).

Previous studies have failed to identify environmentally safe formers which reduce the hydrate dissociation pressure and increase the hydrate dissociation temperature to ambient conditions. This study identifies the most suitable commercially available hydrofluorocarbon former for the formation of hydrates with reduced energy requirements. R14, R32, R116, R152a, R218, R404a, R407c, R410a and R507 are preliminary investigated and R134a is further investigated. Common salts found in industrial wastewater were determined in their respective concentrations. The hydrate phase equilibrium boundary for the chosen former, R134a, was measured and modelled in the presence of pure millipore water as well as with various concentrations of NaCl.

# CHAPTER TWO

## HYDRATES

Hydrates were first discovered in the 19th century by Sir Humphry Davy. Later, in 1823, Michael Farady measured the composition of chlorine hydrates. Research with respect to hydrate formers and hydrate formation conditions were investigated in the 19th century. In the 20th century, the application of hydrates was extended to industrial uses (Eslamimanesh et al., 2012).

Hydrates are crystal-like structures that form at a specific temperature and pressure (usually low temperature and high pressure respectively). Gas hydrates contain a crystal lattice of hydrogen bonded water molecules known as host molecules and are therefore classified as clathrate hydrates. A cavity is found in each crystal-like structure where a non-polar or slightly polar guest molecule is located. Hydrates cannot form without the guest molecule. Van der Waals forces exist between the guest and host molecules, to ensure the hydrate is stable. A stable hydrate is dependent on the guest molecule size, shape and nature. If the guest molecule is too large or too small, the hydrate will not form. It is not necessary for the crystal to be completely filled with the guest molecule for hydrate formation to occur, however, ideally all cavities should be occupied to ensure the hydrate is stable, (Sloan and Koh, 2008). When the temperature is too high or pressure too low, the lattice dissociates. Figure 2.1 indicates the basic structure of a non-stoichiometric clathrate hydrate.

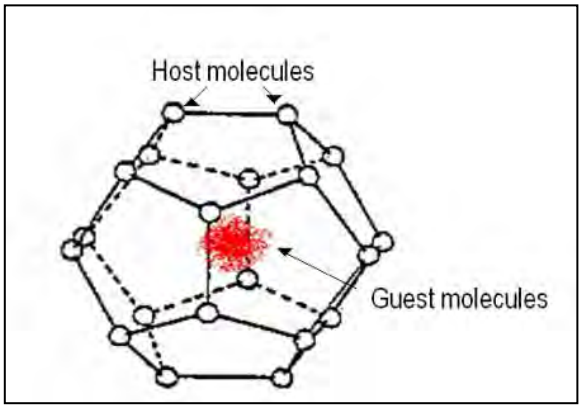


Figure 2.1: Simple structure of a Type I Clathrate Hydrate
(https://sps.esd.ornl.gov/desalinationpage.html, accessed 16 January 2012).

Chapter two introduces the reader to how hydrates are classified and their application. It also describes hydrate formation and dissociation. The result of using various formers on hydrate dissociation is illustrated. Additionally, the effect inhibitors and promoters have on phase equilibrium data is shown in Figures 2.13 and 2.14.

## 2.1 Hydrate structures

From previous studies, hydrate analysis was conducted using Nuclear Magnetic Resonance, Neutron diffraction or Raman spectroscopy (Mooijer-Van Den Heuvel, 2002). Three common hydrate structures were observed. These included cubic structure I, II and H, as seen in Figure 2.2. Each hydrate structure contained different sized cavities, which were classified as either large or small. The type of structure was dependent on the guest molecule diameter (refer to Table 2.1). Type I structures (SI) contained molecules with diameters of 4.2 to 6 Å. Type II structures (SII) contained molecules with diameters below 4.2Å or between 6 and 7Å. Type H structures (SH) contained guest hydrate molecules with diameters between 7 and 9Å. Methane and ethane form SI hydrates while propane and carbon dioxide form SII hydrates. Some comparatively larger molecules such as butane are too large to occupy the cavities (Parrish et al., 1972). Larger molecules can only enter a limited number of cavities and thus require a help gas, also known as a hydrate promoter, to enter into the smaller cavities and increased the hydrate stability.

The nomenclature used for describing hydrate structures is $n_i^{mi}$. "n" was the number of edges in the face type "i", while "mi" was the number of faces with "ni" edges (Sloan and Koh, 2008). The optimum host molecule to guest molecule size ratio is 0.75. If the ratio is smaller, the van der Waals forces are too weak to stabilise the hydrate. If the ratio is greater than 1, the guest molecule was too large to fit in the cavity. Type I and II structures required one guest molecule to ensure the hydrate was stable while type H structures required two different guest molecules, one larger and one smaller, for a stable hydrate to form. For systems containing mixed gases, the gas with the largest molecule size determined the type of structure formed (Sum et al., 1997).

Table 2.1: Properties of various hydrate structures including Type I, Type II and Type H.

| Structure | Cavity type[a] | Shape[a] | Name[a] | Number of cages per unit cell[b] | Average cell radius Å[b] | water molecules per unit cell[b] |
|---|---|---|---|---|---|---|
| Type I | Small | $5^{12}$ | Pentagonal Dodecahedron | 2 | 3.95 | 46 |
| | Large | $5^{12}6^2$ | Hexagonal truncated trapezohedron | 6 | 4.33 | |
| Type II | Small | $5^{12}$ | Pentagonal Dodecahedron | 16 | 3.91 | 136 |
| | Large | $5^{12}6^4$ | Hexadecahedron | 8 | 4.73 | |
| Type H | Small | $5^{12}$ | | 3 | 3.91 | 34 |
| | Small | $4^3 5^6 6^3$ | | 2 | 4.06 | |
| | Large | $5^{12}6^8$ | | 1 | 5.71 | |

[a] (Sloan and Koh, 2008)
[b] (Sloan, 2003)

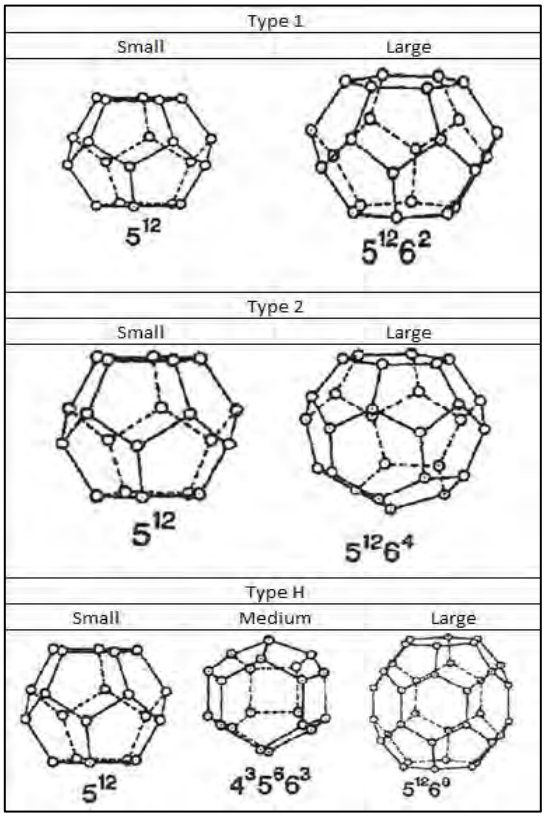


Figure 2.2: Structures of Type I, Type II and Type H Clathrate Hydrates including faces and edges (Zakrzewski et al., 1994).

## 2.2 Industrial prevention and uses

Hydrate formation is considered a nuisance in the petroleum industry as they block pipelines and prevent production, processes and transportation of fluids. Gas hydrates may be useful. Some applications may include carbon dioxide capture and sequestration, storage of gas, air-conditioning systems, concentration of food solutions, flue gas separation and desalination.

### 2.2.1 Hydrate prevention

When natural gas is extracted from reservoirs, water is often present. In the petroleum industry, the natural gas is transported through several heating and cooling processes. At specific conditions, hydrates may form. It is important to know where hydrates form as, if present, they may block pipelines, valves and safety devices. The formation of hydrates in a pipeline reduces the cross sectional area in which the fluid flows. This increases the pressure drop across the pipeline which may increase processing, production and transportation costs. Hydrates are commonly formed in drilling muds as well as oil reservoirs any processes where water and natural gas are found. Hydrates are removed by mechanical methods (physical removal of hydrates), thermal methods (heating the pipelines), thermodynamics (predicting under what conditions hydrates will form) as well as adjusting the activity of water by adding inhibitors (Eslamimanesh et al., 2012).

### 2.2.2 Gas supply and storage

Approximately $10^{16}$ $m^3$ methane is trapped in the form of gas hydrates. This methane can be extracted and used as an energy source. The methane may be produced by reducing the reserve pressure or increasing the reserve temperature to outside of the hydrate stability region. Additionally, inhibitors may be added to alter the conditions at which the hydrate is stable. The use of hydrate technology as a source of energy has not been implemented on an industrial scale (Eslamimanesh et al., 2012).

Hydrates may be used for the storage of gases such as hydrogen, methane and carbon dioxide. Storing gases in hydrate structures have lower process volumes than other storage methods such as liquefaction. Refer to Strobel et al. (2009) for further details on this application.

### 2.2.3 Separation

#### 2.2.3.1 Flue gas separation

Conventional processes used to separate carbon dioxide, methane, hydrogen sulfide, sulfur hexafluoride, $H_2$, $N_2$ and R134a from flue gas include amine absorption and membranes. Gas hydrates is another economically viable solution. Promoters may be added to the gas hydrate process to reduce the energy required to form the hydrates which will decrease operating costs. Additionally, gas hydrate technology may be used as an alternative separation process for the separation of gas and oil (Eslamimanesh et al., 2012).

#### 2.2.3.2 Concentrating food solutions

Clathrate hydrates form at temperatures above the freezing point of ice. It is therefore more cost effective to concentrate dilute aqueous solutions with hydrate technology than crystallisation. Concentration of proteins, lipids, carbohydrates, apple, orange and tomato juices have been reported in literature (Eslamimanesh et al., 2012).

#### 2.2.3.3 Desalination

Current competitive desalination technologies included reverse osmosis (RO) and multiple effect distillation (MED). RO required the system to overcome a high osmotic potential and therefore operate under high energy inputs. Additionally, RO technology contained membranes and is subject to scaling and fouling. MED operated at high temperatures and was subject to corrosion, scaling and fouling. Additionally, MED required energy to overcome the latent heat of vaporisation of the solution.

Gas hydrate technology is being researched in literature as a desalination technology. The proposed process for the desalination of saline waters using gas hydrate technology involved directly mixing the concentrated industrial wastewater with a hydrate former in the hydrate reactor. At a specified temperature and pressure, a hydrate formed excluding the salt particles. The hydrates were transported to a vertical hydraulic wash column where the crystals were separated from the concentrated brine by forcing the brine hydrate mixture up the column. A small quantity of wash water flowed down the column over the hydrates (refer to Figure 2.3). The wash water containing

the brine was removed from the centre of the column as concentrated saline solution. The hydrate crystals were transported to the hydrate decomposer where at a specified temperature and pressure, the hydrate crystals dissociated; the former was released and recycled to the hydrate reactor and fresh water was obtained (McCormack and Andersen, 1995).

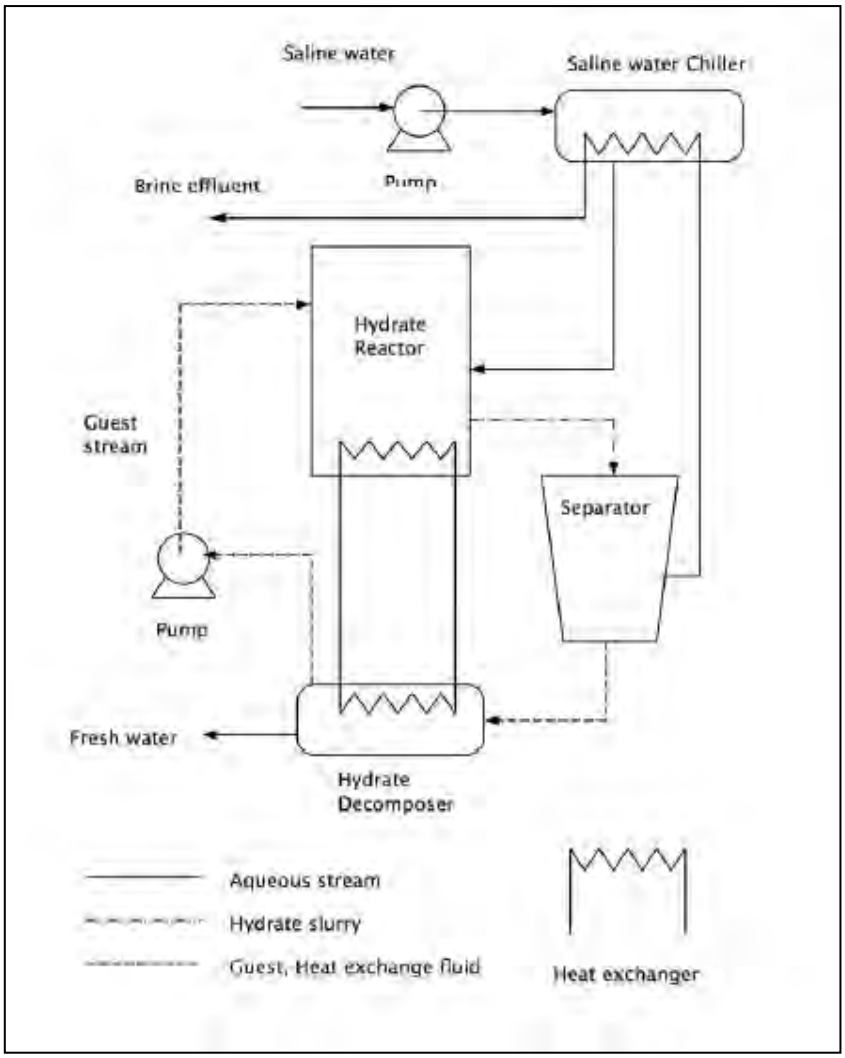


Figure 2.3: Clathrate desalination process (Bradshaw et al., 2008).

## 2.3 Hydrate Kinetics

Hydrate formation is dependent on hydrate nucleation and growth. Hydrate nucleation is the process where critical sized nuclei are formed at the vapour-liquid interface. Hydrate growth is the growth of the stable nuclei to form stable clathrate hydrates. When equilibrium is disturbed, such as an increase in temperature, hydrates dissociate to release the guest molecules trapped in the cavities.

Hydrate formation is path dependent while hydrate dissociation is path independent. The time required for hydrate formation is important for the separation of salt from the hydrate. The longer the time given for hydrate formation, the better the separation between the hydrate and salt. Methods are used to describe hydrate nucleation, growth and dissociation (Sloan and Koh, 2008).

### 2.3.1 Nucleation

Nucleation occurs when a supersaturated solution of excess dissolved hydrate former is in contact with hydrogen bonded water molecules. The water molecules position themselves around the non-polar organic former and a nuclei is formed. This is known as the hydrophobic effect. The location of the supersaturated point in the solution determines where the first nuclei will form. For a non-stirred system, the nuclei may form at the vapour-liquid interface due to a high concentration of both the guest and host molecules, as well as the lower Gibbs‟ free energy. For a stirred system, the nuclei may form anywhere in the solution depending on the position of the highest concentration of the dissolved former (Bishnoi and Natarajan, 1996). If the nuclei size is less than the critical crystal size, the hydrate crystal is not stable. It will therefore continue to grow or break in the solution.

Referring to Figure 2.4, for an isochoric system, nucleation occurs between points A and B. The induction time is dependent on the time required for the nucleation process. For systems which have previously formed hydrates, the induction time is reduced, this is known as the memory effect (Vysniauskas and Bishnoi, 1983). Induction time is dependent on water history and agitation and therefore surface area. Three models have been developed to describe the nucleation process; the reader is referred to (Sloan and Koh, 2008) for further information.

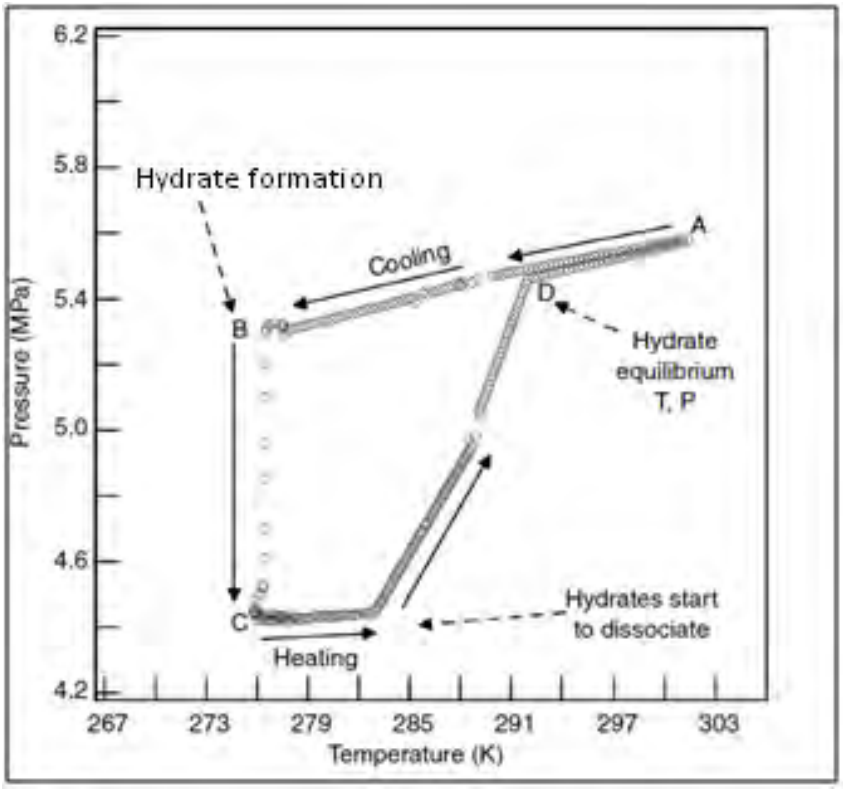


Figure 2.4: Isochoric temperature search technique to determine the hydrate dissociation point extracted from (Tumba, 2010).

### 2.3.2 Crystal growth

Once the hydrate nuclei have obtained critical size, they continue to grow to form clathrate hydrate crystals. During crystal growth, a large drop in pressure is observed due to diffusion and adsorption of guest molecules into the cavities. As a result, stable hydrates are formed (refer to points B to C in Figure 2.4). Englezos et al. (1987) developed a model whereby the dissolved gas diffuses through the surrounding solution (point $f_b$) into the stagnant liquid layer (point $f_s$). The gas then adsorbs into the hydrate, which is assumed spherical (refer to Figure 2.5). The reaction rates for each step are in terms of fugacity and not dissolved gas concentration. At equilibrium, the growth rate per particle can be expressed as (Bishnoi and Natarajan, 1996):

$$\left(\frac{dn}{dt}\right)_p = K^* A_p \left(f_b - f_{eq}\right) \qquad 2.1$$

Several models were developed for hydrate growth (Sloan and Koh, 2008).

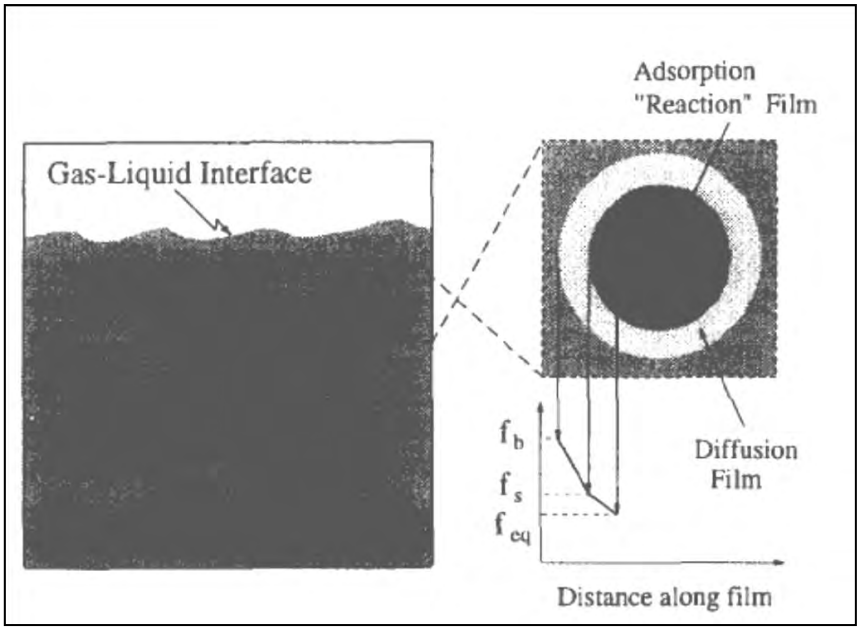


Figure 2.5: Profile of a growing hydrate crystal in terms of fugacity (Bishnoi and Natarajan, 1996).

### 2.3.3 Dissociation

Dissociation may occur due to depressurization, thermal stimulation, thermodynamic inhibitor injection or any combination of the methods mentioned. The most common method used in industry to prevent pipe blockages, is inhibitor injection. In laboratories, pipe blockages are prevented by thermal stimulation. Hydrate dissociation consists of two steps: the destruction of the lattice as well as desorption. At very low temperatures, the molecular motion stops and the hydrate lattice becomes rigid. As temperature increases, the motion due to water molecule reorientation and diffusion causes the hydrate to dissociate. The trapped gas in the hydrate is then released which increases the system pressure (refer to points C to D in Figure 2.4). The dissociation of hydrates is twice as slow as that of ice. This is due to the lower density hydrogen bonds found in hydrates. Hydrate dissociation is an endothermic process. Heat is supplied to break the van der Waals forces between the water and guest molecules, as well as the hydrogen bonds between the water molecules. The surrounding layer of ice conducts heat from an external source and transfers it radially to the hydrate resulting in a temperature gradient. As the hydrate begins to dissociate, a cloud of gas surrounds the hydrate and forms a layer for desorption (refer to Figure 2.6). According to Kim et al. (1987), at equilibrium the dissociation rate per particle may be expressed as (Bishnoi and Natarajan, 1996):

$$-\left(\frac{dn_H}{dt}\right)_p = K_d A_p \left(f_{eq} - f_g^v\right) \qquad 2.2$$

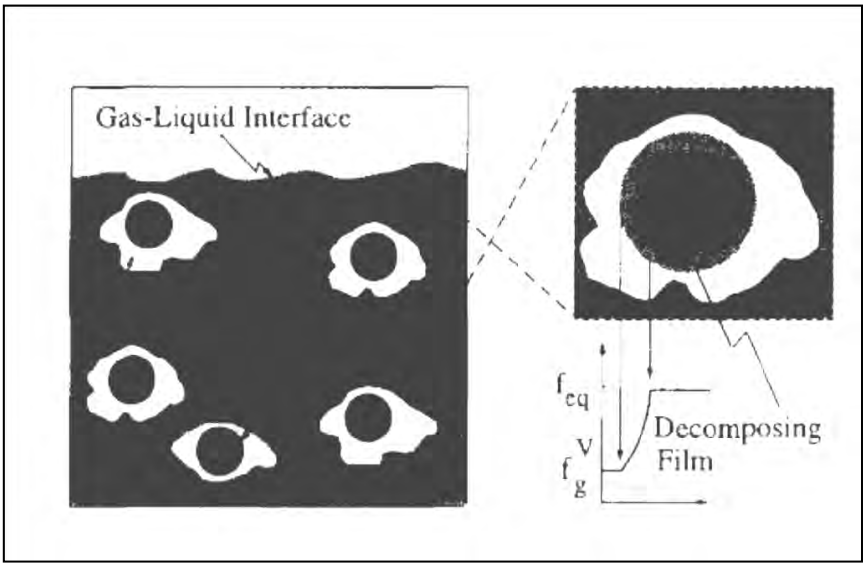


Figure 2.6: Profile of a dissociating hydrate crystal in terms of fugacity, assuming a spherical structure (Bishnoi and Natarajan, 1996).

## 2.4 Formers, promoters and inhibitors

Hydrate formers are a type of guest molecule, required for hydrate formation. Hydrate formation and dissociation were affected by chemicals such as promoters and inhibitors. Promoters increased the temperature or reduced the pressure at which hydrates form, while inhibitors had the opposite effect.

### 2.4.1 Hydrate formers

Hydrate formers were liquid or gas molecules which assisted in hydrate formation. These molecules were usually hydrophobic. Previous studies in literature used methane, ethane, propane and carbon dioxide as common formers for the desalination of saline waters. Common hydrate formers were used as they were easily available at a low cost (refer to Table 2.2). However, they formed hydrates at pressures above 2 MPa and temperatures below 288 K (refer to Figure 2.7) and thus resulted in an energy intensive process.

Table 2.2: Specific criteria used for choosing the best common formers for hydrate formation.

| | **Methane** | **Ethane** | **Propane** | **Carbon dioxide** |
|---|---|---|---|---|
| Upper quadruple point | None[A] | 287.85 K, 3.39 MPa [B] | 280.9K, 0.6 MPa[B,C] | 283 K , 4.8 MPa[B,C] |
| Critical pressure | 4.70 MPa[A] | 4.88 MPa | 4.2 MPa[C] | 7.4 MPa[C] |
| Ecological effect | None | None | None | None |
| Toxicity effect | simple asphyxiant | None | simple asphyxiant | asphyxiant |
| Flammability | yes | yes | yes | Non-flammable |
| Stability | unstable at high temperatures, outside explosive limits | | | Stable |
| Class | I | I | II | I |
| Cost* | R16/$m^3$ | Not available in examined literature | R11.5/$m^3$ | R12.13/$m^3$ |
| Compatibility | compatible with metals at certain temperatures | Oxidizing agents, chlorine dioxide, chlorine | Oxidizing agents | Alkali metals, alkaline earth metals, metal acetylides, chromium, titanium, uranium, , magnesium |
| Solubility in water | Not available in examined literature | 0.05 vol/vol | 0.04 vol/vol | 0.9 vol/vol |
| Availability | Yes | Yes | Yes | Yes |
| Particle diameter (Å)[Ref] | 4.36[B] | 5.5[B] | 6.28[B] | 5.12[B] |

Ref: Diameters approximated using Avogadro; A: Goel (2006), Sloan and Koh (2008); C: Javanmardi and Moeshfeghian (2003).

*Exchange rate: R8.14/US$

Common hydrate formers were investigated to determine how the former properties affect hydrate formation, as well as the effect salts have on hydrate formation. Propane hydrate dissociation

points occurred at a lower pressure or higher temperature than methane, ethane and carbon dioxide. Additionally, the effect of an inhibitor, NaCl (in Figure 2.8) and $CaCl_2$ (in Figure 2.6) on propane dissociation data was less than that of methane, ethane and carbon dioxide. As a result, propane was used to compare common formers with fluorinated hydrating agents, as seen in Figure 2.11.

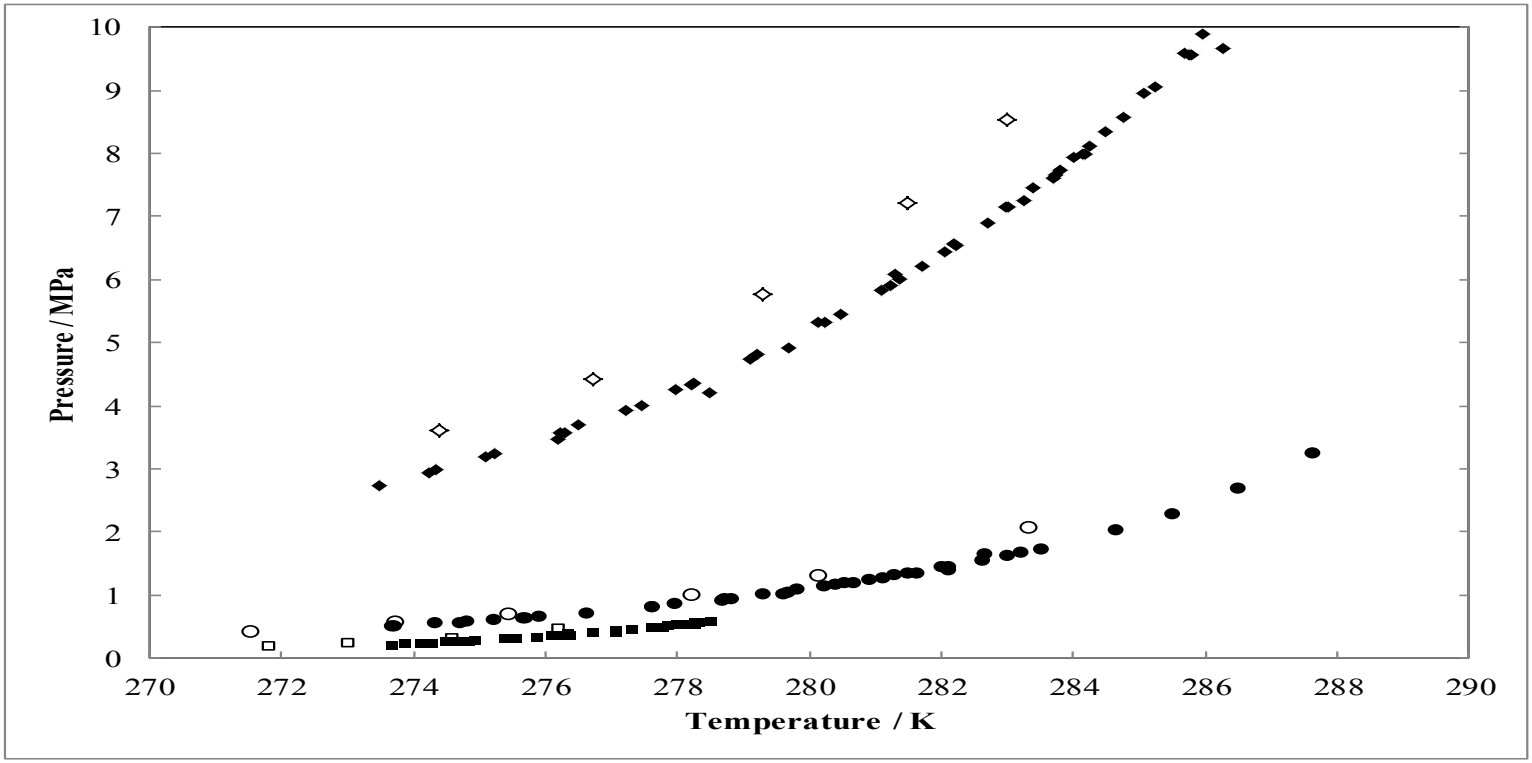


Figure 2.7: Comparison of hydrate dissociation points between hydrate formers and hydrate formers with 5 wt% $CaCl_2$. ◆, $CH_4$ (Jager et al., 2001), (Mohammadi et al., 2005), (Nakamura et al., 2003), (Yang et al., 2001), (Nixdorf et al., 1997); ◇, $CH_4$ and 5 wt% $CaCl_2$ (Mohammadi et al., 2008a); ●, $C_2H_6$ (Nixdorf et al., 1997), (Mohammadi et al., 2008a), (Englezos and Bishnoi, 1991), (Deaton and Frost, 1946), (Morita et al., 2000); ○, $C_2H_6$ and 5 wt% $CaCl_2$ (Mohammadi et al., 2008a); ■, $C_3H_6$ (Nixdorf et al., 1997), (Mohammadi et al., 2008a), (Englezos et al., 1993), (Deaton and Frost, 1946); □, $C_3H_6$ and 5 wt% $CaCl_2$ (Mohammadi et al., 2008a).

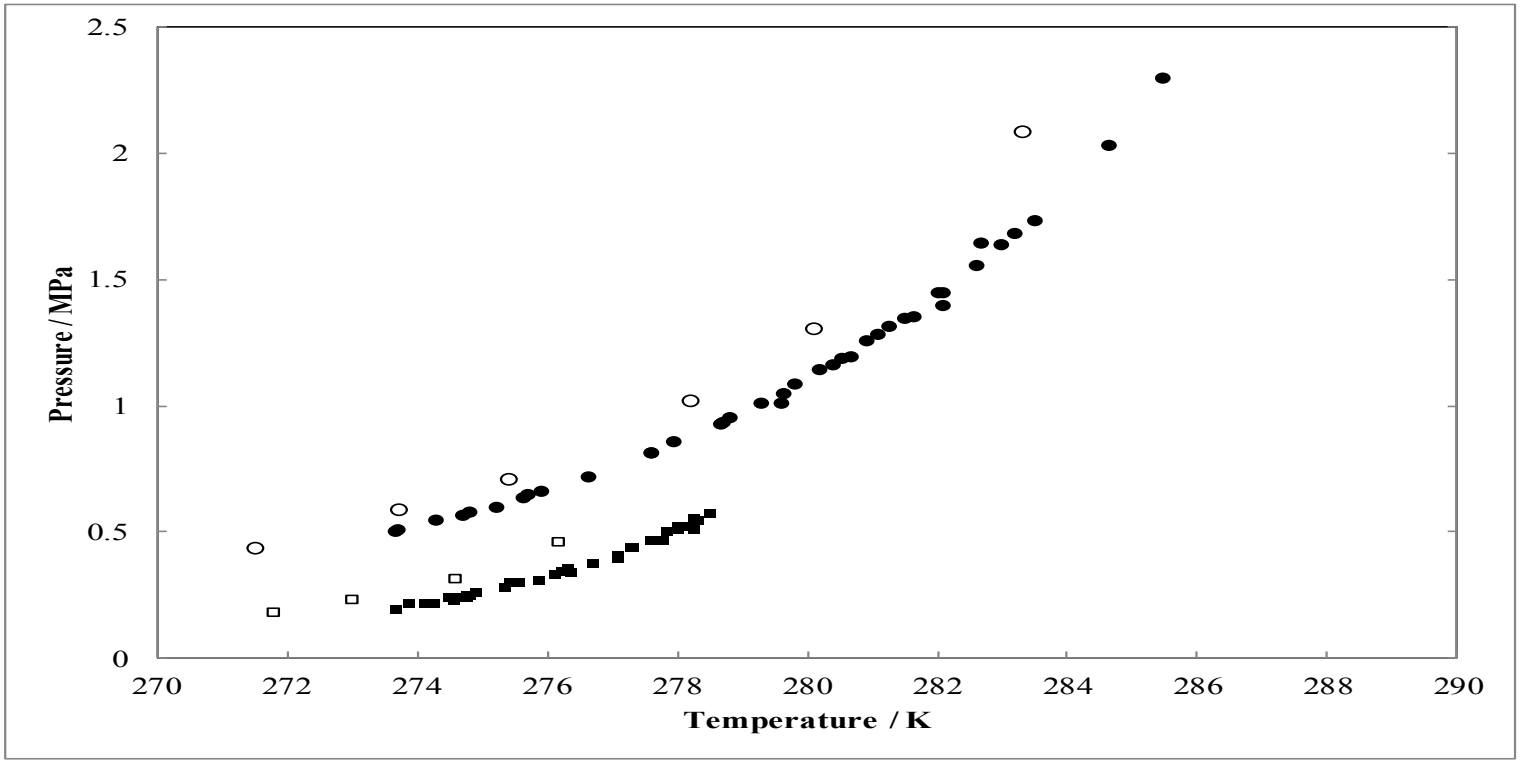


Figure 2.8: Axis magnified - Comparison of hydrate dissociation points between hydrate formers and hydrate formers with 5 wt% $CaCl_2$. ◆, $CH_4$ (Jager et al., 2001), (Mohammadi et al., 2005), (Nakamura et al., 2003), (Yang et al., 2001), (Nixdorf et al., 1997); ◇, $CH_4$ and 5 wt% $CaCl_2$ (Mohammadi et al., 2008a); ●, $C_2H_6$ (Nixdorf et al., 1997), (Mohammadi et al., 2008a), (Englezos and Bishnoi, 1991), (Deaton et al., 1946), (Morita et al., 2000); ○, $C_2H_6$ and 5 wt% $CaCl_2$ (Mohammadi et al., 2008a); ■, $C_3H_6$ (Nixdorf et al., 1997), (Mohammadi et al., 2008a), (Englezos and Ngan, 1993), (Deaton and Frost, 1946); □, $C_3H_6$ and 5 wt% $CaCl_2$ (Mohammadi et al., 2008a).

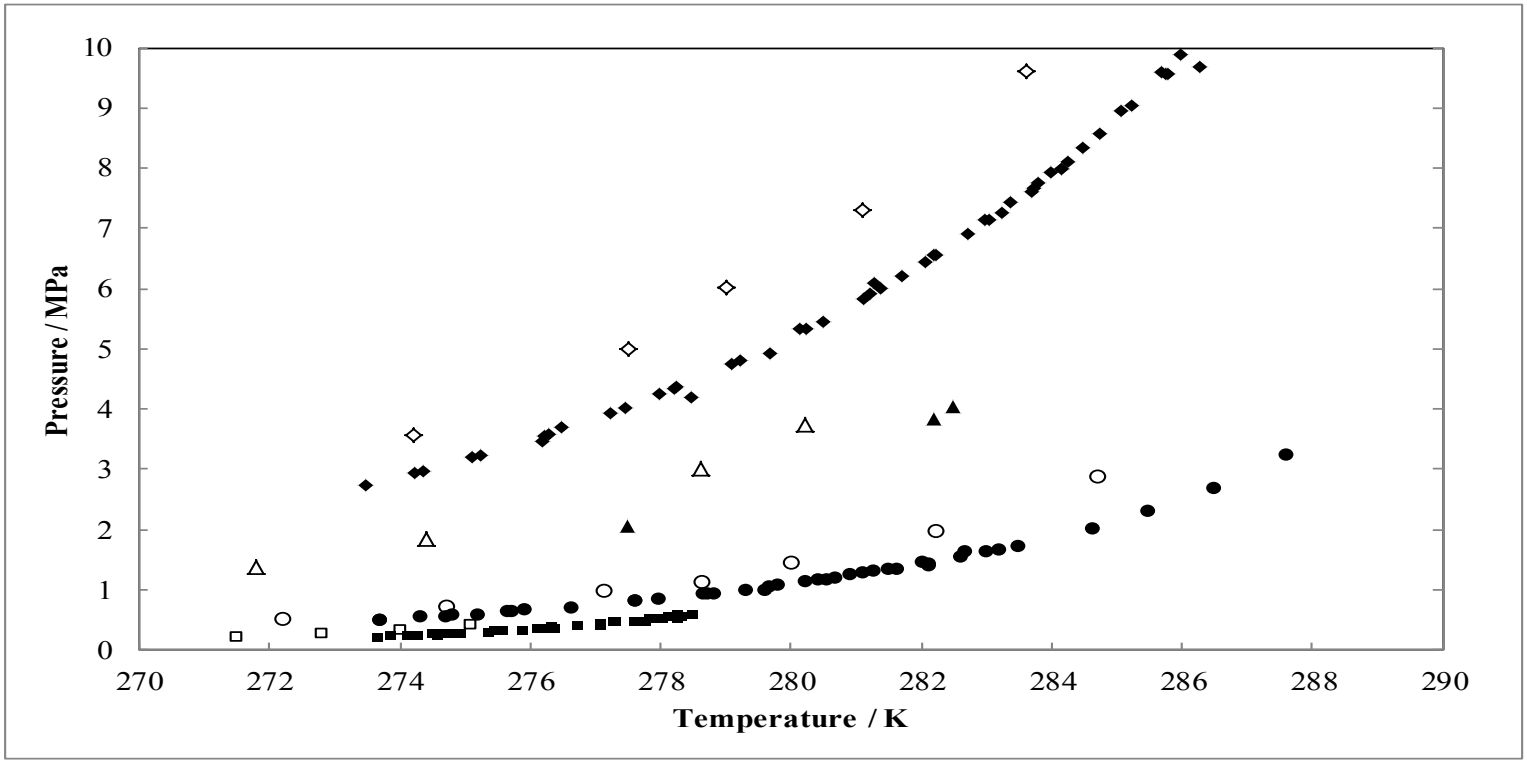


Figure 2.9: Comparison of hydrate dissociation points between hydrate formers and hydrate formers with 5 wt% NaCl. ◆, $CH_4$ (Jager et al., 2001), (Mohammadi et al., 2005), (Nixdorf et al., 1997), (Yang et al., 2001); ◇, $CH_4$ and 5 wt% NaCl (Mohammadi et al., 2008a); ●, $C_2H_6$ (Nixdorf et al., 1997), (Mohammadi et al., 2008a), (Englezos and Bishnoi, 1991), (Deaton and Frost, 1946), (Morita et al., 2000); ○, $C_2H_6$ and 5 wt% NaCl (Mohammadi et al., 2008a); □, $C_3H_6$ (Nixdorf et al., 1997), (Mohammadi et al., 2008a), (Englezos and Ngan, 1993), (Deaton and Frost, 1946),■, $C_3H_6$ and 5 wt% NaCl (Mohammadi et al., 2008a); ▲, $CO_2$ (Mohammadi et al., 2005), (Wendland et al., 1999); △, $CO_2$ and 5 wt% NaCl (Mohammadi et al., 2008a).

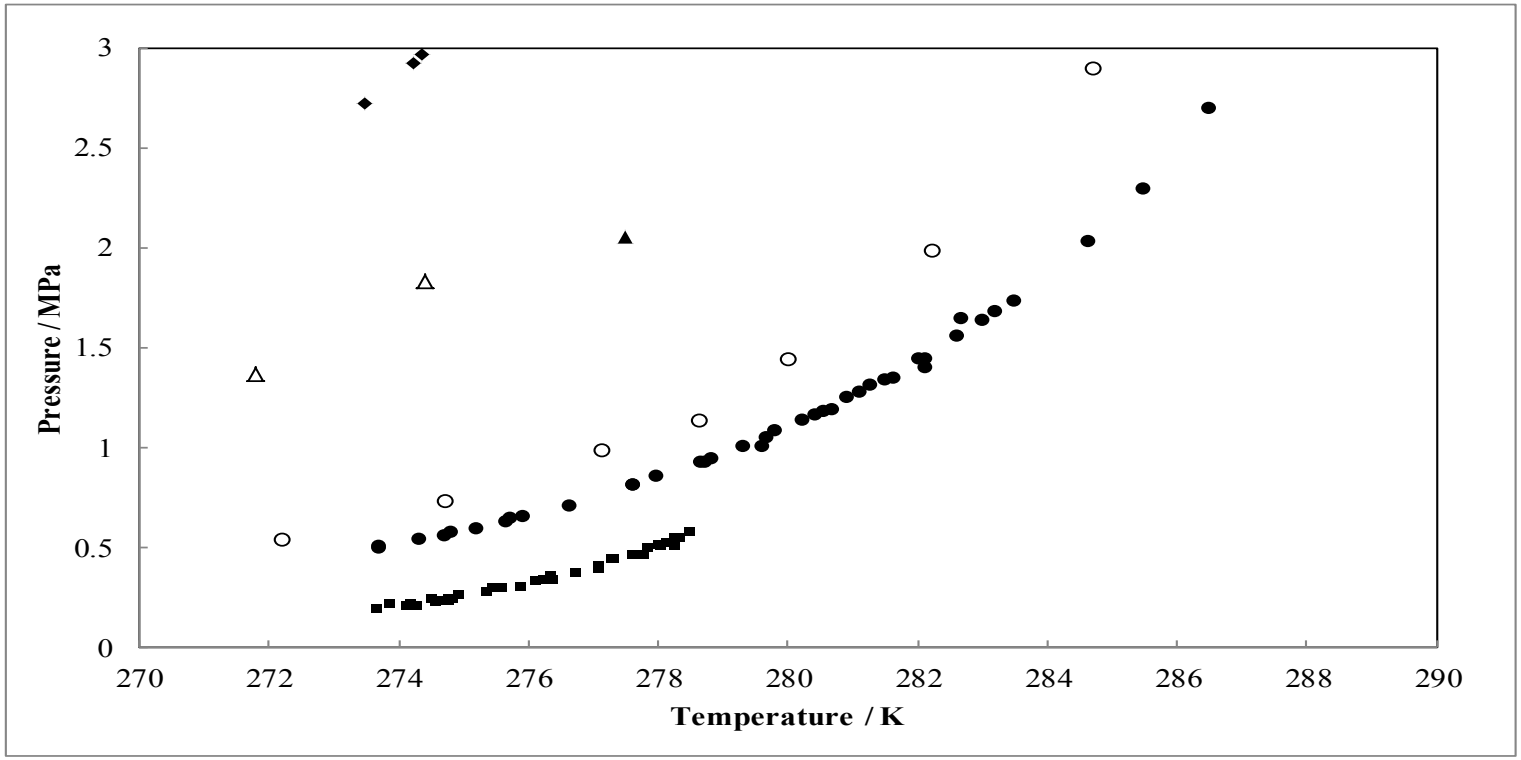


Figure 2.10: Axis magnified - Comparison of hydrate dissociation points between hydrate formers and hydrate formers with 5 wt% NaCl. ◆, $CH_4$ (Jager et al., 2001), (Mohammadi et al., 2005), (Nakamura et al., 2003), (Yang et al., 2001), (Nixdorf et al., 1997); ◇, $CH_4$ and 5 wt% NaCl (Mohammadi et al., 2008a); ●, $C_2H_6$ (Nixdorf et al., 1997), (Mohammadi et al., 2008a), (Englezos and Bishnoi, 1991), (Deaton and Frost, 1946), (Morita et al., 2000); ○, $C_2H_6$ and 5 wt% NaCl (Mohammadi et al., 2008a); □, $C_3H_6$ (Nixdorf and Oellrich, 1997), (Mohammadi et al., 2008a), (Englezos and Ngan, 1993), (Robinson et al., 1971), (Deaton and Frost, 1946); ■, $C_3H_6$ and 5 wt% NaCl (Mohammadi et al., 2008a); ▲, $CO_2$ (Mohammadi et al., 2005), (Wendland et al., 1999); △, $CO_2$ and 5 wt% NaCl (Mohammadi et al., 2008a).

Hydrates, which stabilise at pressures below 0.6 MPa and 288 K were investigated. This was to reduce the energy required for hydrate formation and dissociation. A preliminary investigation was undertaken on commercial fluorinated hydrating agents. The choice of commercial fluorinated hydrating agents was dependent on a number of factors. These included; tests which were conducted in literature as well as similarities in structure between common formers such as methane, ethane, propane and carbon dioxide with commercial fluorinated hydrating agents.

Several criteria were considered when determining suitable commercial fluorinated hydrating agents for the desalination of industrial wastewater. Firstly, a list of commercially available fluorinated compounds was obtained and compared to the Montreal Protocol. The Montreal Protocol considered ozone depletion due to the presence of chlorine as well as greenhouse effect (refer to Table 2.3). Only those refrigerants which were not banned nor will be banned by the Montreal Protocol were considered, as the ultimate purpose for this technology was industrial application. R14, R32, R116, R134a, R152a, R218, R404a, R407c, R410a and R507 underwent a preliminary investigation. R22 will be banned by the Montreal Protocol however, it was used as a test system. This was due to it being one of the few easily available commercial fluorinated hydrating agents which had been measured in literature in its pure form and in the presence of salts (McCormack and Andersen, 1995).

Table 2.3: List of commercially available fluorinated hydrating agents investigated by the Montreal Protocol.

| Name | Common Name | Formulae | Banned by Montreal Protocol |
|---|---|---|---|
| R11 | Trichlorofluoromethane | $CCl_3F$ | Yes |
| R12 | Dichlorodifluoromethane | $CCl_2F_2$ | Yes |
| R12Br | Bromochlorodifluoromethane | $CBrClF_2$ | Yes |
| R14 | Tetrafluoromethane | $CF_4$ | No |
| R21 | Dichlorofluoromethane | $CHCl_2F$ | Yes |
| R22 | Chlorodifluoromethane | $CHClF_2$ | Yes |
| R22Br | Bromodifluoromethane | $CHBrF_2$ | Yes |
| R31 | Chlorofluoromethane | $CH_2ClF$ | Yes |
| R32 | Difluoromethane | $CH_2F_2$ | Will be banned |
| R116 | Hexafluoroethane | $C_2F_6$ | No |
| R134a | 1,1,1,2-Tetrafluoroethane | $H_2FC\text{-}CF_3$ | No |
| R141b | 1,1-Dichloro-1-fluoroethane | $Cl_2FC\text{-}CH_3$ | Yes |
| R142b | 1-Chloro-1,1-difluoroethane | $ClF_2C\text{-}CH_3$ | Yes |
| R152a | Difluoroethane-1,1 | $F_2HC\text{-}CH_3$ | No |
| R218 | Octafluoropropane | $C_3F_8$ | No |
| R404A | Refrigerant blend | 52wt% R143a, 44wt% R125, 4wt% R134a | No |
| R406A | Refrigerant blend | 55wt% R22, 41wt% R142b, 4wt% R600a | Will be banned |
| R407C | Refrigerant blend | 23wt% R32, 25wt% R125, 52wt% R134a | No |
| R408A | Refrigerant blend | 47wt% R22, 46wt% R143a, 7wt% R125 | Will be banned |
| R409A | Refrigerant blend | 60wt% R22, 15wt% R142b, 25wt% R124 | Will be banned |
| R410A | Refrigerant blend | 50wt% R125, 50wt% R32 | No |
| R507 | Refrigerant blend | 50wt% R125, 50wt% R143a | No |

Commercially available fluorinated hydrating agents which were not banned by the Montreal Protocol were preliminary investigated using the specific criteria in Table 2.4. Table 2.5 displays a detailed analysis on each criteria for each potential commercial fluorinated hydrating agent.

Table 2.4: List of specific criteria used for a preliminary investigation to determine suitable fluorinated hydrating agents (McCormack and Andersen, 1995).

| **Characteristic** | **Criteria** |
|---|---|
| Environmental acceptability | The former was approved by the Montreal Protocol as it has low ozone depletion and greenhouse effect. |
| Non-toxicity | The former had a low acute toxicity as it was non-carcinogenic and non-mutagenic. |
| Non-flammability | The flash point temperature of the former was high, this was to reduce the risk of a fire starting. |
| Chemical Stability | The former reacted slowly with chemicals. |
| Compatibility with standard materials | The former had a low chemical activity. |
| Forms a class II hydrate | Easier separation between the hydrate and salt in the wash column was established. |
| Low cost | Operating costs were reduced. |
| Availability | The former was manufactured in commercial quantities from reliable sources. |
| Water solubility | A former with a low water solubility eliminated an extra step in the process to recover the former from the water. |
| Suitable operating temperature and pressure | A former with operating temperatures and pressures close to ambient conditions resulted in lower operating costs. |
| Quadruple point | Operation occurred near the upper quadruple point. This resulted in an operating temperature larger than 278.15 K and an operating pressure lower than 2 MPa. |
| Critical point | To obtain a large heat of vaporisation, the upper quadruple point should be far away from critical point. |

Table 2.5: Specific criteria to determine commercial fluorinated hydrating agents for further investigation.

| | **R14 (CF4)** | **R116 (C2F6)** | **R218 (C3F8)** | **R22 (CHClF2)** | **R141b (CH3CCl2F)** | **R134a (H2FC-CF3)** | **R152a (F2HC-CH3)** | **R32a ($CH_2F_2$)** |
|---|---|---|---|---|---|---|---|---|
| **upper quadruple point**[a] | Not available in examined literature | Not available in examined literature | Not available in examined literature | 289.5 K, 0.77 MPa (Sloan et al., 2008) | 281.5 K, 0.04 MPa (Liang et al., 2001) | 283 K, 0.41 MPa (Liang et al., 2001) | 288 K, 0.44 MPa (Liang et al., 2001) | 293 K, 1.45 MPa (Hashimoto et al., 2010) |
| **critical point** | 227.65 K, 3.74 MPa | 292.85 K, 2.98 MPa | 344.15 K, 2.68 MPa | 369.15 K, 4.94 MPa | 477.65 K, 4.25 MPa | 374.05 K, 4.06 MPa | 387.15 K, 4.76 MPa | 351.6 K, 5.83 MPa |
| **Ecological effect** | Not available in examined literature | Not available in examined literature | Not available in examined literature | Dangerous for the ozone layer | Dangerous for the ozone layer | contribute to the greenhouse effect | contribute to the greenhouse effect | contribute to green house effect |
| **Toxicity effect** | Asphyxiant at high concentrations | Not available in examined literature | Not available in examined literature | Not available in examined literature | Not available in examined literature | irregular heart beat and nervous symptoms | narcotic effects, irregular heart beat and nervous symptoms | produce irregular heart beat and nervous symptoms |
| **Flammability** | Non-flammable | Non-flammable | Non-flammable | Non-flammable | Yes | Non-flammable | Yes | Yes – flammable |
| **Chemical Stability** | Stable, decomposes to react with moisture | stable, decomposes to form harmful products | Stable, hazardous thermal decomposition products | Stable, decomposes to react with moisture | Stable | stable, do not mix with oxygen or air above atmospheric pressure | Stable. form explosive mixture with air, react violently with oxidants, Thermal decomposition yields toxic products: corrosive with moisture | Stable, incompatible with strong oxidizing agents, thermal decomposition, corrosive products in moisture |

Table 2.5: (contd.) Specific criteria to determine commercial fluorinated hydrating agents for further investigation.

| | **R14 (CF4)** | **R116 (C2F6)** | **R218 (C3F8)** | **R22 (CHClF2)** | **R141b (CH3CCl2F)** | **R134a (H2FC-CF3)** | **R152a (F2HC-CH3)** | **R32a ($CH_2F_2$)** |
|---|---|---|---|---|---|---|---|---|
| **Class** | I | Not available in examined literature | Not available in examined literature | I (Chun et al., 2000) | II (Liang et al., 2001) | II (Liang et al., 2001) | I or II (Liang et al., 2001) | I (Hashimoto et al., 2010) |
| **Cost** | Not available in examined literature | R1912/kg | R2500/kg | R32 /kg | Not available in examined literature | R79 /kg | R68/ kg | R2500/kg |
| **Compatibility** | Incompatible with zinc, alkaline earth metals, Group I metals, aluminum and its alloys | React violently with chemically active metals such as sodium, potassium, barium, magnesium , aluminum | Alkali and alkaline earth metals | Alkali metals, Alkaline earth metals, Powdered metals, Powdered metal salts | Hydrochloric acid, alkali or alkaline earth metals, finely powdered metals (aluminum, magnesium, zinc) and strong oxidizers | Freshly abraded aluminum surfaces can chemically react metals: potassium, calcium, powdered aluminum, magnesium, and zinc | Incompatible with alkali or alkaline earth metals- powdered Al, Zn, Be, sodium, calcium | Incompatib le with sodium or sodium oxides, potassium, calcium, alkali metals, |
| **Solubility in water** | 0.005 %V at 293.15 K | Not available in examined literature | Not available in examined literature | 0.78 vol/vol | 4 g/L at 293.15 K | 0.21 vol/vol | 0.54% at 273.15 K | 4.4g/L |
| **Availability** | Not available in examined literature | Not available in examined literature | Difficult to obtain | Not available in examined literature | Not available in examined literature | Not available in examined literature | Not available in examined literature | Not available in examined literature |

Table 2.5: (contd.) Specific criteria to determine commercial fluorinated hydrating agents for further investigation.

| | | | | | | | | |
|---|---|---|---|---|---|---|---|---|
| **Particle diameter [b] (Å)** | 5.2 (Den Heuvel et al., 2002) | 5.414 | 6.598 | 4.57 | Not available in examined literature | 5.411 | Not available in examined literature | Not available in examined literature |
| | **R404A** (52wt% R143a, 44wt% R125, 4wt% R134a) | **R406A** (55wt% R22, 41wt% R142b, 4wt% R600a) | **R407C** (23wt% R32, 25wt% R125, 52wt% R134a) | **R408A** (47wt% R22, 46wt% R143a, 7wt% R125) | **R409A** (60wt% R22, 15wt% R142b, 25wt% R124) | **R410A** (50wt% R125, 50wt% R32) | **R507** (50wt% R125, 50wt% R143a) | |
| **Critical point** | Not available in examined literature | 387.15 K, 45.8 bar | Not available in examined literature | Not available in examined literature | 382.55 K, 46.41 bar | 345.95 K, 48.6 bar[b] | 343.95 K, 37.2 bar | |
| | Not available in examined literature | Not available in examined literature | Not available in examined literature | Irregular heartbeat and nervous symptoms | Irregular heartbeat and nervous symptoms | Irregular heartbeat and nervous symptoms | Irregular heartbeat and nervous symptoms | |
| **Flammability** | Non-flammable | Non-flammable | Non-flammable | Non-flammable | Non-flammable | Non-flammable | Non-flammable | |
| **Chemical Stability** | Stable, avoid open flames and high temperatures, decomposition products may be corrosive with moisture | Stable, decomposition gases dangerous upon contact with hot metallic surfaces | Stable corrosive decomposition products | Stable, release toxic decomposition gases | Stable, | Stable, decomposition gases may be corrosive in the presence of moisture | Stable, release toxic decomposition gases | |

Table 2.5: (contd.) Specific criteria to determine commercial fluorinated hydrating agents for further investigation.

| | **R404A** (52wt% R143a, 44wt% R125, 4wt% R134a) | **R406A** (55wt% R22, 41wt% R142b, 4wt% R600a) | **R407C** (23wt% R32, 25wt% R125, 52wt% R134a) | **R408A** (47wt% R22, 46wt% R143a, 7wt% R125) | **R409A** (60wt% R22, 15wt% R142b, 25wt% R124) | **R410A** (50wt% R125, 50wt% R32) | **R507** (50wt% R125, 50wt% R143a) |
|---|---|---|---|---|---|---|---|
| **Cost*** | R136 /kg | Not available in examined literature | R84 /kg | Not available in examined literature | Not available in examined literature | R130 /kg | R132 /kg |
| **Compatibility** | Incompatible with active metals, alkali or alkaline earth metals, powdered Al, Zn and Be | Incompatible with metallic powders, alkaline earth metals, alkaline metals and alloys, strong bases | Incompatible with potassium, calcium, powdered aluminum, magnesium and zinc | Incompatible with alkali metals, magnesium and alloys, alkali metals, alkali earth metals, sodium, potassium and barium | Incompatible with aluminum surfaces, potassium, calcium, powdered aluminum, magnesium and zinc | Incompatible with aluminum, zinc, beryllium, alkali or alkaline earth metals | Incompatible with alkaline metals and alloy, alkali earth metals, |
| **Availability** | Industrially Available | Industrially Available | Industrially Available | Industrially Available | Industrially Available | Industrially Available | Industrially Available |

*Exchange rate: R8.14/US$

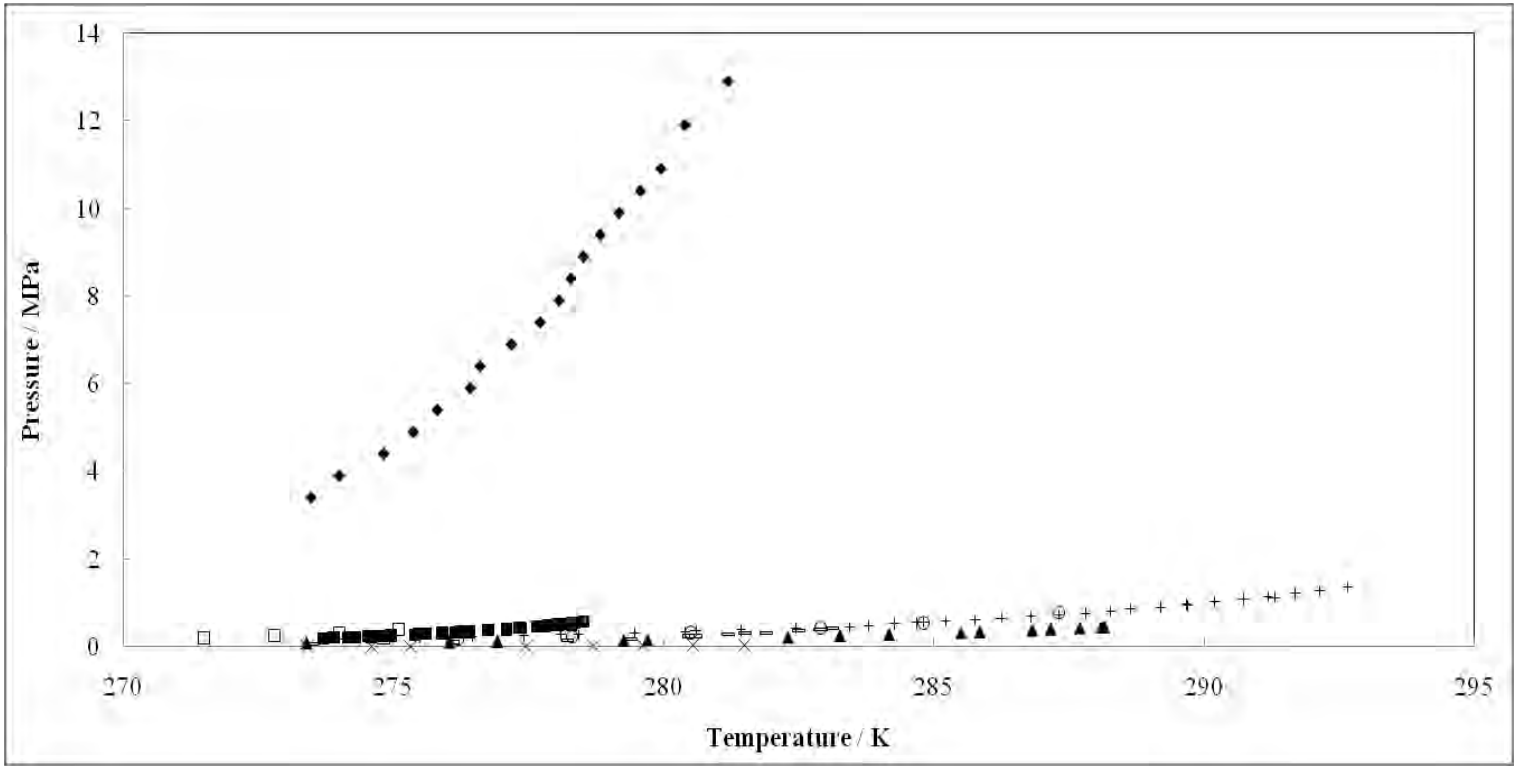


Figure 2.11: Comparison of hydrate dissociation points between commercial fluorinated hydrating agents. -, R134a (Heuvel, 2004), (Mohammadi and Richon, 2010); x, R141b (Heuvel, 2004), (Liang et al., 2001); ▲, R152a (Heuvel, 2004), (Liang et al., 2001), (Mohammadi and Richon, 2010); ○, R22 and 5wt% NaCl (Chun et al., 2000); ◆, $CF_4$ (Heuvel, 2004); ■, $C_3H_8$ (Nixdorf et al., 1997), (Mohammadi et al., 2008a), (Englezos et al., 1993), (Deaton et al., 1946); □, $C_3H_8$ and 5wt% NaCl (Mohammadi et al., 2008a); +, R32 (Hashimoto et al., 2010), (Liang et al., 2001), (Mohammadi and Richon, 2010).

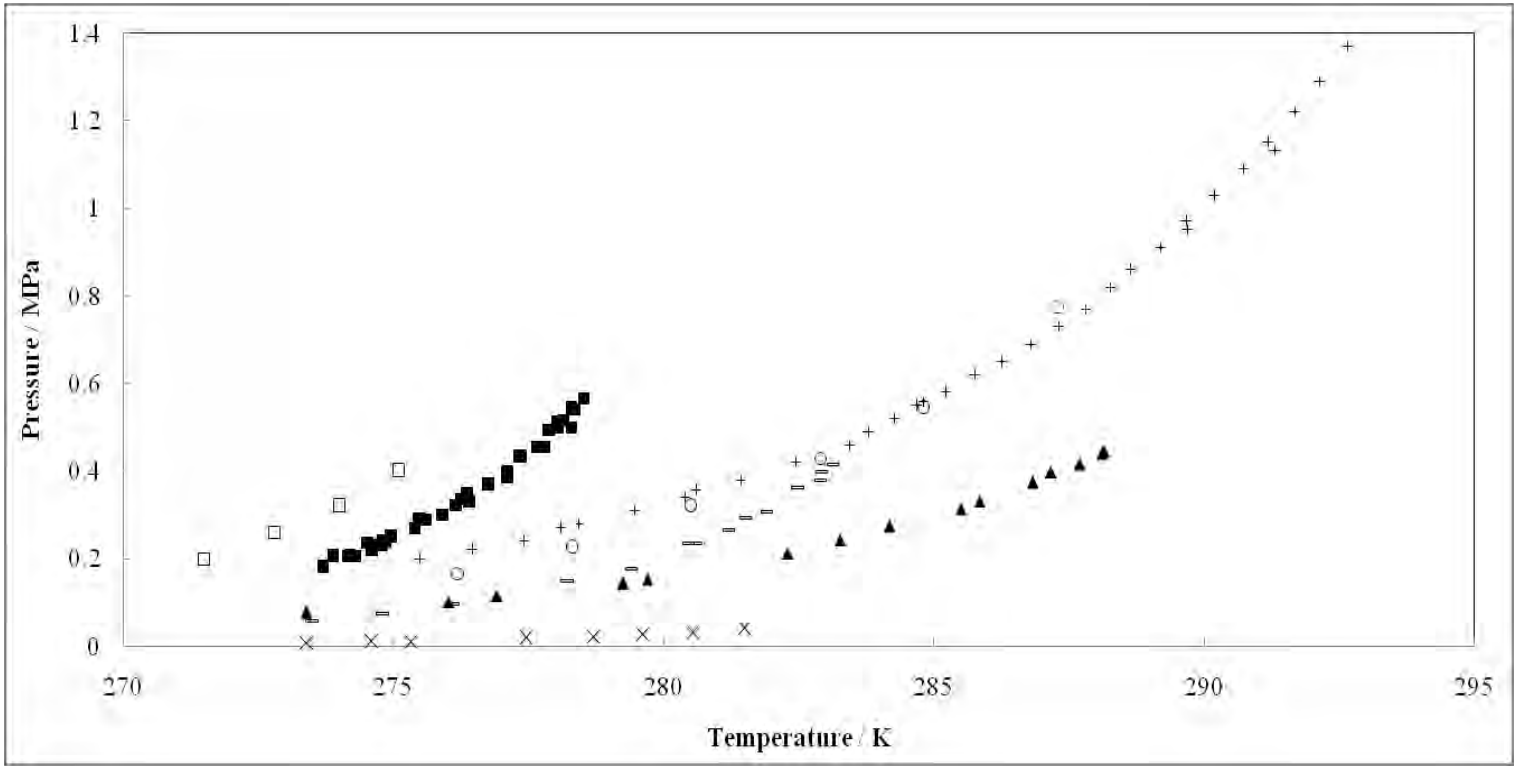


Figure 2.12: Comparison of hydrate dissociation points between commercial fluorinated hydrating agents. -, R134a (Heuvel, 2004), (Mohammadi and Richon, 2010); x, R141b (Heuvel, 2004), (Liang et al., 2001); ▲, R152a (Heuvel, 2004), (Liang et al., 2001), (Mohammadi and Richon, 2010); ○, R22 and 5wt% NaCl (Chun et al., 2000); ■, $C_3H_8$ (Nixdorf et al., 1997), (Mohammadi et al., 2008a), (Englezos and Ngan, 1993), (Deaton and Frost, 1946); □, $C_3H_8$ and 5wt% NaCl (Mohammadi et al., 2008a); +, R32 (Hashimoto et al., 2010), (Liang et al., 2001), (Mohammadi and Richon, 2010).

From Table 2.5, all flammable commercial fluorinated hydrating agents were eliminated due to the high fire risk involved when applied on an industrial scale. These included R141b, R152a and R32a. R14 was eliminated as a possible former as it formed a Type I hydrate structure. A Type I structure was proven to be too difficult to wash during hydrate-salt separation. R116 and R218 were expensive and difficult to obtain in South Africa and therefore would not be economical for industrial application. From the refrigerant blends, R410a and R507 were easily available however, no hydrate phase boundary measurements had been conducted for the system refrigerant blend (1) + water (2). Further investigation was required before the refrigerant blends were considered as possible commercial fluorinated hydrating agents.

From the possible commercial fluorinated hydrating agents, R134a fitted the specific criteria the best. Hydrates formed in the presence of R134a at relatively lower pressures or higher temperatures than that of the other examined refrigerants. R134a was chosen as the most suitable fluorinated hydrating agent which was further investigated while further testing was recommended for R410a and R507.

### 2.4.2 Hydrate promoters

Industrial application of hydrate technology was hindered due to the slow formation of hydrates and the energy costs involved with hydrate formation at low temperature and/or high pressure. Promoters were responsible for the rapid formation of hydrates under the same operating conditions as using only a hydrate former. The addition of a promoter reduced the pressure or increased the temperature at which the hydrate is formed. Promoters reduced mass transfer and kinetic challenges during hydrate formation (Mandal and Laik, 2008).

Promoters were usually hydrophobic and were classified according to their shape, size and chemical nature. The size of the molecules and type of structure occupied affected the position of the gas within the structure of the hydrate. This altered the formation pressure and temperature. Promoters were classified as either water soluble or water insoluble. Promoters like propylene oxide, 1,4-dioxane and THF were water soluble. Benzene, tetrahydropyran, cyclohexane, cyclopentane and neopentane were water insoluble (Tohidi et al., 1997). An additional liquid phase was present in the system, provided the solubility limit of the water insoluble promoter was not reached. As a result, it was easier to separate the water from the promoter.

According to the Gibbs phase rule in thermodynamics, the amount of promoter added will not affect the dissociation point. As a result, it was sufficient to add 5 to 10 vol% of the promoter to a system. In general, hydrates cannot form with only the presence of promoters (Carroll, 2003; Sloan and Koh, 2008). Figure 2.12 indicated how different promoters had different effects on a specific hydrate former.

When a promoter was added to a system, the temperature or pressure shifted. The temperature shift between a system without a promoter and that with a promoter was calculated as follows; cyclopentane, neopentane and cyclohexane were 19.4 K, 13.6 K and 8.1 K respectively.

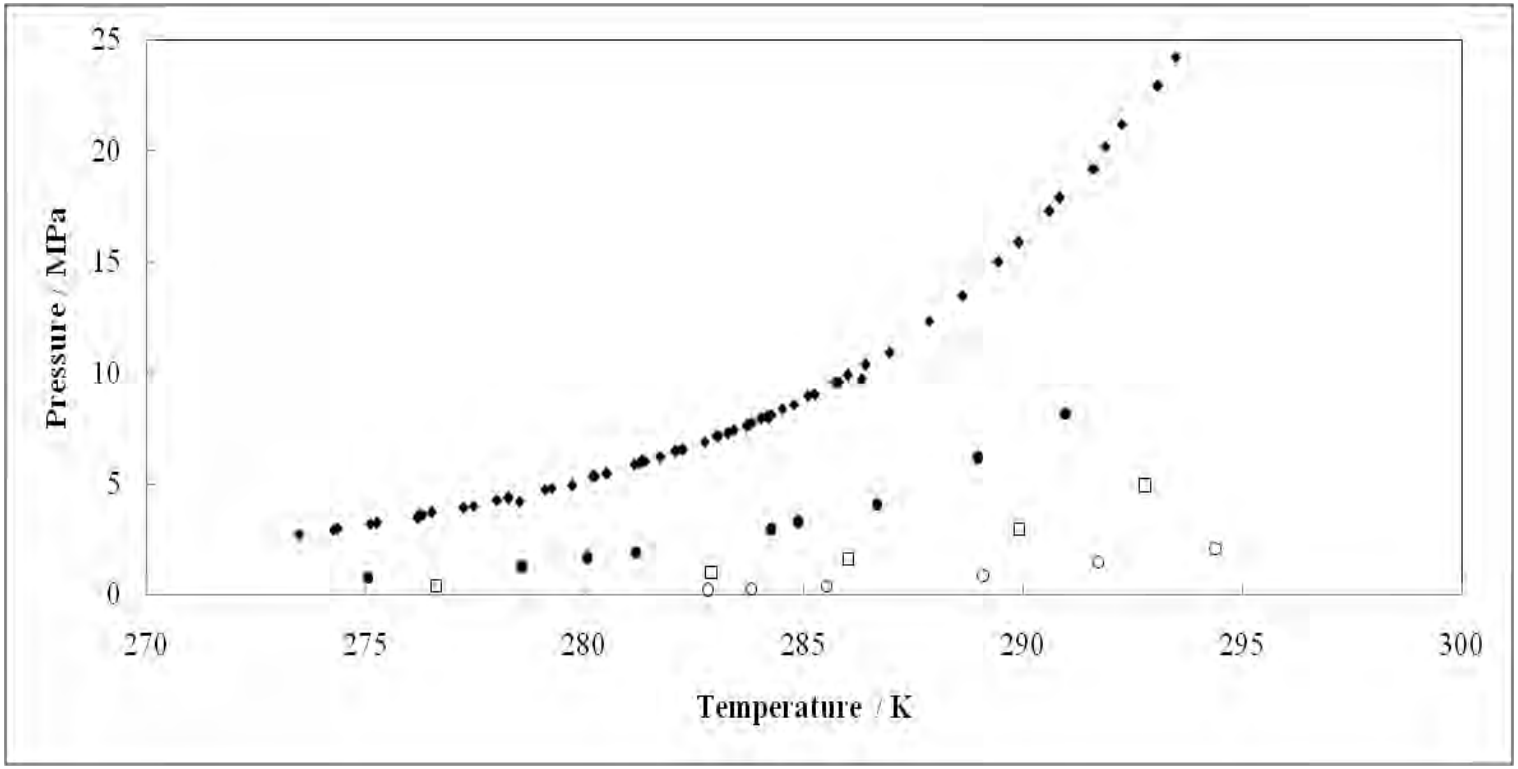


Figure 2.13: Comparison of hydrate dissociation points of methane with various hydrate promoters. ◆, $CH_4$ (Jager and Sloan, 2001), (Mohammadi et al., 2005), (Nakamura et al., 2003), (Yang et al., 2001), (Nixdorf and Oellrich, 1997); ●, cyclohexane, (Tohidi et al., 1996) ; □, neopentane, (Tohidi et al., 1997); ○, cyclopentane, (Tohidi et al., 1997).

In Figure 2.13, it is clear that cyclopentane had the largest effect on the hydrate dissociation point. If cyclopentane was added to a system containing R134a, the hydrate dissociation point may have shifted to ambient conditions. This shift would have decreased the hydrate free region.

### 2.4.3 Hydrate inhibitors

In the petroleum industry, hydrates often cause blockages in pipelines, valves and safety devices. This may have prevented the formation of products and possibly resulted in an explosion. Hydrates were usually controlled using chemicals, such as inhibitors. Inhibitors were added to a mixture to reduce the activity of the water. A decrease in the water activity resulted in an increased pressure or reduced temperature at which hydrates dissociate. As a result the hydrate formation region was reduced. Although this inhibitory effect was advantageous for hydrate formation prevention, its presence proved to be more energy intensive during desalination.

Two classes of inhibitors exist. They included thermodynamic inhibitors such as glycols, alcohols and salts (refer to Sloan and Koh (2008)) and were required in large quantities. Another class of inhibitor was low dosage inhibitors (LDHI‟s). Within the class of LDHI‟s, two inhibitor categories exist. These included kinetic hydrate inhibitors and anti-agglomerants. Kinetic inhibitors were water-soluble polymers, which delayed hydrate formation by preventing nucleation and growth. Anti-agglomerants prevented the formation of large hydrate clusters (Kelland, 2006). All inhibitors increased the time required for hydrate formation (Carroll, 2003).

Salts ionize in solution and interact with the water molecule dipole forces. This columbic bond was much stronger than the hydrogen bond between the water molecules or the van der Waals forces between the crystal structure and the guest molecule. Since the water was attracted to the ions more than that of the hydrate structure, hydrate formation was inhibited. This resulted in a larger pressure or lower temperature at which the hydrates formed. Additionally, the strong forces between the salt and water molecule resulted in a “salting-out” effect where the solubility of the guest molecule was reduced (Sloan and Koh, 2008). An increase in the salt concentration resulted in a larger temperature or pressure shift (refer to Table A.16 for a list of inhibitors).

As the inhibitor concentration increased so the temperature shift became larger. For the system R22 (1) + water (2) + {0, 5, 10 or 15} wt% NaCl (3) reported by (Chun et al., 2000), at higher pressures, the temperature shift for a specific system was slightly larger. The average shift in temperature

between the system containing no salt and the systems containing {5, 10 and 15} wt% NaCl were -2.3 K, -4.6 K and -7.8 K respectively. As the concentration increased, the temperature shift became slightly larger.

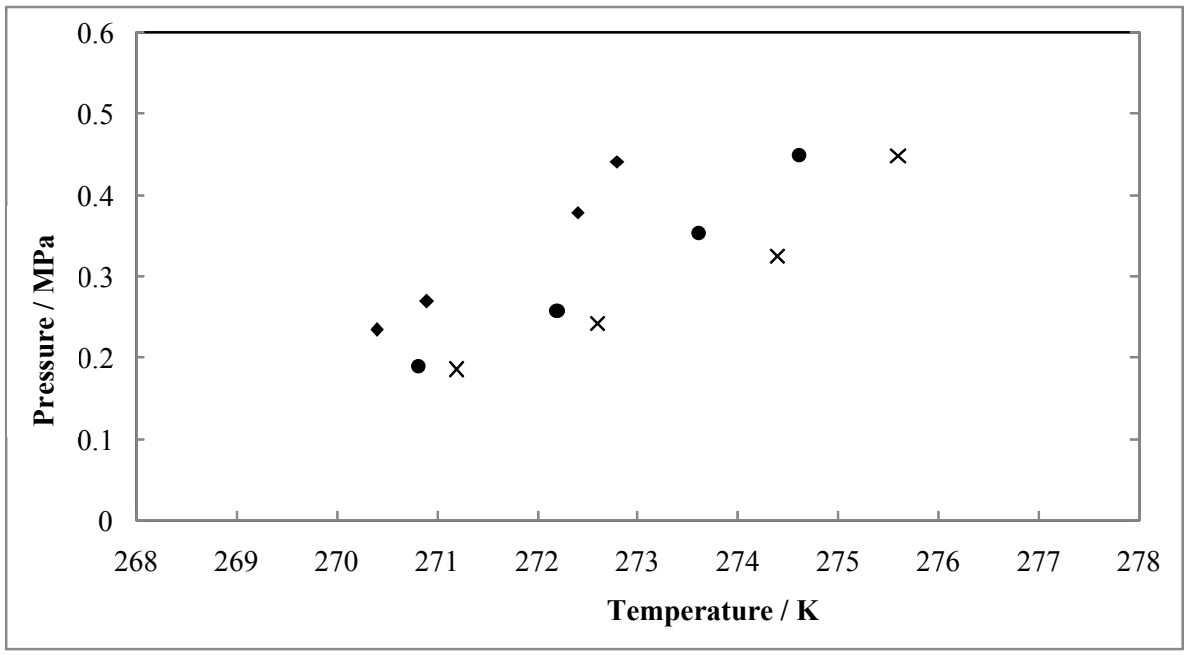


Figure 2.14: Comparison of hydrate dissociation points of propane with various salts. x, 5 wt% NaCl, (Patil, 1987); ●, 10 wt% NaCl, (Patil, 1987); ◆, 5 wt% NaCl and 5 wt% KCl, (Tohidi et al., 1997).

Strong interactions between water and salt depressed the water freezing point and inhibited liquid from vaporising. As a result, the upper and lower quadruple points for systems containing salt were at lower temperatures than that of systems containing no salt. The higher the salt concentration, the lower the temperature for the upper and lower quadruple points (refer to Table 2.6 for freezing point depression data of NaCl in water).

Table 2.6: Freezing point and vapour pressure depression data for NaCl in water.

| Wt% NaCl | Freezing point Δ T / K | Vapour pressure ΔP / MPa |
|---|---|---|
| 5 | 3.05 | 0.02 |
| 10 | 6.56 | Not available in examined literature |
| 15 | 10.92 (by linear interpolation) | Not available in examined literature |

Ref: (Lide, 2005)

In Figure 2.14, it is clear that the dissociation point occured at a higher pressure or lower temperature in the system containing 5 wt% NaCl and 5 wt% KCl when compared to the system containing {5 or 10} wt % NaCl. As a result, mixed salts had more of an inhibitory effect on hydrate dissociation than single salt solutions.

## 2.5 Phase diagrams

According to the Gibbs‟ phase rule (Heuvel, 2004):

$$F = 2 + N - \pi \quad (2.3)$$

F: Degree of freedom
N: Number of components
$\pi$: Number of phases

The degrees of freedom specify the number of fixed independent intensive variables. These variables include temperature, pressure, concentration, volume or density and phase amounts. Volume, density, phase amounts and certain compositions are difficult to measure. As a result, phase equilibria are determined from temperature, pressure and composition. More specifically, hydrate phase equilibria are determined from temperature, pressure, water free former phase composition and water free phase composition which excludes formers but includes inhibitors. The remaining properties may be calculated (Sloan and Koh, 2008). For a more detailed discussion on phase diagrams, refer to Harmens and Sloan (1990), Huo et al. (2003), Katz et al. (1959), Sloan et al. (1986) and Wierzchowski and Monson (2005).

The number of dimensions required to represent the complete phase behaviour of a system is given by:

$$F_{max} = N + 1 \quad (2.4)$$

### 2.5.1 Unary system

Water is an essential component of hydrate formation. The phases that may occur in a unary system of pure water are ice, I, liquid, $L_w$, and vapour, V. Each phase region is bounded by I-$L_w$, $L_w$-V and

I-V equilibrium lines. The equilibrium curves intersect at the triple point, I-$L_w$-V. The $L_w$-V equilibrium curve ends at the critical point. Thereafter the phases become indistinguishable (Heuvel, 2004) . Refer to Table 2.7 for the application of the Gibbs‟ phase rule to a unary system.

Table 2.7: Application of Gibbs‟ phase rule for a unary system (Heuvel, 2004).

| N | π | F | Representation in Figure 2.14 | Representation in Figure 2.14 |
|---|---|---|---|---|
| 1 | 1 | 2 | $L_w$ | Region |
| 1 | 2 | 1 | I-$L_w$ | Curve |
| 1 | 3 | 0 | I-$L_w$-V | Point |

For a unary system, $F_{max}$ is 2 and thus temperature and pressure, temperature and composition or pressure and composition are sufficient to represent the phase behaviour of the system.

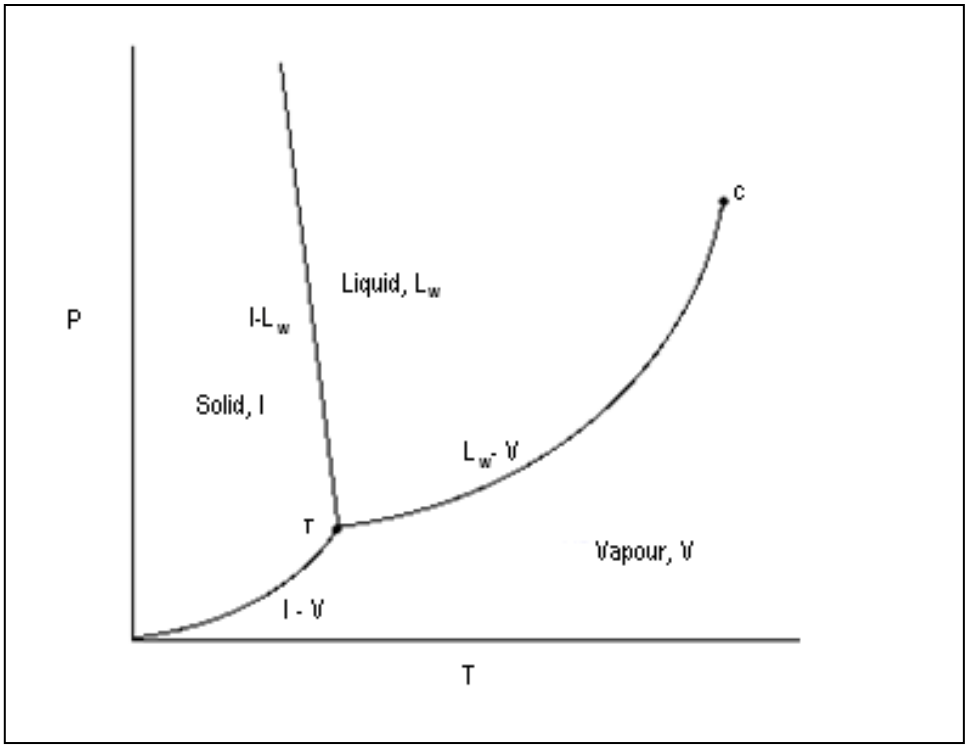


Figure 2.15: Pressure Temperature phase equilibrium diagram for pure $H_2O$ (Heuvel, 2004).

2.5.2 Binary system

The binary system of hydrates consists of water and one guest molecule. A binary system may be represented as a function of the independent intensive variables, temperature, pressure and composition. For a binary system, $F_{max}$ is 3 and thus Figure 2.14 may be projected onto a third axis which shows the dependence of composition on equilibrium conditions. However, it is more advantageous to represent a planar cross-section of the equilibrium conditions at a fixed value of one of the variables. Figure 2.16 and 2.17 show the effect of composition-pressure or composition-temperature on the equilibrium conditions and are able to convey a detailed system of the phase behaviour. Binary phase diagrams for structure I and II hydrates are similar (Sloan and Koh, 2008).

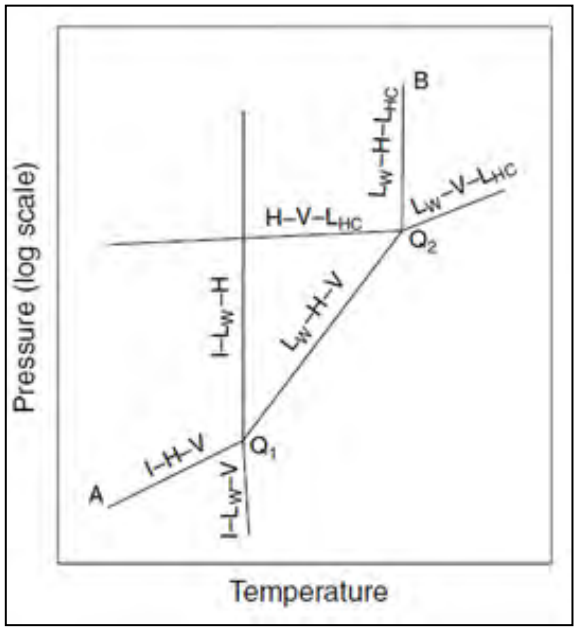


Figure 2.16: Pressure-temperature phase diagram for a binary system at a specific composition (Sloan and Koh, 2008).

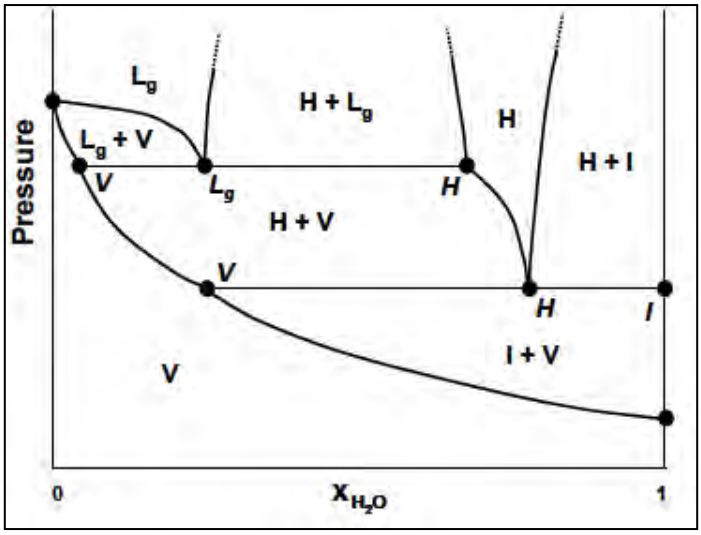


Figure 2.17: Pressure-composition phase diagram for a binary system at a specific temperature (Heuvel, 2004).

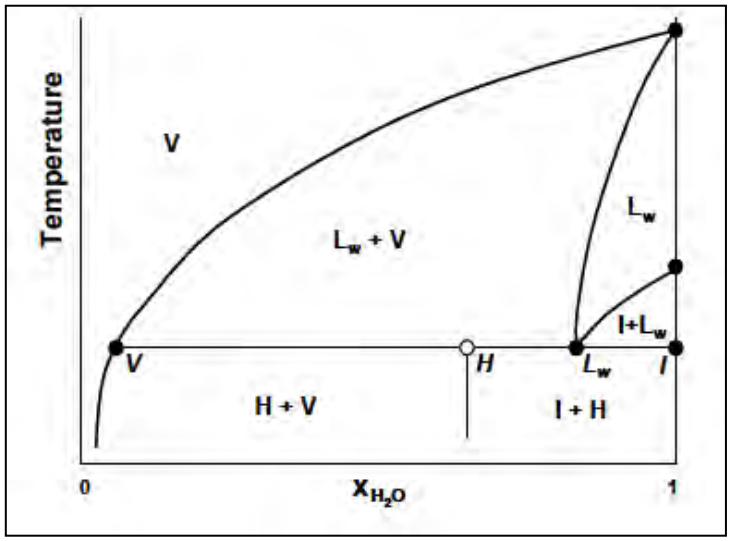


Figure 2.18: Temperature-composition phase diagram for a binary system at a specific pressure (Heuvel, 2004).

The phases which may occur in a binary system are ice, I, liquid water, $L_w$, hydrate, H, vapour, V and liquid guest molecule, $L_g$. Each phase region is bounded by I-H-V, vapour pressure of the guest molecule in the presence of ice, I-$L_w$-V, freezing point of water depression, I-$L_w$-H, H-V-$L_g$, $L_w$-H-V, vapour pressure of hydrate forming substance and water, $L_w$-H-$L_g$, hydrate melting point variation, and $L_w$-V-$L_g$, saturation vapour pressure of hydrate forming substance equilibrium lines. The intersection of the equilibrium lines, I-$L_w$-H, $L_w$-H-V, I-H-V and I-$L_w$-V form the lower

quadruple point, $Q_1$, I-$L_w$-H-V. This point is at approximately 273.15 K for all hydrate formers. However, the lower quadruple point pressure varies considerably between hydrate formers due to the types of bonds present between particles. The intersection of $L_w$-H-V, $L_w$-V-$L_g$, $L_w$-H-$L_g$ and H-V-$L_g$ form the upper quadruple point, $Q_2$, $L_w$-H-V-$L_g$ (Sloan and Koh, 2008). Differences in enthalpy and volume of the vapour and liquid hydrocarbon result in the three phase hydrate formation line change from $L_w$-H-V to $L_w$-H-$L_g$ (Ballard and Sloan, 2001). Refer to Table 2.8 for the application of the Gibbs‟ phase rule to a binary system.

Table 2.8: Application of Gibbs‟ phase rule on a binary system.

| **N** | **π** | **F** | **Represnetation in 2.15** | **Representation in Figure 2.15** |
|---|---|---|---|---|
| **2** | 3 | 1 | I-H-V, I-$L_w$-V, I-$L_w$-H, H-V-$L_g$, $L_w$-H-V, $L_w$-H-$L_g$, $L_w$-V-$L_g$ | Curve |
| **2** | 4 | 0 | I-$L_w$-H-V, $L_w$-H-V-$L_g$ | Point |

Ref: (Heuvel, 2004).

The curve I-$L_w$-H represents the Clapeyron equation while H-V-$L_g$ has a slightly lower pressure than the vapour pressure of the pure guest molecule (Heuvel, 2004). The region below the I-H-V and $L_w$-H-V curves is called the hydrate instability region; hydrates cannot form in this region. To ensure the hydrate instability region is not reached it is important to experimentally obtain points on the $L_w$-H-V equilibrium curve and to model the results to obtain a continuous $L_w$-H-V equilibrium curve. To obtain this curve, the degrees of freedom is 1 (refer to Table 2.8). Thus an independent intensive property must be specified. According to the isochoric method, this property is temperature (Sloan and Koh, 2008).

The binary pressure-temperature phase diagram will be used to represent R22 and water as well as R22, water and salts.

### 2.5.3 Ternary system

For a ternary system, $F_{max}$ is 4. This is difficult to represent and therefore one or two free variables remain constant. Ternary systems are usually represented on a triangular diagram where pressure and temperature remain constant or prisms where pressure or temperature remains constant.

Ternary phase equilibrium systems are dependent on three factors. These include the hydrate formation of the binary system including water, the phase behaviour of the binary systems with water and the guest component, as well as the size of the regions in which the liquid phases will be immiscible. Ternary systems, which include water, guest molecules and an additive, where both components are present in a hydrate lattice and no structural transitions occur may be classified according to the following (Heuvel, 2004):

Type A: One of the guest molecules cannot form hydrates by itself. This includes adding a promoter to a former.

Type B: Both guest molecules can each form hydrates in a binary system with water, where the phase behaviour in the binary systems are the same. Both show gas-like or both show liquid-like behaviour.

Type C: Both guest molecules can each form hydrates in a binary system with water, where the phase behaviour in the binary systems is different. One shows gas-like while the other shows liquid-like behaviour.

*Type A system*

Figure 2.18 and Figure 2.19 portray Type A ternary systems. The mixed structure is classified as Type II. For the binary system, including the guest component and water, Type I structures form. For the system R22 (1) + water (2), Type II hydrates form (Heuvel, 2004).

The assumptions for Type A system are as follows (Heuvel, 2004):

1. Water-guest molecules have immiscible $L_w$ and $L_g$ phases.
2. Water – additive do not form structure H hydrates and $L_w$ and $L_a$ are immiscible.
3. $L_a$ and $L_g$ are immiscible.

In Figure 2.19 there are a number of quintuple points ($Q_t$), including I-$H_{sII}$-$L_w$-$L_a$-V, I-$H_{sI}$-$H_{sII}$-$L_w$-V and $H_{sI}$-$H_{sII}$-$L_w$-$L_a$-V. The hydrate stability region is bounded by I-$H_{sII}$-$L_a$-V, $H_{sII}$-$L_w$-$L_a$-V and $H_{sI}$-$L_w$-$L_a$-V equilibrium curves. In Figure 2.18, the hydrate stability region is bounded by $H_{sII}$-$L_w$-$L_a$-V and $H_{sII}$-$L_w$-$L_a$-$L_g$ (Heuvel, 2004).

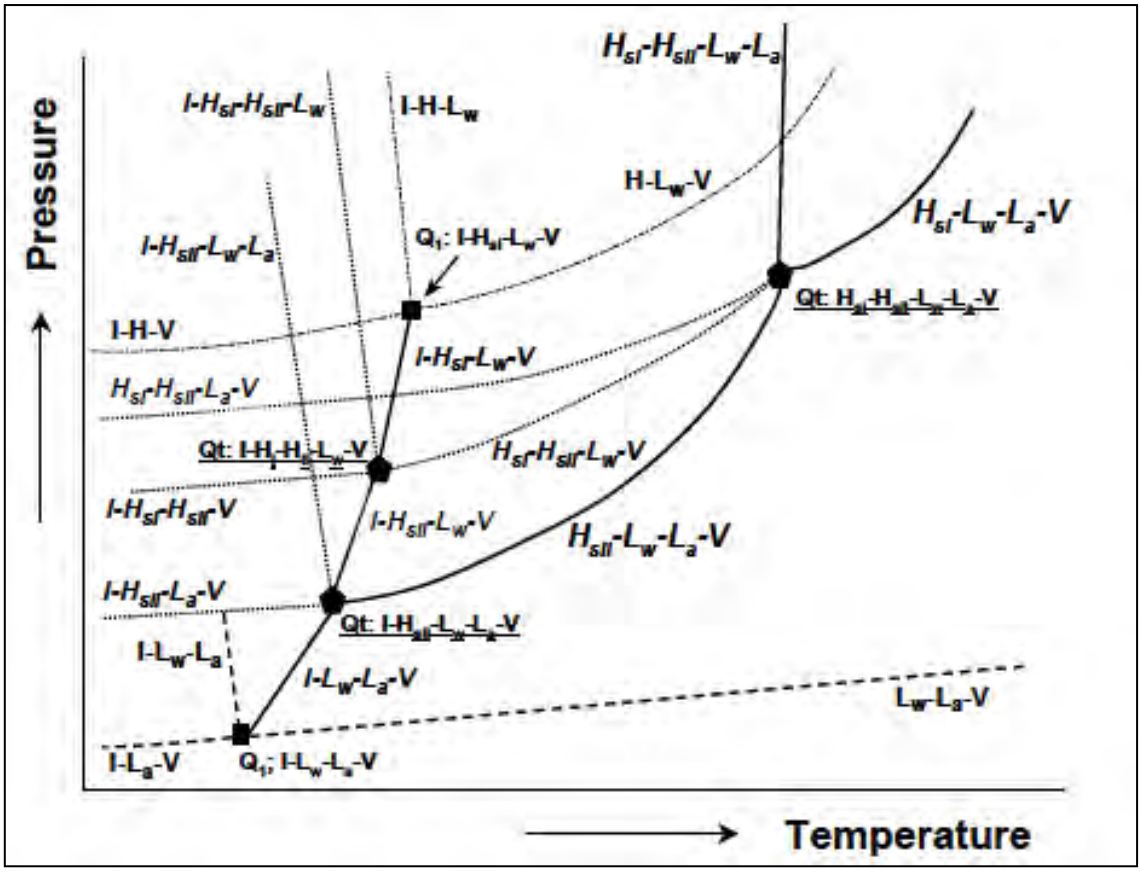


Figure 2.19: Phase diagram for the type A ternary hydrate system where the system shows gas-like behaviour (Heuvel, 2004).

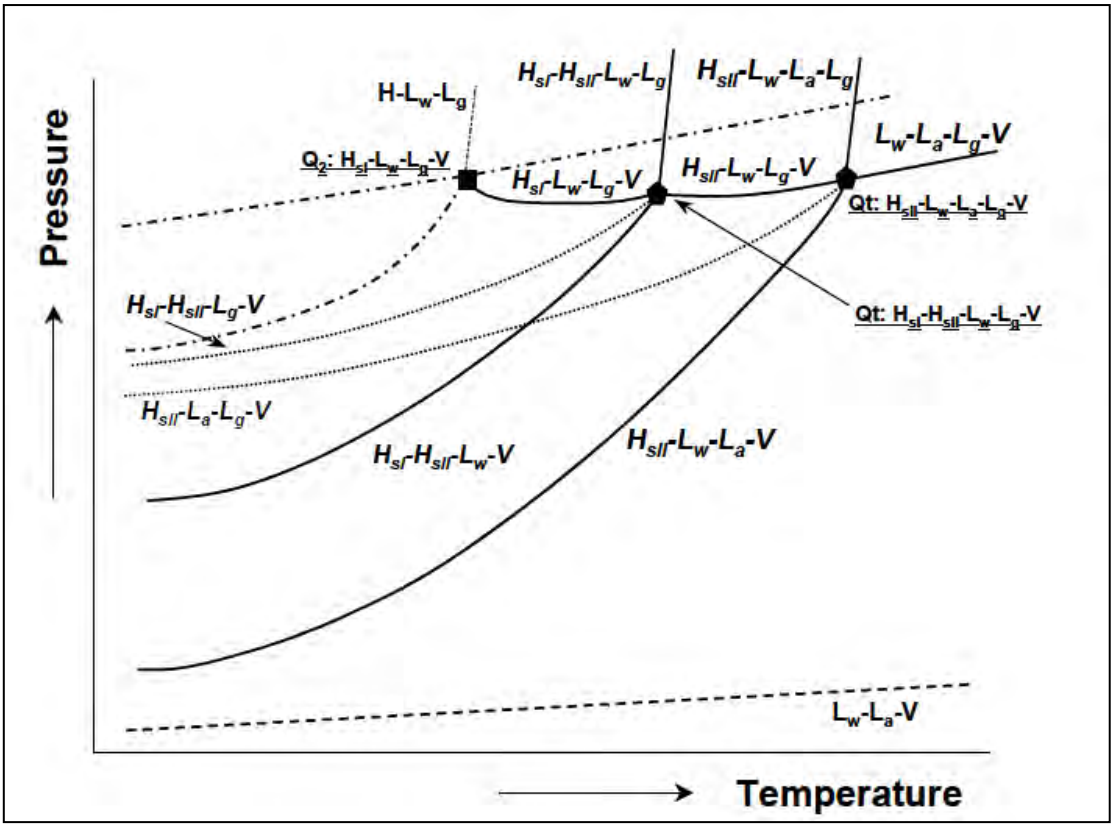


Figure 2.20: Phase diagram for the type A ternary hydrate system where the system shows liquid-like behaviour (Heuvel, 2004).

If the assumption that $L_a$ and $L_g$ are immiscible does not apply, the number of quintuple points decreases (Heuvel, 2004).

*Type B system*

The assumptions for Type B system in Figure 2.20 and Figure 2.21are as follows (Heuvel, 2004):

1. Water-guest molecules form structure I hydrates and have immiscible $L_w$ and $L_g$ phases.
2. Water – additive form structure II hydrates and $L_w$ and $L_a$ are immiscible.
3. $L_a$ and $L_g$ are immiscible in the guest-additive phase.
4. $L_w$, $L_a$ and $L_g$ are immiscible in the water-guest-additive phase.

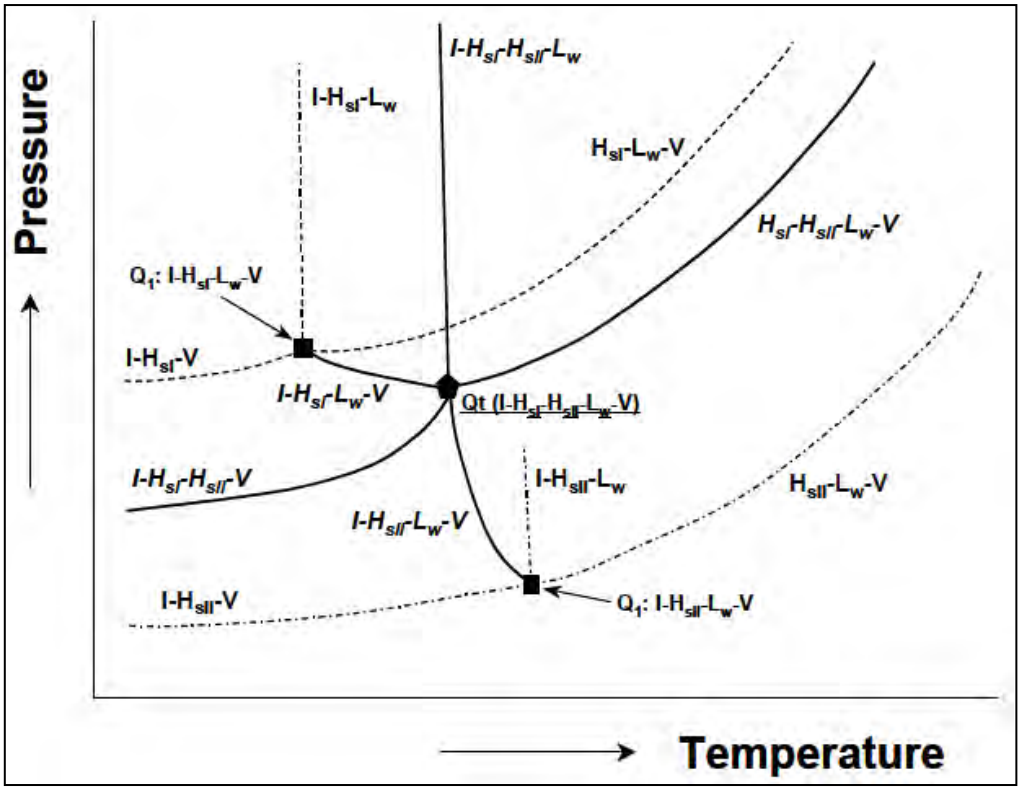


Figure 2.21: Phase diagram for the type B ternary hydrate system where the system shows gas-like behaviour (Heuvel, 2004).

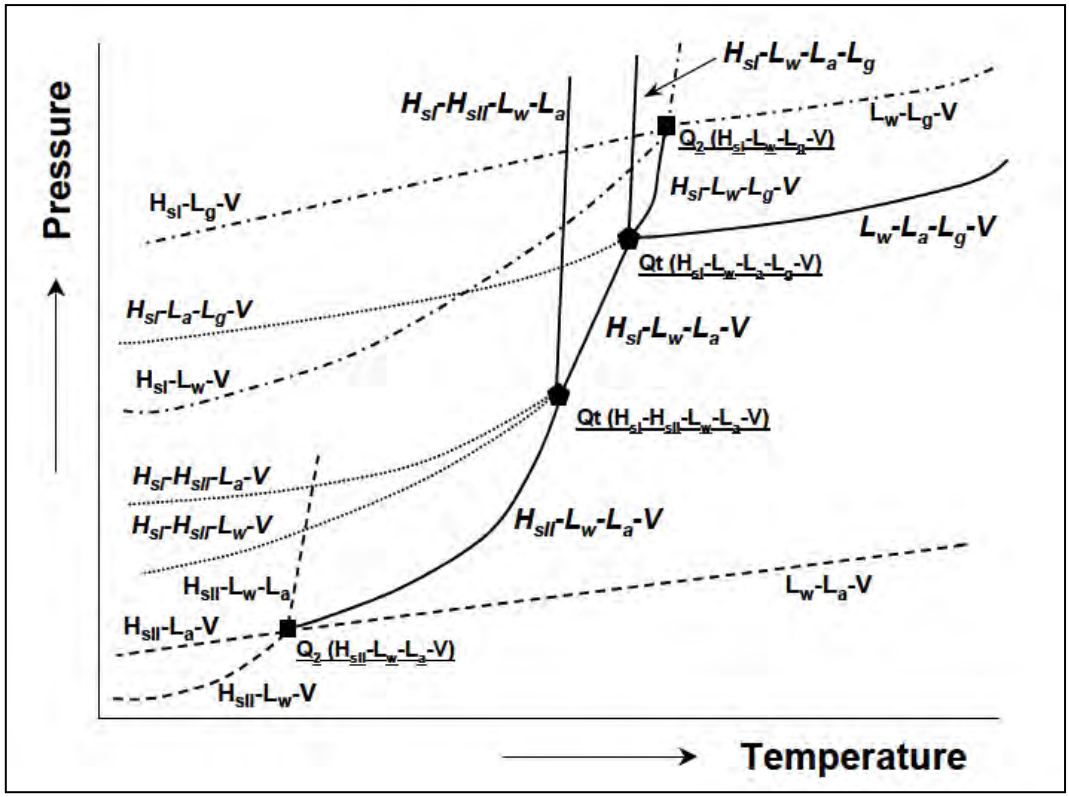


Figure 2.22: Phase diagram for the type B ternary hydrate system where the system shows liquid-like behaviour (Heuvel, 2004).

*Type C system*

The assumptions for Type C system in Figure 2.22 include (Heuvel, 2004):

1. Water-guest molecules form structure I hydrates and have immiscible $L_w$ and $L_g$ phases.
2. Water – additive form structure II hydrates and $L_w$ and $L_a$ are immiscible.
3. $L_a$ and $L_g$ are immiscible in the guest-additive phase
4. $L_w$ and $L_a$ are immiscible in the water-guest-additive phase

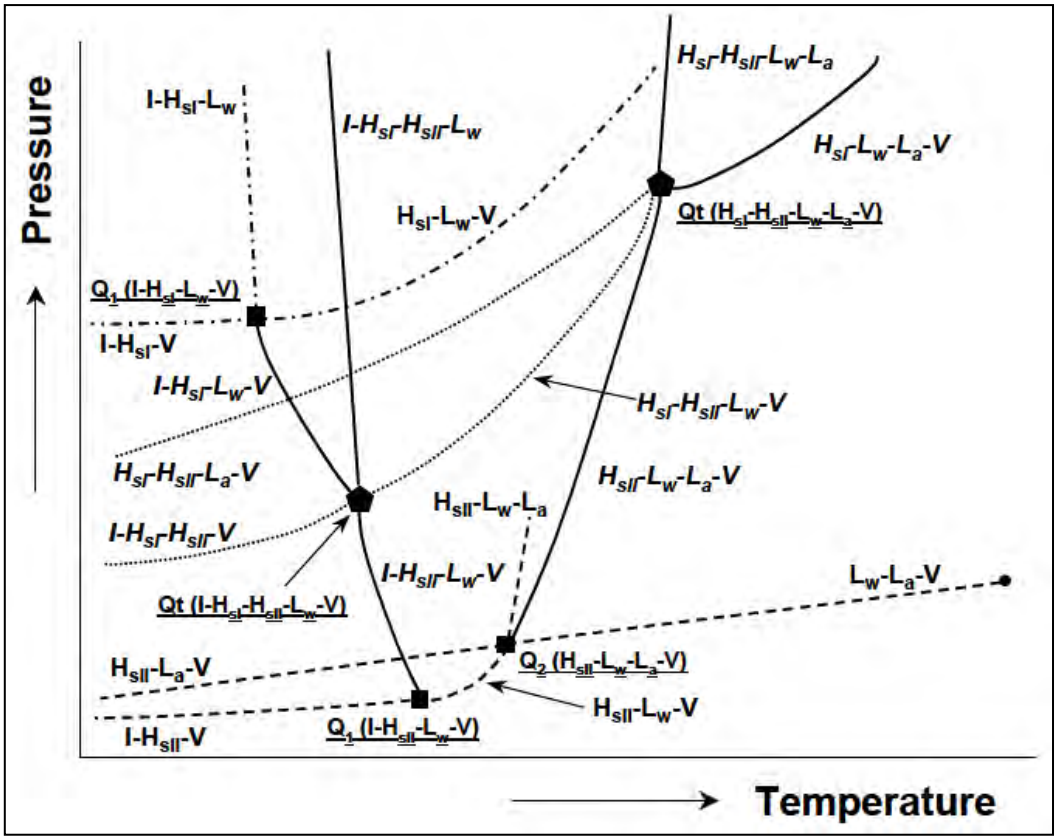


Figure 2.23: Phase diagram for the type C ternary hydrate system where the system shows gas like behaviour for structure I binary system and liquid like behaviour for structure II binary system (Heuvel, 2004).

### 2.5.4 Binary systems with inhibitors

In Figure 2.23 the curve $A_1$-$Q_1$-$Q_2$-B represents the hydrate bounding line when no inhibitors are present. This is equivalent to $A_1$-$Q_1$-$Q_2$-B in Figure 2.16. As the concentration of an inhibitor such as salt, glycol or alcohol, is increased, the point at which ice forms, $Q_1$, is shifted to a higher pressure. This is due to an increase in the energy required to freeze water in the presence of salt. This is advantageous as the formation of ice is avoided in industry. $Q_1$-$Q_2$-B shifts towards the left which decreases the region in which hydrates can form. The extent to which the line is shifted is dependent on the type of inhibitor, as well as the concentration of the inhibitor. The presence of the inhibitor decreases the temperature and increases pressure at which hydrates are able to form due to increased competition for the water molecules (Sloan and Koh, 2008).

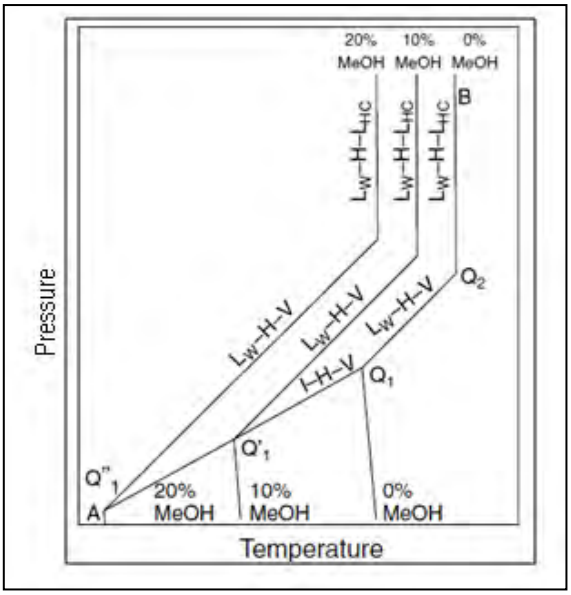


Figure 2.24: Shift in the phase equilibrium boundary due to the presence of various concentrations of the inhibitor, methanol (Sloan and Koh, 2008).

This project focuses on the hydrate phase equilibria between the upper and lower quadruple points, as the presence of pure ice and liquid refrigerant is not desired in the process. The presence of these two phases will require a more energy intensive process with more operating units to recover the pure water, which would increase costs.

### 2.5.5 Enthalpy of dissociation

The heat required to dissociate a hydrate is dependent on the size of the cavity occupied by the guest molecule. The Clapeyron equation may be used to calculate the heat of vaporisation of a pure component using vapour pressure data for univariant systems. The Clausius-Clapeyron equation is able to predict the amount of heat required to dissociate a simple hydrate. The type of guest molecule used has a significant effect on this quantity and therefore must be considered when choosing a possible promoter. The Clausius-Clapeyron equation is given by (Sloan and Koh, 2008):

$$\frac{d\ell nP}{d(1/T)} = -\frac{\Delta H}{zR} \qquad 2.5$$

Semilogarithmic plots of dissociation pressure versus reciprocal temperature results in a straight line. This indicates that the heats of dissociation, compressibility factor, and ratio of water to guest molecules are constant.

Table 2.9: The enthalpy of dissociation for systems containing common hydrate formers measured calorimetrically.

| **System** | **ΔH KJ/mol** | **Reference** |
|---|---|---|
| $CH_4$ ( 1) + water (2) | 53.81 | |
| $C_2H_6$ ( 1) + water (2) | 71.34 | |
| $C_3H_8$ ( 1) + water (2) | 129.2 | |
| $CO_2$ ( 1) + water (2) | 57.66 | (Yoon et al., 2003) |

# CHAPTER THREE

## THERMODYNAMIC MODELLING OF H-V-L EQUILIBRIUM DATA

Phase equilibrium thermodynamic data for systems containing mixtures are important for the design and operation of separation processes. It is not possible to measure all phase equilibrium data for all systems. As a result, thermodynamic methods are applied to available phase equilibrium experimental data in order to predict system properties.

Thermodynamic fundamentals and principles are outlined in this chapter. This includes a general description of thermodynamic chemical phase equilibrium as well as fugacity and activity coefficients for vapour and liquid phases. Furthermore, the $\gamma - \phi$ (combined method) and $\phi - \phi$ (direct method) are described for the regression of vapour-liquid equilibrium data.

The chapter then extends vapour-liquid equilibrium modelling to hydrate-vapour-liquid (H-V-L) equilibrium modelling. Two methods are used to determine H-V-L equilibrium data. These include; prediction techniques based on hand calculations as well as computer-based methods formulated from statistical thermodynamic techniques. Various hydrate phase models and equations of state (EOS) are considered for statistical thermodynamic techniques.

### 3.1 Thermodynamic phase equilibrium

For chemical phase equilibrium to exist in a system, it is necessary for specific criteria to be met. Criteria for chemical phase equilibrium include the following:

1. Equal temperatures and pressures between phases.
2. Equal chemical potential $(\mu)$ between a specific component in each phase.
3. Minimum global Gibbs‟ free energy.

For a system in chemical phase equilibrium, the chemical potential can be expressed as:

$$\mu_i^{\alpha} = \mu_i^{\beta} = \mu_i^{\gamma} \qquad 3.1$$

Fugacity is defined in terms of measurable variables such as pressure, temperature, volume and phase composition. As a result, it is preferred to express the chemical phase equilibrium of a system in terms of fugacity. The fugacity in solution can be in a mixture of real gases or in a solution of real liquids. For species i, where the temperature for each phase is the same, the fugacity in solution is expressed as;

$$\overset{\wedge}{f}_i^{\alpha} = \overset{\wedge}{f}_i^{\beta} = \overset{\wedge}{f}_i^{\gamma} \qquad 3.2$$

3.2 Vapour-liquid equilibrium modelling

The design and operation of separation processes require fluid phase equilibrium data. For systems where this data is not available or difficult to estimate, predictive models are used. These models include EOS with mixing rules and liquid phase activity coefficient models. Phase equilibrium data are regressed with these models to obtain model parameters. These model parameters are unique to the system analysed.

3.2.1 Vapour Phase modelling

The fugacity in solution of the vapour phase specifically for the species water, can be expressed as:

$$\hat{f}_w^V = \hat{\varphi}_w^V y_w P \qquad 3.3$$

An EOS may be used to determine the fugacity coefficient in solution, $\hat{\phi}^V$ .

**Equation of state (EOS)**

The EOS accounts for the following phase behaviour:

1. Liquid-liquid equilibrium.
2. Vapour-liquid equilibrium.
3. Vapour-vapour equilibrium.

It is difficult to select the most appropriate EOS and mixing rule to describe the vapour phase as several hundred EOS and mixing rules are available. Each EOS has its own shortcomings. In literature, three categories of EOS exist, these include:

1. Empirical EOS.
2. Theoretical EOS.
3. Semi-empirical EOS.

Empirical equations or correlations are obtained by fitting experimental data to a function with numerous parameters. This type of EOS requires numerous experimental data and cannot be extended to mixtures. Theoretical equations are applicable to a wider range of systems as they are determined from thermodynamic principles. Semi-empirical methods are a combination of empirical and theoretical models. This method is generally more suitable than the previously mentioned methods.

The van der Waals family of cubic EOS are semi-empirical and are derived for pure fluids. They have been extended to mixtures by replacing the parameters with composition-dependent empirical mixing rules. The following EOS are commonly used in hydrate modelling:

- Soave-Redlich-Kwong (1948): used in Sloan et al. (1987) and Kang et al. (1998) with the modified Huron-Vidal second order mixing rule.
- Peng Robinson (1976): used in Ng and Robinson (1980), Javanmardi et al. (2004) and Sloan et al. (1987).
- Peng-Robinson-Stryjek-Vera: Klauda et al. (2000).
- Patel and Teja, (1982): used in Chen and Guo (1996).
- Trebble-Bishnoi (1988): used in Englezos (1992) with quadratic mixing rules.
- Valderrama (1990): used by Eslamimanesh et al, (2011) and Najibi et al. (2009) with non density dependent mixing rules.

Engelzos and Ngan (1993) stated that any EOS could be used to model the vapour phase. More specifically, it was suggested that the Peng-Robinson, the Soave-Redlich-Kwong, or the Trebble and Bishnoi could be used to describe the vapour phase. The Soave-Redlich-Kwong EOS can be applied to non-polar or slightly polar fluids. The Peng-Robinson EOS was chosen as it requires little input information and obtains good phase equilibrium predictions for hydrocarbon systems.

Disadvantages of the Peng–Robinson EOS include low accuracy for liquid density prediction, inaccurate parameter prediction for non-hydrocarbons (particularly polar fluids) and inaccurate vapour predictions for pressures below 101.325 kPa (Naidoo, 2004).

The Peng-Robinson-Stryjek-Vera EOS improved the vapour pressure predictions of non-polar and polar compounds at the expense of adding more parameters to the Peng-Robinson EOS. The Patel and Teja EOS is developed for non polar systems only. The Valderrama EOS is a modified version of the Patel and Teja EOS. It is able to accurately predict equilibrium data for polar and non-polar compounds. Many papers have been published recently which use the Valderrama EOS with non-density dependent mixing rules.

In Tohidi et al. (1995), the Valderrama EOS including non-density dependent mixing rules was compared to the Peng–Robinson EOS with van der Waals classical mixing rules. It was shown in Tohidi et al. (1995) that both models can be used to determine the fugacity of the liquid or vapour phase for a mixture of non-electrolyte components where gas solubility is low. The Peng-Robinson EOS with van der Waals classical mixing rules is chosen as it compared well to the Valderrama EOS with non-density dependent mixing rules. In Javanmarid et al. (2004) the Peng-Robinson EOS is used for the system R22 (1) + water (2). Although this model is simple, it could not be used for the system R134a (1) + water (2). This is due to no vapour pressure information available in literature. The Peng-Robinson EOS with van der Waals classical mixing rules is given by:

$$\ln \hat{\phi}_i^{\,EOS} = \frac{b_i}{b_m}(z-1) - \ln\left(z - \frac{b_m P}{RT}\right) - \frac{a_m}{2\sqrt{2}b_m RT}\left(\frac{2\sum_k z_k a_{ki}}{a_m} - \frac{b_i}{b_m}\right)\ln\left[\frac{z+\left(1+\sqrt{2}\right)b_m}{z+\left(1-\sqrt{2}\right)b_m}\right] \quad 3.4$$

$$0 = z^3 - \left(1 - \frac{b_m P}{RT}\right)z + \left(\frac{a_m P}{R^2T^2} - 3\left(\frac{b_m P}{RT}\right)^2 - \frac{2b_m P}{RT}\right)z - \left(\frac{a_m b_m P^2}{R^3T^3} - \left(\frac{b_m P}{RT}\right)^2 - \left(\frac{b_m P}{RT}\right)^3\right) \quad 3.5$$

$$a_m = z_i{}^2 a_{ii} + z_j{}^2 a_{jj} + 2z_i z_j \sqrt{a_{ii}a_{jj}}\left(1 - k_{ij}\right) \quad 3.6$$

$$b_m = z_i{}^2 b_{ii} + z_j{}^2 b_{jj} + z_i z_j \left(b_{ii} + b_{jj}\right)\left(1 - l_{ij}\right) \quad 3.7$$

For non-polar components $k_{ij}=l_{ij}=0$, where:

$$a_{ii} = 0.45724 \frac{R^2 T_{c,i}^{\ 2}}{P_{c,i}} \alpha_{ii} \qquad 3.8$$

$$b_{ii} = 0.07780 \frac{R\ T_{c,i}}{P_{c,i}} \qquad 3.9$$

$$\alpha_{ii} = \left[ 1 + \kappa_{ii} \left( 1 - \left( \frac{T}{T_{c,i}} \right)^{0.5} \right) \right]^2 \qquad 3.10$$

$$\kappa_{ii} = 0.37464 + 1.54226\omega_{ii} - 0.26992\omega_{ii}^2 \qquad 3.11$$

Table: 3.1: Properties of components for Equations 3.8 to 3.11 (Poling et al., 2001).

| **Component** | **$P_c$ / MPa** | **$T_c$ / K** | **ω** |
|---|---|---|---|
| water | 22.064 | 647.14 | 0.344 |
| $CH_4$ | 4.599 | 190.56 | 0.011 |
| $C_2H_6$ | 48.72 | 305.32 | 0.099 |
| R22 | 4.986 | 369.28 | 0.221 |
| R134a | 4.059 | 374.26 | 0.326 |

3.2.2 Liquid phase modelling

The fugacity in solution for a liquid phase may be expressed in terms of the fugacity coefficient in solution. This definition of fugacity in solution is used in the Phi-Phi method of thermodynamic data regression (refer to Chapter 3.3.2).

$$\hat{f}_w^L = \hat{\varphi}_w^L x_w P \qquad 3.12$$

An EOS may be used to determine the fugacity coefficient in solution (refer to Chapter 3.2.1 for further details).

The fugacity in solution for a liquid phase may also be expressed in terms of the activity coefficient. This definition of fugacity in solution is used in the Gamma-Phi method of thermodynamic data regression (refer to Chapter 3.3.1).

$$\hat{f}_w^L = \gamma_w^L x_w P_w^{sat} \tag{3.13}$$

For system temperatures above 273.15 K (Eslamimanesh et al.,2011):

$$P_w^{sat} = 10^{-6} \times e^{\left(73.649 - \frac{7258.2}{T} - 7.3037 \ln(T) + 4.1653 \times 10^{-6} T^2\right)} \tag{3.14}$$

For system temperatures below 273.15 K (Eslamimanesh et al.,2011):

$$P_I^{sat} = \frac{\left[10^{\left(\frac{-1032.558}{T} + 51.056 \times \log(T) - 0.0977 T + 7.0357 \times 10^{-5} \times T^2 - 98.512\right)}\right]}{7600} \tag{3.15}$$

The activity or fugacity coefficients represent the non-ideality in the liquid phase. Non-ideality may be due to high system pressures or where solubility in mixtures cannot be ignored. The non-ideality can be classified in terms of long and short range interactions (refer to Equation 3.16). For systems containing an electrolyte component, two approaches are used to predict the phase equilibria. The first includes an EOS with mixing rules for the long and short wave interactions. The second uses an EOS to describe the short wave interactions and an electrostatic term, such as Debye-Hückel, to describe the long-range interactions. Refer to Equation 3.17 for the latter.

$$G = G^{LR} + G^{SR} \tag{3.16}$$

A recent development, described by Aasberg-Petersen et al. (1991), is frequently used in literature. The fugacity coefficient was extended to account for the liquid-liquid equilibrium phase behaviour as well as the electrolyte contribution as follows:

$$\ln \varphi_w^{L} = \ln \varphi_w^{EOS} + \ln \gamma_w^{EL} \qquad 3.17$$

**Electrolyte component described by the activity coefficient model**

Electrolytes may dissolve in solution resulting in hydrate inhibition. This can be observed in the water activity. The electrolyte component accounts for the following interactions:

1. Liquid-salt.
2. Salt-salt (mixture).
3. Vapour-salt.

Electrolyte models can be classified according to the model description as follows (refer to Tables 3.2, 3.3 and 3.4 for further details):

1. Direct extensions of the Debye-Hückel model;
2. Pair correlation functions; and
3. Local composition based models.

Table 3.2: Electrolyte modelling - Direct extensions of the Debye-Hückel model.

| Name | Year developed | Progression | Assumptions | Limitations | Equations | Reference |
|---|---|---|---|---|---|---|
| Debye-Hűckel | 1923 | non ideal electrolyte solutions | electrostatic interactions, point charge ions, continuous solution charge density | Below 0.01 M | B.1 | (Hibbert, 1993) |
| Debye-Hűckel limiting law | | Not available in examined literature | Same as:Debye-Hückel, equal ion interaction | Below 0.1M | B.2 | Not available in examined literature |
| Extended Debye-Hűckel limiting law | 1925 | dielectric constant dependence on composition | Same as: Debye-Hűckel limiting law | Not available in examined literature | B.3 | |
| The Born / Debye and McAulay Theory | 1936 | Transfer ions from solvent to medium, | Not available in examined literature | Not available in examined literature | | (Stokes et al., 1948) |
| The hydration model | 1947 | Ion hydration | Not available in examined literature | Below 4M | B.4 | |

Table 3.2 continued: Electrolyte modelling - Direct extensions of the Debye-Hückel model.

| Name | Year developed | Progression | Assumptions | Limitations | Equations | Reference |
|---|---|---|---|---|---|---|
| The Davies Equation | 1962 | electrical charge | Not available in examined literature | Below 10M | B.5 | (Zhu et al., 2002) |
| B-dot equation | 1969 | Coefficient $\dot{B}$ is dependent on the species electrical charge | Species with the same value hard core diameter and electric charge<br>Below 10M, Up to 575.15K | Not available in examined literature | B.6 | (Zhu et al., 2002) |
| The graphical correlation | 1972 | Not available in examined literature | I = 20,<br>Pure solutions | Not available in examined literature | | (Meissner and Kusik, 1972) |
| One parameter model | 1973 | pure and mixed electrolyte solutions | I=6 | Not available in examined literature | B.7 | (Bromely, 1973) |

Table 3.3: Electrolyte modelling - Pair correlation functions.

| Name | Year developed | Progression | Assumptions | Limitations | Equations | Reference |
|---|---|---|---|---|---|---|
| Mean Spherical approximation model | 1966 | Not available in examined literature | Not available in examined literature | Not available in examined literature | | (Lebowitz and Percus, 1966) |
| Mean Spherical approximation model developments | 1972 | volume effects | Not available in examined literature | Not available in examined literature | | (Waisman and Lebowitz, 1970) |
| Pitzer | 1973 | long range interactions, short wave interactions | ions are in dielectric continuum | 6M binary and ternary ion interactions single solvent systems | B.8 to B.15 | (Chen et al., 1982, Prausnitz et al., 1999) |
| Extended MSA model | 1981 | hard core repulsion forces | Not available in examined literature | Not available in examined literature | | (Planche and Renon, 1981) |

Table 3.4: Electrolyte modelling - Local composition based models.

| Name | Year developed | Progression | Assumptions | Limitations | Equations | Reference |
|---|---|---|---|---|---|---|
| NRTL, Debye-McAulary | 1985 | long range interactions, dielectric constant dependence on ionic concentration, NRTL - short range interactions | Not available in examined literature | Electrolytes: completely / partially dissociated Solvents: un-dissociated | | (Cruz and Renon, 1978) |
| Extended NRTL, Pitzer, Debye-Hűckel | 1982 | Not available in examined literature | large repulsive forces between like charges, zero net local charge, negligible entropy of mixing for non ideal electrolytes | 6M single solvent, single electrolyte multi-component systems | | (Chen et al., 1982) |
| Modified Cruz-Renon | 1985 | ionic molalities, ionic radius | Not available in examined literature | Not available in examined literature | | (Ball et al., 1985) |
| NRTL-NRF with Debye-Hückel | 1986 | From (Chen et al., 1986) – NRTL with NRF not e-NRTL | Not available in examined literature | electrolyte solutions: dilute to saturated | | (Haghtalab and Vera, 1988) |

The addition of electrolyte components decreases the solubility of the guest molecule in the liquid phase. This is due to stronger interactions which exist between the electrolyte and liquid phase as compared to the gas and liquid phases. However, in some cases such (as with $CO_2$), although the solubility decreases with the addition of electrolytes, it does not become negligible. The main shortcoming of the direct extension of the Debye-Hückel models, pair correlation functions and local composition-based models, as mentioned above, is the inability of the models to account for the gas solubility. Little information is available in literature regarding high concentration electrolyte modelling for H-L-V equilibrium data where gas solubility is significant. The reader is referred to the references recorded below for further information regarding models developed based on the following assumptions:

1. Negligible gas-liquid interactions due to high liquid-salt interactions $\varphi_w^{EOS}$ =1, (Zemaitis et al., 1986).
2. Slight gas-liquid interactions due to high liquid-salt interactions (Englezos, 1988).
3. Significant gas-liquid interactions and liquid salt interactions (Englezos, 1992) and (Tohidi et al., 1995).

Menten (1981) was one of the first to develop models that use freezing point data to obtain an empirical model to determine hydrocarbon hydrates with a single salt. This model was extended to salt mixtures, however, the model could not account for gas solubility (Englezos, 1988). Predictive numerical models for determining the hydrate phase equilibrium in the presence of electrolytes is developed in Tohidi et al. (1995) and Engelzos (1992). These models account for gas solubility. The aqueous phase was modelled using an EOS and an electrolyte term as seen in Equation 3.17. As mentioned previously in respect of Tohidi et al. (1995), the Valderrama EOS with non density-dependent mixing rules was used. Additionally, the Peng-Robinson EOS with van der Waals classical mixing rules was used. Englezos (1992) use the Trebble and Bishnoi EOS. Both Tohidi et al. (1995) and Englezos (1992) use the electrolyte model developed by Aasberg-Petersen et al. (1991) with modified Debye-Hückel activity coefficient. This is given by:

$$\ln \gamma^{EL} = \frac{2Ah_{is}MF(BI^{0.5})}{B^3} \qquad 3.18$$

Where:

$$A = 1.327757 \times 10^5 \frac{d_w^{0.5}}{(\varepsilon_m T)^{1.5}} \quad 3.19$$

$$B = 6.359696 \times \frac{d_w^{0.5}}{(\varepsilon_m T)^{0.5}} \quad 3.20$$

$$F(BI^{0.5}) = 1 + BI^{0.5} - \frac{1}{1 + BI^{0.5}} - 2\ln(1 + BI^{0.5}) \quad 3.21$$

$$\varepsilon_m = x_s \varepsilon_N \quad 3.22$$

The dielectric constant of water data was obtained from the CRC handbook of Chemistry and Physics and the correlation developed by Zemitis (1986) is used:

$$\varepsilon_N = 305.7 \exp\left( -\exp(-12.741 + 0.01875T) - \frac{T}{219} \right) \quad 3.23$$

The water-salt or the salt-salt interactions are accounted for in the parameter $h_{is}$ in Equation 3.18. There are two suggested methods to determine the parameters for this term to model hydrate equilibrium data, namely:

1. freezing point depression data with vapour pressure data; and
2. hydrate dissociation point data.

Only the first method is used in literature where the freezing point data for the salt in water is determined at specific temperatures, pressures and salt concentrations. Using freezing point data allows for the direct determination of salt-water interactions while vapour pressure data determined the salt-gas interactions. Englezos (1992) determined this parameter by regressing vapour-liquid equilibrium data for carbon dioxide and water in the presence of a single salt, NaCl. The water-salt interaction parameter is reported as 92.5 by Englezos (1992).

Tohidi et al. (1995), on the other hand, developed a water-salt interaction parameter. The water-salt interaction parameter is determined using a least squares method where freezing point data and

vapour pressure depression data is regressed at 373.15 K for single salt solutions. The model is extended to mixed electrolyte solutions, accounting for salt-salt interactions. This parameter is a function of salt concentration is:

$$h_{ws} = \frac{\left(A + BT + Cw_s + Dw_s^2 + ETw_s\right)}{1000} \qquad 3.24$$

Table 3.5: Regressed constants for the interaction parameter $h_{ws}$ in Equation 3.24 (Tohidi et al., 1995).

| Salt | A | B | C | D | E |
|---|---|---|---|---|---|
| NaCl | -11.91 | $1.037\text{x}10^{-2}$ | $-6.043\text{x}10^{-2}$ | $-5.814\text{x}10^{-3}$ | $3.861\text{x}10^{-4}$ |
| KCl | -12.79 | $1.385\text{x}10^{-2}$ | $5.184\text{x}10^{-2}$ | $-2.152\text{x}10^{-3}$ | $1.436\text{x}10^{-5}$ |
| $CaCl_2$ | -5.672 | $8.037\text{x}10^{-3}$ | $-3.330\text{x}10^{-1}$ | $-1.771\text{x}10^{-3}$ | $5.800\text{x}10^{-4}$ |
| $Na_2SO_4$ | -5.495 | $7.476\text{x}10^{-3}$ | $-1.769\text{x}10^{-2}$ | $-8.905\text{x}10^{-4}$ | $1.083\text{x}10^{-4}$ |
| NaF | -14.82 | $1.758\text{x}10^{-2}$ | $-3.657\text{x}10^{-2}$ | $-5.514\text{x}10^{-2}$ | $1.258\text{x}10^{-3}$ |
| KBr | -14.04 | $1.705\text{x}10^{-2}$ | $1.471\text{x}10^{-1}$ | $-1.657\text{x}10^{-3}$ | $-2.851\text{x}10^{-4}$ |
| $MgCl_2$ | -6.420 | $1.066\text{x}10^{-2}$ | $-6.186\text{x}10^{-1}$ | $-4.556\text{x}10^{-3}$ | $-1.312\text{x}10^{-3}$ |
| $SrCl_2$ | -6.591 | $1.327\text{x}10^{-2}$ | $-2.334\text{x}10^{-1}$ | $9.035\text{x}10^{-4}$ | $1.555\text{x}10^{-4}$ |
| $BaCl_2$ | -5.905 | $8.248\text{x}10^{-3}$ | $-9.799\text{x}10^{-2}$ | $-2.780\text{x}10^{-4}$ | $1.423\text{x}10^{-4}$ |

Javanmardi and Moshfeghian (2003) report the water-salt interaction parameter in terms of salt concentration and pressure. Since the isochoric method is used, where pressure is determined from a step-in temperature, it is more accurate to use temperature in the water-salt interaction parameter than pressure.

Englezos (1992) compares the experimental data for the system $CO_2$ (1) + water (2) + NaCl (3) with the predicted data. An average error of 7.2% was reported. Tohidi et al. (1995) compares the experimental data for single salt solutions and mixed salt solutions for methane, ethane, propane and carbon dioxide. The maximum error in the hydrate formation temperature for ethane and the mixture of carbon dioxide and methane is ±1 K.

The second method to determine the salt-water or salt-salt interactions is not applied in examined literature. This method uses hydrate dissociation data to determine the salt-salt and salt-water interactions. The hydrate dissociation point accounts for the hydrate, liquid and vapour phases at equilibrium, including the respective interactions which occur at each phase. This method requires further investigation.

In this work, the approach reported in Tohidi et al. (1995) is used. It is a generalised approach which can be simplified depending on the systems measured. The Aasberg-Petersen model is chosen for the electrolyte component. This model can predict aqueous solutions under high pressure and it is highly accurate for hydrate formation conditions. The interaction coefficient for this model is determined by using hydrate dissociation point data. No vapour-liquid equilibrium data or freezing point depression data was reported in literature for the system R134a (1) + water (2) + NaCl (3). Additionally, no experimental data were measured for this system in this work.

## 3.3 Vapour-liquid equilibrium data regression

Two common methods used to regress phase equilibrium data include the $\gamma - \phi$ (combined method) and $\phi - \phi$ (direct method). In the combined method, an EOS is used to describe the vapour phase non-ideality while the liquid phase non-ideality is described by the activity coefficient model. The liquid and vapour phase non-idealities are described using an EOS with a mixing rule.

A comparison between the direct and combined methods is obtained from Wichterle (1978a, b) and Ramjugernath and Raal (1999). The comparison is displayed in Table 3.6.

Table 3.6: Comparison between direct and combined methods used to regress vapour-liquid equilibrium data (Wichterle,1978a, b) and (Ramjugernath and Raal, 1999).

| | **Direct Method** | **Combined Method** |
|---|---|---|
| Initial guess sensitivity | Small. | Insignificant in comparison to direct method. |
| Calculation accuracy | Dependent on chosen EOS and mixing rules. | Good out of the critical region. |
| Limitations of conditions | Unreliable at critical region. | Unreliable at critical region. |
| Components in the system | Difficulty in modelling highly polar and structurally complex systems. | Dependent on the EOS and liquid phase model chosen. |
| Time required for computation | Dependent on the model chosen. | Dependent on the models chosen. |
| Input parameters | Dependent on the models chosen. | Choice of standard state is important. |
| Ability to extrapolate | Able to extrapolate using Wong and Sandler mixing rules | No ability to extrapolate. |
| Ability to predict | Interpolation for small ranges. | Not as good as direct method. |
| Ability to interpolate | Predictive capabilities if UNIFAC group contribution model is used. | No predictive capabilities unless UNIFAC group contribution method is used. |

### 3.3.1 Gamma-Phi method ($\gamma - \phi$)

The calculation procedure for the Gamma-Phi method, specifically for an isothermal system is show in Figure 3.1.

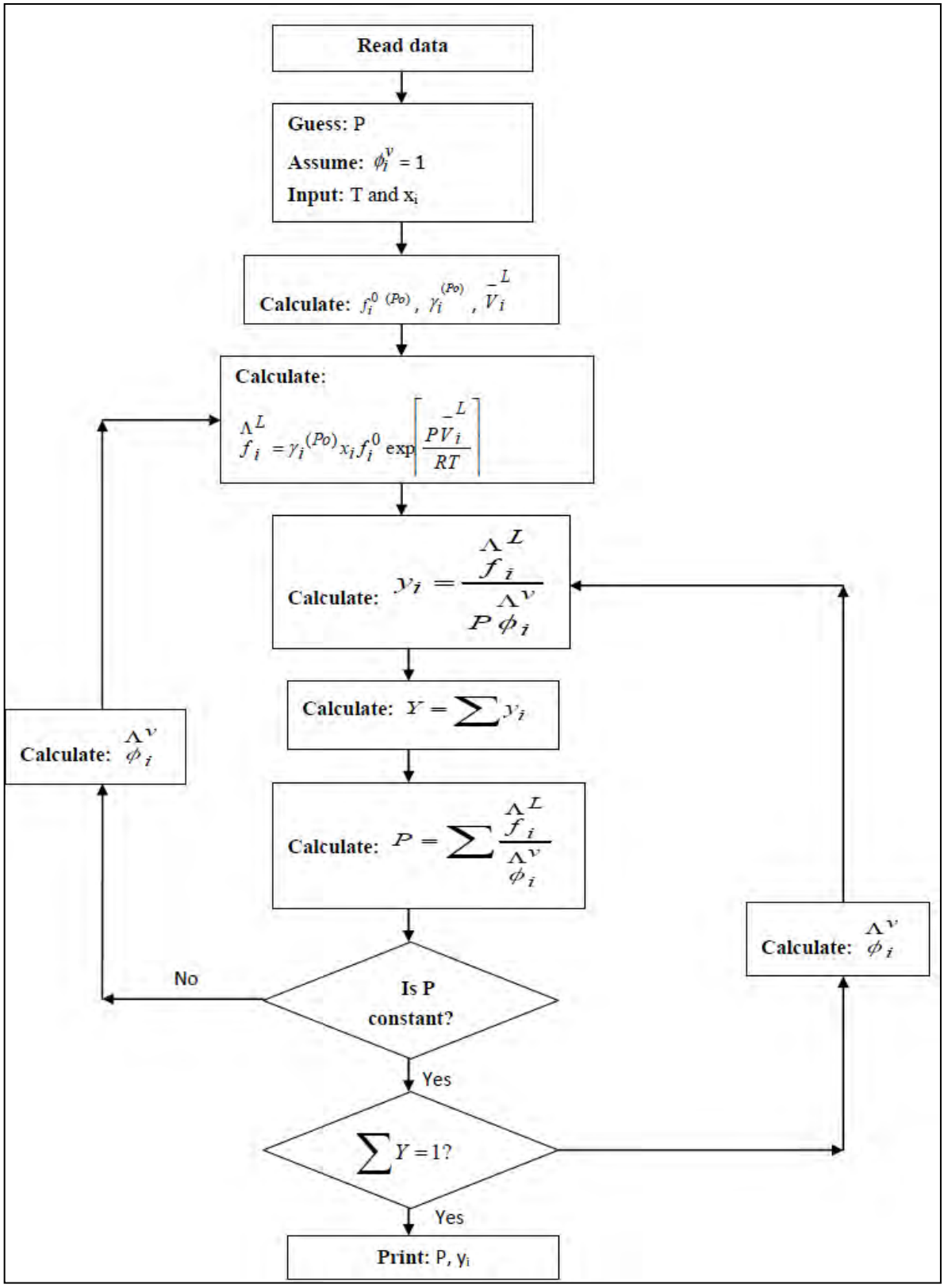


Figure 3.1: Flow diagram for the Gamma-Phi isothermal bubble-pressure method (Prausnitz and Chueh, 1968).

### 3.3.2 Phi-Phi method ($\phi - \phi$)

The calculation procedure for the Phi-Phi method, specifically for an isothermal system is show in Figure 3.2.

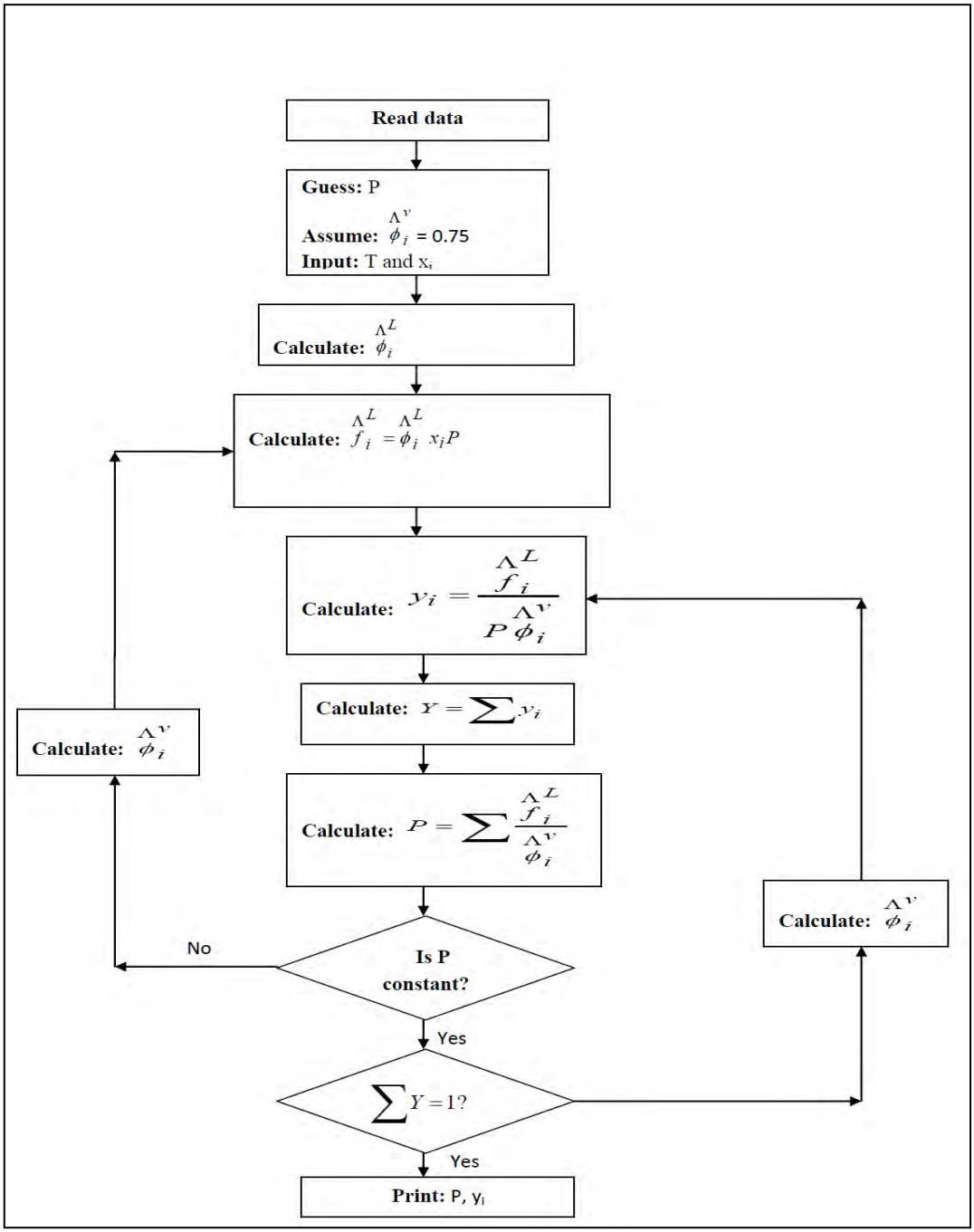


Figure 3.2: Flow diagram for the Phi-Phi isothermal bubble-pressure method (Prausnitz and Chueh, 1968).

## 3.4 Extension of vapour-liquid equilibrium data regression to hydrate-vapour-liquid equilibrium modelling

### 3.4.1 Hand calculation based methods

Hand calculations are useful for determining an estimate of the hydrate dissociation temperature and pressure; however, they are highly inaccurate. Three methods are used namely (Sloan et al., 2008):

1) Gas gravity method.
2) K-factor method.
3) Baillie-Wichert method.

The gas gravity method (Katz et al., 1959) uses enthalpy-entropy charts and isenthalpic expansion to determine hydrate Joule Thompson charts. This method has an accuracy of 20% as it ignores the effect of composition change on temperature and pressure.

The K-factor method (Wilcox et al., 1941) uses the ratio of the gas and hydrate mole fractions. The following assumptions were made:

1. The formation enthalpy for structures I and II for the same guest molecule in a mixture are the same.
2. The gas phase and hydrate phase are ideal.

The first assumption was proven incorrect as this method could not account for the formation of structure I and II hydrates for the same guest molecule in a mixture. The K-factor method has an accuracy of 15% and can only be used for a temperature range of 273.15 to 293.15 K and a pressure range of 0.7 to 7 MPa.

The third method is that of Baillie-Wichert. This method is an extension of the gas gravity method as it accounts for propane and hydrogen sulphide. This method requires an iterative procedure by using an initial guess for the pressure obtained from the gas gravity method.

### 3.4.2 Computer based methods

Hydrate dissociation points occur when the liquid, hydrate and the vapour phases are in equilibrium. Computer based methods require an iterative procedure using equilibrium criteria. The following intermolecular interactions are important and should be accounted for in each phase:

| *Hydrate phase* | *Liquid phase* | *Vapour phase* |
|---|---|---|
| Solid-vapour | Liquid-vapour | Liquid-vapour |
| | Salt-liquid | Vapour-vapour (mixtures) |
| | Liquid-liquid (liquid hydrate formers) | Salt-vapour |
| | Salt-salt (mixtures) | |

The liquid and vapour phases are discussed in Chapter 3.2.1 and 3.2.2. The hydrate phase will be discussed in this section.

Hydrates maintain a regular structure therefore statistical thermodynamics are used to obtain hydrate thermodynamic properties. Van der Waals and Platteeuw (1959) obtained the fundamental equations to calculate the hydrate dissociation pressures using the Lennard-Jones-Devonshire cell model. This method connects the microscopic hydrate properties with the macroscopic thermodynamic properties and forms the basis of all hydrate dissociation condition calculations. Numerous models have been developed from the van der Waals and Platteeuw model. Each attempting to reduce the error between the experimental and modelled H-L-V equilibrium data while ensuring the model is simple to use for industrial purposes.

The hydrate formation process is thermodynamically modelled by considering two steps. The first step considers the formation of an empty hydrate lattice from pure water. The second step is the filling of the hydrate lattice with a guest molecule. The chemical potential change according to the two-step process is resembled in the following equation:

$$\mu_w^H - \mu_w^L = (\mu_w^H - \mu_w^{MT}) + (\mu_w^{MT} - \mu_w^L) = 0 \qquad 3.25$$

The first two terms on the right hand side of Equation 3.25 indicates the stabilisation of the hydrate. Numerous models may be applied to evaluate this term e.g. Van der Waals and Platteeuw (1959), Parrish and Prausnitz (1972), Dharmawardhana et al. (1980a) and Holder and Grigoriou (1980). The second two terms indicate a phase change calculated using thermodynamic models in Parrish and Prausnitz (1972) and Holder and Grigoriou (1980):

$$\frac{\mu_w^{MT} - \mu_w^L}{RT} = \frac{\Delta\mu_w{}^o(T_o, P)}{RT^0} - \int_{T^0}^{T}\left[\frac{\Delta h_w^{MT-L}}{RT^2}\right]_P dT + \int_{P^0}^{P}\left[\frac{\Delta V_w^{MT-L}}{RT}\right]_T dP - \ln a_w^L \qquad 3.26$$

Where:

$$\Delta h_w^{MT-L} = \Delta h_w^{MT-L^o}(T_o) + \int_{T^0}^{T} \Delta C_{p_w}^{MT-L} dT \qquad 3.27$$

$$\Delta Cp_w^{MT-L} = \Delta C_{p_w}^{MT-L^0}(T_o) + \beta^{MT-L}(T - T_o) \qquad 3.28$$

$$a_w^L = \frac{\overset{\Lambda}{f}{}_w^L}{\overset{\Lambda}{f}{}_w^+} \qquad 3.29$$

Table 3.7: Thermodynamic properties for Structures I and II for liquid or ice and an empty hydrate lattice.

| **Property**[a] | **Value** | | **Units / Reference** |
|---|---|---|---|
| | Structure I | Structure II | |
| $\Delta\mu_w{}^0$ | 1264 | 883 | J/mol / (Parrish and Prausnitz, 1972) |
| $\Delta h_w^{MT-L^o}(T_o)$ | -4858 | -5201 | J/mol / (Parrish and Prausnitz, 1972) |
| $\Delta h_w^{MT-I^o}(T_o)$ | 1151 | 808 | J/mol / (Parrish and Prausnitz, 1972) |
| $\Delta C_{p_w}^{MT-L^0}(T_o)$ | -38.13 | | J/(mol.K) / (Parrish and Prausnitz, 1972) |
| $\beta^{MT-L}$ | 0.141 | | J/(mol.K$^2$) / (Parrish and Prausnitz, 1972) |
| $\Delta V_w^{MT-L^0}$ | 4.6x10$^{-6}$ | 5x10$^{-6}$ | m$^3$/mol / (Parrish and Prausnitz, 1972) |
| $\Delta V_w^{MT-I^0}$ | 3.0x10$^{-6}$ | 3.4x10$^{-6}$ | m$^3$/mol / (Parrish and Prausnitz, 1972) |

[a]Reference condition: $T^0$=273.15K, $P^0$=0 Pa

The thermodynamic property $\Delta\mu_w^0$ for structure I was initially determined by van der Waals and Platteeuw (1959) as 700 J/mol where bromine was used as the reference parameter. It was later established by Allen (1963) that bromine is not a structure I hydrate. Parrish and Prausnitz (1972) used the methane hydrate and natural gas hydrate mixtures as their structure I and structure II reference hydrates respectively above 273.15 K. Parrish and Prausnitz (1972) determined the thermodynamic properties $\Delta\mu_w^0$ and $\Delta h_w^{MT-L^o}(T_o)$ for structure I hydrates by a trial and error method which compared calculated and experimental data.

**Van der Waals and Platteeuw model**

The first two terms on the right hand side of Equation 3.25 were first introduced by van der Waals and Platteeuw, (1959). Fundamental statistical thermodynamic equations for gas hydrates are used with concepts of Langmuir gas absorption. The van der Waals and Platteeuw theory assumes the following:

1. The gas phase consists of one gas hydrate former.
2. Each spherical cavity contains at most one gas molecule.
3. Gas molecules are small enough not to distort the hydrate lattice.
4. There are no interactions between the hydrate lattice and the encaged gas molecules.
5. Classical statistics is valid.
6. The behaviour of the gas is ideal.

Van der Waals and Platteeuw (1959) derived an equation using Gibbs Free Energy in terms of internal energy and extensive properties; entropy and volume. For further details the reader is referred to (Sloan and Koh, 2008). The equation is as follows:

$$\frac{\mu_w^{MT} - \mu_w^H}{RT} = -\sum_m \nu_m \ln(1 - \theta_{ml}) \qquad 3.30$$

Where Equation 3.31 accounts for the potential of a cavity to be occupied by a single gas molecule:

$$\theta_{ml} = \frac{C_{ml} P}{\left(1 + C_{ml}\ P\right)} \qquad 3.31$$

The Langmuir constant, $C_{ml}$, accounts for the gas-water interactions using the Lennard-Jones-Devonshire cell theory (refer to Van der Waals and Platteeuw (1959) for further information).

Table 3.8: Ratio of the number of cavities to the number of water molecules in the hydrate structure.

| **Property** | **Value**[a] | |
|---|---|---|
| | Structure I | Structure II |
| $\nu_{small}$ | 1/23 | 2/17 |
| $\nu_{large}$ | 3/23 | 1/17 |

[a]Ref: (Van der Waals and Platteeuw, 1959)

**Parrish and Prausnitz model**

Parrish and Prausnitz (1972) extended the hydrate model proposed by van der Waals and Platteeuw (1959). The extensions included:

1. Multicomponent gas, hydrate formers and non hydrate formers in the gas phase.
2. Non-ideal gas phase, therefore the model could be used for higher pressures.
3. London forces are accounted for in the interaction between the gas and water molecules while polar forces are accounted for in the lattice hydrogen bonding.
4. Kihara potential parameters are used to determine the Langmuir parameters (refer to Parrish and Prausnitz (1972) for further details).

Since the gas hydrate formers compete for a position in a cavity, the probability of the gas occupying the cavity decreases. Therefore Equation 3.30 becomes:

$$\frac{\mu_w^{MT} - \mu_w^H}{RT} = -\sum_m \nu_m \ln\left(1 - \sum_j \theta_{mj}\right) \qquad 3.32$$

And Equation 3.31 becomes:

$$\theta_{ml} = \frac{C_{ml} f_l}{\left(1 + \sum_j C_{ml\,j} f_j\right)} \qquad 3.33$$

Where:

$$f_l = \phi_l y_l P \tag{3.34}$$

$$C_{ml} = \frac{4\pi}{kT}\int_0^{\infty} \exp\left[\frac{-w(r)}{kT}\right] r^2 dr \tag{3.35}$$

Where:

$$w(r) = 2z\varepsilon\left[\frac{\sigma^{12}}{R^{11}r}\left(\delta^{10} + \frac{a}{R}\delta^{11}\right) - \frac{\sigma^{6}}{R^{5}r}\left(\delta^{4} + \frac{a}{R}\delta^{5}\right)\right] \tag{3.36}$$

$$\delta^N = \left[\left(1 - \frac{r}{R} - \frac{a}{R}\right)^{-N} - \left(1 + \frac{r}{R} - \frac{a}{R}\right)^{-N}\right] / N \tag{3.37}$$

Equations 3.36 and 3.37 are functions of the core radius, (a); radial coordinate, (r) and the depth of intermolecular potential well, (ε). Refer to Parrish and Prausnitz (1972) for the parameter values. For systems with a temperature between 260 and 300 K, Equation 3.35 is simplified to:

$$C_{ml} = \frac{A_{ml}}{T}\exp\left(\frac{B_{ml}}{T}\right) \tag{3.38}$$

Table 3.9: Fitted parameters for Langmuir parameters in Equation 3.38, for various gases with an accuracy of ±0.2%.

| **Gas** | **Value[a]/ K** | | | | | | | |
|---|---|---|---|---|---|---|---|---|
| | Structure I | | | | Structure II | | | |
| | Small | | Large | | Small | | Large | |
| | $A_{ml}x10^3$ | $B_{ml}x10^{-3}$ | $A_{ml}x10^2$ | $B_{ml}x10^{-3}$ | $A_{ml}x10^3$ | $B_{ml}x10^{-3}$ | $A_{ml}x10^2$ | $B_{ml}x10^{-3}$ |
| Methane | 3.7237 | 2.7088 | 1.8372 | 2.7379 | 2.9560 | 2.6951 | 7.6068 | 2.027 |
| Ethane | 0.0 | 0.0 | 0.6906 | 3.6316 | 0.0 | 0.0 | 4.0818 | 3.0384 |
| Propane | 0.0 | 0.0 | 0.0 | 0.0 | 0.0 | 0.0 | 1.2353 | 4.4061 |
| Carbon Dioxide | 1.1978 | 2.8605 | 0.8507 | 3.2779 | 0.9091 | 2.6954 | 4.8262 | 2.5718 |

[a]Ref: (Parrish and Prausnitz, 1972)

Variations of the parameters reported in Table 3.9 are reported in van der Waals and Platteeuw (1959), Holder and Grigoriou (1980) and Dharmawardhana et al. (1980b). Cao et al. (2002) discuss how the model prediction or regression is significantly affected by the value of the parameters reported in Table 3.9 and how this may result in significant error.

Recent developments have been made to the model established by Parrish and Prausnitz (1972), particularly for the Langmuir constants. One such development replaced the Kihara potential parameters with correlated experimental data. Klauda and Sandler (2000) proposed that the strength of the hydrogen bonds between the water molecules in the lattice is dependent on the size of the empty hydrate lattice. As a result, the hydrate properties are dependent on the guest molecules. Additionally, the Kihara potential parameters should be determined from the virial coefficient and viscosity data, and the chemical potential should vary according to the guest molecule.

**Sloan, Khoury and Kobayashi model**

From Equation 3.32, with the assumption that the hydrate lattice is composed of pure ice, Sloan (1976) showed that the fugacity of the water in the filled hydrate could be related to the difference in chemical potential in the filled and empty hydrate by:

$$f_w^H = f_w^{MT} \exp \frac{\mu_w^H - \mu_w^{MT}}{RT} \qquad 3.39$$

Where $f_w^{MT}$ is obtained experimentally by determining a corrected value for the saturated vapour of the empty hydrate.

**Ng and Robinson model**

Ng and Robinson (1980) extended the model proposed by Parrish and Prausnitz (1972) for a hydrocarbon liquid former. Additionally, they extended the model proposed by Sloan (1976) by obtaining the term $f_w^{MT}$. This is demonstrated by using correlative methods from vapour-hydrate data for various components. Since an empirical fit is used, $f_w^{MT}$ becomes negative below 285 K and 287 K for structures I and II respectively.

**Sloan, Sparks and Johnson model**

Sloan et al. (1987) modified the model proposed by Ng and Robinson, by fitting vapour pressure data obtained from H-L-V equilibrium data for various components:

$$f_w^{MT} = P_w^{MT}\phi_w^{MT} \exp \int_{P_w^{MT}}^{P} \frac{V_H^{MT}}{RT} dP \qquad 3.40$$

Where for structure I:

$$\ln P_w^{MT} = 17.440 - \frac{6003.925}{T} \qquad 3.41$$

For structure II:

$$\ln P_w^{MT} = 17.332 - \frac{6017.635}{T} \qquad 3.42$$

Since the empty hydrate fugacity coefficient, $\phi_w^{MT}$, is introduced, it is thermodynamically proven the pressure should always remain positive. $\phi_w^{MT}$ is determined using the second virial coefficient and becomes significant at high pressures (refer to Sloan et al. (1987) for further details).

Equation 3.40 may be simplified by the following assumptions:

The hydrate partial molar volume equals the molar volume and is independent of pressure.
$P_w^{MT}$ is in the order of $10^{-3}$MPa therefore $\phi_w^{MT} = 1$.

$$f_w^{MT} = P_w^{MT} \exp \frac{V_H^{MT}\left(P - P_w^{MT}\right)}{RT} \qquad 3.43$$

**Chen and Guo model**

Chen and Guo (1998), developed a model based on a two step hydrate formation mechanism. The first step is the formation of a basic hydrate structure from a quasi-chemical reaction process. This step includes the following assumption:

1. The gas molecules dissolve in the liquid phase, and each guest molecule is surrounded by a cluster of dissolved gas molecules with water molecules.

The second step is the adsorption of the dissolved gas molecules into the empty hydrate cavity. This step can only occur for small gas molecules such as $N_2$, Ar, $O_2$ and $CH_4$. The Langmuir adsorption theory is used to determine this step (refer to Chen and Guo (1998) for further details).

**Mohammadi and Richon model**

Mohammadi et al. (2008b) further simplified the equation developed by Sloan et al. (1987). Making the following assumption:

The Poynting correction term, $\exp \frac{V_H^{MT}\left(P - P_w^{MT}\right)}{RT} = 1$, for pressures up to 2 MPa.

Equation 3.43 becomes:

$$f_w^{MT} = P_w^{MT} \qquad 3.44$$

And Equation 3.39 becomes:

$$f_w^H = P_w^{MT} \exp \frac{\mu_w^H - \mu_w^{MT}}{RT} \qquad 3.45$$

**Eslamimanesh, Mohammadi and Richon model**

Eslamimanesh et al. (2011) simplified the equation developed by Parrish and Prausnitz (1972) by assuming:

1. For systems where the dissociation pressure of the hydrate is low, the vapour phase consisting of pure guest molecules is assumed ideal, therefore:

$$f_l = P \tag{3.46}$$

And Equations 3.32 and 3.33 become:

$$\frac{\mu_w^{MT} - \mu_w^H}{RT} = \sum_m \ln\left(1 + \sum_j C_{mj} P\right)^{-\nu_m} \tag{3.47}$$

Table 3.10: Regressed parameters for Langmuir parameters in Equation 3.47, for various hydrofluorocarbons.

| **Refrigerant** | **Value/ K** | | | | | | | |
|---|---|---|---|---|---|---|---|---|
| | Structure I | | | | Structure II | | | |
| | Small | | Large | | Small | | Large | |
| | $A_{ml}x10^{3}$ | $B_{ml}x10^{-3}$ | $A_{ml}x10^{2}$ | $B_{ml}x10^{-3}$ | $A_{ml}x10^{3}$ | $B_{ml}x10^{-3}$ | $A_{ml}x10^{2}$ | $B_{ml}x10^{-3}$ |
| R134a | 0.0 | 0.0 | 0.0 | 0.0 | 0.0 | 0.0 | 0.5700 | 4.9088 |
| R141b | 0.0 | 0.0 | 0.0 | 0.0 | 0.0 | 0.0 | 3.2600 | 4.9623 |
| R152b | 0.0 | 0.0 | 0.1600 | 4.5854 | 0.0 | 0.0 | 9.3400 | 4.2417 |
| R32 | 0.0041 | 1.0481 | 2.8500 | 3.5782 | 0.0 | 0.0 | 0.0 | 0.0 |

Ref: (Eslamimanesh et al., 2011)

The models mentioned above are simplifications of the van der Waals and Platteeuw model. The models used in literature are dependent on the systems investigated and the significance of the assumptions used in the models. As a result, many literary sources have developed their own modification of the van der Waals and Platteeuw model. Another method used includes molecular simulation; however, this will not be discussed in this work.

It is important to note that since electrolytes are excluded from the hydrate phase during hydrate formation, the systems containing electrolytes cannot affect the chemical potential of the hydrate phase (Sum et al., 1997).

## 3.5 Summary of measured systems in literature

Salt has a high boiling point therefore it was assumed there were no ions in the vapour phase and gas-salt interactions were ignored. Table 3.10 to 3.13 summarise the models used to describe the liquid and vapour phases including the maximum percentage reported error for the systems described in this text.

Table 3.11: Summary of the liquid and vapour phase models used in H-V-L equilibrium modelling, this is discussed in Chapter 3.2 and 3.3.

| **Reference** | **Liquid / Vapour phase** | **Mixing Rule** | **Maximum % AAD[a]** |
|---|---|---|---|
| (Parrish and Prausnitz, 1972) | | | 20.69 |
| (Sloan et al. 1987) | SRK / PR | Modified Huron-Vidal / Van der waals | 5.80 |
| (Chen and Guo, 1998) | PT | none | 40.97 |
| (Mohammadi et al., 2008) | Henry‟s Law | none | <6.00 |
| (Eslamimanesh et al., 2011) | none | none | 30.00 |

[a] $\%ADD = \frac{100}{n}\sum \frac{\left|P^{\exp} - P^{calc}\right|}{P^{\exp}}$

PR=Peng Robinson, PT=Patel and Teja, SRK=Soave-Redlich-Kwong

Table 3.12: Summary of models used in literature of the system R22 (1) + water (2).

| Reference | Liquid / Vapour phase | Mixing Rule | Maximum % AAD[a] |
|---|---|---|---|
| (Javanmardi et al., 2004) | Not available in examined literature | Not available in examined literature | Reported as temperature: very good fit |
| (Chun et al., 2000) | SRK | Modified Huron-Vidal | 4.03 |
| (Chun et al., 1996) | Not available in examined literature | Not available in examined literature | Not available in examined literature |

[a] $\%ADD = \frac{100}{n}\sum\frac{\left|P^{\exp} - P^{calc}\right|}{P^{\exp}}$

SRK Soave-Redlich-Kwong

Table 3.13: Summary of models used in literature of the system R134a (1) + water (2).

| Reference | Liquid / Vapour phase | Mixing Rule | Maximum % AAD[a] |
|---|---|---|---|
| (Akiya et al., 1999) | Not available in examined literature | Not available in examined literature | Not available in examined literature |
| (Liang et al., 2001) | PR | Not available in examined literature | 4.8 |
| (Eslamimanesh et al., 2011) | Not available in examined literature | Not available in examined literature | 4.9 |

[a] $\%ADD = \frac{100}{n}\sum\frac{\left|P^{\exp} - P^{calc}\right|}{P^{\exp}}$

PR Peng Robinson

Table 3.14: Summary of the liquid and vapour phase models reported for electrolyte systems discussed in chapter 3.2.2.

| Reference | Liquid / Vapour phase | Electrolyte | Mixing Rule | Maximum % AAD[a] |
|---|---|---|---|---|
| (Chun et al., 2000) | SRK | Pitzer | Modified Huron-Vidal | 4.03 |
| (Englezos, 1992) | TB | Aasberg Petersen | Not stated | 4.5 |
| (Tohidi et al., 1995) | PR / VPT | Aasberg Petersen | Classical / non density dependent | Not reported: very good fit |

[a] $\%ADD = \frac{100}{n}\sum\frac{\left|P^{\exp} - P^{calc}\right|}{P^{\exp}}$

PR=Peng Robinson, SRK=Soave-Redlich-Kwong, TB=Trebble-Bishnoi, PT=Patel and Teja

## 3.6 Model application

### 3.6.1 Modelling approach

The model published by Parrish and Prausnitz (1972) and modified by Holder and Grigoriou (1980) is used as a general approach to model the H-L-V equilibrium data of a pure hydrate former. It accounts for the gas solubility in the liquid phase as well as the liquid solubility in the gas phase. Systems which are modelled by Parrish and Prausnitz (1972) with include $CO_2$ (1) + water (2) and $C_2H_6$ (1) + water (2) systems. The gas has a high water solubility and therefore was chosen to verify the model programmed in this work. The flow diagram for this predictive model is shown in Figure 6.5.

The model proposed by Parrish and Prausnitz (1972) later modified by Holder and Grigoriou (1980), was simplified specifically for refrigerants by Eslamimanesh et al. (2011). The following assumptions are stated and equations presented:

For the system R134a (1) + water (2):

*Liquid Phase assumptions:*

1. Negligible gas solubility, $\gamma^{L}_{w}=1$.

2. Pure water liquid phase, $x_w$=1.

Equation 3.13 becomes:

$$\hat{f}_w^L = P_w^{sat} \qquad 3.48$$

*Vapour phase assumptions:*

1. Low dissociation pressure, below 2 MPa, $\hat{\varphi}_w^V = 1$ (Mohammadi et al., 2008b).
2. No water in the vapour phase, $y_w = 0$.

This model contains many of the simplifications and assumptions made by Parrish and Prausnitz (1972). This resulted in a simpler approach to modelling hydrate systems containing refrigerants with low water solubility. The flow diagram for this predictive model is shown in Figure 6.8. The objective function used in this model (in terms of the saturated pressure) used the Antoine‟s equation and calculated saturated pressure. In order to extend this model to systems that contain water-soluble hydrate formers, the objective function is altered such that it is in terms of experimental and calculated dissociation pressure. Thus the fugacity coefficient in solution may be used in place of the activity coefficient. The reader is referred to Figure 6.8 for the flow diagram of the model used in this work.

The model mentioned above is later extended to salts by using the interaction coefficient parameters reported in Tohidi et al. (1995). Dissociation data for the systems R22 with {5, 10 and 15} wt% NaCl from the publication of Chun et al. (2000) are predicted. Additionally, Chun et al. (2000) predicts the systems R134a with {5, 10 and 15} wt% NaCl, as measured in this work (refer to Figure 6.14 for the predictive flow diagram).

### 3.6.2 Flow Diagrams

An ASPEN flash calculation is conducted to obtain the equilibrium composition of the vapour and liquid phase components at the dissociation temperature and pressure. Refer to Figure A.6 in Appendix B for the flow diagram of this calculation or for further information refer to Smith et al. (2005).

All regression and predictive models were programmed using MATLAB®.

# CHAPTER FOUR

## A REVIEW OF EXPERIMENTAL METHODS AND EQUIPMENT USED

Hydrate-vapour-liquid equilibrium data have been measured with numerous apparati. Discrepancies have been found between different measurements for the same system. In some cases, it is difficult to describe a system with simplified models and therefore it is important to obtain reliable experimental results.

This section contains a summary of current apparati which have been used in literature to measure hydrate phase equilibrium. The Quartz crystal microbalance, Cailletet, Rocking cell, High pressure differential scanning calorimetry, Differential thermal analysis and High pressure auto clave cell are researched. The High pressure autoclave cell with sapphire windows is used in this work for hydrate measurements. It is simple to operate, easily available and the observation of hydrate formation and dissociation are possible.

### 4.1 Equipment Review

#### 4.1.1 Quartz crystal microbalance

The apparatus, as seen in Figure 4.1, consists of two electrodes separated by a thin quartz disk. When an electric current is passed though the electrodes, the crystal oscillates at a specific frequency. A drop of water is added to the crystal surface and placed into the high pressure cell. The temperature is reduced to allow the water to freeze. The cell is evacuated and experimental fluids are inserted into the cell. An initial hydrate forming temperature and pressure are chosen. During hydrate formation, a mass attaches itself to the crystal surface thus changing the resonant frequency. A stepwise increase in temperature is initiated and the pressure and frequency are recorded at each step (Mohammadi et al., 2003). The point at which the frequency changes, usually the highest frequency, is taken as the hydrate dissociation point. Since samples are small and the device is sensitive to changes in mass, the time required to determine the hydrate dissociation point is reduced. From a literature review, the Quartz crystal microbalance is not chosen for the measurement of hydrate phase equilibrium as it is not guaranteed that the hydrate will attach itself to the crystal and therefore there is a risk of inaccurate results (Sloan and Koh, 2008).

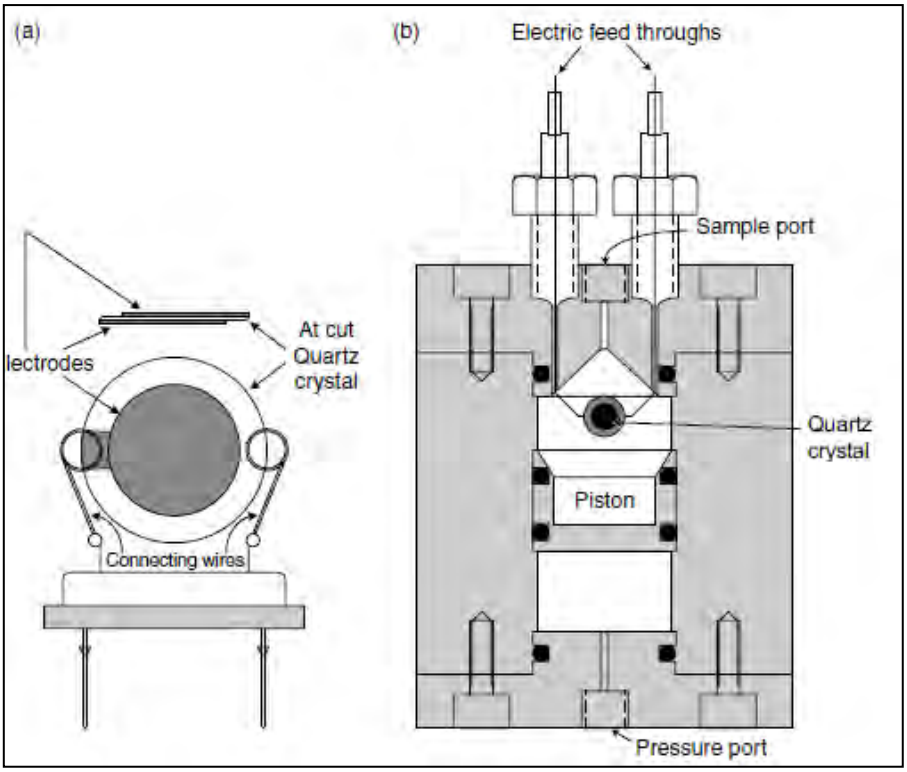


Figure 4.1: (a) Quartz crystal microbalance (b) Quartz crystal microbalance in high pressure apparatus extracted from (Sloan and Koh, 2008) and (Mohammadi et al., 2003).

### 4.1.2 Cailletet

The Cailletet tube is filled with the test fluid and the sample is degassed. Mercury is pressed on a known quantity of ethane gas at the top of the measuring tube and simultaneously cooled with liquid nitrogen, as seen in Figure 4.2. The Cailletet is placed in the high pressure equipment. The temperature is set to a specific value while the volume is adjusted until hydrate formation occurs. The pressure is measured and monitored until a constant pressure is obtained. This is known as the hydrate dissociation point. This equipment requires visual observation and may be used for temperatures between 250 K and 450 K with pressures up to 18 MPa (Peters et al., 1987). From examined literature, this apparatus is no longer used as mercury is highly toxic and the equipment is vulnerable to mechanical degradation due to the regular volume adjustments.

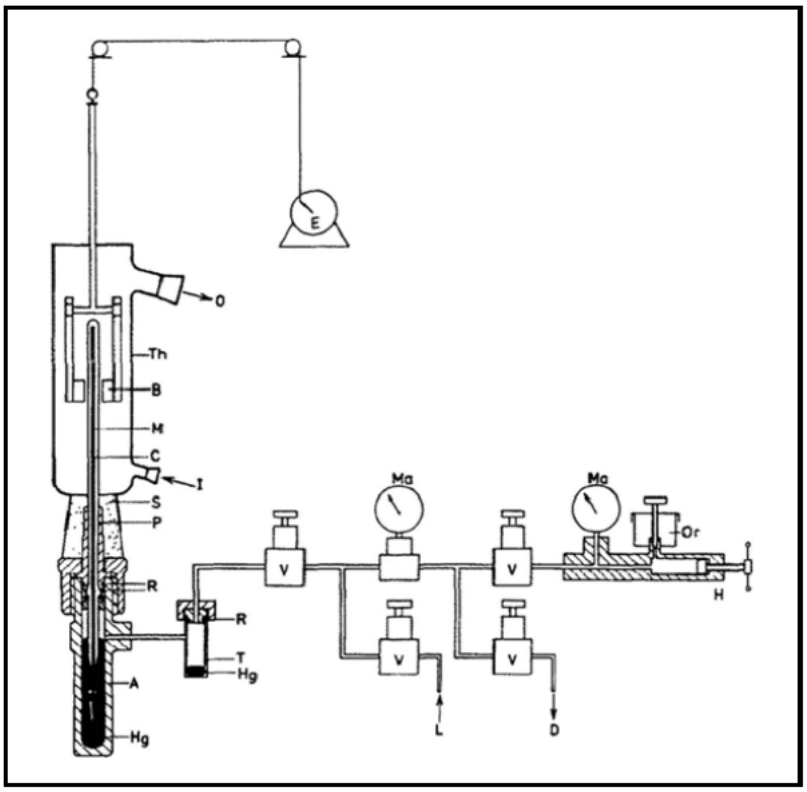


Figure 4.2: Cailletet apparatus. A, autoclave; B, magnets; C, Capillary glass tube; D, drain; E, motor; F, metal stirrer; Hg, mercury; I, thermostat liquid - in; L, line to dead weight pressure gauge; M, investigated mixer; Ma, manometers; O, I, thermostat liquid – out; Or, hydraulic oil reserve; P, closing plug; R, viton O rings; S, silicon rubber stopper; T, mercury trap; Th, glass thermostat; V, valve (Sabil and Bin, 2009).

### 4.1.3 Rocking cell

A high pressure cell is placed on a horizontal pivot for 180° pneumatic controlled rocking, as seen in Figure 4.3. The rate at which the cell is rocked is dependent on the required degree of mixing. This type of equipment can withstand a pressure of 50 MPa, a temperature range of 243.15 K to 323.15 K and is usually used in an isochoric experimental method (Najibi et al., 2009). From reviewing literature, the rocking cell experimental set up is no longer used as it is subject to mechanical deterioration due to the continuous rocking motion. Other methods of agitation include magnetic stirring (Mohammadi et al., 2008a), the flow wheel (Sloan and Koh, 2008), ultrasonic vibration (Maeda et al., 2008) and the use of a Thermolyne orbital shaker (Makogen and Sloan, 1994).

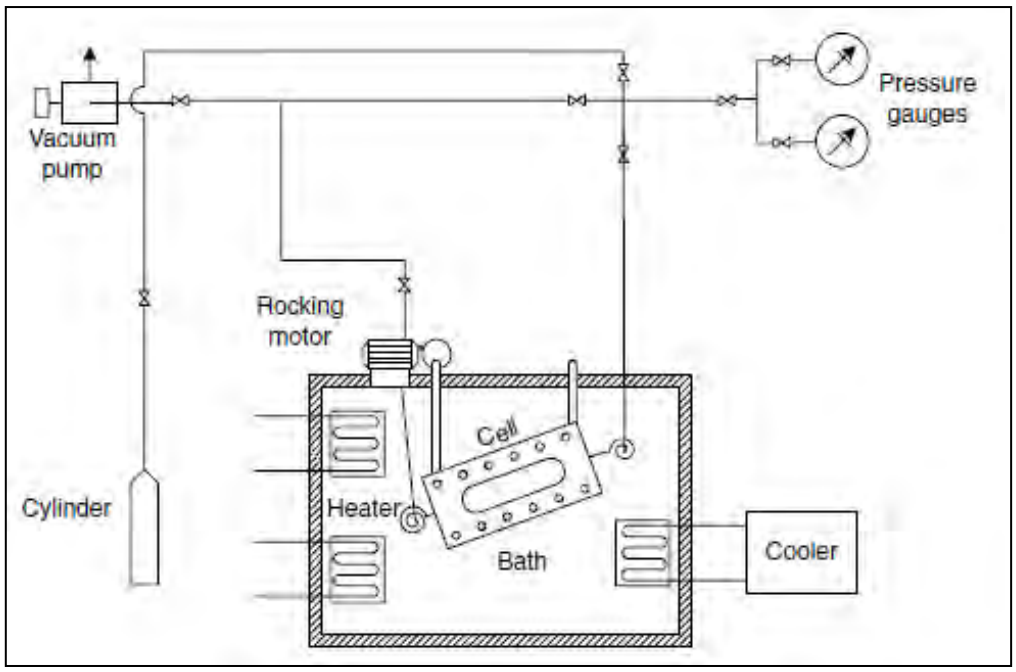


Figure 4.3: Rocking hydrate equilibrium apparatus (Sloan and Koh, 2008).

4.1.4 High pressure differential scanning calorimetry

The differential scanning calorimetry device contains two pressure-controlled cells, a sample cell which contains the fluid and the reference cell which remains empty. The sample cell is placed in the furnace, as seen in Figure 4.4, where it is purged and the pressure is set to a constant specified value (Mayoufi et al., 2009). The isochoric pressure search method is used to obtain the hydrate dissociation point. The hydrate dissociation temperature is the crest of the hydrate progressive dissociation peak as seen in Figure 4.5 (Deaton and Frost, 1946). From a literature analysis, this type of equipment was not chosen as interpreting the results may prove complex and measurement uncertainty may prove to be large.

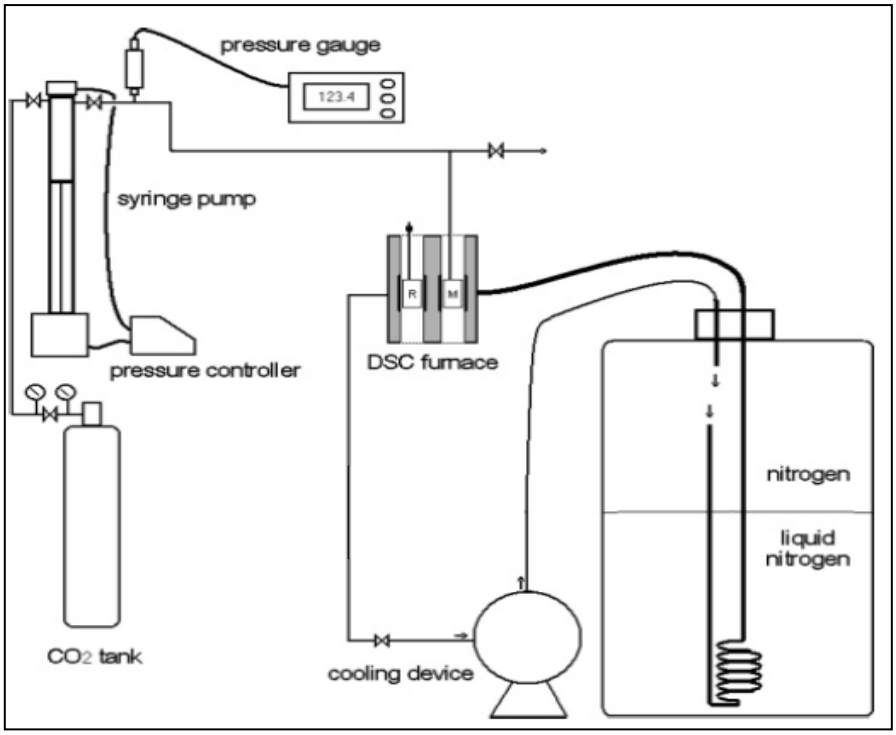


Figure 4.4: High pressure differential scanning calorimetry equipment (Delahaye et al., 2005).

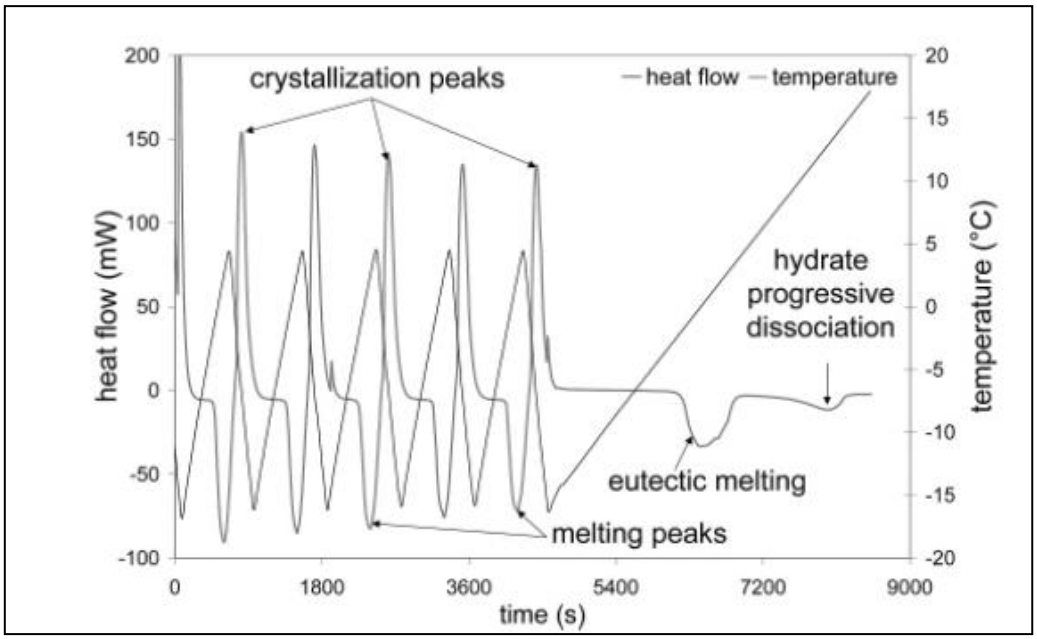


Figure 4.5: Temperature and heat flow signals of a hydrate formation and dissociation for high pressure differential scanning calorimetry (Delahaye et al., 2005).

4.1.5 Differential thermal analysis (DTA)

The DTA signal is obtained from the difference between two cell temperatures (refer to Figure 4.7). The increasing peaks indicate the formation of crystals while the decreasing peaks indicate hydrate decomposition. This can be observed in Figure 4.6. The temperature at the crest of the dissociation peak is known as the hydrate dissociation temperature (Delahaye et al., 2005). The dissociation temperatures may be obtained by maintaining a constant temperature while increasing and decreasing the pressure in cycles to obtain the cooling and heating rates (Fournaison et al., 2004). From a literature review, this equipment was not chosen due to its complex set up and the potential difficulty in interpreting results.

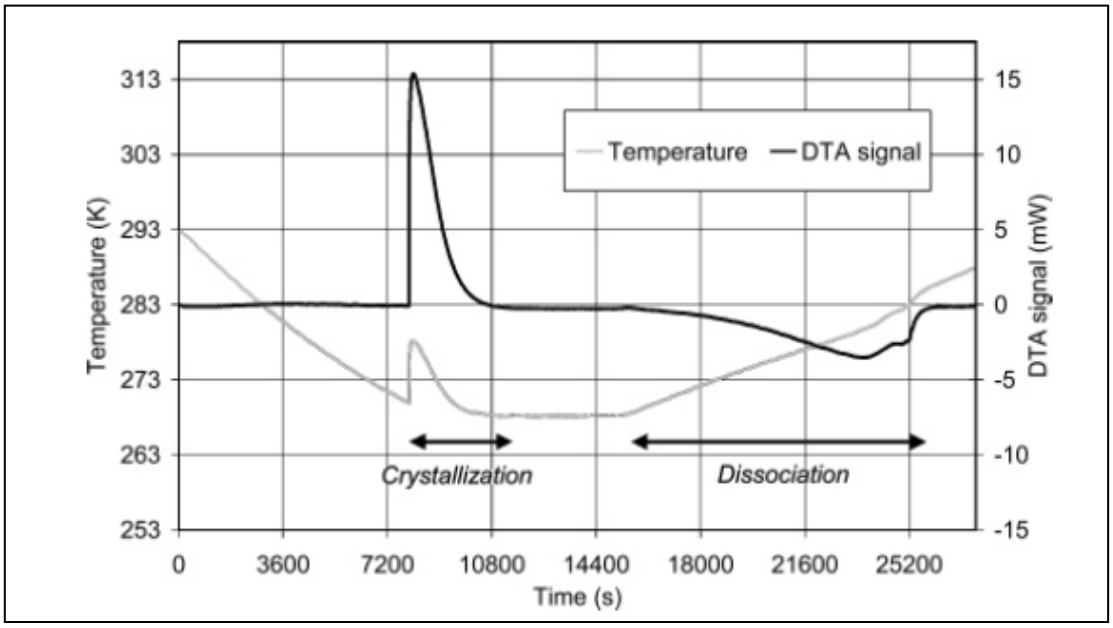


Figure 4.6: Temperature and DTA signals of a hydrate formation and dissociation for differential thermal analysis (Delahaye et al., 2005).

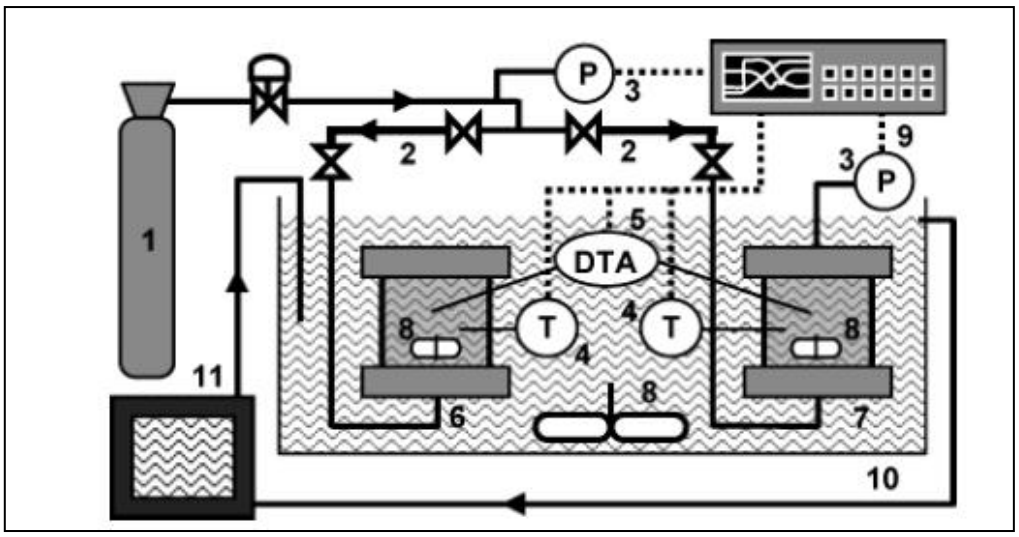


Figure 4.7: Differential thermal analysis equipment. 1, Gas cylinder; 2, injection tube; 3, pressure gauge; 4, thermocouples; 5, differential thermal analyzer; 6, reference cell; 7, measuring cell; 8, stirrer; 9, acquisition interface; 10, temperature controlled bath; 11, cooling/ heating unit (Fournaison et al., 2004).

### 4.1.6 High pressure autoclave cell

A high pressure cell may be composed of sapphire or 316 stainless steel. The cell volume may be between 30cm$^3$ and 2000 cm$^3$; this is dependent on whether the cell has a variable or fixed volume (Kang, Chun et al., 1998; Herri, Bouchemoua et al., 2011). The cell volume is varied using a floating piston. The high pressure autoclave cell may be non-visual or visual; for the latter there are two sapphire or flexi glass windows fitted into the cell for observation. The high pressure cell is immersed in a bath, containing ethanol, ethylene glycol or silicon oil, for temperature control. The type of solution used in the bath is dependent on the temperature range required. Due to their heat capacity, ethanol is used for low temperatures, ethylene glycol for moderate temperatures and silicon oil for high temperatures. A magnetic stirrer is placed in the cell for agitation. In some high pressure autoclave cells, baffles are used to reduce vortex formation (Lee et al., 2005). One of three experimental methods; isothermal pressure search, isobaric temperature search or isochoric pressure search methods, is used to determine the hydrate dissociation point. This type of setup was chosen as it is simple to construct and operate, is capable of sampling the cell contents if required, is compatible with many chemicals and all fittings and o-rings are easily available for replacement. This type of high-pressure equilibrium cell with the auxiliary equipment is easily in the laboratories

for measurements. Slight modifications are necessary for gas hydrate measurements; this is discussed in Chapter 5.

## 4.2 Experimental method review

### 4.2.1 Isothermal pressure search

Two procedures are available for this method: the visual and non-visual techniques. The visual technique requires setting the temperature to a specified value and increasing the pressure higher than that predicted for equilibrium. Once hydrates are observed, the pressure is gradually reduced to allow the hydrates to dissociate. When all the hydrates have disappeared, the pressure is increased in small increments until hydrates appear. If the hydrates disappear, the pressure is raised slightly until the hydrates reappear. At the specified temperature and pressure, if the hydrates are able to remain intact for 6 hours, the hydrate equilibrium pressure is obtained (refer to Figure 4.8). To avoid errors due to hysteresis, this process is repeated a number of times for the specific temperature (Englezos and Ngan, 1994). This process may be time-consuming as it is a trial-and-error method.

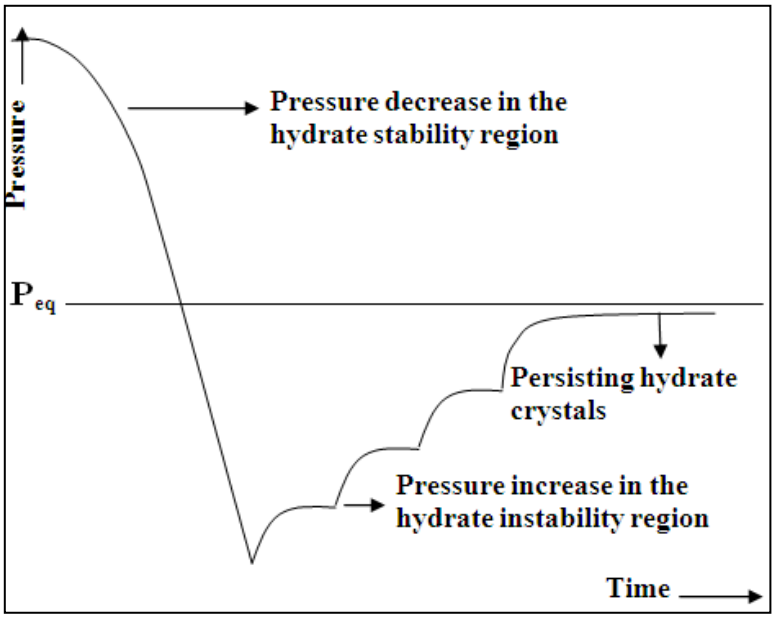


Figure 4.8: Visual isothermal pressure search technique extracted from (Tumba, 2010).

The non visual technique involves setting the temperature to a specified value and allowing hydrate formation which is noted by the decrease in pressure. Once equilibrium is established, the pressure is decreased below the expected equilibrium by gas ventilation. The hydrates dissociate thus increasing the pressure to a new equilibrium point and the pressure is then increased (refer to Figure 4.9). This process is repeated until a 2% error is obtained between the upper and lower equilibrium pressures (Makogon and Sloan, 1994). As with the visual method, this process may be time consuming as it is a trial-and-error method.

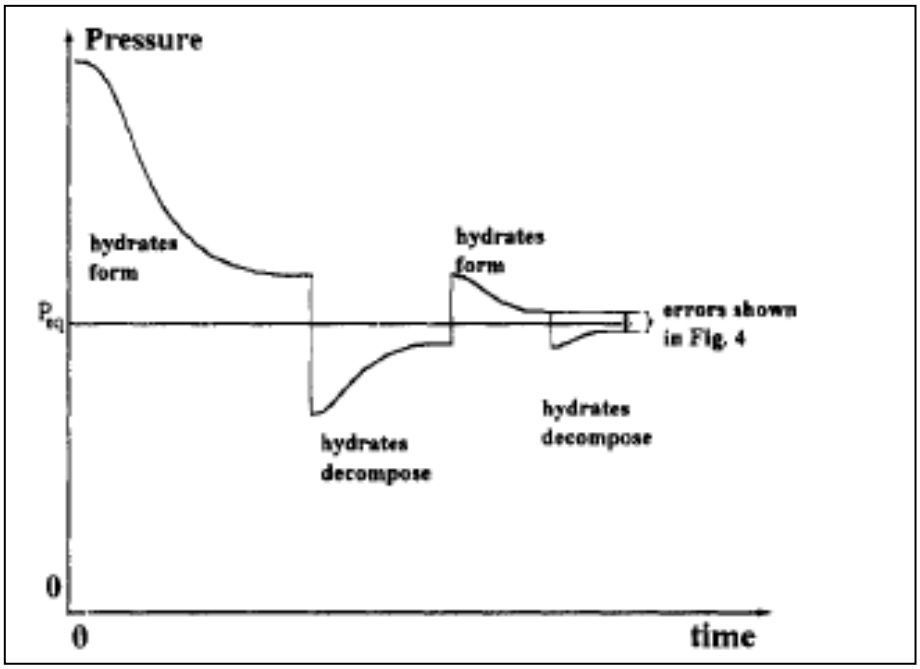


Figure 4.9: Non Visual isothermal pressure search technique (Makogen and Sloan, 1994).

4.2.2 Isobaric temperature search

The pressure is set to a specified constant value where the hydrate phase, vapour phase, liquid water phase and organic liquid phase are established. The temperature is increased in increments of 0.5 K every 10 minutes until hydrate dissociation occurs (refer to Figure 4.10). When bubbles are observed, the temperature is increased by 0.1 K until the hydrates dissociate completely. The temperature at which this occurs is called the hydrate dissociation temperature (Sabil and Bin, 2009). A clear window is required to observe the bubbles.

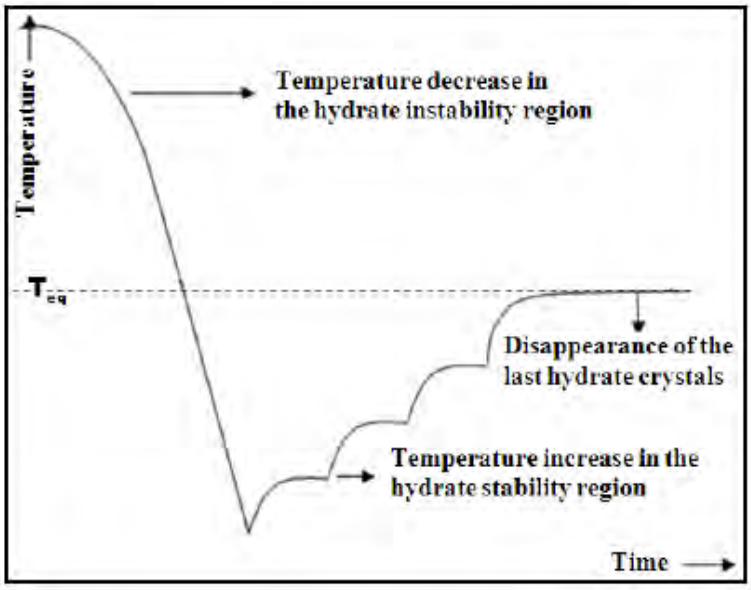


Figure 4.10: Isobaric temperature search technique extracted from (Tumba, 2010).

### 4.2.3 Isochoric pressure search

The initial temperature and pressure is set in the hydrate instability region. The cell temperature is lowered, from A to B (refer to Figure 2.4), known as the induction period, resulting in a decrease in pressure. The induction time is dependent on the degree of mixing, the rate of mass or heat transfer, the surface area available and the composition of the mixture. At point B, known as the turbidity point, hydrates form and the pressure suddenly decreases to point C, known as the catastrophic growth period or the stationary point. The temperature is increased by 0.1 K/h thus increasing pressure as the hydrates dissociate. At point D, the hydrates are fully dissociated as all the gas is released from the crystal. The hydrate dissociation temperature and pressure occurs at point D, the intersection of the heating and cooling curves. This method is chosen as it is independent of the visual observation. With the setup being a closed system, it is safer to use under high pressures (Sloan and Koh, 2008; Sabil, Duarte et al., 2010).

# CHAPTER FIVE

## DESCRIPTION OF THE EXPERIMENTAL APPARATUS AND PROCEDURE

The static method was chosen to determine hydrate-vapour-liquid equilibria. This was due to reduced time and cost for construction and maintenance. Additionally spare parts for this method were easily available when compared to the dynamic method.

This chapter describes the apparatus used in this work which includes the high pressure static equilibrium cell, agitator, liquid bath, temperature controllers as well as temperature probes and pressure transducers. The instrument accuracy and limitations were also discussed. Additionally, the type of materials used and their purity are mentioned.

The experimental procedure including leak testing, temperature and pressure calibrations, cell preparation, sample preparation and vapour pressure testing are discussed in this chapter.

### 5.1 Experimental apparatus

A high pressure static apparatus (Tshibangu, 2010) was used for the experimental measurements. The apparatus consists of:

- the equilibrium cell;
- equilibrium cell content agitation;
- the liquid bath;
- temperature controllers ; and
- temperature and pressure sensors.

The reader is referred to Figures 5.1 and 5.2 for the equipment layout.

The equipment commissioned by Tshibangu (2010), was modified to measure hydrate phase boundaries. This included replacing the air bath with a polycarbonate liquid bath, to withstand the temperature during hydrate formation and dissociation, and to view the contents in the cell. A second transducer was added to the equipment by means of a “T-junction” separated by a 1.5 mm

Two-way valve. This allowed for the measurement of low pressure (0-1 MPa) and high pressure (0 to 10 MPa). As a result, it was easier to obtain measurements for pressures in a desired pressure range. The valve was closed off when the pressure reached above 1 MPa. This ensured that no high pressure was applied on the low pressure transducer.

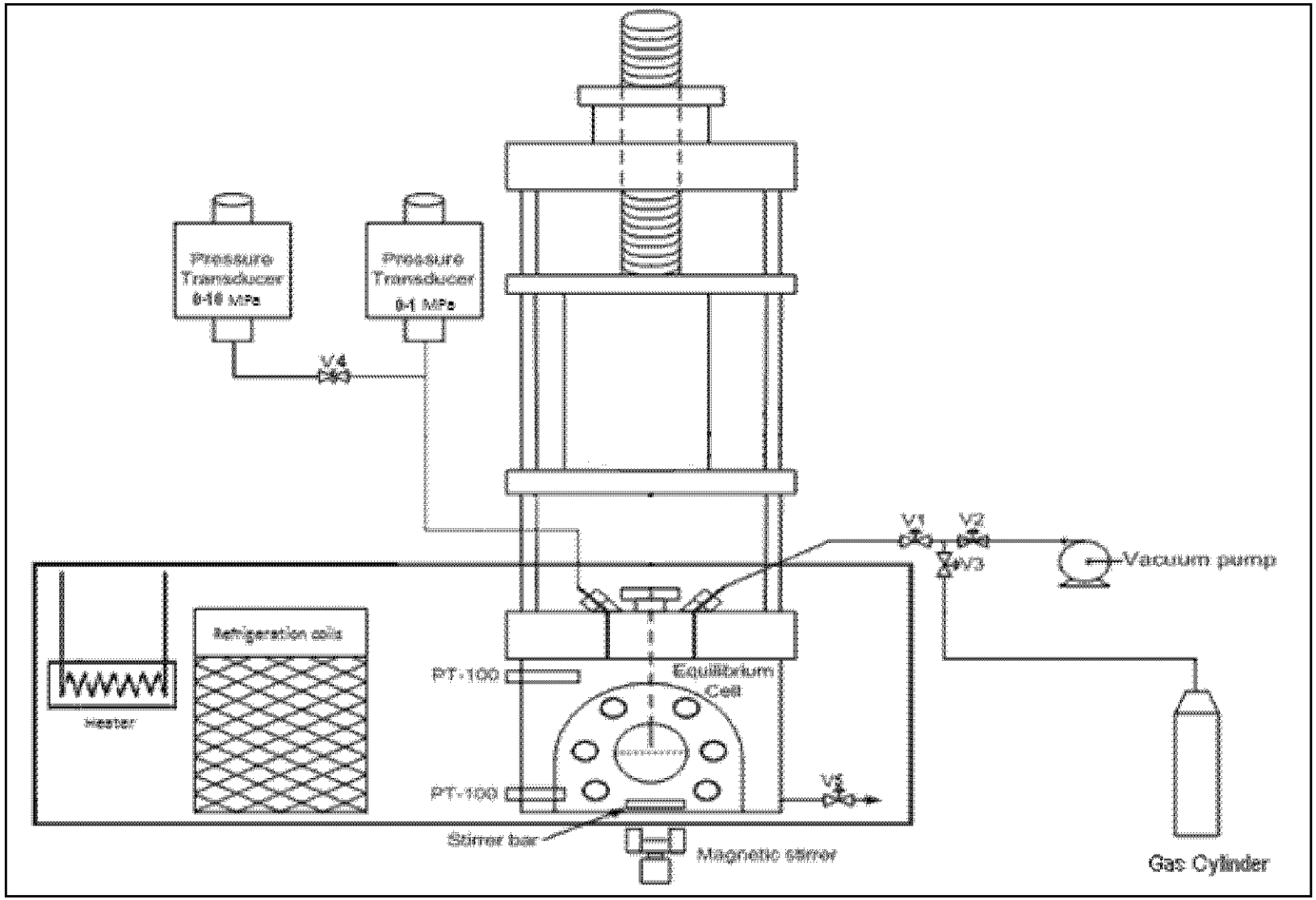


Figure 5.1: Layout of the experimental apparatus for high pressure phase equilibrium measurements (Tshibangu, 2010).

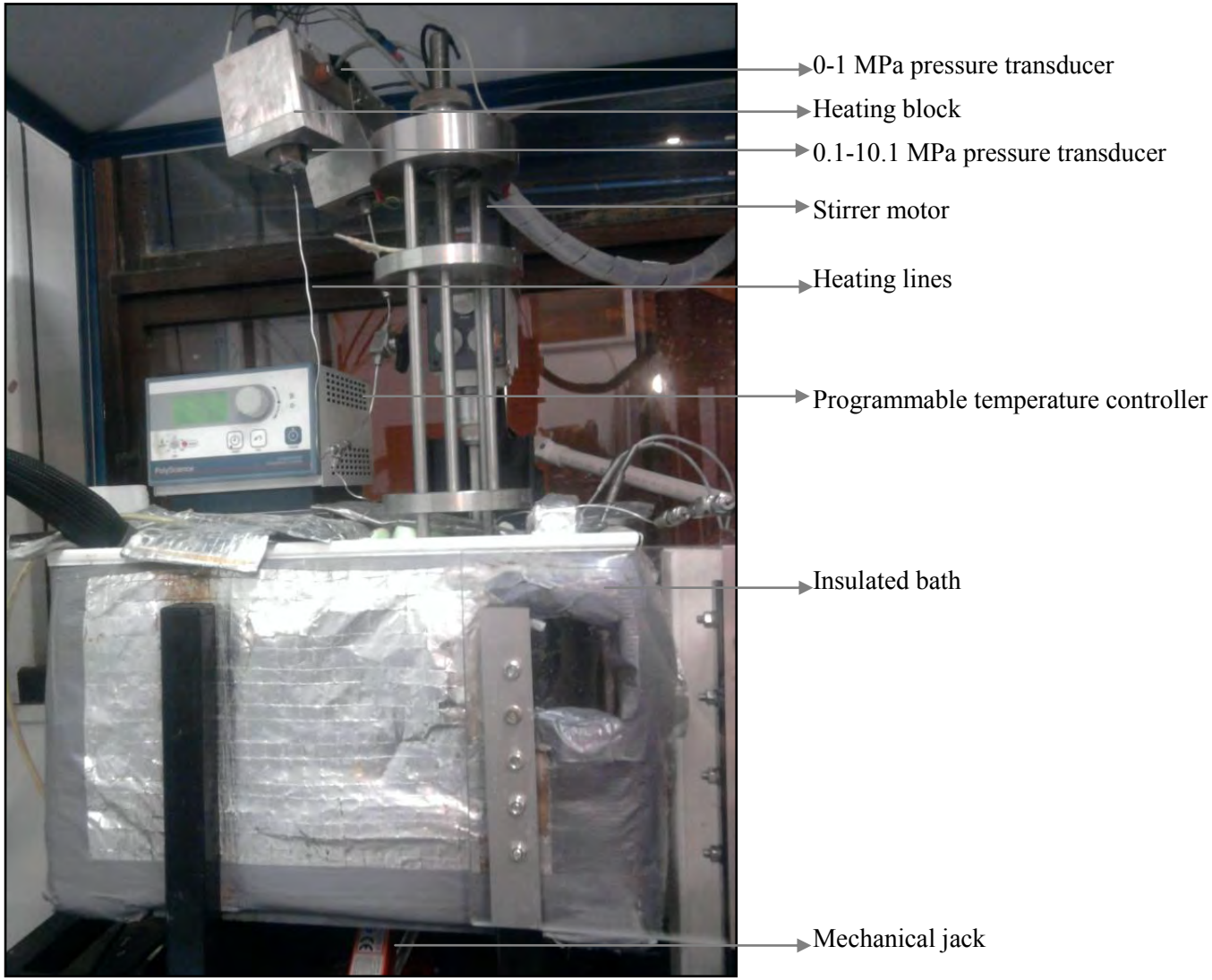


Figure 5.2: Photograph showing the layout of the experimental apparatus for high pressure phase equilibrium measurements.

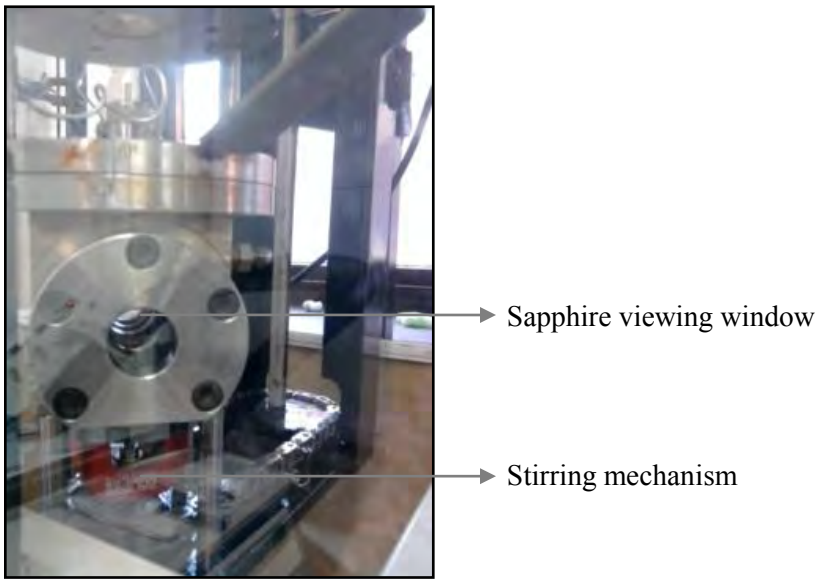


Figure 5.3a: Photograph showing the high pressure static equilibrium cell.

Figure 5.3b: Photograph showing hydrates within the static equilibrium cell.

### 5.1.1 High pressure static equilibrium cell

The equilibrium cell was constructed of 316 stainless steel, due to its magnetic properties and resistance to corrosion. It has a height of 100 mm and a diameter of 60 mm. A cylindrical cavity 30 mm in diameter and 85 mm in length was drilled in the cell providing a volume of approximately 60 $cm^3$ for the cell contents. Two sapphire windows were situated on each side of the cell for observation. The windows were 15 mm thick and 33 mm in diameter and can withstand pressures of up to 20 MPa. EPG „ο"-rings, gaskets and 5 mild steel bolts ensured the windows were completely sealed on the cell (Tshibangu, 2010) (refer to Figure 5.3).

Three holes, each with a 3 mm diameter, were drilled into the equilibrium cell. The first hole, on the top right of the cell, was used for filling and evacuation of the cell contents. The second, located on the top left of the cell was used to provide the pressure transducers with vapour for pressure measurements. The third, located at the bottom of the cell, was for the discharge of liquid. All valves were bidirectional, the liquid discharge valve was supplied by Whitey while the remaining valves were supplied by Swagelok. These valves were able to withstand a pressure of up to 17 MPa and a temperature of up to 423 K (Tshibangu, 2010).

Composition analysis was not required and therefore the sampling apparatus capillary was blocked using a stainless steel stopper. This was to eliminate the sampling lines during the process of leak detection.

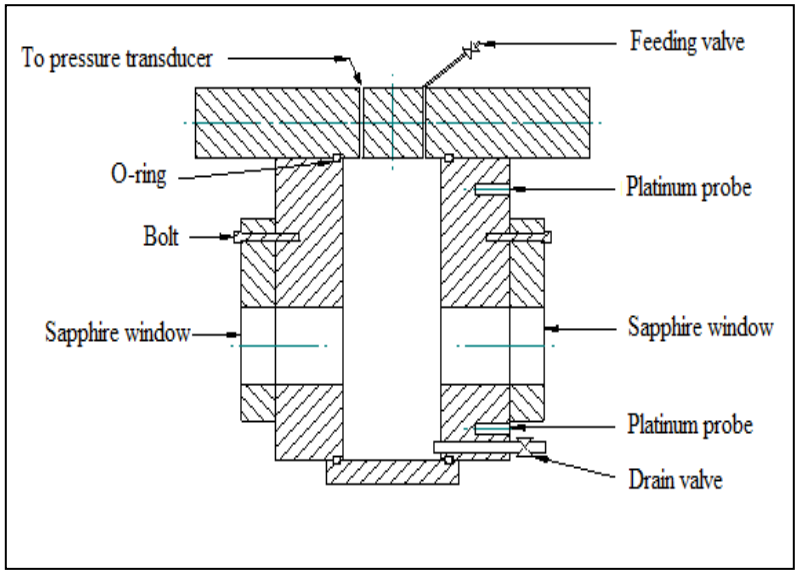


Figure 5.4: Schematic of the high pressure equilibrium cell (Tshibangu, 2010).

### 5.1.2 Agitation of cell contents

Agitation is required to reduce the time required for equilibrium to be reached. This is achieved using an impeller that has an embedded rare earth magnet, located inside the cell. A Heidolph RZR 2041 motor was used to rotate the shaft and operated between 40 and 2000 rpm with an accuracy of 0.1% of the final value.

### 5.1.3 Liquid bath

The equilibrium cell was submerged in a liquid bath to ensure an isothermal environment was created. The bath was 43 cm in length, 35 cm in width and 26 cm in height. The bath was constructed of 10 cm thick polycarbonate for observation. It contained a 30 L mixture of 80 wt% colourless ethylene glycol (supplied by Polychem) and 20 wt% water. This allowed for an operating temperature between 228 K (melting point at atmospheric pressure) and 397 K (boiling point at atmospheric pressure). The bath was completely insulated to prevent heat loss or gain from the environment.

### 5.1.4 Temperature controllers

Two heating cartridges, each with a 7 mm diameter and 40 mm length, were situated in each heating block housing the pressure transducers. This ensured the pressure transducers were maintained at a fixed temperature. The pressure transducer readings were highly sensitive to fluctuations in temperature. The transducers were maintained at 313.15 K which was the maximum temperature the experimental apparatus was expected to reach.

All lines connecting the pressure transducers to the equilibrium cell were heated with nichrome wire. This prevented condensation in the lines leading to the pressure transducer for pressure measurements.

The bath temperature was controlled using a Model 7312 programmable controller supplied by PolyScience®. The controller temperature range was 278.15 K to 473.15 K. It contained an immersion circulator pump with an internal temperature probe. The programmable controller heated or cooled the ethylene glycol water mixture in the bath which in turn heated or cooled the equilibrium cell contents to the required temperature. A programmable controller was used to control the temperature of the equilibrium cell contents at a specified rate to ensure that adequate separation between the hydrates and the salts was achieved.

An immersion cooler, supplied by PolyScience®, was used to cool the bath contents. It operated at temperatures down to 173.15 K. The refrigeration unit was composed of an evaporator, condenser, compressor and throttling valve.

### 5.1.5 Temperature and pressure sensors

*Temperature*

Two platinum resistance thermometers (Pt-100) were used to measure temperature in the equilibrium cell. The Pt-100‟s sensed temperatures between 73.15 K and 1073.15 K with an accuracy of ± 0.15 K. The probes were fixed on the equilibrium cell; one at the top and one at the bottom. This was to monitor the temperature gradient within the cell, usually 0.2 K. As a result, bath temperature uniformity could be checked. The bottom probe was used for temperature measurements as hydrates form at the bottom of the cell. The temperature probes were connected to an Agilent data acquisition where the temperature readings were electronically displayed with respect to time.

*Pressure*

Two pressure transducers, each with a stated accuracy of ±0.05% (full span) were used to provide pressure readings. Each pressure transducer was able to measure between 0-1 MPa and 1-10 MPa respectively. The 0-1 MPa pressure transducer was connected to the system by a bidirectional valve. At low pressures, the 0-1 MPa pressure transducer was used as it senses accurate pressure readings as compared to the 0-10 MPa pressure transducer. The total pressure exerted in the cell was the sum of the 1-10 MPa pressure transducer and the atmospheric pressure was measured from the DPG 2400 digital pressure gauge. The DPG 2400 was manufactured by Mensor with a stated uncertainty of ±0.012 MPa. If pressure exceeded 1 MPa, the valve was closed to ensure the pressure transducer was not damaged. The transducers were connected to an Agilent data acquisition unit (connected to a computer to log the data) which enabled pressure to be electronically displayed with time.

## 5.2 Materials

Table 5.1: Purity and supplier of the gases used in vapour-liquid equilibrium and hydrate measurements.

| Compound | Formula | CAS number | Purity / vol% | Supplier |
|---|---|---|---|---|
| R410A | | | | AFROX Ltd |
| R 507 | | 150621-87-7 | | AFROX Ltd |
| Chlorodifluoromethane, R22 | $CHClF_2$ | 74-45-6 | | AFROX Ltd |
| 1,1,1,2-Tetrafluoroethane, R134a | $C_2H_2F_4$ | 811-97-2 | > 99.9 | AFROX Ltd |

Table 5.2: Purity and supplier of the salts used in hydrate measurements.

| Compound | Formula | Purity / wt % | Supplier |
|---|---|---|---|
| Anhydrous Sodium Sulphate | $Na_2SO_4$ | > 99 | Merck (Pty) Ltd |
| Calcium SulfateDihydrate | $CaSO_4.2H_2O$ | > 99 | Merck (Pty) Ltd |
| Sodium Chloride | NaCl | > 99 | Merck (Pty) Ltd |
| Calcium Chloride Dihydrate | $CaCl_2.2H_2O$ | > 99 | Merck (Pty) Ltd |

The ultrapure water was supplied by the University of KwaZulu-Natal Chemistry Department with a 3μS conductivity. All chemicals were used without additional purification.

## 5.3 Experimental procedure

### 5.3.1 Leak testing

Leak testing was conducted to reduce errors. A leak test was executed after a line had been disconnected or a fitting replaced. This was typically done before calibrating or before hydrate or vapour pressure measurements. During low pressure leak testing, the cell was filled to a pressure of 0.9 MPa with nitrogen and the inlet valve to the equilibrium cell was closed. The equilibrium cell was filled with nitrogen gas to approximately 9 MPa at 288.15 K for high pressure leak testing. This ensured nitrogen did not condense which would have resulted in vapour-liquid equilibrium. The bath was maintained at a constant temperature to eliminate temperature fluctuations. A leak detecting fluid (SNOOP®) was applied on all fittings and connections. A leak was detected at a fitting by observing the presence of foam or bubbles. All fittings, at which such leaks were observed to occur were tightened, wrapped with thread tape or coated with Locktight. The equilibrium cell was left under vacuum to ensure the Locktight was drawn into the fittings and dried. The experimental set up was left at 9 MPa or 0.9 MPa (dependent on which lines to the pressure

transducers were checked) and 288.15 K for the same time period as the experiment. This ensured no significant pressure losses were detected over this time frame. The pressure and temperature were monitored on the data logging program; if leaks continued to occur, the valves, „o"-rings and gaskets were checked. If no leaks were detected, or the leak rate was less than the pressure transducer error over a 1 hour period, calibrations were conducted.

### 5.3.2 Calibrations

*Temperature*

Probes were placed in a silicon bath with a standard CTH 6500 probe, supplied by WIKA. For the temperature range between 73.15 K and 473.15 K, the standard state had a standard accuracy of ±0.05K. The maximum calibrated temperature accuracy was ±0.024 K. At a specific stabilised temperature, readings from the probes and standard probe were recorded. If the temperature was initially low, the temperature was increased then decreased stepwise. The effect of hysteresis was then considered. The temperature displayed on the standard probe was plotted against the Pt-100 temperature readings.

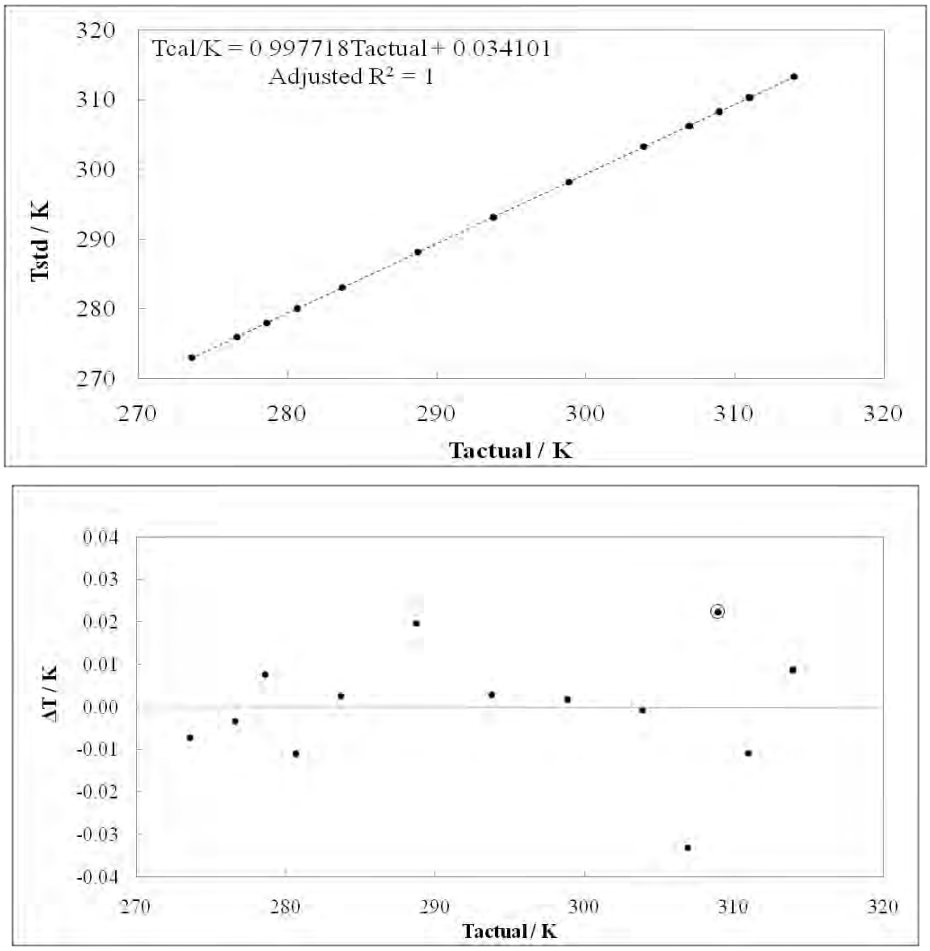


Figure 5.5: Calibration of the temperature transducer for the high pressure static cell apparatus. *Left:* First order relation between the standard and transducer temperatures. This was conducted on 31 May 2011 and verified by undertaking vapour pressure measurements in August. *Right:* Deviations from the standard temperature due to the first order relation. The symbol, ⦿; indicated the maximum deviation from the standard temperature, ±0.027 K.

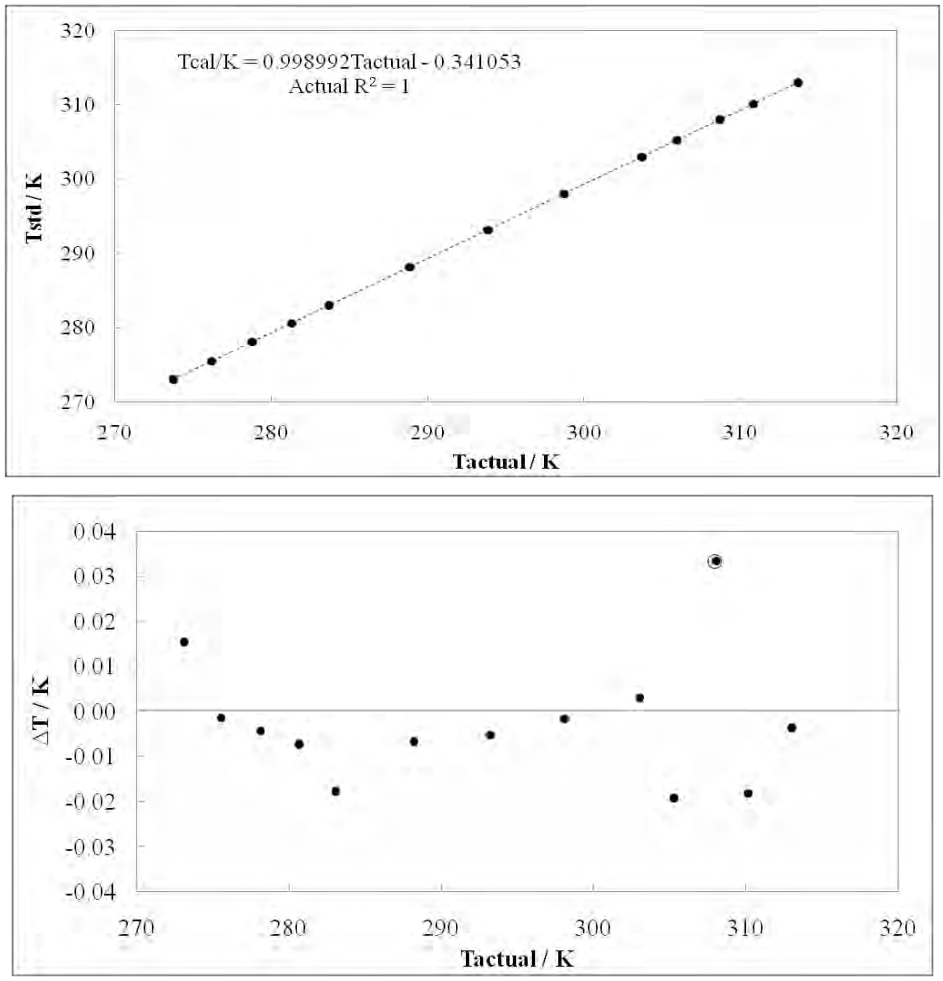


Figure 5.6: Calibration of the temperature transducer for the high pressure static cell apparatus. *Left:* First order relation between the standard and transducer temperatures. This was conducted on 22 April 2011. *Right:* Deviations from the standard temperature due to the first order relation. The symbol, ⦿; indicated the maximum deviation from the standard temperature, 0.033 K. Pressure.

*Pressure*

The pressure transducers were calibrated internally against a standard CPH 6000, supplied by WIKA. The standard transducer was able to measure pressures from 0 – 25 MPa with a stated full scale accuracy of ±0.025%. Each pressure transducer was connected to a common pressure manifold together with the standard. The standard transducer was calibrated for a temperature of 298.15 K. As a result, the standard transducer was therefore maintained at room temperature, while the transducer housing was maintained at a constant temperature of 313.15 K. The transducer was maintained at this temperature during measurements to eliminate the effect of fluctuating temperature on the calibration. At a specific pressure, the pressure readings from the pressure

transducer and the standard pressure transducer were recorded. If the initial pressure was low, the pressure was increased and later decreased stepwise. As a result, the effects of hysteresis was accounted for. The pressure transducer measurements were plotted against the standard pressure measurements and a first or second order polynomial was fitted to the data points. This was dependent on which resulted in the lowest variance.

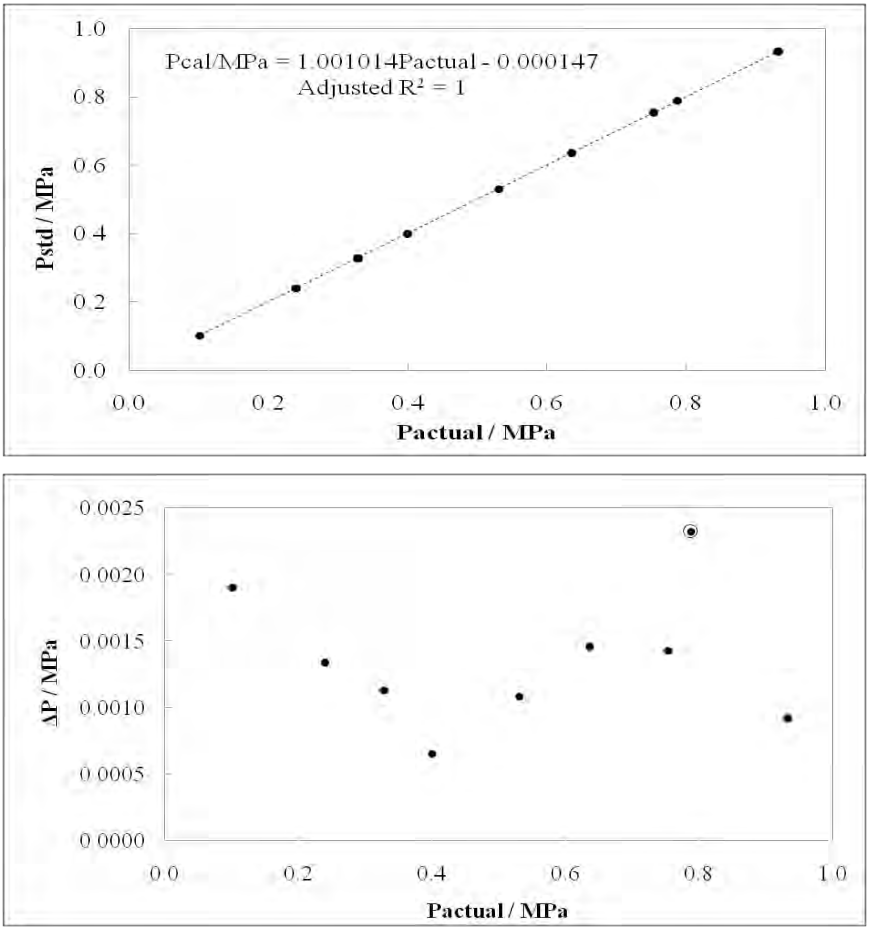


Figure 5.7: Calibration of the 0-1 MPa pressure transducer for the high pressure static cell apparatus. *Left:* First order relation between the standard and transducer pressures, conducted on 7 July 2011 and verified with vapour pressure measurements conducted in August. *Right:* Deviations from the standard pressure due to the first order relation. The symbol,⦿; indicated the maximum deviation from the standard pressure, ±2.3 kPa.

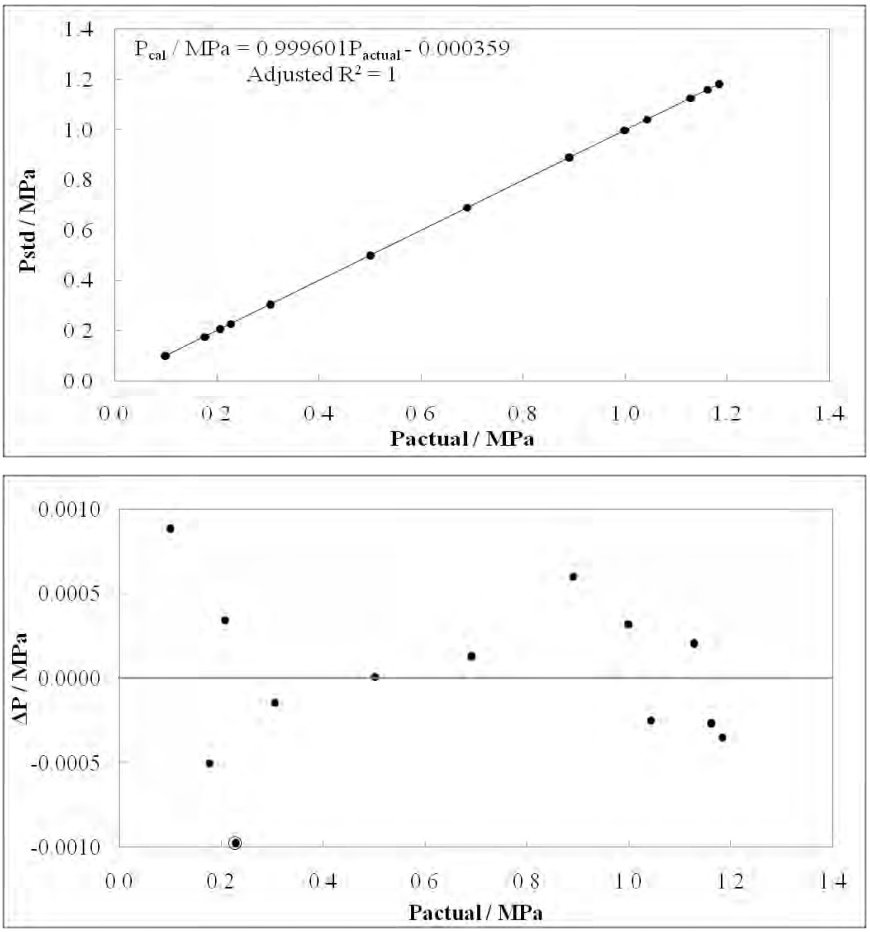


Figure 5.8: Calibration of the 0-1.6 MPa pressure transducer for the high pressure static cell apparatus. *Left:* First order relation between the standard and transducer pressures, conducted on 31 May 2011. *Right:* Deviations from the standard pressure due to the first order relation. The symbol, ⦿; indicates the maximum deviation from the standard pressure, 1kPa.

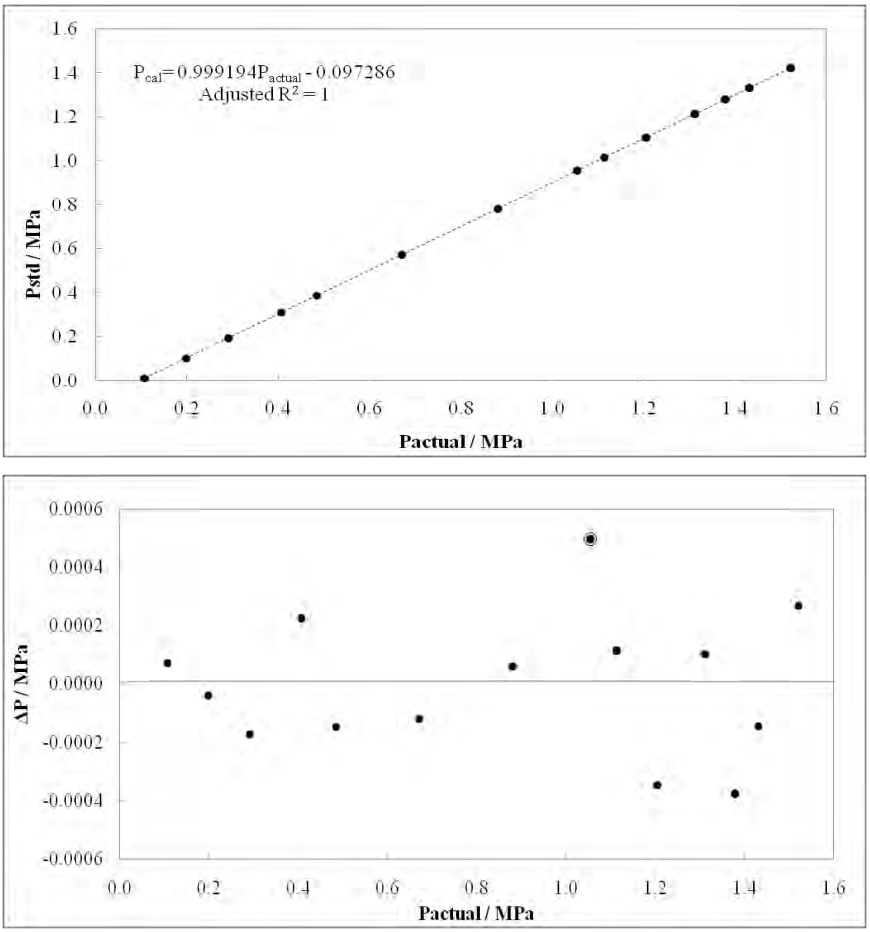


Figure 5.9: Calibration of the 0-1.6 MPa pressure transducer for the high pressure static cell apparatus. *Left:* First order relation between the standard and transducer pressures, conducted on 26 April 2011. *Right:* Deviations from the standard pressure due to the first order relation. The symbol, ⦿; indicated the maximum deviation from the standard pressure, 0.5kPa.

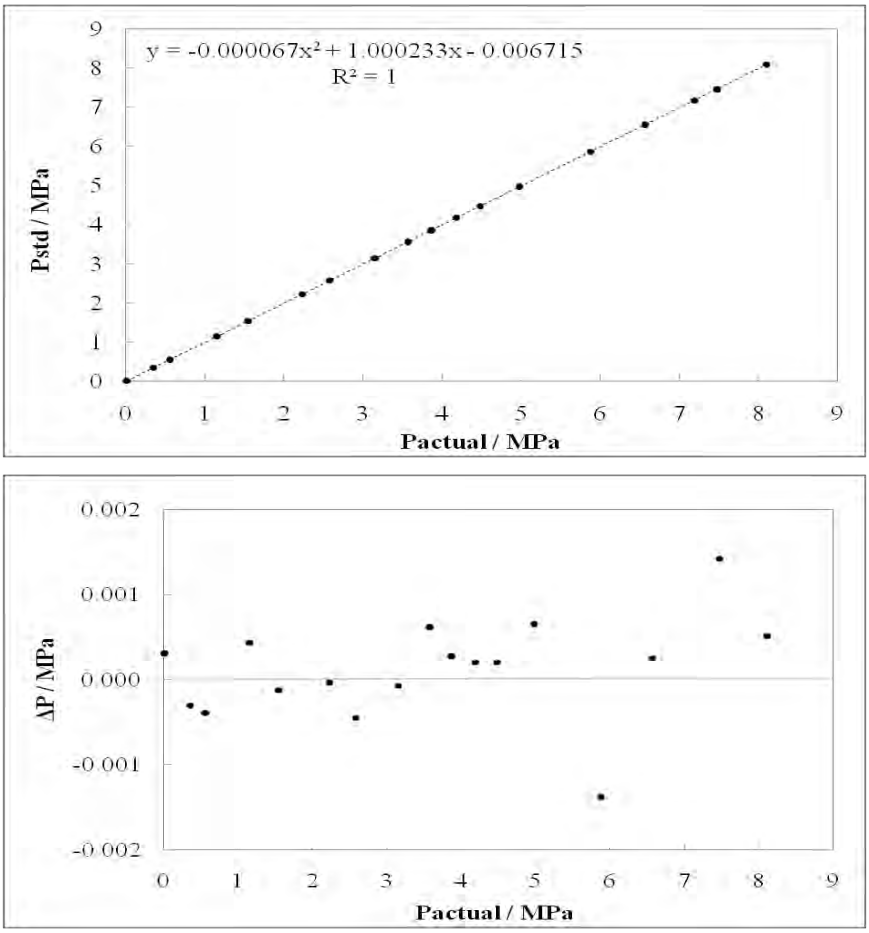


Figure 5.10: Calibration of the 0-10 MPa pressure transducer for the high pressure static cell apparatus. *Left:* Second order relation between the standard and transducer pressures, conducted on 23 June 2011. *Right:* Deviations from the standard pressure due to the second order relation. The symbol, ⦿; indicates the maximum deviation from the standard pressure, 2 kPa.

### 5.3.3 Cell preparation

The equilibrium cell was cleaned before every run to reduce contamination of the cell contents. It was initially placed under vacuum, 0.2 kPa, for 30 minutes to remove any air or volatile residue present in the cell. Thereafter, it was pressurized with 3 MPa nitrogen and flushed through the drain valve to remove any water droplets which remained in the cell. Each time the cell was placed under vacuum, the cell was observed to ensure all the residue was removed. This was repeated twice. The cell was placed under vacuum for 30 minutes and thereafter flushed through with the gas used for measurements. This was repeated twice. Once the contents were discharged and the cell was placed under vacuum for 2 hours thereafter the hydrate measurements were conducted.

5.3.4 Sample preparation

The specific quantity of salt was weighed using a mass balance with a ± 0.0001 g uncertainty. It was added to 10 $cm^3$ of 3μS millipore water and heated and stirred at 298 K for 20 minutes. This was to ensure the salt was completely dissociated in the water. This allowed for easy injection of the solution into the equilibrium cell, eliminating changes in the initial salt concentration and preventing initial salt precipitation in the cell.

5.3.5 Vapour pressure and hydrate measurements

Calibrations were conducted and vapour pressure data were measured to verify the calibrations. After cell preparation and loading, the isochoric method was used to determine the hydrate dissociation point.

The prepared solution was filled into the evacuated cell. The line connecting the gas cylinder to the cell was evacuated prior to filling the cell to remove any air trapped in the line which could cause the composition to change. The equilibrium cell was pressurized to the initial starting pressure with the gas of the system investigated. For systems which had been previously measured, such as R22 (1) + water (2) or R134a (1) + water (2), the system was initially set to the expected hydrate dissociation pressure and a temperature outside the expected hydrate stability region (refer to the right of the equilibrium curve A-$Q_1$-$Q_2$-B in Figure 2.7). If no literature data was available such as for the system R134a (1) + NaCl (2) + water (3), the system was set to 298.15 K with the pressure below the vapour-liquid equilibrium curve at 298.15 K. This was in the hydrate instability region (refer to Figure 2.7, below the curve $Q_2$-B).

The magnetic stirrer was switched on and set to 350 rpm. Once adsorption had occurred and the system stabilised, the programmable temperature controller was set to 10 K below the expected hydrate dissociation temperature. If the temperature was above 273.15 K, hydrate phase and water phase were in equilibrium. If the temperature was below 273.15 K the hydrate was in equilibrium with ice (refer to the equilibrium curve A-$Q_1$-$Q_2$ in Figure 2.15). The temperature was slowly decreased at a rate of 1 K/h to ensure hydrate formation and a good separation between the hydrate and salt. This is known as the cooling curve. Two distinct gradients were observed in the cooling curve. A small decrease in pressure in the cooling curve indicated the nucleation process was occurring where the pressure change was primarily a function of change in temperature. This was

indicated by the vapour-liquid isochoric curve in Figure 2.4. A large decrease in pressure indicated hydrate growth had occurred and therefore hydrates had formed (refer to Figure 2.4). If no large pressure drop was observed, the temperature was further decreased or gas was added to the system to increase the pressure, until a pressure drop was observed. The formation of ice resulted in a small drop in pressure, while the formation of hydrates resulted in a large drop in pressure as the amount of gas in the vapour space was being reduced.

Once the system stabilized, temperature was increased stepwise. At each step in temperature, the system temperature and pressure were allowed to stabilize. The first step in temperature was large, 5 K. As the pressure increased to the dissociation pressure, the temperature steps became smaller until the temperature was increased in steps of 0.2 K. Two distinctive gradients were observed in the heating curve. The point at which the gradient changed was the hydrate dissociation point. Before this point, the pressure increase was large due to the hydrates dissociating and releasing the guest molecule into the vapour space. This was indicated by the hydrate-liquid-vapour curve in Figure 5.7. After the dissociation point, the change in pressure was primarily a function of temperature, indicated by the vapour-liquid isochor in Figure 5.11.

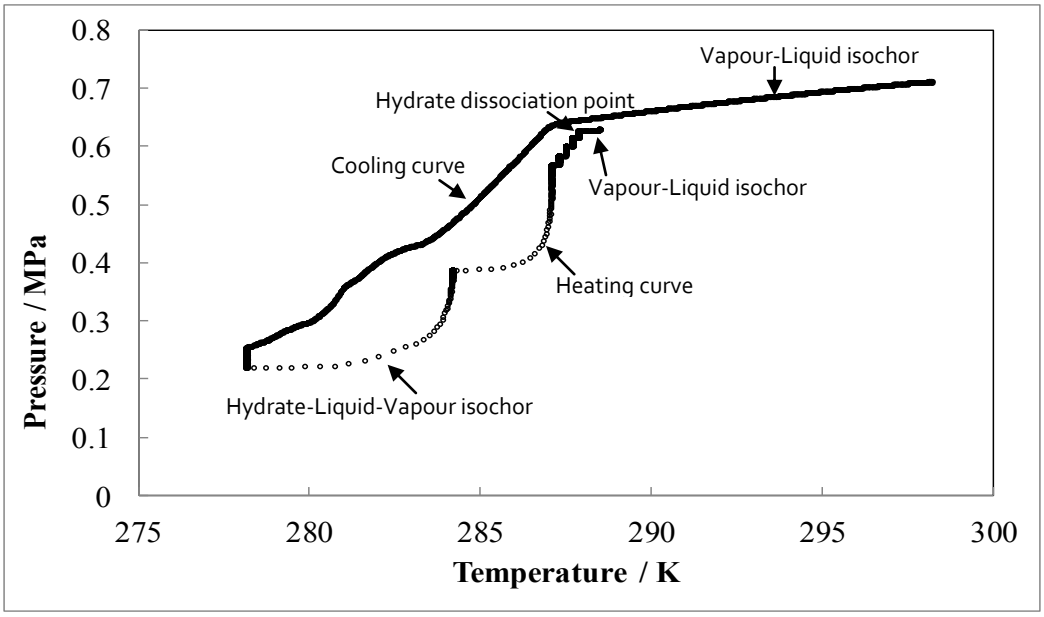


Figure 5.11: Heating and cooling curves for the system R22 (1) + water (2)

For every phase equilibrium point measured, at least three temperature steps were obtained before and after the point. This reduced the error when determining the hydrate dissociation point. At each step in temperature, the average temperature and pressure, from the last 60 minutes of each

stabilised step in temperature (including their corresponding reproducibility"s) was calculated. Second order polynomials were fitted to each gradient by considering the average temperature and pressure at each step in temperature. Solver (program in Excel) was used to find the pressure and temperature intersection of the two polynomials; this was the hydrate dissociation point (refer to Figure 5.12).

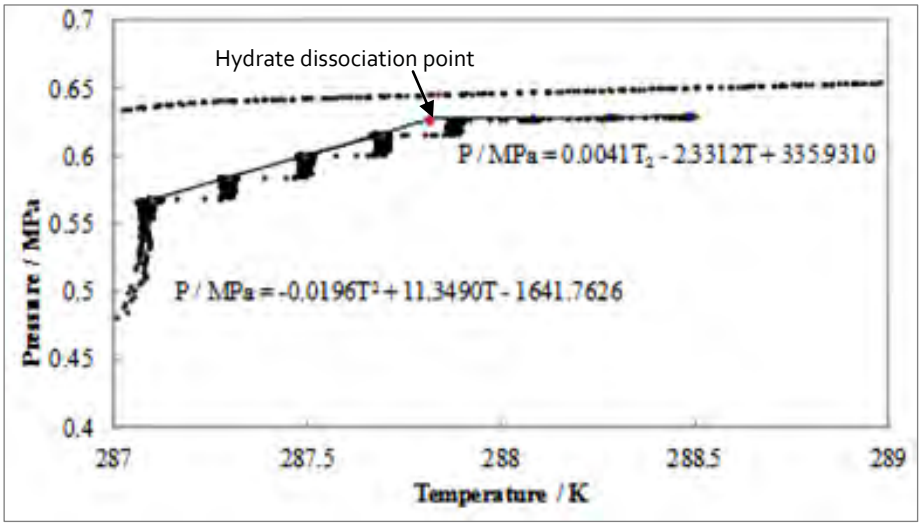


Figure 5.12: Analysis of heating and cooling curves for the system R22 (1) + water (2) to determine the hydrate dissociation point.

The hydrate dissociation point may have been found using either a linear fit or second order polynomial. The residual error when using each fit was determined and compared in Figure 5.12. The second order polynomial resulted in slightly less error and thus was used to determine the hydrate dissociation point.

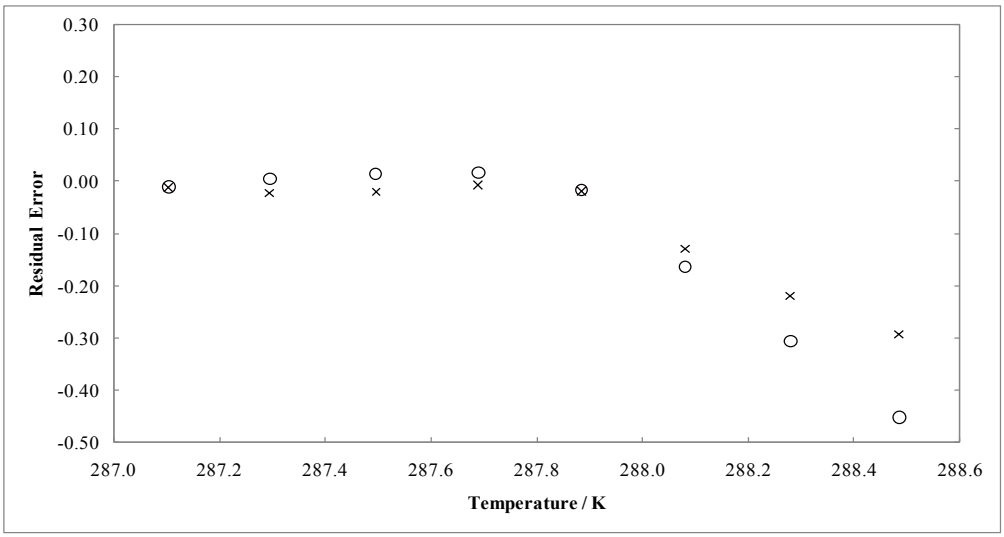


Figure 5.13: Plot of residual error; ○, linear fit and; x, second order polynomial fit for the heating curve to determine the hydrate dissociation point (refer to Figure 5.12).

In Figure 5.11, at a specific pressure, multiple temperature readings can be obtained. This was due to the bath stability. The hydrate dissociation point may be obtained by either fitting a second order polynomial to the minimum temperature, average temperature or maximum temperature at each step in pressure. The effect each method has on the hydrate dissociation point was reported in Table 5.3. An average temperature was used where the uncertainty was taken into account in terms of the repeatability of the measured variable.

Table 5.3: Uncertainty analysis in determining the hydrate dissociation point by either fitting a second order polynomial to the minimum temperature, average temperature or maximum temperature at each step in pressure.

| | **Temperature / K** | **Pressure / MPa** |
|---|---|---|
| Minimum Temperature | 287.41 | 0.63 |
| Average Temperature | 287.79 | 0.63 |
| Maximum Temperature | 287.86 | 0.63 |

The hydrate dissociation point was measured as opposed to the hydrate formation point. The latter was path-dependent and therefore was difficult to replicate. This was unsuitable for industrial purposes.

## 5.4 Uncertainty analysis for H-L-V equilibrium data and vapour pressure measurements

It was important to differentiate between accuracy, precision, error and uncertainty. Accuracy referred to how well the measured data resembled the actual data. This can be used in calibrations or in comparing literature and experimental measurements. Precision referred to how repeatable the measured data was. Error referred to how much the measured data differed from the literature or true data. Uncertainty was an interval around the set of measured data such that if a point was repeated, the result will lie within the stated interval.

### 5.4.1 Estimating uncertainty

It was important to represent uncertainty as a combination of all possible sources of uncertainty. When more than one source was found, uncertainty may be represented as the combined standard uncertainty. Uncertainty was conveyed according to NIST guidelines for reporting uncertainties; (refer to Taylor and Kuyatt (1994)).

$$u_c(x) = \pm\sqrt{\sum_i u_i(x)^2} \qquad 5.1$$

Type A uncertainties for temperature and pressure transpired from multiple transducer readings for a stable system. Type B uncertainties for temperature and pressure transpired from the polynomial used in the calibrations as well as the manufacturer"s specifications. The combined standard uncertainty for a particular variable which may be temperature or pressure:

$$u_c(x) = \pm\sqrt{u_{instrument}(x)^2 + u_{calibration}(x)^2 + u_{repeatability}(x)^2} \qquad 5.2$$

The upper and lower uncertainty limit from the temperature calibration was determined from the first order polynomial. In Figure 3.4, the uncertainty was, a = ±0.03K. Similarly for the pressure calibration in Figure 3.5, the uncertainty was, a = ±0.001 MPa and a = ±0.002 MPa for the 0-1 MPa and 0-10 MPa pressure transducers respectively. From these limits, a rectangular probability distribution was formed where there was a 100% probability the calibration uncertainty would fall in the interval. The rectangular distribution was determined by:

$$u_{calibration}(x) = \frac{b}{\sqrt{3}} \tag{5.3}$$

$$u_{instrument}(x) = \frac{b}{\sqrt{3}} \tag{5.4}$$

$$b = \left( \frac{a_{+} \pm a_{-}}{2} \right) \tag{5.5}$$

Where

Table 5.4: Pressure and temperature calibration uncertainty.

| Calibration | B | $u_{calibration}$ |
|---|---|---|
| Temperature / K | 0.03 | 0.02 |
| Pressure 0-1 MPa transducer / kPa | 0.01 | 0.40 |
| Pressure 0-10 MPa transducer/ kPa | 0.02 | 0.20 |

During an experiment, temperature fluctuations occurred as a result of inefficient liquid circulation in the bath as well as heat loss or gain to and from the environment. Additionally, the temperature and pressure fluctuations resulted from the instrument manufacturer error. The uncertainty in the temperature and pressure repeatability was measured by noting the temperature and pressure every 30 seconds for 30 minutes. From this, the uncertainty was calculated using the following equations:

$$u_{repeatabilty}(x) = \left( \frac{1}{n(n-1)} \sum_{k=1}^{n} \left( x_{i,k} - \bar{x}_i \right)^2 \right)^{0.5} \tag{5.6}$$

Where

$$\bar{x}_i = \frac{1}{n} \sum_{k=1}^{n} x_{i,k} \tag{5.7}$$

The most significant factor in the temperature measurement uncertainty was the instrument while the pressure was a contribution of the pressure calibration and instrument uncertainty (refer to Appendix F for further details) .

### 5.4.2 Reporting uncertainty

Uncertainty may be reported as the combined standard uncertainty or by including a coverage factor which indicates the measurement with its particular confidence interval. In this report, a coverage factor was not used as precise measurements were required.

$$U(x) = ku_c(x) \tag{5.8}$$

# CHAPTER SIX

## RESULTS AND DISCUSSION

### 6.1 Experimental apparatus

The two main contributions to temperature and pressure uncertainty during measurements are heat gain from the environment and fluctuating temperatures within the environment. For temperatures below ambient conditions, heat gain from the environment is reduced by placing insulation around and on top of the bath thus increasing bath stability. Fluctuating environmental temperatures are prevented by using heating blocks on the pressure transducers. This maintains these devices at a constant temperature. The block temperature set at the maximum temperature which the system measurements are expected to reach. This is 313.15 K. Although the maximum rating on the pressure transducers is 333.15 K, the pressure transducers are maintained at 313.15 K during calibrations.

Since refrigerants are not volatile, the system temperature and pressure remained below the vapour pressure curve for the systems investigated. Therefore, the stainless steel lines and fittings from the equilibrium cell to the transducers are not insulated or heated and no condensation occurred in the line. This is verified by conducting measurements on the test systems R22 (1) + water (2) and R134a (1) + water (2).

For hydrates to undergo the process of nucleation (refer to Chapter 2.3.1) the liquid phase is supersaturated with the hydrate former. With no agitation, this process requires a long time to occur. However, when the agitation is too vigorous, needle-like hydrates form. This is not desired since needle-like crystals are difficult to wash in the desalination of industrial wastewater.

### 6.2 Experimental procedure

To prevent system contamination, the static equilibrium cell is cleaned before a new system is measured. In some instances, the static equilibrium cell is washed with ethanol as it has a low vapour pressure. As a result, the ethanol can be vaporised under vacuum. The ROLSI (sampling device) and the sampling section of the apparatus is disconnected and therefore it is uncertain

whether all the ethanol is removed. To reduce this uncertainty, high pressured nitrogen is used to flush the cell. This is to remove any liquid remaining in the cell, thereafter the cell is placed under vacuum. This flushing and evacuating procedure is repeated numerous times. Very good results were obtained for the measured test systems R22 (1) + water (2) and R134a (1) + water (2), verifying that little or no contaminants were present in the cell. The cleaning procedure is undertaken for all measured systems.

Hydrate dissociation was conducted using the isochoric method (refer to Figure 2.1). It is important to start hydrate dissociation measurements outside the hydrate formation region as it allows for easier graphical observation of the hydrate dissociation point. For systems where no hydrate dissociation data and no vapour pressure data are available, such as R134a (1) + water (2) + {5, 10 or 15} wt% NaCl (3), a trial and error method is used to determine the starting temperature and pressure. The temperature is initially set to a specified value and the cell pressure adjusted until the system is in vapour-liquid equilibrium. The pressure is then released until it is several kilopascals below vapour-liquid equilibrium and the starting temperature is increased.

During hydrate dissociation, the heating curve may be obtained in one of two ways: firstly, through continuously increasing temperature with time and secondly through increasing the temperature in steps and allowing the pressure to stabilise at each step in temperature. Each process has its own sources of error. The first method is dependent on how quickly pressure changes with increasing temperature. Therefore there is a high possibility of obtaining a hydrate dissociation point at an elevated temperature. The second method is dependent on how long the system pressure is allowed to stabilise. The second method was used as it provides reduced measurement uncertainty. At a specific step in temperature, if the change in pressure over a period of one hour is less than the error on the pressure transducer as stated by the manufacturer, the system is considered stable.

Initially each hydrate dissociation point took 3 to 4 days to measure. The stirring speed was 166 rpm which required 9 hours for the pressure (at each temperature step) to stabilise. Additionally, at every step in temperature, the pressure was allowed to stabilise. Several factors were considered in order to reduce the time required for each experiment. It had no effect on the hydrate dissociation point since it is path independent. The stirrer speed was increased to 325 rpm thus requiring 5 to 7 hours for the pressure (at each temperature step) to stabilise. Complete stabilisation for the first few temperature steps in the heating curve was not required. Only the points close to the hydrate dissociation point required complete stabilisation. Although the stirrer speed was increased, it

should be noted that if the stirrer speed was too high, the temperature might have increased due to resistance created by the stirrer. As a result, the time required for cooling decreased at the expense of good separation between the salt and the hydrate.

## 6.3 Calibrations

Reliable experimental techniques are important in determining precise experimental data for phase equilibrium. Isochoric data were obtained for four unary systems. This is to verify pressure and temperature calibrations. A list of gases and their respective suppliers are provided in Table 6.1.

Table 6.1: Vapour pressure data measured for this work.

| Component | Temperature range / K | Pressure range / MPa |
|---|---|---|
| Chlorodifluoromethane (R22) | 273.0 –295.1 | 0.50– 1.45 |
| Hexafluoropropylene Oxide | 273.0 – 293.0 | 0.31 – 0.59 |
| Carbon Dioxide | 273.0 - 298.1 | 3.47 – 6.32 |
| 1,1,1,2-Tetrafluoroethane (R134a) | 273.0 - 303.0 | 0.29 – 0.77 |

The vapour pressure for the gases listed in Table 6.1 were measured and reported in Tables 6.2 to 6.5. These measured data included the components R22 and R134a. This was due to hydrate phase equilibrium data being measured for the systems containing these components. The calibrated temperature range was between 273.15 K and 313.15 K and therefore the vapour pressure measurements for each gas remained in this temperature range. Since all gas hydrate measurements were conducted below 305 K, all vapour pressure measurements were limited to this temperature.

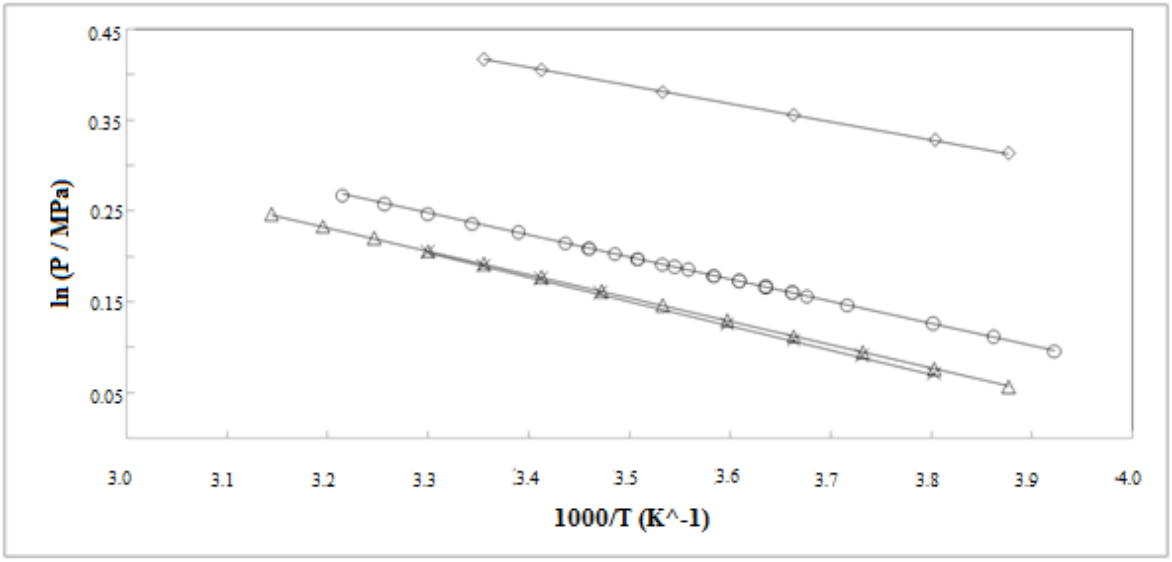


Figure 6.1: Vapour pressure data for the systems: R22: o, measured; modelled, NIST software and (Poling et al., 2001). R134a: x, measured; NIST software and (Poling et al., 2001). Hexafluoroprorylene oxide: Δ, measured; (Dicko et al., 2011). Carbon dioxide:◇, NIST software and (Poling et al., 2001). Linearly regressed data: -.

Table 6.2: Vapour pressure data for chlorodifluoromethane

| This work | | Ref 1 | Ref 2 |
|---|---|---|---|
| T / K | P /kPa | ΔP / kPa | ΔP / kPa |
| 273.03 | 494.58 | ±2.03 | ±2.26 |
| 275.03 | 527.56 | ±2.30 | ±2.43 |
| 277.04 | 562.38 | ±2.41 | ±2.56 |
| 285.06 | 718.31 | ±3.72 | ±3.66 |
| 286.94 | 761.28 | ±1.78 | ±1.65 |
| 289.04 | 806.88 | ±4.08 | ±3.93 |
| 283.04 | 677.17 | ±2.57 | ±2.49 |
| 281.03 | 636.82 | ±2.66 | ±2.72 |
| 279.03 | 598.69 | ±2.39 | ±2.56 |
| 291.06 | 854.83 | ±4.50 | ±4.25 |
| 295.05 | 955.32 | ±5.51 | ±5.11 |

Ref 1: Poling et al., 2001
Ref 2: Taylor. B. N et al., 2011

The eleven data points measured for the component chlorodifluoromethane were obtained using the 0-1.6 MPa pressure transducer between the temperature ranges stated in Table 6.1. Temperatures outside of this range resulted in a high bath instability. The results were compared to NIST software and a cubic spline fit of Poling et al. (2001) using MATLAB resulted in a maximum deviation of ±5 kPa and ±6 kPa respectively. A maximum pressure error between literature and experimental data of ±0.8 kPa was reported in Giuliani et al. (1995). There was a larger deviation in the results of this work when compared to Giuliani et al. (1995). However the percent relative error remains below 0.6%. The uncertainty in the cell content gas purity may have led to the slight deviations between literature and this work. From Equation 5.2, the measurement pressure and temperature uncertainties were ±1 kPa and ±0.09 K respectively. The calibration and instrument uncertainty were the largest contributing factors to the combined standard uncertainty.

Table 6.3: Vapour pressure data for hexafluoropropylene oxide.

| This work | | Ref 1 |
|---|---|---|
| T / K | P / MPa | ΔP / kPa |
| 293.04 | 587.79 | ±1.03 |
| 288.03 | 505.04 | ±0.62 |
| 283.02 | 431.47 | ±0.33 |
| 278.01 | 366.17 | ±0.07 |
| 273.00 | 308.61 | ±0.16 |

Ref 1: Dicko et al., 2011

There were limited vapour pressure data for hexafluoropropylene oxide in literature. Five experimental data points were measured with the 0-1.6 MPa pressure transducer between 273 K and 293 K, as seen in Table 6.3. The results were compared to a cubic spline fit of (Dicko et al., 2011) in MATLAB where the maximum deviation was ±1 kPa with a maximum relative percent error of 0.1%. The maximum literature deviation was the same as the pressure deviation as calculated using Equation 5.2 with a temperature deviation of ±0.09 K. The measured vapour pressure of hexafluoropropylene oxide was reliable and proved the temperature and pressure calibrations were correct.

Table 6.4: Vapour pressure data for carbon dioxide.

| This work | | Ref 1 | Ref 2 |
|---|---|---|---|
| T / K | P / kPa | ΔP / kPa | ΔP / kPa |
| 283.02 | 4405.81 | ±18.21 | ±5.44 |
| 272.98 | 3386.77 | ±16.50 | ±3.76 |
| 293.04 | 5626.99 | ±12.29 | ±11.11 |
| 298.05 | 6323.42 | ±4.46 | ±7.60 |

Ref 1: NIST software
Ref 2: DDBST software

The vapour pressure data for carbon dioxide was measured using the 0-10 MPa pressure transducer and compared to NIST and DDBST software; the maximum pressure deviations were ±18 kPa and ±11 kPa respectively with a maximum relative percentage error of 0.5%. A possible cause of this may have been due to a slightly contaminated gas sample, as mentioned above. The four data points measured contained temperature and pressure uncertainties of ±0.033 K and ±1 kPa respectively.

Table 6.5 Vapour pressure data for 1,1,1,2-tetrafluoroethane.

| This work | | Ref 1 | Ref 2 |
|---|---|---|---|
| T / K | P / kPa | ΔP / kPa | ΔP / kPa |
| 273.00 | 299.23 | ±0.55 | ±1.75 |
| 278.01 | 358.34 | ±0.54 | ±1.43 |
| 288.05 | 499.69 | ±0.63 | ±1.23 |
| 293.04 | 584.65 | ±0.66 | ±1.10 |
| 298.04 | 669.98 | ±0.63 | ±0.89 |
| 303.03 | 771.24 | ±0.33 | ±0.38 |

Ref 1: NIST software
Ref 2: Poling et al., 2001

The maximum temperature and pressure uncertainties for the vapour pressure data of 1,1,1,2-tetrafluoroethane were ±0.09 K and ±0.7 kPa respectively. While the maximum deviation between the six measured data points and from the NIST software was ±0.7 kPa, when compared to a spline fit of Poling et al. (2001) it was ±2.7 kPa. The maximum relative percentage error between the literature and experimental data was 0.6%. This system was measured with the 1 MPa pressure transducer and proved the temperature and pressure calibrations were correct.

The vapour pressure data for R134a was checked each time the pressure transducers or temperature probes were disturbed to ensure the calibrations were still valid. To ensure the purity of each gas in the cell remained as proximate to the cylinder purity, the cell was flushed numerous times with the measured gas and the contents were degassed prior to recording the measurements.

## 6.4 Uncertainties

Measurement uncertainties such as repeatability, calibration and instrument error was discussed in Chapter 5.4. They were represented in terms of temperature and pressure. An additional uncertainty is the water composition used in hydrate measurements. Millipore water was used to minimise the ions found in the water. This minimised the inhibition effect of the ions on the hydrate formation for systems containing no salts. A sample of millipore water with a conductivity of 1.5 μS was used for each system measured; this eliminated the effect of the initial water composition on the measurements.

Table 6.6 summarises the measurement uncertainty, which was calculated using the Equations 5.1 to 5.8 reported in Chapter 5.4. The combined standard uncertainty reported in Table 6.6 applies to all measurements conducted in this work.

Table 6.6: Summary of measurement uncertainty conducted in this work

| | **T / K** | **P / kPa** | |
|---|---|---|---|
| | | **Low pressure transducer** | **High pressure transducer** |
| Instrument error[a] | ±0.09 | ±0.50 | ±5.00 |
| Calibration uncertainty[b, c] | ±0.02 | ±0.40 | ±0.20 |
| Repeatability uncertainty[b, c] | ±0.00 | ±0.01 | ±0.04 |
| Combined Standard Uncertainty[c] | ±0.09 | ±0.64 | ±5.00 |

[a] Specified by supplier

[b] Measured

[c] $u_c(x) = \pm\sqrt{u_{instrument}(x)^2 + u_{calibration}(x)^2 + u_{repeatability}(x)^2}$

High pressure transducer: 0-10.1 MPa
Low pressure transducer: 0-1 MPa

Javanmardi et al. (2004) measured the system R22 (1) + water (2) and reported the pressure uncertainty as ±7 kPa, using a 1.378 MPa pressure transducer and temperature uncertainty of ±0.2K. Liang et al. (2001) reported a temperature uncertainty of ±0.05 K and a pressure uncertainty of ±9

kPa using a 0.9 MPa pressure transducer. The measurement uncertainties in this work were very good in comparison to literature.

## 6.5 Measured data

Table 6.7: Binary systems measured with water for HVL equilibrium

| System | Wt % Salt | Temperature / K | Pressure / kPa |
|---|---|---|---|
| R22 (1) + water(2) | 0 | 278.9 – 288.3 | 181 – 645 |
| R134a (1) + water (2) | 0 | 277.1 – 282.6 | 114 – 382 |
| R134a (1) + water (2) + NaCl (3) | 5 | 274.6 – 280.6 | 98 – 383 |
| R134a (1) + water (2) + NaCl (3) | 10 | 273.3 – 277.1 | 138 – 337 |
| R134a (1) + water (2) + NaCl (3) | 15 | 268.1 – 273.4 | 86 - 299 |

### 6.5.1 Test systems

The experimental apparatus and procedure were verified by measuring the systems chlorodifluoromethane (R22) (1) + water (2) and 1,1,1,2-tetrafluoroethane (R134a) (1) + water (2). Measurements were conducted between the upper and lower quadruple points as this was the desired operating region where no ice was present. The upper quadruple point was determined by the vapour pressure of the system measured, while the lower quadruple point was determined by the freezing point of ice (or the solution, water in this case). The difference between the experimental data and literature data may be reported in terms of temperature or pressure. Since the isochoric method was used, the error was reported in terms of pressure since the dissociation pressure was determined from the intersection of two second-order polynomials (refer to chapter 5.3.5).

#### 6.5.1.1 R22 (1) + water (2)

Table 6.8: Hydrate dissociation measurements for the system R22 (1) + water (2) system, the maximum temperature and pressure uncertainties were T = ±0.09 K and P = ±0.6 kPa respectively.

| This work | | Ref 1 | Ref 2 | Ref 3 |
|---|---|---|---|---|
| T/K | P/kPa | ΔP / kPa | ΔP / kPa | ΔP / kPa |
| 278.9 | 181.00 | ±1.58 | ±2.88 | ±6.78 |
| 282.2 | 292.62 | ±4.63 | ±9.73 | ±6.93 |
| 283.6 | 349.77 | ±5.44 | ±13.94 | ±6.33 |
| 285.7 | 467.72 | ±2.82 | ±8.12 | ±12.92 |
| 286.9 | 534.60 | ±4.34 | ±11.18 | ±14.88 |
| 287.8 | 629.92 | ±6.00 | ±8.00 | ±14.80 |
| 288.3 | 645.21 | ±3.50 | ±5.79 | ±13.33 |

$\Delta P = \left| P_{literature} - P_{experimental} \right|$

Ref 1: (Wittstruck et al., 1961)
Ref 2: (Javanmardi et al., 2004)
Ref 3: (Chun et al., 1996)

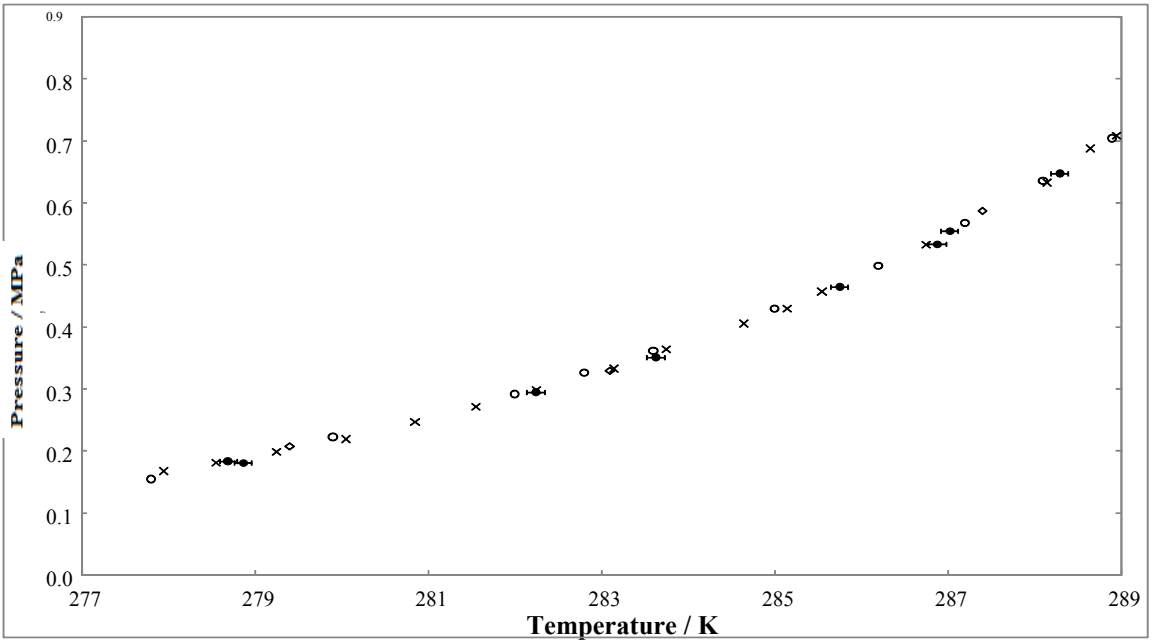


Figure 6.2: Hydrate phase boundary for the system chlorodifluoromethane (1) + water (2). •, Measured with error bars; o, (Wittstruck et al., 1961); x , (Chun et al., 1996); ◇, (Javanmardi et al., 2004).

The hydrate system R22 (1) + water (2) was measured with a combined standard measurement uncertainty of ±0.09 K and ±1.1 kPa. These uncertainties were very good in comparison to ±0.2 K and ±7 kPa, reported in Javanmardi et al. (2004) which used a glass tube equilibrium cell under isochoric conditions. No uncertainties were reported by Wittstruck et al. (1961).

A small amount of scatter was observed when comparing the data measured to those reported by Chun et al. (1996) and Javanmardi et al. (2004).A maximum pressure deviation between the literature data of ±20.80 kPa was obtained when a cubic spline curve was fitted, using MATLAB, between the data of Chun et al. (1996) and Wittstruck et al. (1961). This comparison was conducted at the temperatures measured in this work. A maximum pressure deviation of ±14.88 kPa between measured data and literature data was observed when fitting a cubic spline curve using MATLAB to the data by Chun et al. (1996) with a percentage relative error of 2.7%.

Additionally, Chun et al. (1996) compared their data to that of Berecz et al. (1983) The maximum deviation between the two data sets was ±6.7 kPa. Since the maximum deviation reported between measured data and literature data was smaller than the deviation amongst literature data, the measured data were found to be in good agreement with literature.

A pressure deviation of ±6.00 kPa between the measured data and that reported by Wittstruck et al. (1961) was considerably smaller than the other literature sources (refer to Table 6.7). The apparatus used by Wittstruck et al. (1961) was similar to that used in this work. However, the experimental procedure was considerably different. Large deviations were observed between measured data and the data reported by Chun et al. (1996). The isochoric experimental procedure was similar to that used in this publication with the following exception: the hydrate nucleation and dissociation steps were repeated. This was to reduce hysteresis while visual observation was used to determine the hydrate dissociation point.

The measured data for the system for R22 (1) + water (2) compared very well with that reported in literature. This ensured the experimental technique for determining the hydrate dissociation temperature and pressure was reliable.

6.5.1.2 R134a (1) + water (2)

Table 6.9: Hydrate dissociation measurements for the system R134a (1) + water (2).

| This work | | Ref 1 | Ref 2 | Ref 3 |
|---|---|---|---|---|
| T/K | P/kPa | ΔP / kPa | ΔP / kPa | ΔP / kPa |
| 280.7 | 249.07 | ±12.36 | ±7.94 | ±9.66 |
| 282.4 | 381.89 | ±16.87 | ±2.33 | ±10.37 |
| 281.0 | 269.40 | ±11.14 | ±9.16 | ±4.84 |
| 279.0 | 173.17 | ±7.89 | ±3.91 | ±6.21 |
| 277.1 | 114.01 | ±6.49 | ±10.41 | ±19.31 |
| 282.6 | 381.89 | ±22.27 | ±1.73 | ±11.67 |

$\Delta P = \left| P_{literature} - P_{experimental} \right|$

Ref 1:(Liang et al., 2001)
Ref 2: (Akiya et al., 1999)
Ref 3:(Eslamimanesh et al., 2011)
Predicted: $\Delta P = \left| P_{experimental} - P_{predicted} \right|$

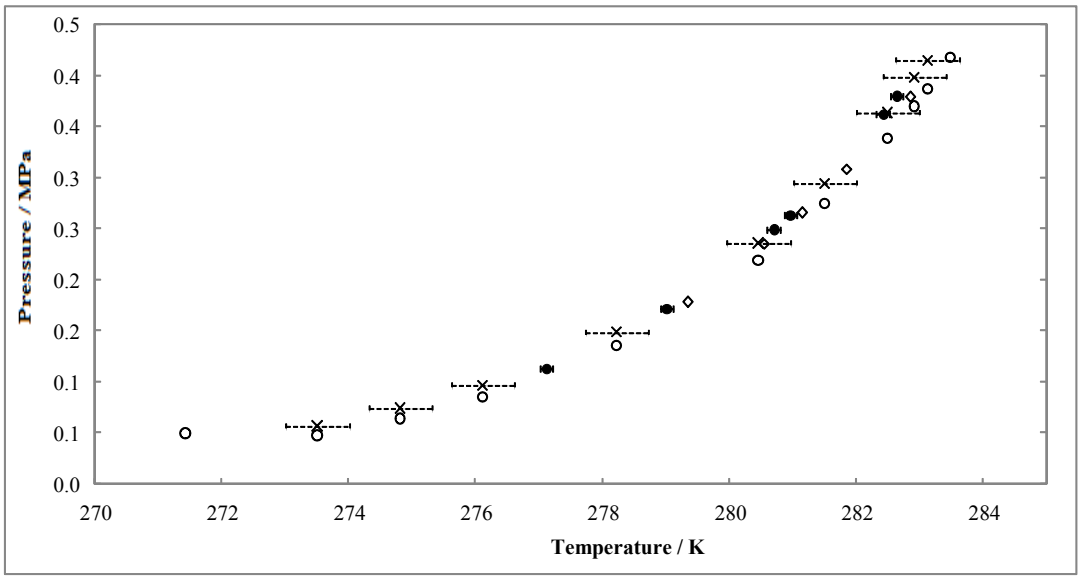


Figure 6.3: Hydrate phase boundary for the system 1,1,1,2-tetrafluoroethane (1) + water (2). •, measured with error bars; o, (Liang et al., 2001); x, (Eslamimanesh et al., 2011) with error bars; ◇, (Akiya et al., 1999).

A fair amount of scatter was observed when comparing the data of Chun (1996), Liang (2001), Akiya (1999) and Eslamimanesh et al. (2011). This was due to the uncertainties in the measurement as can be seen by the error bars in Figure 6.3. When taking the error bars into account, the measured

data for the system for R134a (1) + water (2) compared very well with that reported in literature data, thus confirming the experimental technique for determining the hydrate dissociation temperature and pressure.

At temperatures measured in this work (refer to Table 6.8) the maximum pressure deviation between the literature data of ±25.80 kPa was obtained when fitting a cubic spline curve, using MATLAB, between the data of Eslamimanesh et al. (2011) and Liang et al. (2001). A maximum pressure deviation of ±22.27 kPa between measured data and literature data was observed when fitting a cubic spline curve using MATLAB to the data of Liang et al. (2001) with a relative percentage error of ±6 %. As a result, the measured data was in good agreement with literature.

The pressure deviations between the measured data and Akiya et al. (1999) were smaller when compared with the other literature data (refer to Table 6.8). This may be due to both measurements taking place using the isochoric method. Akiya et al. (1999) reported a gas purity of 99.9 wt% and the equilibrium cell contained a four blade stirrer which may have resulted in efficient stirring. The pressure deviations between the data of Liang et al. (2001) and this work were larger than in other reported literature data. Although the same experimental procedure was used with a similar stirring mechanism, the gas purity was 99.7%. This slight difference in purity may have resulted in the deviation.

### 6.5.2 New systems

Salt depressed the water freezing point and inhibited liquid from vaporising due to the strong interactions between water and salt (refer to Table 2.13). The highest and lowest hydrate dissociation points measured were dependent on the freezing point and vapour depression data. Desalination of industrial wastewater using gas hydrate technology was not intended for operation below 273.15 K due to high energy consumption. As a result, few measurements were conducted below this temperature.

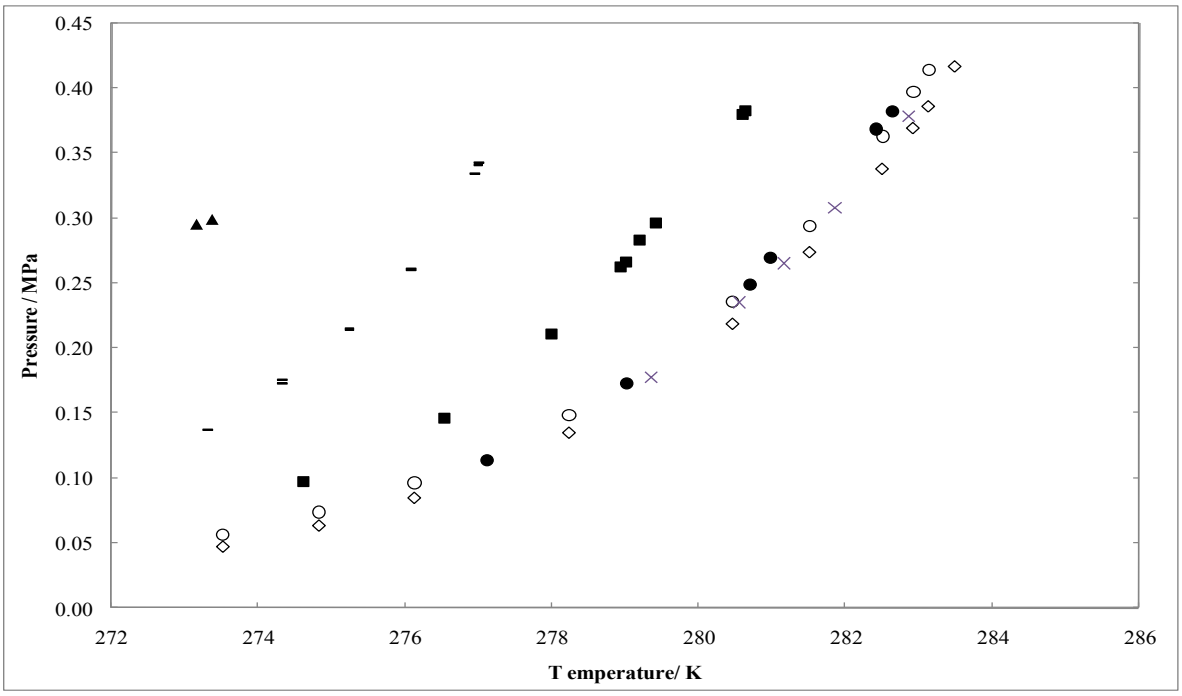


Figure 6.4: Hydrate phase boundary for the system 134a (1) + water (2) + salt (3):
o, (Liang et al., 2001) no salt; x,(Eslamimanesh et al., 2011) no salt; ◇,(Akiya et al., 1999) no salt; ● , this work; ■, this work, 5 wt% NaCl; ♦ , this work, 10 wt% NaCl; ▲ , this work, 15 wt% NaCl.

Three methods were used to verify the results as these systems had not been measured in literature. Firstly, when conducting the measurements, the measurements were not obtained in order of increasing pressure but were rather scattered. Secondly, two dissociation points were repeated which showed reliability and repeatability in the experimental technique. Lastly, a linear regression was conducted on the hydrate dissociation points using Equation 2.5 assuming compressibility was negligible. The results were in good agreement as they showed a highly linear relationship when the hydrate dissociation points were plotted on a lnP versus 1/T scale.

An increase in the system salt concentration resulted in an increased shift in temperature for a particular system for all pressures. The temperature shift for a particular system was slightly larger for higher pressures. The average shift in temperature between the system containing no salt and the systems containing {5, 10 and 15} wt% NaCl were 1.9 °C, 4.8 °C and 8.1 °C lower in temperature respectively. Therefore, as the concentration increased so the temperature shift became slightly larger. This temperature shift was similar to that of R22 with the same salt concentrations. This shift may also be reported in terms of pressure; however, to determine this shift, hydrate dissociation data beyond the HLV equilibrium curve should be measured.

Table 6.10: Hydrate dissociation measurements for the system 1,1,1,2-tetrafluoroethane (1) + water (2) + {5, 10 or 15} wt% NaCl (3).

| **5wt% / 69.4 mS/cm** | | **10wt% / 127.3 mS/cm** | | **15wt% / 171.7 mS/cm** | |
|---|---|---|---|---|---|
| **T / K** | **P / kPa** | **T / K** | **P / kPa** | **T / K** | **P / kPa** |
| 279.0 | 266.78 | 276.9 | 334.46 | 268.1 | 86.00 |
| 278.9 | 263.20 | 277.1 | 336.64 | 269.6 | 128.00 |
| 280.6 | 382.84 | 273.3 | 137.57 | 271.0 | 176.00 |
| 276.5 | 146.74 | 275.2 | 214.92 | 272.8 | 257.00 |
| 274.6 | 97.61 | 276.1 | 260.77 | 273.2 | 295.57 |
| 278.0 | 210.71 | 277.0 | 342.70 | 273.4 | 299 |
| 279.4 | 296.94 | 274.3 | 173.17 | | |
| 279.2 | 283.22 | 274.3 | 176.00 | | |
| | | 277.0 | 340.99 | | |

If the promoter cyclopentane is added to this system, it could possibly increase the hydrate dissociation temperature by 19.4 K at a constant temperature (refer to chapter 2.4.2). Had the temperature shift been used for the system R134a (1) + water (2) + 15wt% NaCl (3) + cyclopentane (4) the expected dissociation temperature range would be 287.5 K to 292.8 K. The temperature would be close to ambient conditions while the pressure less than 0.3 MPa. Therefore R134a could possibly be a suitable fluorinated hydrating agent for the desalination of industrial wastewater.

## 6.6 Enthalpy of dissociation

The enthalpy of dissociation for the systems investigated were estimated using Equation 2.5.

Table 6.11: Calculated enthalpy of dissociation for measured systems from the Clapeyron equation.

| **System** | **ΔH / kJ/mol.K** |
|---|---|
| R22 (1) + water (2) | 88.81 |
| R134a (1) + water (2) | 143.48 |
| R134a (1) + water (2) + 5wt% NaCl (3) | 146.86 |
| R134a (1) + water (2) + 10wt% NaCl (3) | 154.59 |
| R134a (1) + water (2) + 15wt% NaCl (3) | 143.23 |

Table 6.11 displays the enthalpy of dissociation calculated for the systems measured in this work (refer to Equation 2.1). Systems which formed hydrates at a lower temperature or higher pressure, such as R22 (1) + water (2), have a lower enthalpy of dissociation when compared to R134a (1) + water (2). Since salt did not take part in hydrate formation, the enthalpy of dissociation was independent on the salt concentration. However, the enthalpy of dissociation was dependent on the hydrate structure when calculated per molecule of hydrate dissociated. There was uncertainty in obtaining the enthalpy of dissociation using the Clausius-Clapeyron equation as the compressibility was assumed negligible. Therefore the enthalpy of dissociation should be measured using other recommended techniques such as calorimetrically.

## 6.7 Modelling

### 6.7.1 Description of models used

Two modelling approaches were used, one which considered gas solubility and one which assumed negligible solubility. The first approach was modelled according to Parrish (1972) while the latter was modelled according to Eslamimanesh et al. (2011).

The first approach used the direct ($\varphi$-$\varphi$) method whereby Equation 3.12 was used to describe the water fugacity coefficient in the liquid phase. The second incorporated the combined ($\gamma$-$\varphi$) method where the water fugacity coefficient in the liquid phase was described using Equation 3.13.

From Table 2.9, the solubility of $CO_2$ in water was reported as 0.9 vol/vol which cannot be neglected as reported in Tohidi, (1995). Since the solubility of R22 in water at ambient conditions was 0.78 vol/vol while R134a was 0.21 vol/vol, as seen in Table 2.11, the solubility should be taken into account in the modelling, particularly for R22. The PR EOS with Van der Waals mixing rules was used to describe the non-ideality. This EOS is common and was used due to limited information available regarding mixing parameters and vapour pressure data for the systems containing refrigerants.

Model 1: The modelling approach applied initially by Parrish and Prausnitz (1972), which was later modified by Holder and Grigoriou, (1980) was a predictive model used to verify the program. The systems $CO_2$ (1) + water (2) and $C_2H_6$ (1) + water (2) were used as test systems.

Model 2: The second modelling approach used the assumptions stated by Eslamimanesh et al. (2011). The (ϕ-ϕ) method was used in conjunction with the PR EOS to account for solubility. Therefore the objective function in terms of the calculated and experimental dissociation pressures where R134a (1) + water (2), was used as a test system. This was known as the regressed Modified Eslamimanesh et al.ʺs, Mohammadi and Richon model (MReg-EMR model). This model was then extended to account for solubility which was known as the Modified Regression Eslamimanesh et al.ʺs model extended for solubility (MReg-EMR solubility model).

Model 3: A model was then used to account for the salt in the system. The model developed by Aasberg-Petersen, et al. (1991) where the water-salt interaction coefficient was accounted for using the parameters reported in Tohidi et al. (1995). This was known as the predictive, modified Eslamimanesh, Mohammadi and Richon model extended for solubility and salts (Pred-EMR model (salt)). The system R22 (1) + water (2) + {5, 10 or 15} wt% NaCl (3) was used to verify the model while the measured system R134a (1) + water (2) + {5, 10 or 15} wt% NaCl (3) was modelled.

It was important that the optimisation function obtained the global minimum and was insensitive to changes in the initial guess for particular parameters. As a result, a differential evolution strategy was used Eslamimanesh et al. (2011). To obtain the optimal values for the predicted pressure, several adjusted parameters in the optimization algorithm may be altered. These include crossover, mutation, number of population, tolerance and bounds. The optimised value was determined by the performance of the optimised algorithm.

### 6.7.2 Model 1: Parrish and Prausnitz predictive model

This model was a predictive model used for verification of the systems $CO_2$ (1) + water (2) and $C_2H_6$ (1) + water (2). Solubility of the hydrate former was accounted for using the PR EOS with van der Waals mixing rules. The literature data used to model these systems was that reported in Parrish and Prausnitz (1972). These included the data of Morrison, (1952) for the system containing $C_2H_6$ and by Bartholome, (1956), Morrison et al. (1952) and Wiebe, (1941). For the system containing $CO_2$ small and large structure I hydrates were formed. While $C_2H_6$ formed only large structure I hydrates. The flow diagram used to predict the pressure was given in Figure 6.5 where the ASPEN flash calculation was shown in Figure C.6 in Appendix C.

Figures 6.6 and 6.7 showed the literature data as well as the predictive model for the systems $CO_2$ (1) + water (2) and $C_2H_6$ (1) + water (2) respectively. The literature data in Figure 6.7 is quite scattered. The model described the solubility at lower temperatures and pressures for both systems very well; however at higher pressures and temperatures, the model deviated from literature data. This was expected since at high temperatures and pressures, phase non-ideality became significant and the PR EOS with van der Waals mixing rules were not sufficient in describing the liquid density. Other fugacity-based models which could be used include the Patel and Teja, (1982), Trebble and Bishnoi, (1988) and Valderrama, (1990) models including quadratic or non density dependent mixing rules. An alternative was to use an activity-based model to describe the liquid phase and a fugacity-based model for the vapour phase.

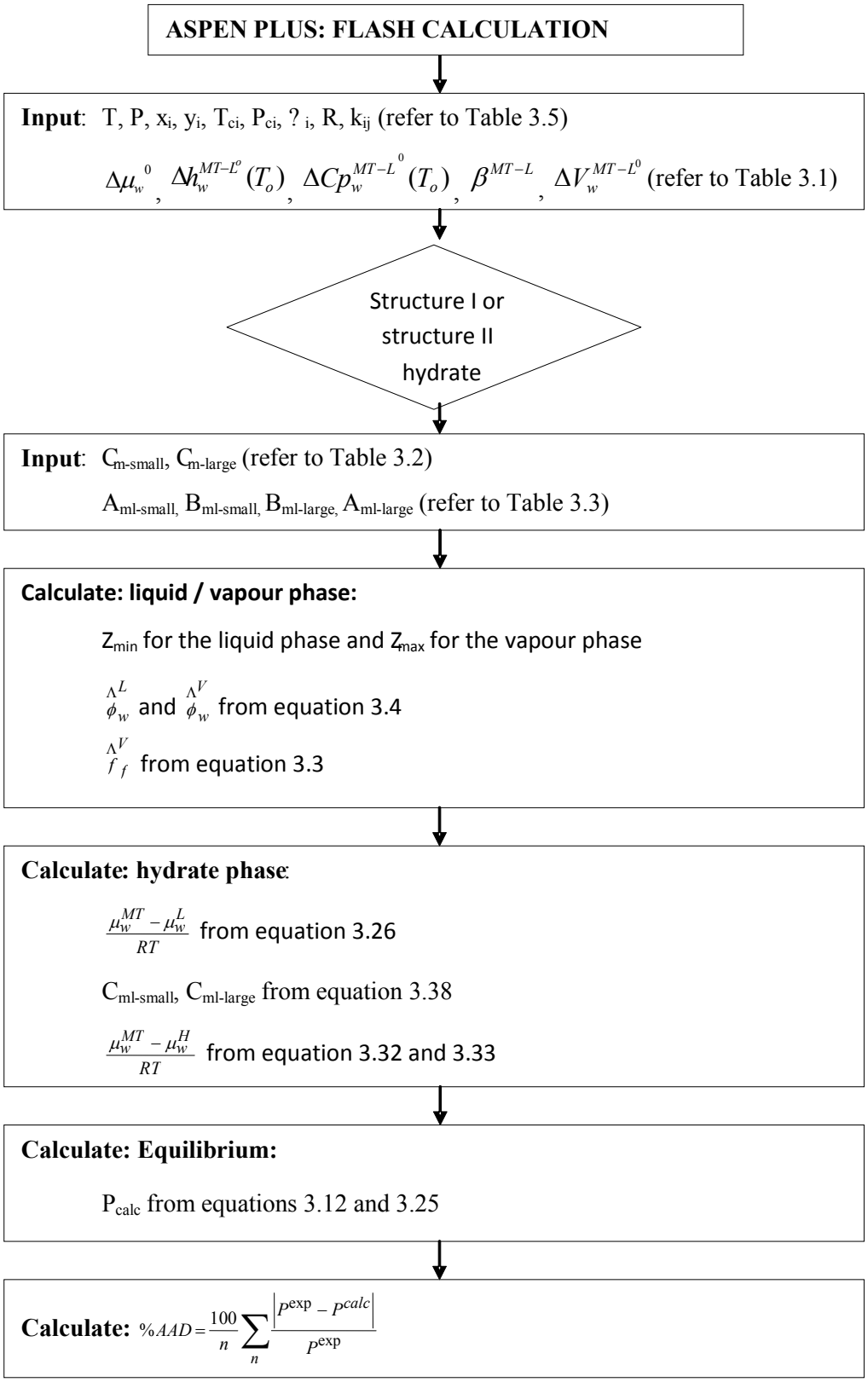


Figure 6.5: Predictive computation flow chart to verify the model developed by (Parrish and Prausnitz, 1972) which includes the solubility of the hydrate formers $C_2H_6$ and $CO_2$.

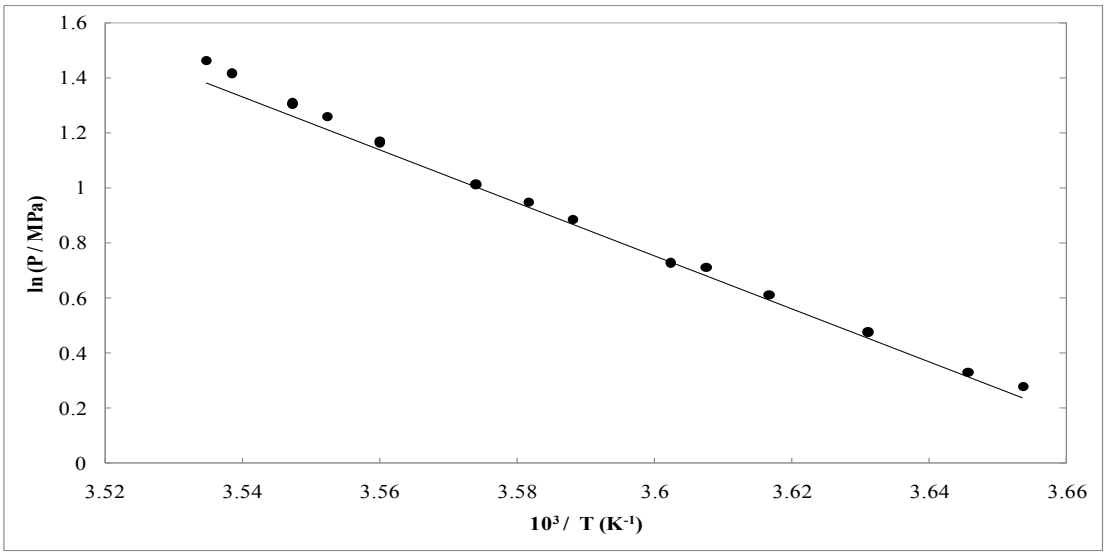


Figure 6.6: H-L-V equilibrium data for the system $CO_2$ (1) + water (2); •, Deaton and Frost (1946), Unruh and Katz, (1949);—, model 1 Parrish and Prausnitz (1972).

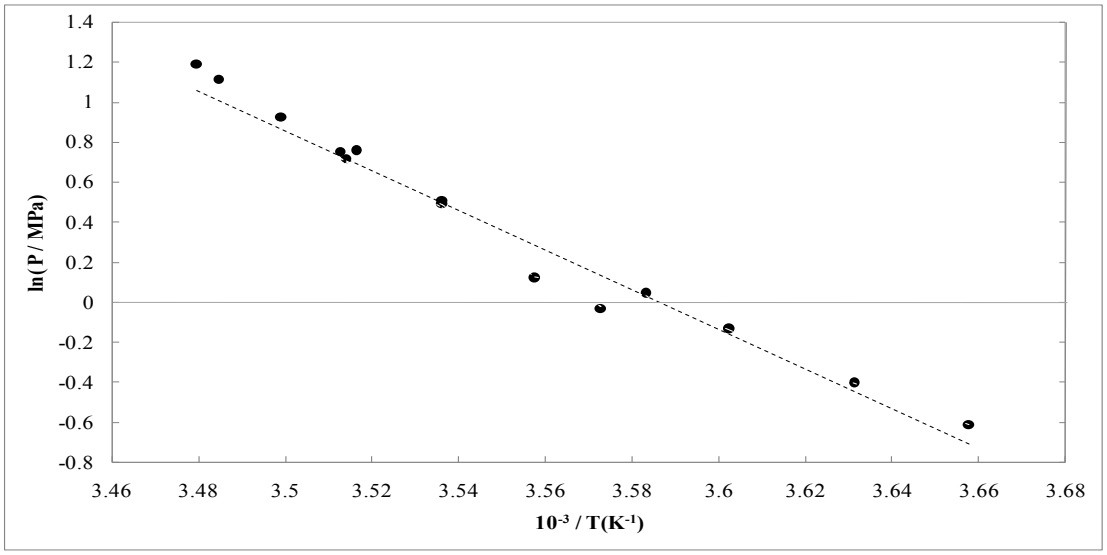


Figure 6.7: H-L-V equilibrium data for the system $C_2H_6$ (1) + water (2); •, Reamer, (1952), Roberts, (1941); —, model 1 Parrish and Prausnitz (1972).

Table 6.12: Hydrate dissociation data for the systems $CO_2$ (1) + water (2) and $C_2H_6$ (1) + water (2).

| $CO_2$ (1) + water (2) | | | $C_2H_6$ (1) + water (2) | | |
|---|---|---|---|---|---|
| Ref 1 | | Predicted | Ref 2 | | Predicted |
| T/K | P / kPa | Δ P / kPa | T/K | P / kPa | Δ P / kPa |
| 273.7 | 1324.0 | ±18.9 | 273.4 | 545.0 | ±3.0 |
| 274.3 | 1393.0 | ±17.7 | 275.4 | 669.0 | ±1.7 |
| 275.4 | 1613.0 | ±27.9 | 277.6 | 876.0 | ±5.8 |
| 276.5 | 1848.0 | ±38.6 | 279.1 | 1048.0 | ±10.5 |
| 277.2 | 2041.0 | ±51.0 | 279.9 | 972.0 | ±6.9 |
| 277.6 | 2075.0 | ±46.2 | 281.1 | 1131.0 | ±2.3 |
| 278.7 | 2427.0 | ±70.5 | 282.8 | 1641.0 | ±36.3 |
| 279.2 | 2586.0 | ±80.7 | 282.8 | 1666.0 | ±39.4 |
| 279.8 | 2758.0 | ±89.3 | 284.4 | 2137.0 | ±74.3 |
| 280.9 | 3227.0 | ±126.0 | 284.6 | 2055.0 | ±60.9 |
| 280.9 | 3213.0 | ±124.0 | 284.7 | 2129.0 | ±68.6 |
| 281.5 | 3530.0 | ±151.6 | 285.8 | 2537.0 | ±101.3 |
| 281.9 | 3689.0 | ±161.5 | 287.0 | 3054.0 | ±143.4 |
| 281.9 | 3709.0 | ±164.5 | 287.4 | 3298.0 | ±164.8 |
| 282.6 | 4130.0 | ±201.0 | | | |
| 282.9 | 4323.0 | ±217.5 | | | |

Ref 1: (Morrison, 1952), (Culberspn, 1950);
Ref 2: (Reamer, 1952), (Roberts, 1941);
Predicted: $\Delta P = \left| P_{experimental} - P_{predicted} \right|$

The parameters reported in Table 3.1 were altered according to the values reported in Cao et al, (2002). For $CO_2$, the %AAD increased from 3.20 to 3.46 while for $C_2H_6$, the %AAD increased from 2.23 to 2.52. Although this increase was not significant it was large enough to change the calculated pressure. Altering the $k_{ij}$ interaction parameter had no effect on the calculated pressure.

### 6.7.3 Models of Eslamimanesh et al.

#### 6.7.3.1 Predictive models of Eslamimanesh et al.

The model proposed by Eslamimanesh, (2011), was a predictive model used to verify the system R134a (1) + water (2). The literature data used to model these systems were that reported in Liang et al. (2001) and Akiya et al. (1999). The model flow diagram can be seen in Figure 6.8. The model was then altered such that the parameters for the measured systems R22 (1) + water (2) and R134a (1) + water (2) could be regressed (refer to Figures 6.9 and 6.10). R22 formed large structure I hydrates (Chun et al., 2000) while R134a formed large structure II hydrates.

This model used a number of assumptions which were tested using either system R22 or R134a. This was due to the solubility of the gas being significant and the hydrates formed at a lower temperature or higher pressure than the system R134a (1) + water (2). $P_w^{MT}$ was in the order of 1 kPa; however, by varying $\phi_w^{MT}$ the %AAD varied significantly. The Poynting factor was assumed equal to 1 for systems where the pressure was below 2 MPa; however, the %AAD varied significantly if this value was varied. Additionally, the fugacity of the refrigerant in the vapour phase was assumed equal to the dissociation pressure. This assumption had no affect on the %AAD.

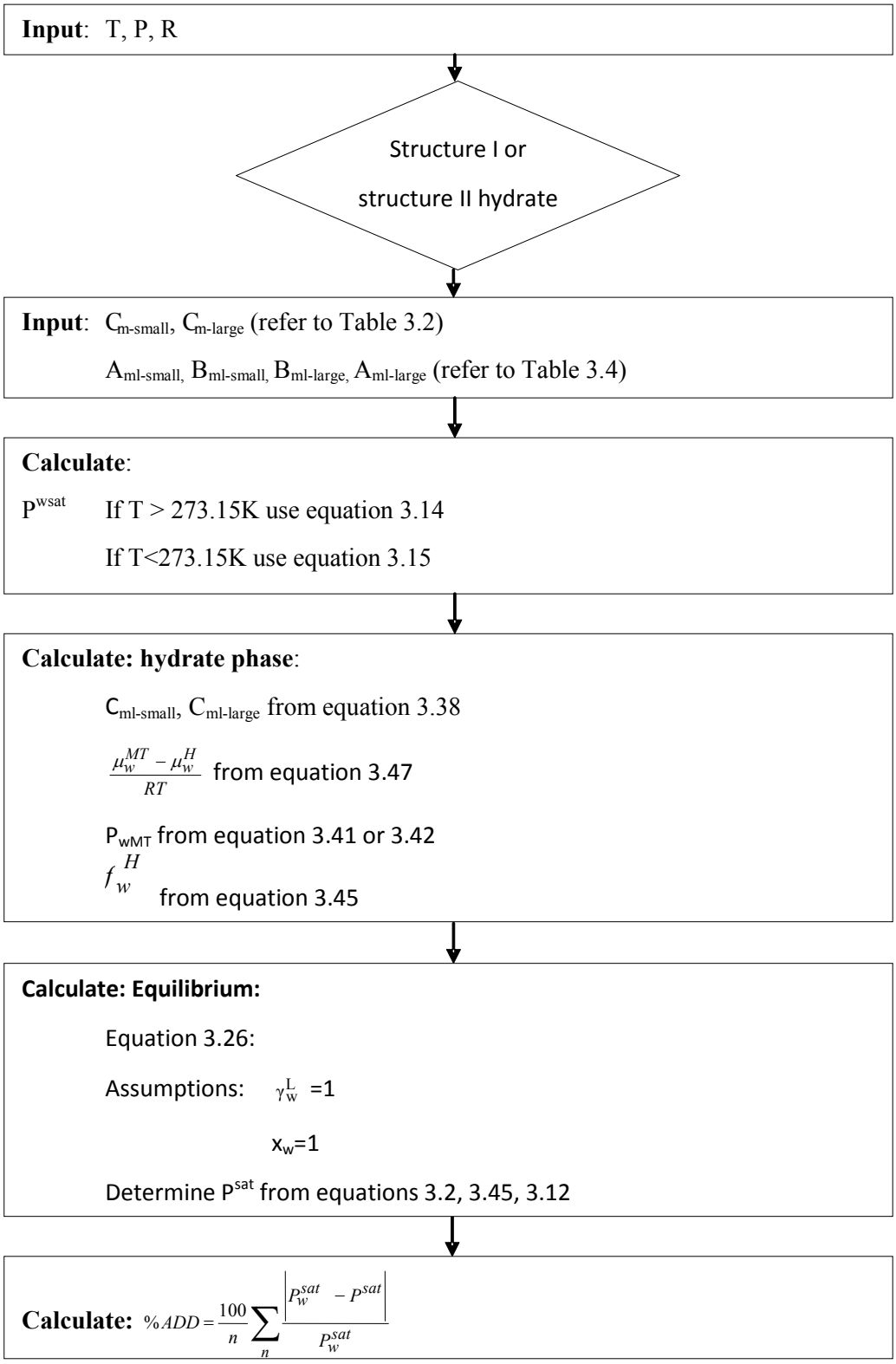


Figure 6.8: Computation flow chart to verify the predictive model stated in Eslamimanesh et al. (2011) for the system R134a (1) + water (2).

The model was altered such that the objective function was in terms of the fugacity coefficient as opposed to the activity coefficient in order to account for the solubility. The minimised objective function was in terms of the dissociation pressure as opposed to the saturated pressure, as seen in Figure 6.9.

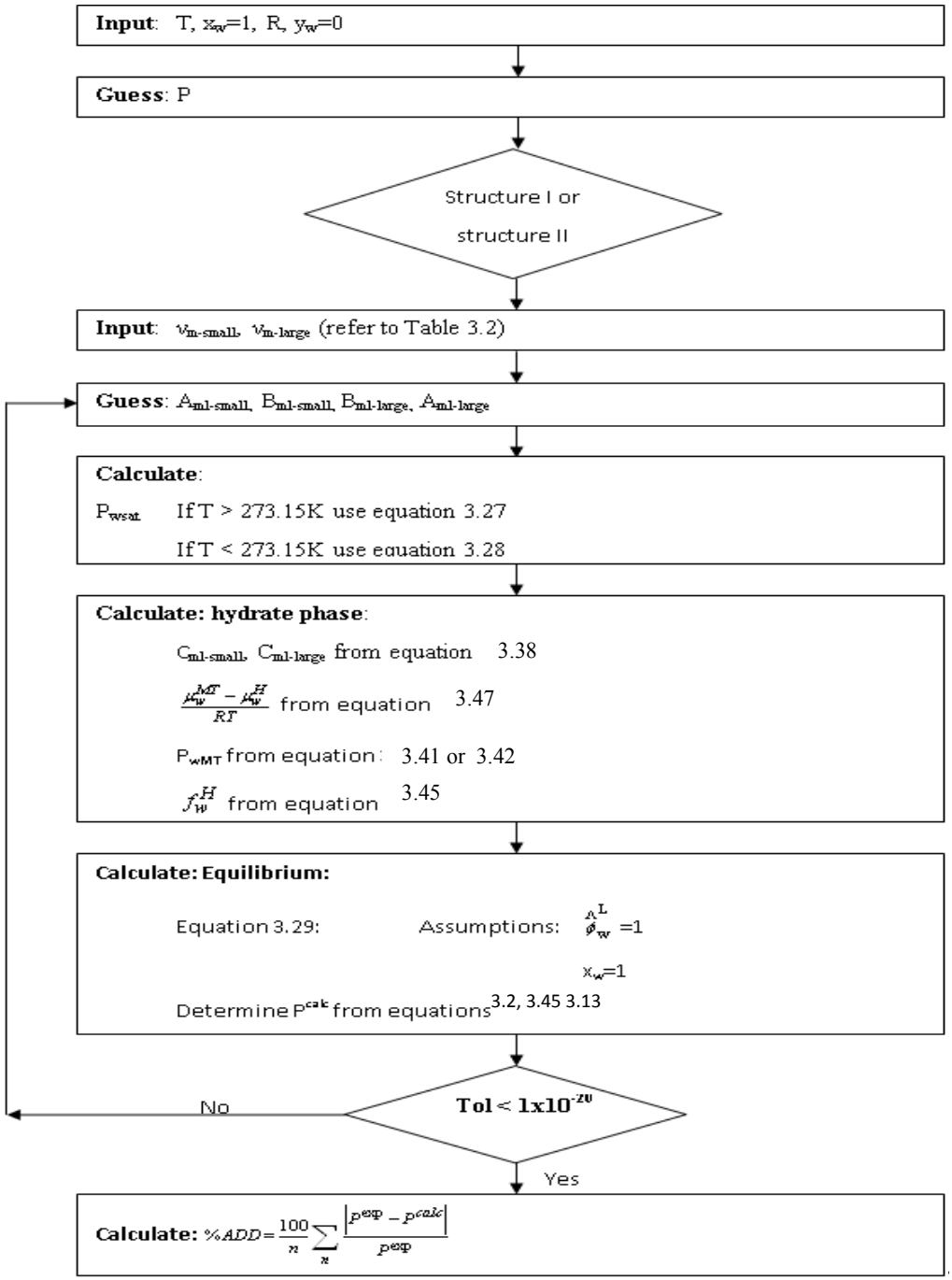


Figure 6.9: Computation flow chart for the regression of the Langmuir parameters for the hydrate formers R134a and R22.

6.7.3.2 Model 2: Regression model of Eslamimanesh et al

Langmuir parameters were regressed in this model and compared to the predictive parameters reported in Eslamimanesh et al. (2011). The parameters were the same. However, the error was higher when using a different objective function in terms of dissociation pressure rather than the saturated pressure. Figures 6.9 and 6.10 show the results of the predicted and regressed models as mentioned above. Both models fitted the data very well with little deviation between the experimental and calculated data.

For the system R22 (1) + water (2), Chun et al. (1996) and Wittstruck et al. (1961) did not report modelled data. Javanmardi et al. (2004) reported the error between the literature and experimental data in terms of temperature and thus cannot be compared to this work. Although Javanmardi et al. (2004) followed a similar experimental technique as this work, the pressure was chosen as the regressed variable whereby the error was minimized between the experimental and predicted values. This was due to a higher uncertainty in the pressure measurements as the temperature was the fixed variable during hydrate measurements.

The maximum deviation between the experimental data and that predicted by the model for the system R134a (1) + water (2) was ±3.2 kPa. Akiya et al. (1999) did not report modelled data. Liang et al. (2001) reported a maximum percentage error between the literature and experimental data as 4.5% of the dissociation pressure (refer to Table 6.11 for a comparison between experimental and modelled data).

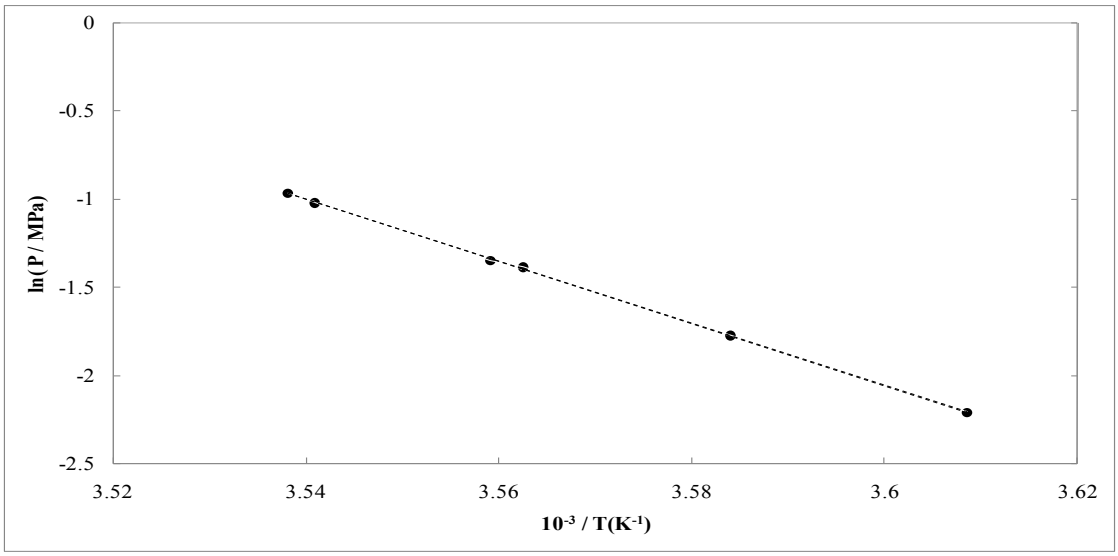


Figure 6.10: H-V-L equilibrium data for; R134a (1) + water (2); —, modelled using the predictive model by Eslamimanesh et al; ——, modelled using the modified regression model by Eslamimanesh et al; •, measured this work.

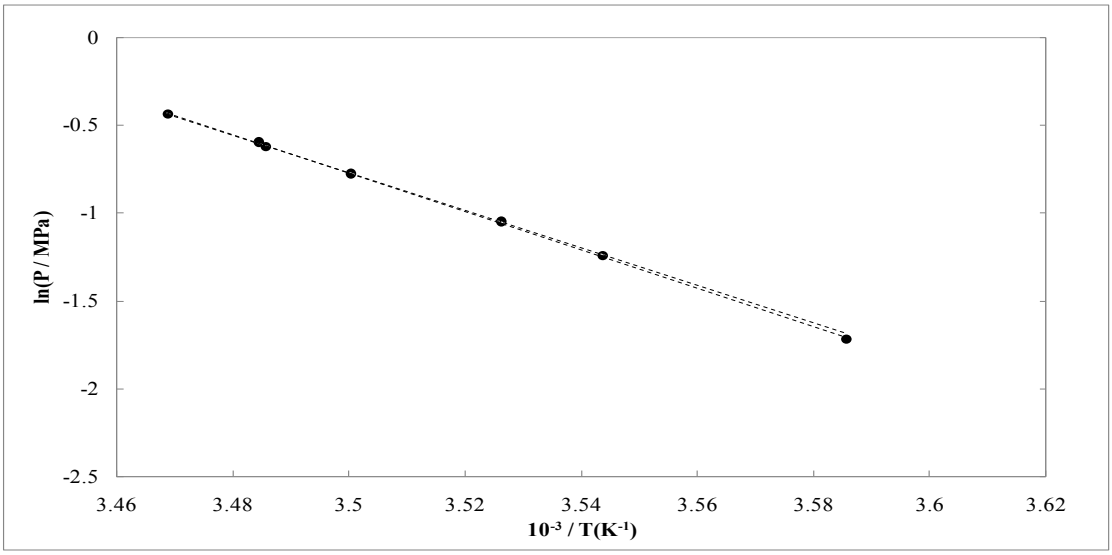


Figure 6.11: H-V-L equilibrium data for the system R22 (1) + water (2); —, modelled using predictive model by Eslamimanesh et al; ——, modelled using modified regressive model by Eslamimanesh et al; •, the measured this work.

6.7.3.3 Model 3: Modified regression model extended for solubility by Eslamimanesh et al

The modified Eslamimanesh et al.″s model was then extended to account for solubility by replacing the γ-φ method with the φ-φ method as mentioned previously. The PR EOS and the van der Waals

mixing rules were used to account for the solubility. Since no vapour-liquid equilibrium data were available in literature for the systems R22 (1) + water (2) and R134a (1) + water (2), an ASPEN flash calculation was used to obtain the equilibrium liquid and vapour compositions. At a specific dissociation temperature and pressure the equilibrium liquid and vapour compositions were obtained. The property method used was PR EOS and the initial temperature, pressure and feed composition had no effect on the results. The interaction mixing parameter $k_{ij}$ was obtained from ASPEN. For both systems, it was zero due to little information available on the systems modelled. This was acceptable since changing the parameter $k_{ij}$ had no effect on the results.

Two approaches were used. The first was a predictive model which used the regressed constants from model 2. The model took into account solubility of the fluorinated hydrating agent in the liquid phase. This model was represented in Figures 6.11 and 6.12 as a solid line.

The second approach was a regressed model known as model 3. Parameters were obtained using the differential evolution strategy optimisation function. This regressive model was represented in Figures 6.11 and 6.12 as a dotted line.

In Figures 6.11 and 6.12, since there was a large shift between the two models, it is evident the change in the Langmuir parameters was large when solubility was accounted for. Model 3 fitted the experimental data very well and contained a %AAD of 0.33 for R22 (1) + water (2) and 0.33 for R134a (1) + water (2).

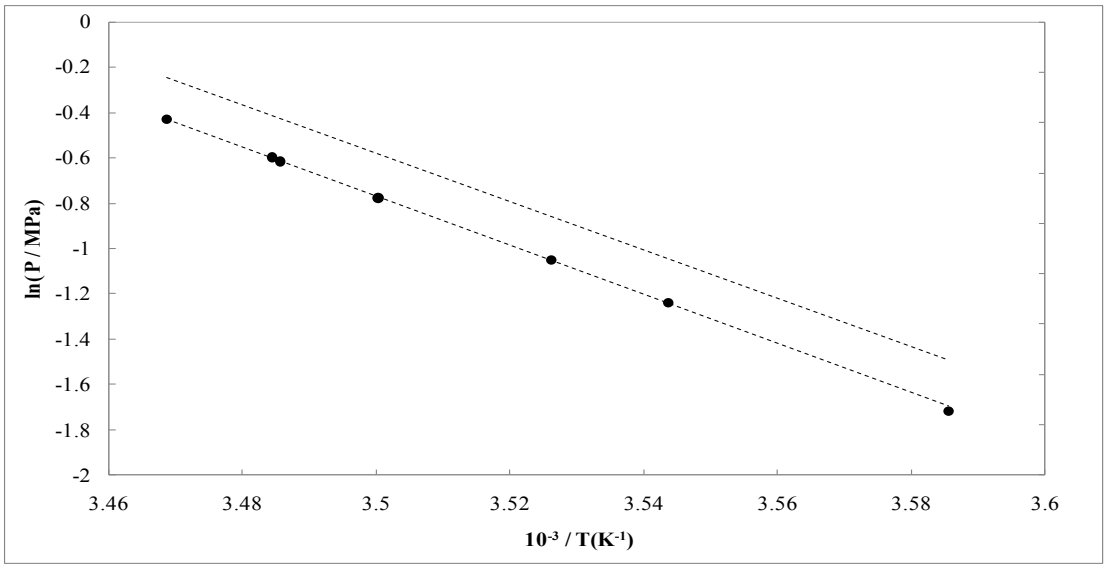


Figure 6.12: H-V-L equilibrium data for the measured system R22 (1) + water (2); •, measured in this work;—, modelled using Langmuir constants established in Figure 6.7 using (Eslamimanesh et al., 2011); ——,modelled using regressed constants using the Eslamimanesh et al. (2011) and Parrish et al. (1972).

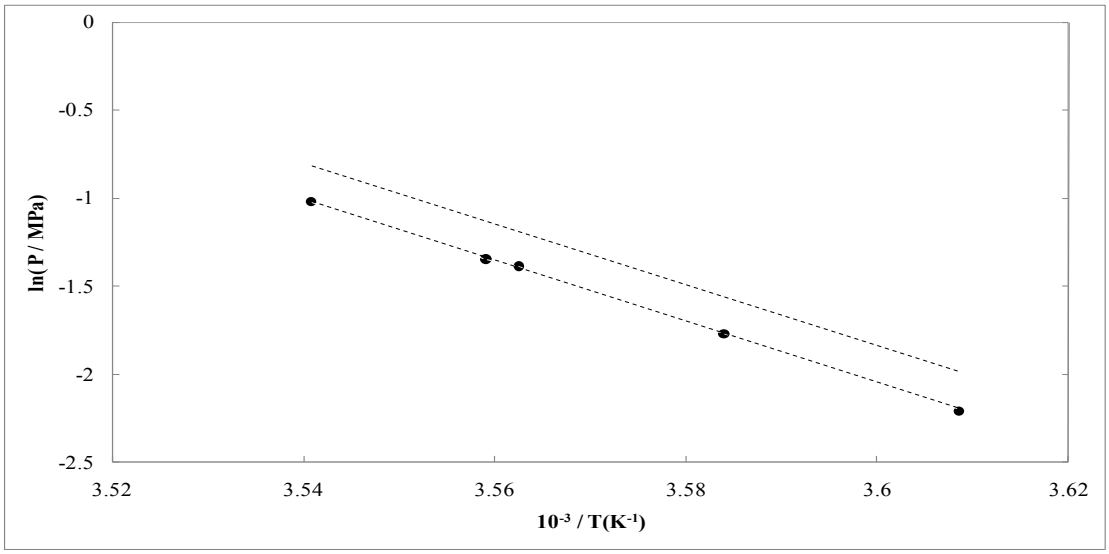


Figure 6.13: H-V-L equilibrium data for the measured system R134a (1) + water (2); •, measured in this work; —, modelled using Langmuir constants established in Figure 6.8 using Eslamimanesh et al. (2011); ——, modelled using regressed constants using Eslamimanesh et al. (2011) and Parrish et al. (1972).

### 6.7.4 Model 4: Modified predictive model extended for solubility and salts by Eslamimanesh et al

The initial salt concentration in the liquid phase was slightly different from the salt concentration at the dissociation point due to the fluorinated hydrating agent water solubility. Although solubility cannot be ignored, particularly for the system containing R22, the change in salt composition in the liquid phase due to gas solubility was negligible. At the point at which the last hydrate dissociates-the dissociation point-the water from the hydrate was in the liquid phase. Therefore the salt concentration at the hydrate dissociation point was assumed the same as the initial salt concentration in the feed.

Model 3 was extended to account for the salt in the system. This model used the model reported in Aasberg-Peterson et al. (1991) modified by Tohidi et al. (1995) to account for salts. This was known as the modified Eslamimanesh et al predictive model extended for solubility and salts. The system R22 (1) + water (2) + {5, 10 or 15} wt% NaCl (3) was used to verify the model using literature data from Chun et al. (2000). Additionally the measured system R134a (1) + water (2) + {5, 10 or 15} wt% NaCl (3) was modelled using this method (refer to Figure 6.13 for flow diagram).

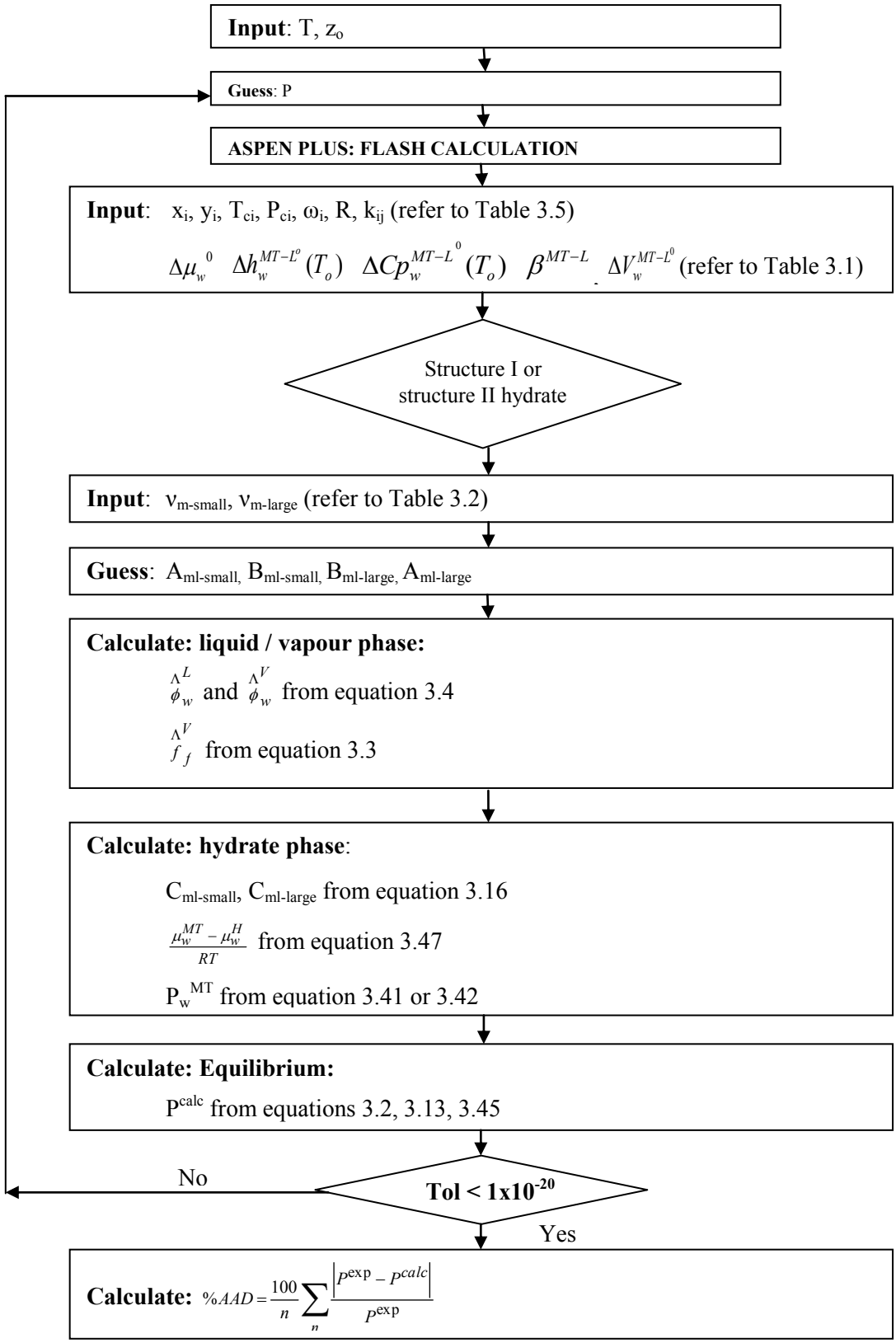


Figure 6.14: Computation flow chart for the predictive model for the hydrate formers R134a and R22 with various concentrations on NaCl.

Figure 6.14 shows a very good model fit to the experimental data. The %AAD reported in Chun et al. (2000) was 4.03 while this system had a %AAD of 8.28. The larger error may be due to the more advanced EOS (RSK) and mixing rule (Huron-Vidal) used to describe the liquid phase, thus accounting for the density of the liquid phase. The electrolyte component was described by Pitzer (1973) as seen in Table 3.13.

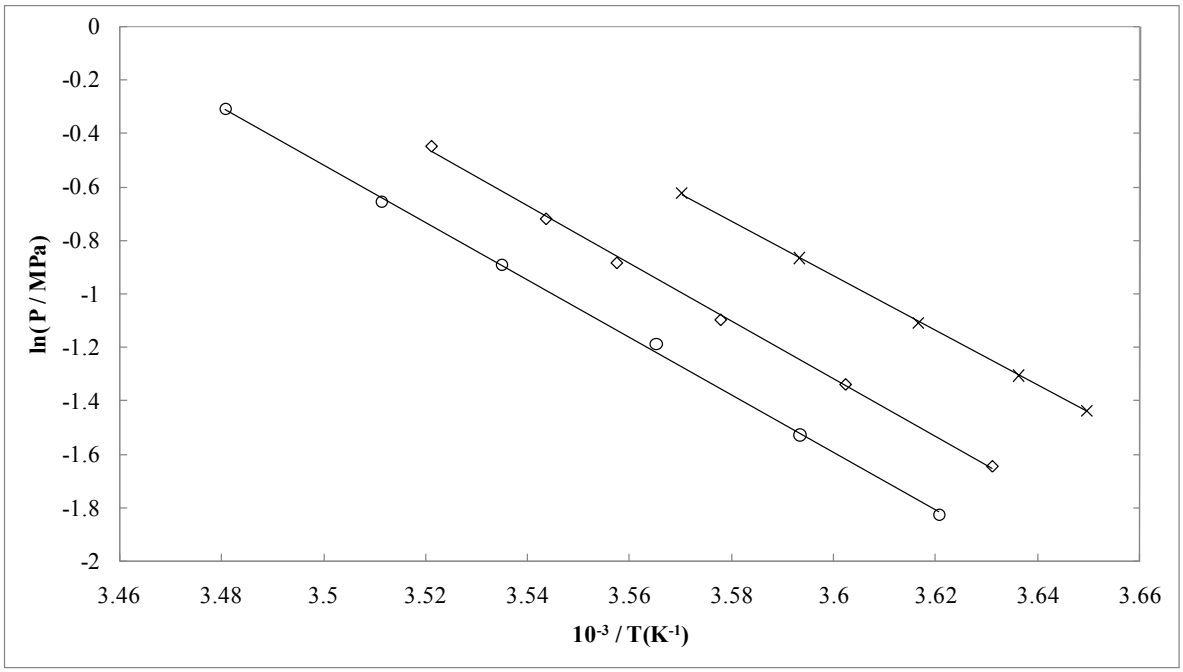


Figure 6.15: H-L-V equilibrium data for the system R22 + water + salt (Chun et al., 1996); ○, 5 wt% NaCl; 10 wt% NaCl; x, 15 wt% NaCl; —, modelled using the model 4.

.

Table 6.13 displays the Langmuir constants which have either been regressed or used in model predictions. The values obtained are similar to those reported in Parrish et al. (1972) (refer to Table 3.3).

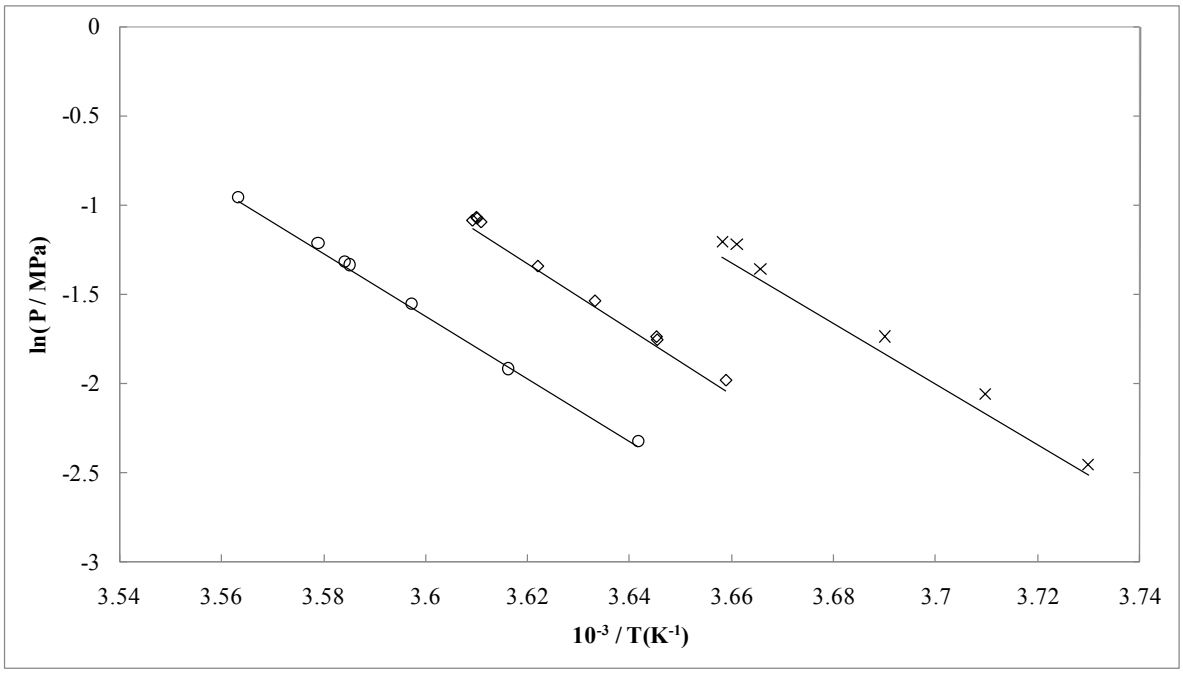


Figure 6.16: H-L-V equilibrium data for the system R134a + water + salt (Chun et al., 1996); ○, 5 wt% NaCl; ◊, 10 wt% NaCl; x, 15 wt% NaCl; —, modelled using model 4.

Table 6.13 shows the regressed Langmuir constants a, b, c and d. The differential evolution strategy was used to obtain the optimal values for the Langmuir constants. The bounds for the differential strategy were either fixed or allowed to reach their optimum value. This can be seen as either bounded or unbounded in Table 6.13.

Table 6.13: Regressed Langmuir constants for the systems R134a (1) + water (2) and R22 (1) + water (2).

| | | a | b | c | d | %AAD[a,b] |
|---|---|---|---|---|---|---|
| **R134a** | Ref | 0 | 0 | 0.005700 | 4908.75 | 5.30 |
| | Figure 6.8 bounded (verification) | 0 | 0 | 0.005700 | 4908.69 | 0.31 |
| | Figure 6.8 unbounded | 0 | 0 | 0.000008 | 6750.38 | 0.03 |
| | Figure 6.9 unbounded | 0 | 0 | 0.000008 | 6750.38 | 0.55 |
| | Figure 6.5 unbounded (solubility) | 0 | 0 | 0.000004 | 7927.59 | 0.33 |
| | Figure 6.13 unbounded (salt) | 0 | 0 | 0.000004 | 7927.59 | 8.28 |
| **R22** | Figure 6.8 bounded | 0 | 0 | 0.000035 | 5576.53 | 0.08 |
| | Figure 6.9 bounded | 0 | 0 | 0.000035 | 5576.53 | 0.63 |
| | Figure 6.9 unbounded | 0 | 0 | 0.000004 | 7927.59 | 0.33 |
| | Figure 6.5 unbounded (solubility) | 0 | 0 | 0.000003 | 6756.64 | 0.41 |
| | Figure 6.13 unbounded (salt) | 0 | 0 | 0.000003 | 6756.64 | 5.14 |

Ref: Eslamimanesh et al. (2011)

[a] $AAD\% = \frac{100}{N}\sum_{i}^{N}\frac{|P_i^{Cal.} - P_i^{Exp.}|}{P_i^{Exp.}};$ [b] $AAD\% = \frac{100}{N}\sum_{i}^{N}\frac{|P_i^{Pred.} - P_i^{Exp.}|}{P_i^{Exp.}}$

[c] $\%Error = 100\left|\frac{Literature - This\ \ Work}{Literature}\right|$

# CHAPTER SEVEN

## CONCLUSIONS

In order to reduce measurement uncertainty to less than that reported in literature, a number of procedures were undertaken. These included preventing heat gain and fluctuations in temperature by using insulation and heating blocks. Additionally, the water composition was verified by conducting measurements on test systems and using the same cleaning procedure as the test systems. Vapour pressure data were measured to verify calibrations.

Pressure calibrations for the 0-1 MPa WIKA pressure transducer and temperature calibrations for the Pt100 temperature probes were conducted with an uncertainty of ±0.01 MPa and ±0.02K respectively. Calibrations were verified by measuring vapour pressure data for the systems hypofluoropropyleneoxide, $CO_2$, R22 and R134a.

The experimental technique, equipment and calibrations were verified by measuring the test systems R22 (1) + water (2) and R134a (1) + water (2). The measured hydrate dissociation data for the systems R22 (1) + water (2) and R134a (1) + water (2) compared very well to literature data.

New systems measured included R134a (1) + water (2) + {5 wt%, 10 wt% or 15 wt%} NaCl (3). The measurement uncertainties were ±0.092K and ±0.640 kPa.

The measured systems were modelled using two methods of approach: one where solubility was included, (Parrish et al., 1972) and the other where solubility was ignored (Eslamimanesh et al., 2011). It was found that although solubility was small, it may not be neglected. The hydrate phase was modelled using modifications of van der Waals and Platteeuw model, (Parrish et al., 1972). The liquid and vapour phases were modelled using Peng Robinson EOS with classical mixing rules (Peng et al., 1976). The electrolyte component was modelled using Aasberg-Petersen et al. (1991) modified by Tohidi et al. (1995). The %AAD for the system and the model, including solubility, was 0.41 for R22 (1) + water (2) and 0.33 for R134a (1) + water (2). For the system R134a (1) + water (2) + {5, 10 or 15} wt% NaCl (3) the %AAD was 5.14.

The addition of a salt to the system resulted in a shift of the H-V-L equilibrium phase boundary to low temperatures: high pressures. As the salt concentration increased so, the shift became

more significant. The average shift in temperature between the system R134a (1) + water (2) containing no salt and the systems containing {5, 10 and 15} wt% NaCl were -1.9K, -4.8K and -8.1K respectively.

Using the hydrate former, R134a, is insufficient to ensure gas hydrate technology is competitive with other desalination technologies. Hydrate dissociation temperature should be increased and pressure decreased further to ambient conditions.

# CHAPTER EIGHT

## RECOMMENDATIONS

A number of measurements may be conducted as a continuation of this work. These include a measurement of systems containing R134a as a fluorinated hydrating agent or other fluorinated hydrating agents such as R410a and R507. The addition of a promoter to the system such as cyclopentane, to determine whether ambient operating conditions could be reached is a further recommendation. Additionally, measuring systems with other common salts such as $CaCl_2$, $Na_2SO_4$ and $CaSO_4$ as well as mixtures of these salts would contribute to literature.

If gas hydrate technology for the desalination of industrial wastewater proves to be successful, gas hydrate technology for wastewater purification could be investigated. HLV equilibrium measurements containing pollutants such as metals, organic compounds, inorganic compounds, solvents, polymers and oil may be conducted.

Since the PR EOS with van der Waals mixing rules did not account for the non-ideal liquid and vapour phases at high temperatures and pressures very accurately, other EOS and mixing rules may be used such as Patel and Teja (1982), Trebble and Bishnoi (1988) and Valderrama (1990) including quadratic or non density-dependent mixing rules.

Since very little solubility data is available for systems containing salt, vapour liquid equilibrium data (including the composition of components in each phase) can be measured to increase the accuracy in modelling the vapour and liquid phases.

The electrolyte may be modelled using other methods mentioned in Chapter 3.2.2. If the method which was presented in Tohidi et al. (1995) is found to be the most suitable option for modelling the electrolyte components, additional measurements may be conducted to determine the freezing point data for the salt used.

# REFERENCES

Aasberg-Petersen, K., Stenby, E. and Fredenslund, A., 1991. Prediction of high-pressure gas solubilities in aqueous mixtures of electrolytes. *Industrial & Engineering Chemistry Research,* 30**,** 2180-2185.

Adisasmito. S, Frank. R. J and Sloan. D, 1991, Hydrates of carbon dioxide and methane mixtures, *J. Chem. Eng. Data,* 36, (1), 68-71.

Akiya, T., Shimazaki, T., Oowa, M., Matsuo, M. and Yoshida, Y., 1999. Formation Conditions of Clathrates Between HFC Alternative Refrigerants and Water. *International Journal of Thermophysics,* 20**,** 1753-1763.

Atik. Z, Windmeier. C and Oellrich. L. R., 2006, Experimental Gas Hydrate Dissociation Pressures for Pure Methane in Aqueous Solutions of $MgCl_2$ and $CaCl_2$ and for a (Methane + Ethane) Gas mixture in an aqueous solution of (NaCl + $MgCl_2$), *J. Chem. Eng. Data,* 51, (5), 1862-1867.

Avlonitis. D., 1988. Multiphase equilibria in oil-water hydrate forming systems M.Sc. Thesis, 1988: Heriot-Watt University, Edinburgh.

Ball, F. X., Fürst, W. and Renon, H., 1985. An NRTL model for representation and prediction of deviation from ideality in electrolyte solutions compared to the models of Chen (1982) and Pitzer (1973). *AIChE Journal,* 31**,** 392-399.

Ballard, A. L. and Sloan, E. D., 2001. Hydrate phase diagrams for methane + ethane + propane mixtures. *Chemical Engineering Science,* 56**,** 6883-6895.

Bishnoi, P. R. and Natarajan, V., 1996. Formation and decomposition of gas hydrates. *Fluid Phase Equilibria,* 117**,** 168-177.

Bradshaw, R. W., Greathouse, J. A., Cygan, R. T., Simmons, B. A., Dedrick, D. E. and Majzoub, E. H., 2008. *Desalination Utilizing Clathrate Hydrates (LDRD Final Report)* [Online]. California: Sandia National Laboratories. Available: http://prod.sandia.gov/techlib/access-control.cgi/2007/076565.pdf [Accessed].

Bromely, L. A., 1973. Thermodynamic Properties of Strong Electrolytes in Aqueous Solutions. *AlChE Journal,* 19**,** 7.

Cao. Z, Tester. J. W and Trout. B. L, 2002, Sensitivity Analysis of Hydrate Thermodynamic Reference Properties Using Experimental Data and ab Initio Methods, *J. Phys. Chem. B,* 106, 7681-7687.

Carroll, J. J., 2003. Natural gas hydrates: a guide for engineers Gulf Professional Pub.

Chen, C.-C., Britt, H. I., Boston, J. F. and Evans, L. B., 1982. Local composition model for excess Gibbs energy of electrolyte systems. Part I: Single solvent, single completely dissociated electrolyte systems. *AIChE Journal,* 28**,** 588-596.

Chen, G.-J. and Guo, T.-M. 1998. A new approach to gas hydrate modelling. *Chemical Engineering Journal,* 71**,** 145-151.

Chen, G.-J. and Guo, T.-M., 1996. Thermodynamic modeling of hydrate formation based on new concepts. *Fluid Phase Equilibria,* 122**,** 43-65.

Chinworth, H. E. and Katz, D. L., 1947, Refrigerant Hydrates, *Refrig. Eng.,* 54, 359-362.

Chun, M.-K., Lee, H. and Ryu, B.-J., 2000. Phase Equilibria of R22 (CHClF2) Hydrate Systems in the Presence of NaCl, KCl, and MgCl2. *Journal of Chemical & Engineering Data,* 45**,** 1150-1153.

Chun, M.-K., Yoon, J.-H. and Lee, H., 1996. Clathrate Phase Equilibria for the Water + Deuterium Oxide + Carbon Dioxide and Water + Deuterium Oxide + Chlorodifluoromethane (R22) Systems. *Journal of Chemical & Engineering Data,* 41**,** 1114-1116.

Cruz, J.-L. and Renon, H., 1978. A new thermodynamic representation of binary electrolyte solutions nonideality in the whole range of concentrations. *AIChE Journal,* 24**,** 817-830.

De Roo. J. L, Peters. C. J, Lichtenthaler. R. N and Diepen. G. A. M, 2004, Occurance of methane hydrate in saturated and unsaturated solutions of sodium chloride and water in dependence of temperature and pressure, *AIChE journal,* 29, (4), 651-657.

Deaton, W. M. and Frost, E. M. J., 1946. Gas hydrates and their relation to the operation of natural-gas pipe lines.

Delahaye, A., Fournaison, L., Marinhas, S., Chatti, I., Petitet, J.-P., Dalmazzone, D. and Fürst, W., 2005. Effect of THF on Equilibrium Pressure and Dissociation Enthalpy of CO2 Hydrates Applied to Secondary Refrigeration. *Industrial & Engineering Chemistry Research,* 45**,** 391-397.

Desalination, accessed at https://sps.esd.ornl.gov/desalinationpage.html, accessed on: 16 January 2012.

Dharmawardhana, P. B., Parrish, W. R. and Sloan, E. D., 1980a. Experimental thermodynamic parameters for the prediction of natural gas hydrate dissociation conditions. *Ind. Eng. Chem. Fundam,* 19**,** 410-414.

Dharmawardhana, P. B., Parrish, W. R. and Sloan, E. D., 1980b. Experimental Thermodynamic Parameters for the Prediction of Natural Gas Hydrate Dissociation Conditions. *Industrial & Engineering Chemistry Fundamentals,* 19**,** 410-414.

Dicko, M., Belaribi-Boukais, G., Coquelet, C., Valtz, A., Brahim Belaribi, F., Naidoo, P. and Ramjugernath, D., 2011. Experimental Measurement of Vapor Pressures and Densities at Saturation of Pure Hexafluoropropylene Oxide: Modeling Using a Crossover Equation of State. *Industrial & Engineering Chemistry Research,* 50**,** 4761-4768.

Dortmund Data Bank, (2010), DDBST Software and Separation Technology GmbH, DDB Software Package Version 2011, Oldenburg

Englezos. P and Bishnoi. P. R, 2004, Prediction of gas hydrate formation conditions in aqueous electrolyte solutions, *AIChE journal,* 34, (10), 1718-1721.

Englezos, P., 1993. Clathrate Hydrate. *Ind. Eng. Chem. Res,* 32**,** 1251-1274.

Englezos, P. and Bishnoi, P. R., 1991. Experimental study on the equilibrium ethane hydrate formation conditions in aqueous electrolyte solutions. *Industrial & Engineering Chemistry Research,* 30**,** 1655-1659.

Englezos, P., Kalogerakis, N., Dholabhai, P. D. and Bishnoi, P. R., 1987. Kinetics of formation of methane and ethane gas hydrates. *Chemical Engineering Science,* 42**,** 2647-2658.

Englezos, P. and Ngan, Y. T., 1993. Incipient equilibrium data for propane hydrate formation in aqueous solutions of NaCl, KCl, and $CaCl_2$. *Journal Name: Journal of Chemical and Engineering Data; (United States); Journal Volume: 38:2***,** Medium: X; Size: Pages: 250-253.

Englezos, P. and Ngan, Y. T., 1994. Effect of polyethylene oxide on gas hydrate phase equilibria. *Fluid Phase Equilibria,* 92**,** 271-288.

Englezos. P, 1992, Computation of the Incipient Equilibrium Carbon Dioxide Hydrate Formation Conditions in Aqueous Electrolyte Solutions, *Ind. Eng. Chem. Res.* 31, 2232-2237.

Eslamimanesh, A., Mohammadi, A. H. and Richon, D., 2011. Thermodynamic model for predicting phase equilibria of simple clathrate hydrates of refrigerants. *Chemical Engineering Science,* 66**,** 5439-5445.

Eslamimanesh, A., Mohammadi, A. H., Richon, D., Naidoo, P. and Ramjugernath, D., 2012. Application of gas hydrate formation in seperation processes: A review of experimental studies. Journal of *Chemical Thermodynamics,* 46**,** 62-71.

Fan. S-S, Chen. G-, Ma. Q-L and Guo, T-M, 2000, Experimental and modeling studies on the hydrate formation of $CO_2$ and $CO_2^-$, *Chemical Engineering Journal,* 78, (2-3), 173-178.

Fan. S-s and Guo. T-M, 1999, Hydrate Formation of $CO_2$-Rich Binary and Quaternary Gas Mixtures in Aqueous Sodium Chloride Solutions, *J. Chem. Eng. Data.* 44, (4), 829-832.

Fournaison, L., Delahaye, A., Chatti, I. and Petitet, J.-P., 2004. CO2 Hydrates in Refrigeration Processes. *Industrial & Engineering Chemistry Research,* 43**,** 6521-6526.

Galloway. T. J, Ruska. W, Chappelear. P. S amd Kobayashi. R, 1970, Experimental Measurement of Hydrate Numbers for Methane and Ethane and Comparison with Theoretical Values, *Ind. Eng. Chem. Fundamen.,* 9, (2), 237-243.

Giuliani, G., Kumar, S., Zazzini, P. and Polonara, F., 1995. Vapor Pressure and Gas Phase PVT Data and Correlation for 1,1,1-Trifluoroethane (R143a). *Journal of Chemical & Engineering Data,* 40**,** 903-908.

Goel, N., 2006. In situ methane hydrate dissociation with carbon dioxide sequestration: Current knowledge and issues. *Journal of Petroleum Science and Engineering,* 51**,** 169-184.

Haghtalab, A. and Vera, J. H., 1988. A nonrandom factor model for the excess gibbs energy of electrolyte solutions. *AIChE Journal,* 34**,** 803-813.

Harmens, A. and Sloan, E. D., 1990. The phase behaviour of the propane-water system: A review. *The Canadian Journal of Chemical Engineering,* 68**,** 151-158.

Hashimoto, S., Miyauchi, H., Inoue, Y. and Ohgaki, K., 2010. Thermodynamic and Raman Spectroscopic Studies on Difluoromethane (HFC-32) + Water Binary System. *Journal of Chemical & Engineering Data,* 55**,** 2764-2768.

Herri. J.-M., Bouchemoua. A., Kwaterski. M., Fezoua. A., Ouabbas. Y and Cameirao. A., 2011, Gas hydrate equilibria for $CO_2$-$N_2$ and $CO_2$-$CH_4$ gas mixtures-Experimental studies and thermodynamic modelling, *Fluid Phase Equilibria,* 301, 171-190.

Heuvel, M. M. M. V. D., 2004. Phase Behaviour and Structural Aspects of Ternary Clathrate Hydrate Systems. *The Role of Additives.* Technische Universiteit Delft.

Hibbert, D. B., 1993. *Introduction to electrochemistry / D. Brynn Hibbert,* Basingstoke :, MacMillan.

Holder. G. D and Hand. J. H, 2004, Multiple-phase equilibria in hydrates from methane, ethane, propane and water mixtures, *AIChE journal,* 28, (3), 440-447.

Holder, G. D. and Grigoriou, G. C., 1980. Hydrate dissociation pressures of (methane + ethane + water) existence of a locus of minimum pressures. *The Journal of Chemical Thermodynamics,* 12**,** 1093-1104.

Huo, Z., Hester, K., Sloan, E. D. and Miller, K. T., 2003. Methane hydrate nonstoichiometry and phase diagram. *AIChE Journal,* 49**,** 1300-1306.

Jager, M. D. and Sloan, E. D., 2001. The effect of pressure on methane hydration in pure water and sodium chloride solutions. *Fluid Phase Equilibria,* 185**,** 89-99.

Javanmardi, J., Ayatollahi, S., Motealleh, R. and Moshfeghian, M., 2004. Experimental Measurement and Modeling of R22 (CHClF2) Hydrates in Mixtures of Acetone + Water. *Journal of Chemical & Engineering Data,* 49**,** 886-889.

Javanmardi, J. and Moshfeghian, M., 2003. Energy consumption and economic evaluation of water desalination by hydrate phenomenon. *Applied Thermal Engineering,* 23**,** 845-857.

Jhaven. J and Robinson. D. B, 2009, Hydrates in the methane-nitrogen system, *The Canadian Journal of Chemical Engineering,* 43, (2), 75-78.

Kang, S.-P., Chun, M.-K. and Lee, H., 1998. Phase equilibria of methane and carbon dioxide hydrates in the aqueous MgCl2 solutions. *Fluid Phase Equilibria,* 147**,** 229-238.

Katz, D. L., Cornell, D., Kobayashi, R., Poettmann, F. H., Vary, J. A. and Weinaug, C. F., 1959. Handbook of Natural Gas Engineering. New York: McGraw-Hill.

Kharrat. M and Dalmazzone. D., 2003. Experimental determination of stability conditions of methane hydrate in aqueous calcium chloride solutions using high pressure differential scanning calorimetry, *J. Chem. Thermodynamics,* 35, 1489-1505.

Kim. H. C, Bishnoi. P. R, Heidemann. R. Aand Rizvi. S. S. H, 1987, Kinetics of methane hydrate decomposition, *Journal of Chemical Engineering Science,* 42, (7), 1646-1653.

Klauda, J. B. and Sandler, S. I., 2000. A Fugacity Model for Gas Hydrate Phase Equilibria. *Industrial & Engineering Chemistry Research,* 39**,** 3377-3386.

Knox, W. G., Hess, M., Jones, G. E. and Smith, H. B., 1961. Title unknown. *Chem. Engng Prog.,* 57**,** 66.

Kobayashi, R. and Katz, D. L., 1949, Methane hydrate at high pressure, *AIME journal,* 186, 66-70.

Kubota. H, Shimizu. K, Tanaka. Y and Makita. T, 1984, Thermodynamic Properties of R13 (CClF3), R23 (CHF3), R152a (C2H4F2) and Propane Hydrates for Desalination of Sea Water, *Journal of Chemical Engineering of Japan,* 17, (4), 423-429.

Larson, S. D., 1955, Phase studies of the two-component carbon dioxide-water system involving the carbon dioxide hydrate, Ph.D Thesis, University of Illinois, 84.

Lebowitz, J. L. and Percus, J. K., 1966. Mean Spherical Model for Lattice Gases with Extended Hard Cores and Continuum Fluids. *Physical Review,* 144**,** 251.

Lee, J. D., Susilo, R. and Englezos, P., 2005. Kinetics of Structure H Gas Hydrate. *Energy & Fuels,* 19**,** 1008-1015.

Liang, D., Guo, K., Wang, R. and Fan, S., 2001. Hydrate equilibrium data of 1,1,1,2-tetrafluoroethane (HFC-134a), 1,1-dichloro-1-fluoroethane (HCFC-141b) and 1,1-difluoroethane (HFC-152a). *Fluid Phase Equilibria,* 187-188**,** 61-70.

Lide, D. R., 2005. *Handbook of Chemistry and Physics,* BocaRaton, Taylor and Francis Group.
Maeda, K., Katsura, Y., Asakuma, Y. and Fukui.K, K., 2008. Concentration of sodium chloride in aqueous solutions by chlorofluoromethane gas hydrate. *Journal of chemical Engineering and Processing,* 47**,** 2281-2286.

Makogon, T. Y. and Sloan, E. D., Jr., 1994. Phase Equilibrium for Methane Hydrate from 190 to 262 K. *Journal of Chemical & Engineering Data,* 39**,** 351-353.

Mandal, A. and Laik, S., 2008. Effect of the Promoter on Gas Hydrate Formation and Dissociation. *Energy & Fuels,* 22**,** 2527-2532.

Mariah, L., Buckley, C. A., Brouckaert, C. J., Curcio, E., Drioli, E., Jaganyi, D. and Ramjugernath, D., 2006. Membrane distillation of concentrated brines--Role of water activities in the evaluation of driving force. *Journal of Membrane Science,* 280**,** 937-947.

Mayoufi, N., Dalmazzone, D., FüRst, W., Delahaye, A. and Fournaison, L., 2009. CO2 Enclathration in Hydrates of Peralkyl-(Ammonium/Phosphonium) Salts: Stability Conditions and Dissociation Enthalpies. *Journal of Chemical & Engineering Data,* 55**,** 1271-1275.

McCormack, R. A. and Andersen, R. K., 1995. Clathrate desalination plant preliminary research study. Available: http://www.usbr.gov/pmts/water/media/pdfs/report005.pdf [Accessed 28 January 2011].

McLeod. H. O, Campbell. J. M and The U. of Oklahoma, 1961, Natural Gas Hydrates at Pressures to 10 000 psia, *Journal of Petroleum Technology,* 13, (6), 590-594.

Menten. P. D, Parrish. W. R and Sloan. E. D, 1981, Effect of inhibitors on hydrate formation, *Ind. Eng. Chem. Process Des. Dev.,* 20, (2), 399-401.

Meissner, H. P. and Kusik, C. L., 1972. Activity coefficients of strong electrolytes in multicomponent aqueous solutions. *AIChE Journal,* 18**,** 294-298.

Miller, B. and Strong, E. K., 1946. Title unknown. *Amer. Gas Assoc. Monthly,* 28**,** 63.

Miller, J. E., 2003. *Review of Water Resources and Desalination Technologies* [Online]. California: Sandla National Laboratories. Available: http://prod.sandia.gov/techlib/access-control.cgi/2003/030800.pdf [Accessed 14 January 2011].

Mohammadi, A. H., Afzal, W. and Richon, D., 2008a. Gas hydrates of methane, ethane, propane, and carbon dioxide in the presence of single NaCl, KCl, and CaCl2 aqueous solutions: Experimental measurements and predictions of dissociation conditions. *The Journal of Chemical Thermodynamics,* 40**,** 1693-1697.

Mohammadi, A. H., Anderson, R. and Tohidi, B., 2005. Carbon monoxide clathrate hydrates: Equilibrium data and thermodynamic modeling. *AIChE Journal,* 51**,** 2825-2833.

Mohammadi, A. H. and Richon, D., 2010. Pressure Temperature Phase Diagrams of Clathrate Hydrates of HFC-134a, HFC-152a and HFC-32, AIChE Annual Meeting 2010.

Mohammadi, A. H., Tohidi, B. and Burgass, R. W., 2003. Equilibrium Data and Thermodynamic Modeling of Nitrogen, Oxygen, and Air Clathrate Hydrates. *Journal of Chemical & Engineering Data,* 48**,** 612-616.

Mooijer-van den Heuvel., Peters. C.J and de Swaan Arons. J., 2002. Gas hydrate equilibria for propane in the presence of additive components, *Fluid Phase Equilibria,* 193, 245-259.

Morita, K., Nakano, S. and Ohgaki, K., 2000. Structure and stability of ethane hydrate crystal. *Fluid Phase Equilibria,* 169**,** 167-175.

Morrison. T. J, Billett. F, 1952, The slting-out of non-electrolytes. Part II. The effect of variation in non-electrolyte, *J . Chem. Soc.,* 3819-3822.

Naidoo, P., (2004), PhD Dissertation: High-Pressure Vapor-Liquid Equilibrium Studies, University of KwaZulu Natal, Durban, South Africa.

Najibi, H., Chapoy, A., Haghighi, H. and Tohidi, B., 2009. Experimental determination and prediction of methane hydrate stability in alcohols and electrolyte solutions. *Fluid Phase Equilibria,* 275**,** 127-131.

Nakamura, T., Makino, T., Sugahara, T. and Ohgaki, K., 2003. Stability boundaries of gas hydrates helped by methane--structure-H hydrates of methylcyclohexane and cis-1,2-dimethylcyclohexane. *Chemical Engineering Science,* 58**,** 269-273.

Nakona, S., Moritoki, M and Ohgaki, K., 1999. High-Pressure Phase Equilibrium and Raman Microprobe Spectroscopic Studies on the Methane Hydrate System. *J. Chem. Eng. Data,* 44, 254-257.

Ng, H. J. and Robinson, D. B., 1980. A Method for Predicting the Equilibrium Gas Phase Water Content in Gas-Hydrate Equilibrium. *Industrial & Engineering Chemistry Fundamentals,* 19**,** 33-36.

Nixdorf, J. and Oellrich, L. R., 1997. Experimental determination of hydrate equilibrium conditions for pure gases, binary and ternary mixtures and natural gases. *Fluid Phase Equilibria,* 139**,** 325-333.

Ohgaki. K, Makihara. Y and Takano. K, 1993, Formation of $CO_2$ Hydrate in Pure and Sea Waters, *Journal of Chemical Engineering of Japan,* 26, (5), 558-564.

Parrish, W. R. and Prausnitz, J. M., 1972. Dissociation Pressures of Gas Hydrates Formed by Gas Mixtures. *Industrial & Engineering Chemistry Process Design and Development,* 11**,** 26-35.

Patel. N. C., and Teja. A. S., 1982, title unknown, *Chem. Eng. Sci.,* 37, (3), 463-473.

Peters, C., Roo, J. D. and Arons, J., 1987. Three phase equilibria in binary mixtures of ethane and n-pentacosane. *Journal of Chemical thermodynamics,* 19**,** 265-272.

Planche, H. and Renon, H., 1981. Mean spherical approximation applied to a simple but nonprimitive model interaction for electrolyte solutions and polar substances. *The Journal of Physical Chemistry,* 85**,** 3924-3929.

Poling, B., Prausnitz, J. and O'connell, J., 2001. The Properties of Gases and Liquids. 5th Edition ed. New York: McGRAW-HILL.

Prausnitz, J., Lichtenthaler, R. and Azevedo, E. G. D., 1999. *Molecular Thermodynamics of Fluid-Phase Equilibria (3rd Edition),* New Jersey, Prentice Hall Inc.

Ramjugernath, D. and Raal, J. D., 1999. Modelling, Prediction and Extrapolation of High Pressure Vapour-Liquid Equilibrium Data: Direct versus Combined Methods, Proceedings of the International Conference, Progress in Computing of Physicochemical Properties*,* 18-20 November, Warszawa, Poland: 308-322.

Reamer. H. H, Selleck. F. T, Slage. B. H, 1952, Some properties of mixed paraffinic and olefinic hydrates, *Petroleum Transactions, American Institute for Mechanical Engineers,* 195, 197-205.

Ribeiro, J., 1996. Desalination Technology Survey and Prospects.

Roberts. O. L, Brownscombe. E. R, Howe. L. S and Ramser. H, 1941, Phase Diagrams of Methane and Ethane Hydrates, *Petroleum Engineer,* 12, 56

Robinson, D. B. and Mehta, B. R., 1971. Hydrates In the PropaneCarbon Dioxide- Water System. *Journal of Canadian Petroleum Technology,* 10**,** 33-35.

Sabil. M, and Bin, K., 2009. Phase Behaviour, Thermodynamics and Kinetics of Clathrate Hydrate Systems of Carbon Dioxide in Presence of Tetrahydrofuran and Electrolytes.

Sloan. E, Khoury. F and Kobayashi. R, 1976. Water Content of Methane Gas in Equilibrium with Hydrates, *Ind. Eng. Chem., Fundam.,* 15, (4), 318-323.

Sloan, E. D., 2003. Fundamental principles and applications of natural gas hydrates. *Nature,* 426**,** 353-363.

Sloan, E. D. and Koh, C., 2008. *Clathrate Hydrates of Natural Gases, Third Edition,* USA, CRC Press Taylor & Francis Group.

Stroble T. A., Hester K. C, Koh C. A., Sum E. D and Sloan E. D., 2009. *Chem Phys*, (478), 97-109.

Stokes, R. H. and Robinson, R. A., 1948. Ionic Hydration and Activity in Electrolyte Solutions. *Journal of the American Chemical Society,* 70**,** 1870-1878.

Sum. A. K, Burruss. R. C and Sloan. D. E, 1997, Measurement of Clathrate Hydrates via Raman Spectroscopy, *J. Phys. Chem. B,* 101, (38), 7371-7377.

Taylor, B. N, Mohr, P. J. and Douma, M, (2011), "The NIST Reference on Constants Units, and Uncertainty", available online from: www.physics.nist.gov/cuu/index.html

Thakore. J. L and Holder. G. D, 1987, Solid vapor azeotropes in hydrate-forming systems, *Ind. Eng. Chem. Res.,* 26, (3), 462-469.

Tohidi, B., Danesh, A., Burgass, R. W. and Todd, A. C., 1996. Equilibrium Data and Thermodynamic Modeling of. Cyclohexane Gas Hydrates. *Chem. Eng. Sci,* 51**,** 159–163.

Tohidi, B., Danesh, A. and Todd, A. C., 1995. Modelling single and mixed electrolyte solutions and its applications to gas hydrates. *IChemE,* 73**,** 464 - 472.

Tohidi, B., Danesh, A., Todd, A. C., Burgass, R. W. and Østergaard, K. K., 1997. Equilibrium data and thermodynamic modelling of cyclopentane and neopentane hydrates. *Fluid Phase Equilibria,* 138**,** 241-250.

Trebble. M. A and Bishnoi. P. R, 1987, Extension of the Trebble-Bishnoi equation of state to fluid mixtures, *Fluid Phase Equilibria,* 40, (1-2), 1-21.

Tshibangu, M. M., 2010. Measurements of HPVLE data for fluorinated systems, MSc Thesis. University of Kwa-Zulu Natal.

Tumba, A. K., 2010. Application of Gas Hydrates to the Separation of close boiling components in petroleum streams. KwaZulu-Natal: Thermodynamics research department, school of Chemical Engineering, University of KwaZulu-Natal

Unruh, C. H. and Katz, D. L., 1949, Gas hydrates of carbon dioxide-methane mixture, . *Pet. Trans. AIME,* 186, 83.

Valderrama. J. O., 1990, A generalized Patel-Teja equation of state for polar and nonpolar fluids and their mixtures, *Journal of Chemical Engineering of Japan,* 23, 87-91

Van Der Bruggen, B. and Vandecasteele, C., 2002. Distillation vs. membrane filtration: overview of process evolutions in seawater desalination. *Desalination,* 143**,** 207-218.

Van Der Waals, J. H. and Platteeuw, J. C., 1959. Clathrate solutions. *Adv Chem Phys,* 2**,** 1-57.

Verma, V. K., 1974, Gas Hydrates from Liquid Hydrocarbon-Water System. Ph.D. Dissertation, University of Mischigan, Ann Arbor, MI.

Vlahakis, J. G., Chen, H.-S, Suwandi, M. S and Barduhn, A. J., 1972, The growth rate of ice crystals: properties of carbon dioxide hydrate, a review of properties of 51 gas hydrates, Syracuse University Research and Development Report 8330, US Department of the Interior.

Vysniauskas, A. and Bishnoi, P. R., 1983. A kinetic study of methane hydrate formation. *Chemical Engineering Science,* 38**,** 1061-1072.

Waals, J. H. V. D. and Platteeuw, J. C., 2007. *Clathrate Solutions*, John Wiley & Sons, Inc.

Waisman, E. and Lebowitz, J. L., 1970. Exact Solution of an Integral Equation for the Structure of a Primitive Model of Electrolytes *Journal of Chemical Physics* 52.

Wendland, M., Hasse, H. and Maurer, G., 1999. Experimental Pressure−Temperature Data on Three- and Four-Phase Equilibria of Fluid, Hydrate, and Ice Phases in the System Carbon Dioxide−Water. *Journal of Chemical & Engineering Data,* 44**,** 901-906.

Wichterle, I., 1978a. High Pressure Vapour-Liquid Equilibria. IV – Quantitative Description. Part 2," *Fluid Phase Equilibria,* **2**: 59-78.

Wichterle, I., 1978b. High Pressure Vapour-Liquid Equilibria. V – Quantitative Description. Part 3," *Fluid Phase Equilibria,* **2**: 143-159.

Wierzchowski, S. J. and Monson, P. A., 2005. Calculating the Phase Behavior of Gas-Hydrate-Forming Systems from Molecular Models. *Industrial & Engineering Chemistry Research,* 45**,** 424-431.

Wiebe, R., 1941, The binary system carbon dioxide-water under pressure, *Chem. Rev.,* 29, (3), 475-481.

Wilcox. W. I., Carson. D. B. and Katz, D. L., 1941, Natural Gas Hydrates, *Ind. Eng. Chem.,* 33, (5), 662-665.

Wittstruck, T. A., Brey, W. S., Buswell, A. M. and Rodebush, W. H., 1961. Solid Hydrates of Some Halomethanes. *Journal of Chemical & Engineering Data,* 6**,** 343-346.

Yang, S. O., Cho, S. H., Lee, H. and Lee, C. S., 2001. Measurement and prediction of phase equilibria for water + methane in hydrate forming conditions. *Fluid Phase Equilibria,* 185**,** 53-63.

Yoon, J-H., Yamamoto. Y., Komai, T and Haneda, H., 2003. Rigorous approach to the prediction of the heat of dissociation of gas hydrates, *Ind. Eng. Chem. Res.,* 42, (5), 1111-1114.

Zakrzewski. M, Klug. D. D and Ripmeester. J. A, 1994, On the pressure-induced phase transformation in the structure II clathrate hydrate of tetrahydrofuran, *Journal of Inclusion Phenomena and Macrocyclic chemistry,* 17, (3), 237-247.

Zemaitis, J . F., Clark. D. M., Rafal, M. and Scrivner, N. D., 1986, Handbook of aqueous electrolyte thermodynamics, American Institute of Chemical Engineers, New York.

Zhu, C. and Anderson, G., 2002. Environmental applications of geochemical modeling. United Kingdom: Cambridge University Press.

# APPENDICES

## APPENDIX A Desalination Technologies

A.1 Membrane Processes

### A.1.1 Electrodialysis

In Figure A.1, the feed is pumped through numerous chambers, which are bound by alternating permeable membranes, to cations or anions. The compartments on either end contain electrodes which pass direct current through all the chambers. Cations and anions travel in opposite directions in response to the voltage applied. Due to the membrane selectivity, the concentration of the ions increases and decreases in alternating chambers (Miller, 2003). The salt concentration decreases from the centre chamber and increases in adjacent chambers. This method is suited for solutions with allow salt concentration. At concentrations above 12 g/L TDS, the cost of operating an electrodialysis plant becomes too high. Membranes require cleaning due to salt (Ribeiro, 1996). The "pure" water stream may contain 0.14g/L TDS with a 94% recovery.

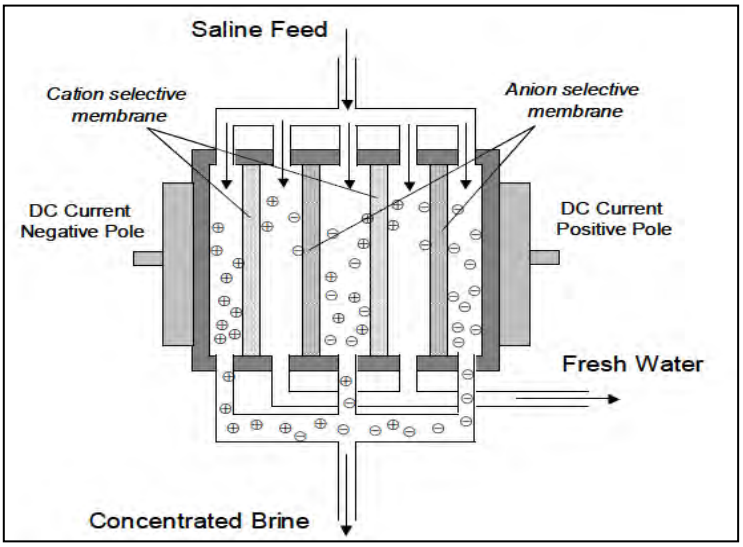


Figure A.1: Electrodialysis process (Miller, 2003).

### A.1.2 Membrane distillation

Supplied energy is used to create a temperature gradient across a hydrophobic microporous membrane which forms a vapour pressure gradient. A water vapour flux is created through the membrane. This enables the concentration of the aqueous brine solution which results in nucleation and crystallization. This process can operate at high solute concentrations, low concentration gradients, moderate temperatures and atmospheric pressure Ribeira (1996) and Mariah, Buckley et al. (2006).

A.1.3 Reverse Osmosis

In the RO process, (refer to Figure A.2), after pretreating through microfiltration and ultrafiltration, the saline feed water enters between two thin semi-permeable spiral or hollow fibre membranes which are supported by a number of non-selective membranes. The membranes are permeable to water however the dissolved salt cannot pass through as the membrane pore size is roughly 0.1 nm. A pressure higher than the feed water osmotic pressure, between 1 MPa and 5 MPa, is exerted on the salt water to allow the pure water to pass through the membrane to the permeate while leaving the concentrated brine, retentate, behind. The energy required is dependent on the concentration of the salt in the feed, roughly 5 g/L salt Ribeiro (1996) and Van der Bruggen and Vandecasteele (2002) and results in a recovery of up to 60% with a permeate concentration of 0.2g/L TDS.

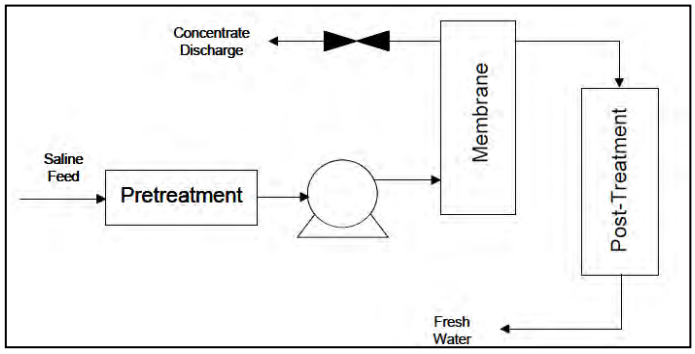


Figure A.2: Reverse osmosis process (Miller, 2003).

A.2 Thermal Processes

### A.2.1 Multiple stage flash distillation

In Figure A.3: the feed is heated and transported to a series of chambers where it is flashed at progressively lower pressures to produce vapour. The vapour condenses on tubes due to the exchange of heat and is collected in trays. Recovery may be 50% with a "pure" water stream of 0.05 g/L TDS (Ribeiro, 1996) and (Van Der Bruggen et al., 2002).

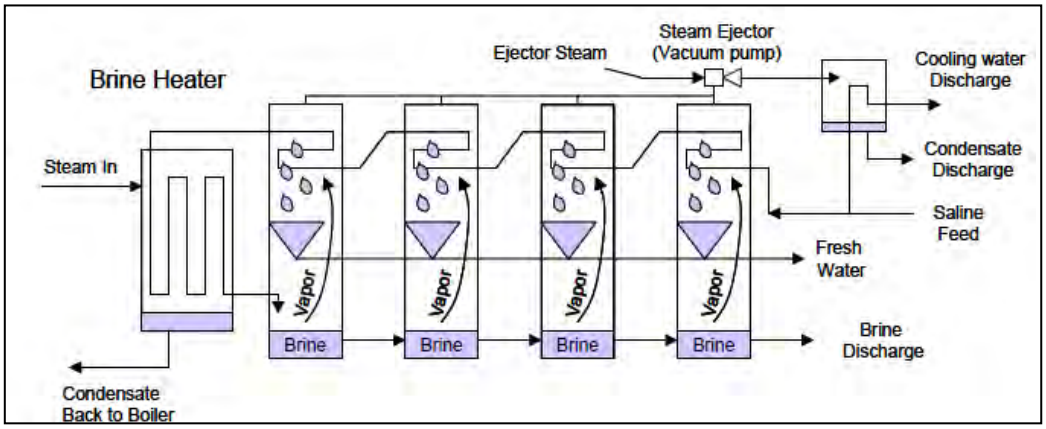


Figure A.3: Multiple Stage Flash distillation process (Miller, 2003).

A.2.2 Vapour compression distillation

According to Ribeiro (1996), in Figure 2.5, the feed is preheated, boiled and the vapour is released. However, the released vapour is compressed with a mechanical compressor or steam ejector and is passed through tubes where it condenses. The latent heat released is used to boil the feed and a vent is used to remove the non-condensable gases. During start up, an initial steam supply is required. A 50% recovery is possible with 0.01g/L TDS in the water product.

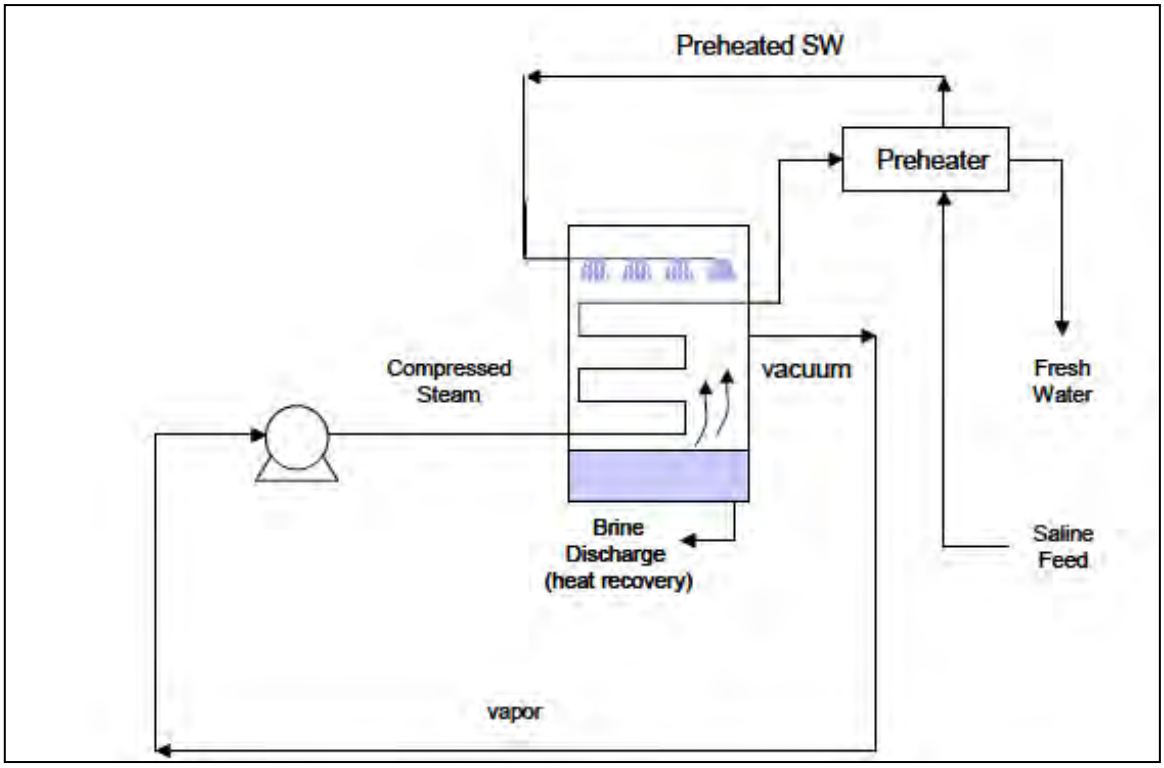


Figure A.4: Vapour compression distillation process (Miller, 2003).

### A.2.3 Multiple Effect Distillation

In the MED process, in Figure 1.2, vapour from the first evaporator condenses in the second evaporator, releasing latent heat. The latent heat is used to evaporate the feed to the second evaporator. This applies to all evaporators in the system; the vapour from the last effect is condensed using a cooling stream of feed. To maintain a pressure gradient between the condensing steam and concentrated salt water, each effect operates at a lower pressure than the previous effect. High heat transfer rates are obtained due to the film boiling and condensation techniques (Van Der Bruggen et al., 2002). The tubes in each effect may be vertical, where condensation occurs on the outside of the tubes, or horizontal, where condensation occurs inside the tubes. Additional steam is required from turbines for low temperature distillation, 233.15 K, which reduces the required energy (Ribeiro, 1996). The “pure” water stream may contain 0.01g/L TDS with a 65% recovery.

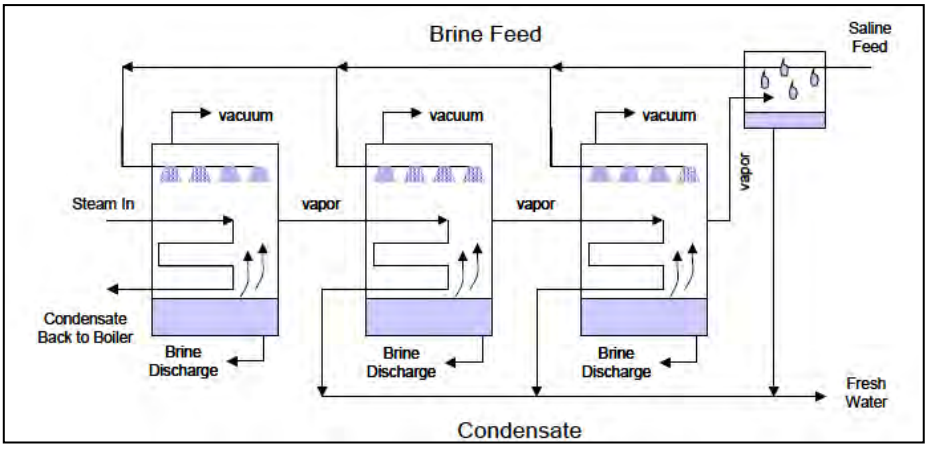


FigureA.5: Multiple effect distillation process (Miller, 2003).

## APPENDIX B Flow Diagrams

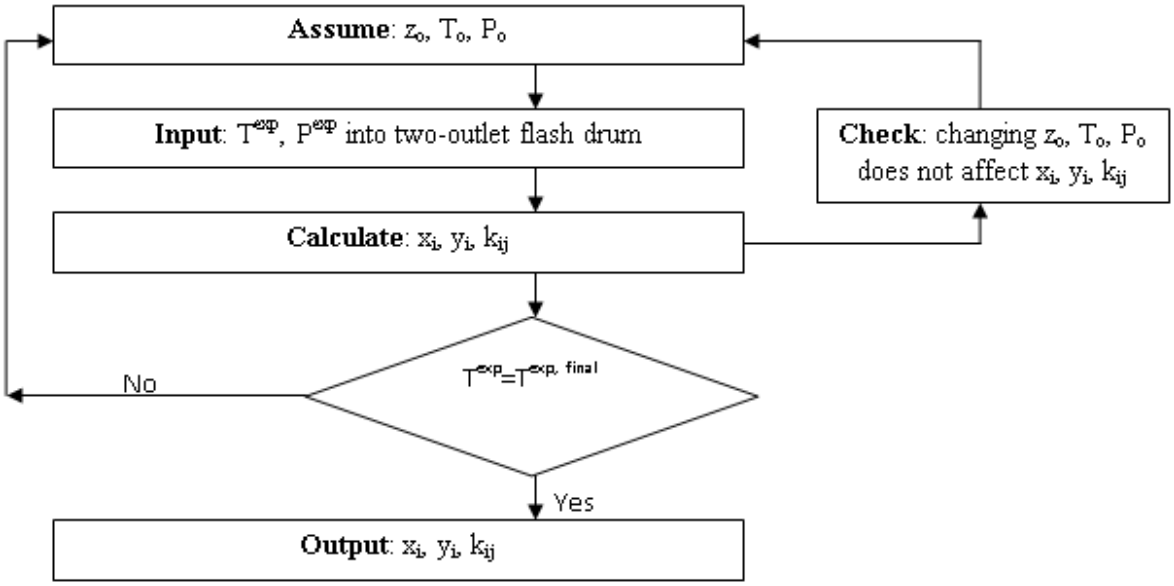


Figure A.6: Computation flow chart for determining solubility data using Aspen Plus flash calculation.

## APPENDIX C Tables

Table A.1: List of references which have measured HLV equilibrium data for the system $CH_4$ (1) + water (2).

| System | T range / K | P range / MPa | Reference |
|---|---|---|---|
| $CH_4$ (1) + water (2) | 280.9-286.7 | 5.847-10.80 | Roberts et al., 1941 |
| | 273.7-281.5 | 2.77-6.06 | Deaton and Frost, 1946 |
| | 295.7-302.0 | 33.99-77.50 | Kobayashi and Katz, 1949 |
| | 285.7-301.6 | 9.62-68.09 | McLeodet al., 1961 |
| | 290.2-320.1 | 15.9-397 | Marshall et al., 1964 |
| | 273.2-294.3 | 2.65-28.57 | Jhaveri and Robinson, 1965 |
| | 283.2-288.7 | 7.10-13.11 | Galloway et al., 1970 |
| | 275.2-291.2 | 3.02-18.55 | Verma, 1974 |
| | 273.3-286.0 | 2.69-10.04 | de Roo et al., 1983 |
| | 275.4-281.2 | 2.87-6.10 | Thakore and Holder, 1987 |
| | 273.4-286.4 | 2.68-10.57 | Adisasmito et al., 1991 |
| | 273.5-293.6 | 2.72-24.96 | Nixdorf and Oellrich, 1997 |
| | 305.1-320.5 | 98.0-493 | Nakano et al., 1999 |
| | 276.5-286.3 | 3.68-9.66 | Yang et al., 2001 |
| | 291.9-303.5 | 20.19-72.26 | Jager et al., 2001 |
| | 274.3-285.8 | 2.92-9.54 | Nakamura et al., 2003 |
| | 274.6-298.3 | 3.06-47.86 | Mohammadi et al., 2005 |
| | 283.2-286.5 | 7.11-10.28 | Kuo et al., 2010 |

Table A.2: List of references which have measured HLV equilibrium data for the system $C_2H_6$ (1) + water (2).

| System | T range / K | P range / MPa | Reference |
|---|---|---|---|
| $C_2H_6$ (1) + water (2) | 273.4-287.0 | 2.06-6.84 | Roberts et al., 1940 |
| | 273.7-286.5 | 0.51-2.73 | Deaton and Frost, 1946 |
| | 279.9-287.4 | 0.97-3.30 | Reamer et al., 1952 |
| | 277.6-282.5 | 0.81-1.55 | Galloway et al., 1970 |
| | 277.5-286.5 | 0.78-2.62 | Holder and Grigoriou, 1980 |
| | 278.8-288.2 | 0.95-3.36 | Holder and Hand, 1982 |
| | 277.8-287.2 | 0.85-3.08 | Avlonitis, 1988 |
| | 274.3-283.0 | 0.55-1.64 | Englezos and Bishnoi, 1991 |
| | 273.7-287.6 | 0.50-3.24 | Nixdorf et al., 1997 |
| | 275.2-282.1 | 0.60-1.40 | Mohammadi et al., 2008a |

Table A.3: List of references which have measured HLV equilibrium data for the system $C_3H_8$ (1) + water (2).

| System | T range / K | P range / MPa | Reference |
|---|---|---|---|
| $C_3H_8$ (1) + water (2) | 273.2-278.0 | 0.17-4.72 | Miller and Strong, 1946 |
| | 273.7-277.1 | 0.18-0.39 | Deaton and Frost, 1946 |
| | 274.3-277.2 | 0.24-0.41 | Reamer et al., 1952 |
| | 274.3-277.8 | 0.21-0.46 | Robinson and Mehta, 1971 |
| | 273.9-278.0 | 0.19-0.51 | Verma, 1974 |
| | 274.2-278.4 | 0.21-0.54 | Kubota et al., 1984 |
| | 274.2-278.2 | 0.22-0.51 | Thakore and Holder, 1987 |
| | 273.6-278.0 | 0.21-0.51 | Patil, 1987 |
| | 274.2-278.3 | 0.21-0.55 | Englezos et al., 1993 |
| | 273.5-282.5 | 0.19-0.57 | Nixdorf and Oellrich, 1997 |
| | 276.8-278.6 | 0.37-0.55 | Mooijer-van den Heuvel et al., 2002 |
| | 274.6-278.3 | 0.22-0.50 | Mohammadi et al., 2008a |

Table A.4: List of references which have measured HLV equilibrium data for the system $CO_2$ (1) + water (2).

| System | T range / K | P range / MPa | Reference |
|---|---|---|---|
| $CO_2$ (1) + water (2) | 273.7-282.9 | 1.32-4.32 | Deaton and Frost, 1946 |
| | 277.2-281.9 | 2.04-3.69 | Unruh and Katz, 1949 |
| | 273.4-283.2 | 1.23-4.50 | Larson, 1955 |
| | 273.9-282.0 | 1.38-3.84 | Robinson and Mehta, 1971 |
| | 279.6-282.8 | 2.74-4.36 | Ng and Robinson, 1985 |
| | 273.6-283.2 | 1.30-4.51 | Vlahakis et al., 1972 |
| | 274.3-282.9 | 1.42-4.37 | Adisasmito et al., 1991 |
| | 273.4-281.1 | 1.34-4.09 | Ohgaki et al., 1993 |
| | 273.6-282.0 | 1.31-4.02 | Fan and Guo, 1999 |
| | 273.9-282.2 | 1.37-3.85 | Wendland et al., 1999 |
| | 274.7-279.7 | 1.50-2.78 | Fan et al., 2000 |
| | 276.5-282.5 | 1.82-4.01 | Mooijer-van den Heuvel et al., 2002 |
| | 277.5-298.3 | 2.05-47.86 | Mohammadi et al., 2005 |

Table A.5: List of references which have measured HLV equilibrium data for the system R22 (1) + water (2).

| System | T range / K | P range / MPa | Reference |
|---|---|---|---|
| R22 (1) + water (2) | 276.3-287.1 | 0.14-0.59 | Chun et al 1996 |
| | 277.8-289.4 | 0.15-0.77 | Javanmardi et al., 2004 |
| | 273.9-289.5 | 0.10-0.77 | Wittstruck et al., 1961 |
| | 274.0-290.4 | 0.41-0.94 | Chinworth and Katz, 1947 |

Table A.6: List of references which have measured HLV equilibrium data for the system R134a (1) + water(2).

| System | T range / K | P range / MPa | Reference |
|---|---|---|---|
| R134a (1) + water (2) | 273.5-283.1 | 0.06-0.41 | Liang et al., 2001 |
| | 273.5-283.5 | 0.04-0.42 | Akiya et al., 1999 |
| | 279.4-282.9 | 0.18-0.38 | Eslamimanesh et al., 2011 |

Table A.7: List of references which have measured HLV equilibrium data for the system R141b (1) + water(2).

| System | T range / K | P range / MPa | Reference |
|---|---|---|---|
| R141b (1) + water (2) | 273.4-281.5 | 0.01-0.04 | Liang et al., 2001 |

Table A.8: List of references which have measured HLV equilibrium data for the system R152a (1) + water(2).

| System | T range / K | P range / MPa | Reference |
|---|---|---|---|
| R152a (1) + water (2) | 273.4-28 | 0.08-0.44 | Liang et al., 2001 |

Table A.9: List of references which have measured HLV equilibrium data for the system R32 (1) + water(2).

| System | T range / K | P range / MPa | Reference |
|---|---|---|---|
| R32 (1) + water (2) | 275.5-290.7 | 0.20-1.09 | Hashimoto et al., 2010 |
| | 274-294.1 | 0.17-1.49 | Akiya et al., 1999 |

Table A.10: List of references which have measured HLV equilibrium data for the system $CH_4$(1) + water(2) + salt (3).

| System | T range / K | P range / MPa | Reference |
|---|---|---|---|
| $CH_4$ (1) + water (2) + NaCl (3) | 274.4-303.5 | 7.92-72.26 | Jager et al., 2001 |
| | 275.1-277.7 | 5.88-8.57 | Kharrat and Dalmazzone, 2003 |
| | 274.2-283.6 | 3.58-9.60 | Mohammadi et al., 2008a |
| $CH_4$ (1) + water (2) + $CaCl_2$ (3) | 274.2-283 | 2.81-9.01 | Mohammadi et al., 2008a |
| | 273.5-282.3 | 4.92-10.22 | Kharrat and Dalmazzone, 2003 |
| | 276.3-282.2 | 10.15-22.93 | Atik et al., 2006 |
| $CH_4$ (1) + water (2) + KCl (3) | 273.7-283.2 | 3.35-8.69 | Mohammadi et al., 2008a |

Table A.11: List of references which have measured HLV equilibrium data for the system $C_2H_6$ (1) + water (2) + salt (3).

| System | T range / K | P range / MPa | Reference |
|---|---|---|---|
| $C_2H_6$ (1) + water (2) + NaCl (3) | 273.7-280.4 | 0.88-2.17 | Tohidi et al., 1997 |
| | 272.2-284.7 | 0.54-2.90 | Mohammadi et al., 2008a |
| $C_2H_6$ (1) + water (2) + $CaCl_2$ (3) | 273.7-283.3 | 0.59-2.09 | Mohammadi et al., 2008a |
| | 273.3-275.2 | 1.25-1.61 | Englezos and Bishnoi, 1991 |
| $C_2H_6$ (1) + water (2) + KCl(3) | 273.3-282.3 | 0.58-2.11 | Mohammadi et al., 2008a |
| | 274.7-278.4 | 0.96-1.56 | Englezos and Bishnoi, 1991 |
| $C_2H_6$ (1) + water (2) + KCl(3) + NaCl (4) | 273.1-276.5 | 1.40-1.85 | Englezos and Bishnoi, 1991 |
| $C_2H_6$ (1) + water (2) + $CaCl_2$ (3) + NaCl (4) | 273.9-276.1 | 1.27-1.73 | Englezos and Bishnoi, 1991 |
| $C_2H_6$ (1) + water (2) + $CaCl_2$ (3) + KCl (4) | 274.1-276.4 | 1.03-1.45 | Englezos and Bishnoi, 1991 |
| $C_2H_6$ (1) + water (2) + $CaCl_2$ (3) + KCl (4) + NaCl (5) | 273.6-278.4 | 0.99-1.97 | Englezos and Bishnoi, 1991 |
| $C_2H_6$ (1) + water (2) + $CaCl_2$ (3) + KCl (4) + NaCl (5) + KBr (6) | 273.6-278.8 | 1.06-2.19 | Englezos and Bishnoi, 1991 |

Table A.12: List of references which have measured HLV equilibrium data for the system $C_3H_8$(1) + water(2) + salt (3).

| System | T range / K | P range / MPa | Reference |
|---|---|---|---|
| $C_3H_8$ (1) + water (2) + NaCl (3) | 274.0-275.1 | 0.32-0.40 | Mohammadi et al., 2008a |
| $C_3H_8$ (1) + water (2) + $CaCl_2$ (3) | 274.6-276.2 | 0.31-0.46 | Mohammadi et al., 2008a |
| $C_3H_8$ (1) + water (2) + KCl (3) | 274.3-276.2 | 0.31-0.46 | Mohammadi et al., 2008a |

Table A.13: List of references which have measured HLV equilibrium data for the system $CO_2$(1) + water(2) + salt (3).

| System | T range / K | P range / MPa | Reference |
|---|---|---|---|
| $CO_2$ (1) + water (2) + NaCl (3) | 273.2-276.1 | 2.15-3.61 | Tohidi et al., 1997 |
| | 274.4-280.2 | 1.83-3.73 | Mohammadi et al., 2008a |
| $CO_2$ (1) + water (2) + KCl (3) | 273.8-278.0 | 2.01-3.35 | Mohammadi et al., 2008a |

Table A.14: List of references which have measured HLV equilibrium data for the system R22 (1) + water (2) + salt (3).

| System | T range / K | P range / MPa | Reference |
|---|---|---|---|
| R22 (1) + water (2) + NaCl (3) | 274.0-284.8 | 0.17-0.54 | Chun and Lee, 2000 |
| R22 (1) + water (2) + KCl (3) | 275.1-285.3 | 0.14-0.63 | Chun and Lee, 2000 |
| R22 (1) + water (2) + $MgCl_2$ (3) | 273.9-286.5 | 0.32-0.68 | Chun and Lee, 2000 |

Table A.15: List of proven formers (Carroll, 2003) and (Sloan and Koh, 2008).

| Name | Type | Cavity | Help gas |
|---|---|---|---|
| Methane | I | Pentagonal dodecahedron | |
| Ethane | I | | |
| Hydrogen Sulphide | I | Pentagonal dodecahedron | |
| Carbon Dioxide | I | | |
| Propane | II | hexakaidecahedron | |
| Nitrogen | II | Pentagonal dodecahedron | |
| Isobutane | II | hexakaidecahedron | |
| Ethylene | | | |
| Acetylene | | | |
| Propylene | | | |

Table A.15 contd.

| Name | Type | Cavity | Help gas |
|---|---|---|---|
| Propyne | | | |
| Fluorine | | | |
| Bromine | | | |
| Argon | II | Pentagonal dodecahedron | |
| Krypton | II | Pentagonal dodecahedron | |
| Xenon | | | |
| Radon | | | |
| Oxygen | II | Pentagonal dodecahedron | |
| Sulphur Dioxide | | | |
| Methanethiol | | | |
| Ethanethiol | | | |
| Propanethiol | | | |
| Ethylene Oxide | I | | |
| Nitrous Oxide | | | |
| Hydrogen Selenide | | | |
| Sulfur Hexafluoride | | | |
| Phosphine | | | |
| Arsine | | | |
| Stibine | | | |
| Perchloryl Fluoride | | | |
| Trimethylene Oxide | II | hexakaidecahedron | |
| | I | tetrakaidecahedron | |
| Cyclopropane | II | hexakaidecahedron | |
| | I | tetrakaidecahedron | |
| Ethylene sulphide | II | hexakaidecahedron | |
| | I | tetrakaidecahedron | |
| Tetrahydrofuran | II | | |
| Cyclobutanone | | | |
| Tetrahydropyran | | | |
| Chloroform | | | |
| Benzene | II | | Xenon |
| CH3F | I | | |

Table A.15 contd.

| Name | Type | Cavity | Help gas |
|---|---|---|---|
| CHF3 | I | | |
| CF4 | I | | |
| C2H3F | I | | |
| C2H5F | I | | |
| CH3CHF2 | I | | |
| (CH3)3CF | II | | |
| Chlorine | I | | |
| Bromine Chloride | I | | |
| CH3Cl | I | | |
| CH2Cl2 | II | | |
| CHCl3 | II | | |
| C2H3Cl | II | | |
| C2H5Cl | II | | |
| CH3CHCl2 | II | | |
| CH2CIF | I | | |
| CHCIF2 | I | | |
| CHCl2F | II | | |
| CCl2F2 | II | | |
| CCl3F | II | | |
| CH3CClF2 | II | | |
| CH3Br | I | | |
| C2H5Br | II | | |
| CH3I | II | | |
| CBrF3 | II | | |
| CBr2F2 | II | | |
| CBrCIF2 | II | | |
| CH3SH | I | | |
| Dimethyl ether | II | | |
| Propylene Oxide | II | | |
| 1,3-Dioxolne | II | | |
| 2,5-Dihydrofuran | II | | |

Table A.15 contd.

| Name | Type | Cavity | Help gas |
|---|---|---|---|
| Clyclohexane | II | | Xenon |
| Cyclohexene oxide | II | | Xenon |
| Isobutylene | II | | Xenon |
| Cis-2-butene | II | | Xenon |
| Allene | II | | Xenon |
| n-butane | II | | Hydrogen sulphide, methane, Xenon |
| Norbornane | II | | Xenon |
| Bicycloheptadiene | II | | Xenon |
| Methyl Formate | II | | Xenon |
| Acetonitrile | II | | Xenon |
| Neopentane | II | | Xenon |
| 1,4-dioxane | | | methane |
| 1,3-dioxane | | | methane |
| CCl4 | | | Carbon dioxide, nitrogen |
| C2H5I | | | Nitrogen |
| CS2 | | | Nitrogen, oxygen |
| CH2CICH2Cl | | | Air |

Table A.16: List of inhibitors (Sloan and Koh, 2008).

| Name | Reference |
|---|---|
| Helium | |
| Methanol | |
| Ethylene Glycol | |
| Triethylene Glycol | |
| Sodium Chloride | |
| Ethanol | |
| Diethylene glycol | |
| Potassium Chloride | |
| Calcium Chloride | |
| Monoethylene glycol | |
| Sodium dodecyl sulfate | (Mandal and Liak, 2008) |
| Para-toluene sulfonic acid | (Mandal and Liak, 2008) |
| Sodium dodecyl benzene sulfonate | (Mandal and Liak, 2008) |
| Potassium oxalate monohydrate | (Mandal and Liak, 2008) |

## APPENDIX D Equations

**Debye-Hűckel** (Hibbert, 1993)

$$\ln \gamma_{\pm}^{(LR)} = \frac{-A|z_1 z_2|\sqrt{I}}{1 + Ba\sqrt{I}} \qquad \text{B.1}$$

$$\ln \gamma_{\pm}^{(LR)} = -A|z_1 z_2|\sqrt{I} \qquad \text{B.2}$$

$$\ln \gamma_{\pm}^{(LR)} = \frac{-A|z_1 z_2|\sqrt{I}}{1 + Ba\sqrt{I}} + CI \qquad \text{B.3}$$

**The hydration model** (Stokes and Robinson, 1948)

$$\log \gamma = -\frac{0.5092 z_1 z_2 \sqrt{I_v}}{1 + 0.3286 \overset{0}{a} \sqrt{I_v}} - \frac{n}{z_1 + z_2} \log a_w - \log\left[1 - 0.018(n - (z_1 + z_2))m\right] \qquad \text{B.4}$$

**The Davies Equation** (Zhu and Anderson, 2002)

$$\log \gamma_{\pm}^{(LR)} = -A_{\gamma,10} |z_i|^2 \left( \frac{\sqrt{I}}{1 + \sqrt{I}} + 0.2I \right) \qquad \text{B.5}$$

**B-dot equation** (Zhu and Anderson, 2002)

$$\log \gamma_{\pm}^{(LR)} = -A_{\gamma,10} |z_i|^2 \frac{\sqrt{I}}{1 + \overset{o}{a}_i B_\gamma \sqrt{I}} + \dot{B} I \qquad \text{B.6}$$

**One parameter model** (Bromely, 1973)

$$\log \gamma_{\pm} = -A_\gamma |z_i|^2 \frac{\sqrt{I}}{1 + a\sqrt{I}} + \frac{(0.06 + 0.6\dot{B})|z_i|^2 I}{\left(1 + \frac{1.5}{|z_i|^2} I\right)^2} + \dot{B} I \qquad \text{B.7}$$

**Pitzer** (Chen et al., 1982) and (Prausnitz et al., 1999)

$$\ln \gamma_{\pm}^{(LR)} = \left|z_+ z_-\right| f^{\gamma} + m\left(\frac{2\nu_+\nu_-}{\nu}\right)B_{MX}^{\gamma} + m^2\left[\frac{2\left(\nu_+\nu_-\right)^{3/2}}{\nu}\right]C_{MX}^{\gamma} \qquad \text{B.8}$$

Where

$$\beta^{\gamma} = 2\beta^{(0)} + \frac{2\beta^{(1)}}{x_1^2}\left[1 - e^{-x_1}(1 + x_1 - 0.5x_1^2)\right] + \frac{2\beta^{(2)}}{x_2^2}\left[1 - e^{-x_{21}}(1 + x_2 - 0.5x_2^2)\right] \qquad \text{B.9}$$

$$f^{\gamma} = f^{\phi} + \left(\frac{2}{b}\right)A_{\phi}\ln\left(1 + bI^{1/2}\right) \qquad \text{B.10}$$

$$f^{\phi} = -A_{\phi}\left[\frac{I^{1/2}}{1 + bI^{1/2}}\right] \qquad \text{B.11}$$

$$x_1 = \alpha_1 I^{1/2} \qquad \text{B.12}$$

$$x_2 = \alpha_2 I^{1/2} \qquad \text{B.13}$$

$$A_{\phi} = \frac{1}{3}\left(\frac{2\pi N_o d_s}{1000}\right)^{1/2}\left(\frac{e^2}{\varepsilon kT}\right)^{3/2} \qquad \text{B.14}$$

$$I = \frac{1}{2}\sum m_i z_i^2 \qquad \text{B.15}$$

**Van der Waals and Platteeuw**(Waals and Platteeuw, 2007)

$$\mu_w^{\,H} - \mu_w^{\,\beta} = -RT\sum_m \nu_m \ln\left(1 - \sum_j \Theta_{mj}\right) \qquad \text{B.16}$$

Where

$$\Theta_{ml}(T,P) = \frac{C_{ml}(T)P}{1 + \sum_j C_{mj}(T)P} \qquad \text{B.17}$$

$$\mathrm{C_{ml}(T)} = \frac{4\pi}{\mathrm{kT}} \int_0^{\mathrm{Rcav}} \exp(-\mathrm{w(r)/kT})\mathrm{r}^2 \mathrm{dr} \qquad \text{B.18}$$

**Extended Van der Waals and Platteeuw**(Parrish and Prausnitz, 1972)

$$\mu_w^{\,H} - \mu_w^{\,\beta} = -RT\sum_m \nu_m \ln\left(1 - \sum_j \Theta_{mj}\right) \qquad \text{B.19}$$

$$\Theta_{ml}(T,P) = \frac{C_{ml}(T)\overset{\Lambda}{f}_j}{1 + \sum_j C_{mj}(T)\overset{\Lambda}{f}_j} \qquad \text{B.20}$$

**Klauda and Sandler** (Klauda and Sandler, 2003)

$$f_w^{\,H} = f_w^{\,\beta} \qquad \text{B.21}$$

$$f_w^{\,H} = f_w^{\,\beta} \exp\left(\frac{-\Delta\mu_w^H}{RT}\right) \qquad \text{B.22}$$

Where

$$f_w^{\,\beta} = P_w^{sat,\beta}\phi_w^{sat,\beta} \exp\left(\frac{V_w^{\beta}(P - P_w^{sat,\beta})}{RT}\right) \qquad \text{B.23}$$

$$\mu_w^{\,H} - \mu_w^{\,\beta} = -RT\sum_m \nu_m \ln\left(1 - \sum_j \Theta_{mj}\right) \qquad \text{B.24}$$

## APPENDIX E Figures

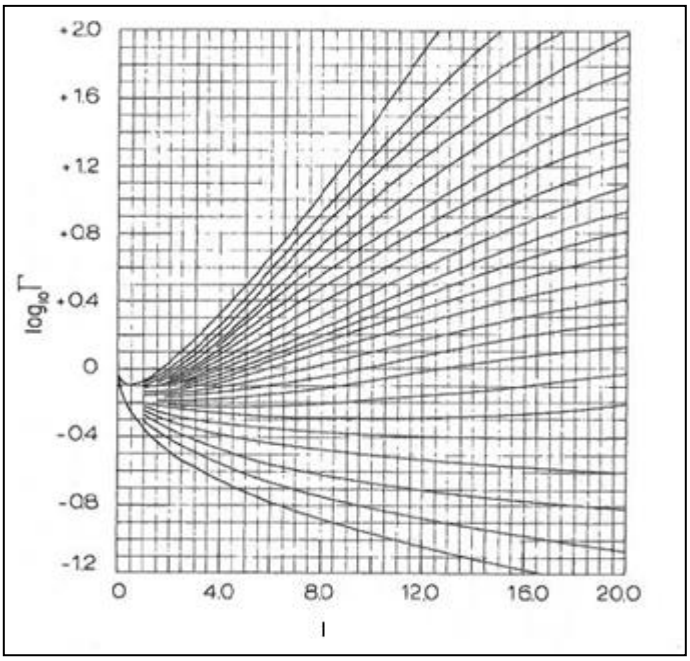


Figure A.7: Reduced activity coefficient (Γ) versus ionic strength between (I) 1 and 20. (Meissner and Kusik, 1972)

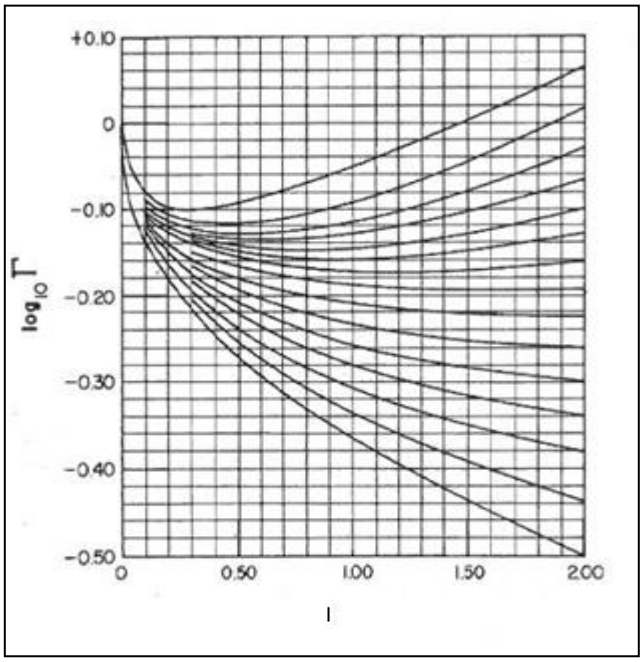


Figure A.8: Reduced activity coefficient (Γ) versus ionic strength (I) between 0.1 and 2. (Meissner and Kusik, 1972)

## APPENDIX F Worked Examples

Estimation of uncertainties

This section demonstrates the procedure for determining the experimental uncertainties. The system (1) Chlorodifluoromethane and (2) water will be used in this example.

Calibration

Two sources of uncertainty are present for the temperature calibration:

- The Pt-100 contains a maximum possible error of ±0.15 K.
- The calibration polynomial, conducted on 31 May 2011, Tcal / K = 0.9977Ttrans + 0.0341, is ±0.027 K.

The uncertainty for each error using the rectangular distribution is:

$$u_{\text{reference}}(T) = \frac{0.15\text{K}}{\sqrt{3}} = 0.087\text{K}$$

$$u_{\text{calibration}}(T) = \frac{0.027\text{K}}{\sqrt{3}} = 0.016\text{K}$$

Similarly for pressure, two sources of uncertainty are present for the pressure calibration: There are two pressure transducers, 0-1 MPa and 0-10 MPa. The latter will be used for pressures above 1 MPa and thus will not be used for the (1) chlorodifluoromethane + (2) water system as at low pressure the transducer is less accurate than the 0-1 MPa transducer.

- The 0-1 MPa contains a maximum possible error of ±0.5 kPa.
- The calibration polynomial, conducted on 7 July 2011, Pcal/MPa = 1.0001Ptrans-0.00015, is ± 1 kPa.

The uncertainty for each error using the rectangular distribution is:

$$u_{reference,0-1MPa}(P) = \frac{0.0005MPa}{\sqrt{3}} = 0.0003\text{MPa}$$

$$u_{calibration,0-1MPa}(P) = \frac{0.01MPa}{\sqrt{3}} = 0.006\text{MPa}$$